Calderas and their volcano-tectonic controls on hydrothermal fluid transport

A thesis submitted in partial fulfilment of the requirements for the degree of Doctor of Philosophy in Geology at the University of Canterbury by

Thomas Owain Garden

2017

View from the head of Alpine Gulch, near the centre of the resurgent dome of Lake City caldera. Photo looking northeast.

ABSTRACT

Silicic caldera volcanoes are often spatially associated with hydrothermal systems that are economically important for geothermal power and the localisation of ore deposits, and also influence their restless behaviour and associated hazards. However, despite their potential importance, the influence that caldera-related structures, lithologies and magmatism have on controlling hydrothermal fluid pathways, and the physiochemical conditions of the fluid is not fully understood. Ancient, exhumed calderas provide an opportunity to examine fossil fluid pathways in a more complete structural, lithological and magmatic context than is possible in poorly-exposed modern calderas. In this thesis I use a combination of field mapping, scanline transects, reflectance spectroscopy, alteration mineralogy, vein textures and fluid inclusion microthermometry to reconstruct and better understand the volcano-tectonic controls on hydrothermal fluid flow at the 22.9 Ma Lake City caldera in Colorado, U.S.A.

Field mapping, scanline transects and petrographic analyses are used in Chapter 2 to characterise the architecture of the caldera margin and the structural and lithological controls on the distribution of veins and alteration at Lake City. The caldera margin consists of relatively straight segments linked by more structurally complex intersections; these structural intricacies produce a zone of deformation that can reach >300 m wide. Structural analyses show that the wide (up to ~60 m) fault core of the ring fault contains abundant sub-parallel veins, with orientations similar to that of the caldera margin. Smaller displacement faults inside the caldera generally have narrow (<1 m), hydrothermally cemented fault cores with more variably oriented veins in the surrounding damage zone. These field data suggest that fluid flow is controlled by fault connectivity, the location and displacement of faults, and lithology. I propose a conceptual model where permeability is enhanced by: 1) the presence of permeable lithologies, 2) a high density of faults and fractures, and 3) orientations of faults and fractures that promote the formation of permeable discontinuity intersections.

Secondary alteration minerals form due to interaction between country rock and hydrothermal fluid. Mineral assemblages and compositions can be used to estimate physiochemical parameters of the hydrothermal system (e.g. pH, temperature, water/rock ratio) that are important for geothermal and ore exploration. The composition of hydrothermal white mica is sensitive to changes in physiochemical conditions. Short wave

infrared (SWIR) reflectance spectroscopy is a well-established tool for investigating alteration mineralogy, including white mica composition. However, the newest high spatial resolution, automated systems, such as the Corescan HCI-3, are poorly represented in the literature compared to older low spatial resolution systems, such as the ASD TerraSpec. In Chapter 3, I compare the performance of Corescan and TerraSpec SWIR systems in measuring the composition of white mica, as estimated using the wavelength position of the ~2200 nm AlOH absorption feature (λ_{AlOH}). The Corescan and TerraSpec correlate well with each other, although there are small absolute differences that should be taken into account if combining data from both systems. The Corescan results for λ_{AlOH} correlate slightly better than TerraSpec with the aluminium content of white mica as determined by scanning electron microscope (SEM) energy-dispersive x-ray spectroscopy (EDS). The spatial distribution of white mica composition at Lake City caldera suggests that high-Al white mica generally correlates with quartz-sericite-pyrite alteration and low $\delta^{18}O$ compositions in the centre of the caldera, although there are significant deviations from this pattern on the western caldera margin. These results confirm the usefulness of SWIR reflectance spectroscopy and white mica composition as a tool for studying hydrothermal alteration.

In Chapter 4 reflectance spectroscopy is combined with a suite of data from alteration mineralogy, vein textures, and fluid inclusions to characterise the physiochemical conditions of the Lake City caldera hydrothermal system. It is determined that the hydrothermal system was dominantly moderate temperature (up to ~290°C), low salinity (<3% NaCl equivalent) and neutral to weakly acidic pH, with boiling conditions more common with decreasing paleodepth. Based on the lack of high-temperature, hypersaline fluid inclusions within the caldera centre, we interpret that the resurgent syenite intrusions (batch A magmas) provided little magmatic fluid input and had cooled significantly by the time the hydrothermal system had established. In contrast, in the eastern portion of the caldera, late distinct magma batches (batch B) provided high temperature (up to ~540°C) and hypersaline (up to ~65% NaCl eq.) magmatic fluid input above intrusions. These data show the contrasting hydrothermal manifestations of a waning, degassed magma batch (batch A) and fresh, volatile-rich magma (batch B), and our conceptual model re-emphasises the importance of fault intersections in facilitating permeability.

The modern calderas of the Taupō Volcanic Zone (TVZ) in New Zealand, and Valles and Long Valley calderas in the U.S.A. have morphologies that are strongly influenced by regional structure. The position of hydrothermal fluid flow is generally influenced by the location of fault intersections, such as where the caldera margin cuts across the regional structural grain, although this relationship is equivocal in some cases. This thesis shows how a variety of methods can be used to reconstruct a fossil hydrothermal system and provide guidelines for geothermal exploration in modern caldera-related settings.

ACKNOWLEDGEMENTS

During my research I received funding from the GNS Science Geothermal Resources of New Zealand Project Water-Rock Interactions, the Mercury Energy-sponsored Source to Surface Project, and the University of Canterbury Department of Geological Sciences Mason Trust Fund. I am really grateful for the support I received from all of these funders.

Thank you to my supervisors, Darren Gravley, Ben Kennedy, Chad Deering, and Isabelle Chambefort, without whom none of this would be possible. Darren – thanks for being crazy enough to send me off to Colorado, and always offering opportunities for teaching, short courses and conferences. And not to mention welcoming me as part of the family! Ben – thanks for your support and creativity, and always making time. Chad – thanks for setting me in the right direction in the field, hosting me at Oshkosh and Michigan Tech, and for your critical eye when needed. Isabelle – thank you for the encouragement and guidance, your hours of patiently explaining water-rock interaction, and for your warm hospitality in Taupō.

I'd like to acknowledge the old guard of Lake City researchers who have encouraged and inspired me during my research. Ken Hon – I'm really grateful for you hosting me in Hilo and giving me much needed advice at the very start of the project. Pete Lipman – thanks for your support and immense knowledge; it was an honour and an eye-opener to get into the field with you. Peter Larson – thanks for your encouragement and continued enthusiasm for work at Lake City.

I'd like to thank all the staff of the UC Geology Department, in particular Jim Cole for always being supportive and willing to read another draft, Rob Spiers for making an unreasonable number of thin sections, Kerry Swanson for teaching me CL, and Pat Roberts and Rebekah Hunt for solving all administrative hurdles. And to all the other staff who made UC such a great place to be – DHB, Travis, Matt, Janet, Sacha, Grim, Alex, Cathy, Catherine, Stefan, Kari, Kate, Pashwell, Sam, Jonathan and more – thanks heaps!

The geothermal and volcanology group staff and students at the GNS Science Wairakei Research Centre always made me feel welcome. Thanks to all of you, Fiona, Lauriane, Andrew, Mike, Bruce, and in particular Mark Simpson for all the help with learning fluid inclusion microthermometry and TerraSpec. Also, thanks to Jamil and Lily for putting up with me visiting, and thanks for all the clothes Jamil!

A huge thanks to those who helped me out in the field: Matt, Annie, and especially Cameron Windham. Cam – what can I say, such good times! To the people of Lake City who made my time in your little mountain town such an unforgettable experience and a home away from home, but also probably less productive than it could've been – Lucky, Patrick, Hannah, Preston, Kelly, JT, Kris, and many more. You're awesome! The staff of the UW Oshkosh and Michigan Tech were really helpful during my time there, thanks in particular to Bob Barron and Tom Suszek. The Sloshkosh crew and MTU bros, thanks for making my USA college experiences such a hoot. Carlo – what a dude, thanks for all the fun and chopping of rocks, and Jordan – too much to say, but the fact you let me stay at your house and invade your personal space for weeks on end speaks volumes in itself.

The UC postgrads (and undergrads), old and new, have made my time here super awesome; thanks for all the laughs, banter, support, beer, wine, distraction and rants. And for putting up

with (and being secretly jealous of) my boundless desire for puns. Louise, Rhodent, Nick, Frazzle, Jo, Simon, Becs, Stan, Liz, Sozzle, HamHam, Pashwell, Paul S, Flo, Jonathan, Ali, George, Moz, Clem, Lorelei, Kay, Regine, Lydia, Jackie, Steph, Jess, Albus, Ellery, Elodie, Alan, Shamu, Andrea, Gabby, Josh S, Josh B, Josh H, Donna, Narges, Michael, Carolyn and everyone else – niiiiice is all I'll say. And of course Alison, who put up with me as an office mate the whole time and shared so many ups and downs. My non-geology friends also helped keep me sane, get me out into the hills, and keep jamming. You all know who you are and you're the best mates I could imagine.

To my family who've been such an inspiration my whole life – Barb, Emily, Kitty, Sally and Danny, and the dearest late Bruce, Char and Lin, I love you all. And especially Mum and Dad, thanks for always fostering my interest in science and the natural world, and encouraging me to give this Ph.D. thing a go…

Finally, to my lovely Mary. Thank you for all your love and always making me happy. I won't say much except that you're the best and I can't wait for whatever comes next!

CONTENTS

LIST OF FIGURES

Chapter 1

Chapter 2

Chapter 3

Chapter 4

Chapter 5

LIST OF TABLES

Chapter 1. Introduction

1. Chapter 1. Introduction

1.1. BACKGROUND TO RESEARCH QUESTIONS AND AIMS

Calderas formed during large silicic eruptions are spectacular yet enigmatic volcano-tectonic features of the Earth's crust (Lipman, 2000a; Branney and Acocella, 2015). As well as being an enormous potential hazard (Acocella et al., 2015), calderas can also provide great economic opportunity as the host for hydrothermal systems (Lipman, 1992; Stix et al., 2003; Stelling et al., 2016). Active hydrothermal systems can be exploited for geothermal electricity generation, and their fossil equivalents for hydrothermal ore deposits (Henley and Ellis, 1983). The successful exploitation of hydrothermal systems relies on locating active or extinct fluid pathways, the creation of which involves a complex interplay of volcanic, tectonic and lithological factors (Hedenquist et al., 2000; Micklethwaite, 2009; Rowland and Simmons, 2012). Understanding and modelling unrest in active calderas is also informed by estimation of crustal fluid pathways (De Natale et al., 2001).

In modern, active settings however, the structures and hydrothermal fluid outflows on the surface do not necessarily reflect deep permeable pathways. Near surface fluid flow is strongly influenced by the hydrology of shallow aquifers and near-surface faulting. These controls may be different from deeper crustal discontinuities, which can only be constrained by data from drilling and/or geophysical methods. An example is the central Taupō Volcanic Zone (TVZ) of New Zealand, which is host to numerous calderas, tectonic structures, and geothermal systems (Wilson and Rowland, 2016). In such a setting, determining the controls on permeability, and predicting favourable sites for new exploration, is not a trivial task. For example, calderas have been considered a primary control on the location of geothermal fields in the TVZ by some studies (e.g. Wood, 1995; Kissling and Weir, 2005), while this is disputed by others (e.g. Rowland and Sibson, 2004), and their importance is still being discussed in the literature (Chambefort, et al., 2017; Villamor et al., 2017). There is, therefore, considerable uncertainty about the influence of calderas and their related structures in controlling permeability, and how this is affected by interaction with regional structure.

In exhumed fossil hydrothermal systems, veins and alteration leave a record of the location of fluid pathways. Geological data can be integrated from a variety of scales in a way not possible in active systems, so that the location of fluid pathways can be related to structural

elements of the caldera volcano-tectonic system. The vein and alteration mineralogy can also be used to assess the physiochemical conditions of the hydrothermal system, and their spatiotemporal variation.

In this thesis, I use the 22.9 Ma Lake City caldera, in Colorado, U.S.A. as an ancient analogue with the aim of helping understand and predict outcrop- to regional-scale controls on permeability in modern geothermal systems that are spatially associated with silicic calderas. The uncertainties in the current understanding of calderas and their controls on hydrothermal fluid flow can be summarised by the research questions listed in Table 1 that drove my work at Lake City caldera. These questions show that this thesis is centred on understanding meso- to mega-scale fluid flow in caldera-related hydrothermal systems.

Chapter two focuses on field-based evidence of controls on permeability. In order to further characterise the physiochemical conditions of the hydrothermal fluid and reconstruct the hydrothermal system, one of the key emerging techniques I used was short wave infrared (SWIR) reflectance spectroscopy, which enables quick identification of key hydrothermal minerals and their compositions. In the course of using this technique it became clear that a gap existed in the current knowledge of how results compare from high versus low spatial resolution spectrometers, particularly with regards to the composition of white mica minerals. This led to two additional questions being explored in Chapter three (see Table 1). To fully reconstruct the Lake City hydrothermal system, I used the data presented in Chapters two and three, as well as a broad suite of additional data and tools, the results of which are integrated into a conceptual model in Chapter four. The results from Chapter four and the previous chapters are then used to help understand and predict controls on hydrothermal fluid flow in modern caldera-related geothermal systems in Chapter 5.

Table 1: Summary of the main research questions that are explored in this thesis.

Question	Specific Aims	Chapter
What is the lithological and permeability architecture of a caldera margin and what structural and lithological factors are favourable for the creation of permeable fluid pathways in caldera settings?	Characterise caldera architecture and lithologies (especially fault rocks) by detailed geological mapping of well-exposed portions of the Lake City caldera margin. Use scanline transects across fault outcrops to characterise the density and orientation of veins in different parts of the caldera.	Chapter 2
How comparable are the results from low spatial resolution (e.g. TerraSpec) and high spatial resolution (e.g. Corescan) SWIR reflectance spectroscopy techniques, with regards to white mica composition?	Analyse samples of altered rock with both TerraSpec and Corescan spectrometers. Compare spectral proxy for white mica composition with white mica composition as determined by scanning electron microscope (SEM) energy-dispersive x-ray spectroscopy (EDS).	Chapter 3
How useful is variation in white mica composition for understanding fluid-rock åinteraction?	Contour white mica composition data across Lake City caldera and visually compare with independent, previously published alteration mineralogy and oxygen isotope data.	Chapter 3
What are the magmatic and structural controls on the physiochemical conditions of the Lake City hydrothermal fluid, and how do these change throughout the evolution of the caldera system?	Analyse alteration mineralogy, vein textures, and fluid inclusions at Lake City caldera, and assess how data relate to caldera magmatism, structure, and temporal evolution.	Chapter 4
How can we use these data from an ancient analogue to inform our understanding of modern caldera-related geothermal systems such as those in the Taupō Volcanic Zone of New Zealand?	Use the answers to the previous questions in this thesis to compare Lake City caldera with other systems worldwide. Suggest general implications for geothermal exploration.	Chapter 5

1.2. SCIENTIFIC CONTEXT

In this section I present the general background to the scientific ideas that are explored in this thesis. In particular, I introduce the most important components of hydrothermal systems, the

volcano-tectonic elements of silicic calderas, and the types of data that can be used to understand the physiochemical conditions of a hydrothermal system. The study area that is the focus of this thesis is then introduced. A full literature review is not conducted, as each chapter is self-contained with its own introduction. However, sufficient context is presented in this section to articulate the knowledge gaps that led to the work in this thesis being undertaken. The Thesis Format section below (section 1.3) will discuss the specific research questions that each chapter investigates, and the data used to address these questions.

The two most important ingredients to form a circulating hydrothermal system are, (1) a source of heat, and (2) sufficient permeability to allow fluid flow (Norton, 1984). Magmatic heat sources are associated with many of the world's most vigorous active or ancient hydrothermal systems, as is exemplified by the presence of high-enthalpy geothermal systems in volcanically active areas such as Iceland, the Taupō Volcanic Zone of New Zealand, and Yellowstone (Henley and Ellis, 1983; Arnórsson, 1995; Hurwitz and Lowenstern, 2014; Wilson and Rowland, 2016). Systems with dominantly non-magmatic heat sources are not the focus of this thesis.

Permeability for fluid through the brittle crust is facilitated by discontinuities such as fractures or faults and by lithologies with interconnected pore spaces (Norton, 1984; Rowland and Simmons, 2012; Heap and Kennedy, 2016). Connections between pores can be primary depositional features (Heap et al., 2014) or formed through secondary processes such as chemical dissolution (Moore et al., 2004). In some parts of Earth, high heat flux in the crust and upper mantle is manifested in the assembly of large silicic magma bodies, which can be the source of large caldera-forming eruptions (Gravley et al., 2016; Wilson and Rowland, 2016). The processes of caldera formation involve the collapse of a portion of the uppermost crust into an evacuating magma chamber(s), and this subsidence results in the formation or re-activation of crustal discontinuities (Branney and Acocella, 2015). The combination of high heat flow with potentially permeable discontinuities makes calderas potentially favourable for the formation of hydrothermal systems (Stix et al., 2003).

The relationship between silicic calderas and hydrothermal systems has been a subject of research for decades, with aims of understanding how they may be utilised for geothermal energy, as hosts for ore deposits, and in the context of understanding their restless behaviour (e.g. Smith and Bailey, 1968; Fournier, 1989; Lipman, 1992; Rytuba, 1994; Wood, 1995;

Stix et al., 2003). The basic volcano-tectonic components of a silicic caldera relevant to hydrothermal fluid flow are: 1) faults that accommodate caldera subsidence, often called ring faults, 2) caldera infill, which is usually mostly ignimbrite from the caldera forming eruption, but also products of post-caldera magmatism and related structures, and 3) regional structures, that may be re-activated during caldera subsidence and post-collapse magmatism (Fig. 1). The variable combination of these different components defines the complex permeability architecture in caldera settings. For example, in the Taupō Volcanic Zone of New Zealand, the location of geothermal systems has been attributed to caldera structures, regional structures or accommodation zones, and individual magmatic intrusions (e.g. Wood, 1995; Rowland and Sibson, 2004; Kissling and Weir, 2005; Bertrand et al., 2015; Wilson and Rowland, 2016). In particular, caldera margin faults have often been cited as potentially favourable sites for hydrothermal fluid flow (e.g. Duex and Henry, 1981; Wood, 1994; Guillou-Frottier et al., 2000; Stix et al., 2003). Contrary to numerous detailed studies conducted on fault zone architecture in different rock types and their effect on permeability (e.g. Flodin et al., 2002; de Joussineau and Aydin, 2007; Walker et al., 2012; Soden and Shipton, 2013), detailed studies on caldera ring faults are globally rare mainly due to the lack of well-exposed ring faults outcrops (Geyer and Martí, 2014). The only outcrop-scale studies on caldera margin faults have been volcanologically-focussed studies (Shannon, 1988; Moore and Kokelaar, 1998; Miura, 1999; Kokelaar, 2007; Henry et al., 2017). To my knowledge, no studies attempt to characterise the permeability architecture and heterogeneity of ring faults, or how this differs from other types of fault. This knowledge gap motivated the research questions and aims of this thesis.

In hydrothermal systems, veins form from mineral precipitation in channelized, dilational fluid conduits such as fractures or faults, while hydrothermal alteration forms from chemical exchange between the fluid and country rock (Reed, 1997; Bons et al., 2012). In fossil hydrothermal systems, the location of veins and alteration can therefore be used to identify sites of past fluid flow and chemical sealing, as Chapter 2 demonstrates (Fig. 1). The orientation and kinematics of veins can be used to determine the controls on the formation of structures that become fluid conduits, and the stress regime at the time of hydrothermal activity (Hodgson, 1989; Peters, 1993; Sibson, 1996; Bons et al., 2012).

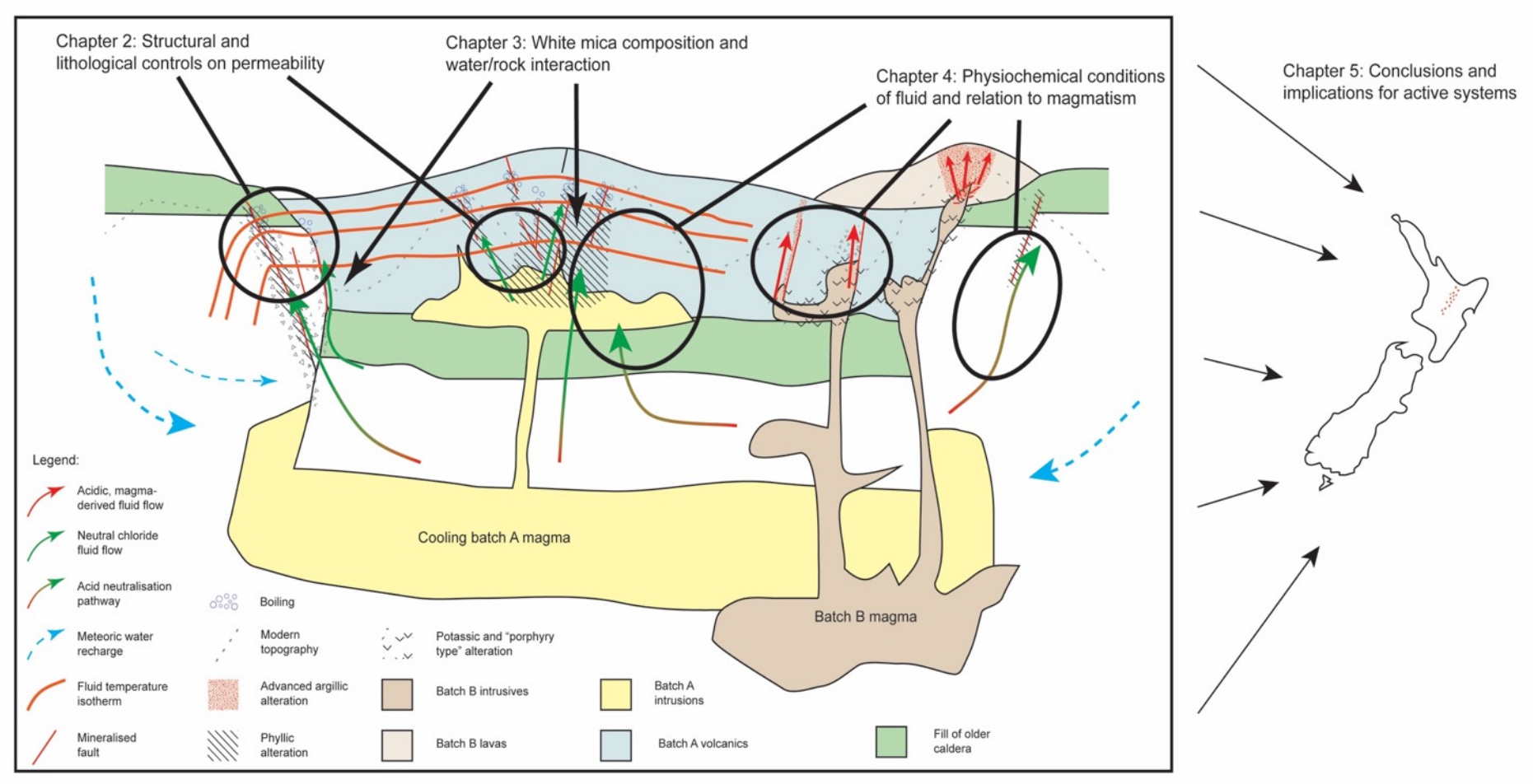

Figure 1: Simplified conceptual cartoon for hydrothermal fluid flow at Lake City caldera (cf. Chapter 4), showing which parts of the thesis provide the elements needed to create this model and apply it to active systems such as those in the Taupō Volcanic Zone of New Zealand.

The secondary alteration mineral phases and their compositions (such as white mica – see Chapter 3) are controlled by the physiochemical conditions of the hydrothermal fluid, such as its temperature, pH, composition and flow rate and its interaction with the rock (Browne, 1978; Henley and Ellis, 1983; Giggenbach, 1984; Reed, 1997). Fluid-rock interaction also affects the oxygen isotope composition of rocks, with lower $\delta^{18}O$ compositions resulting from increased interaction with meteoric water (Taylor, 1974). Fluid inclusion microthermometry in vein minerals allows direct estimates of the temperature and salinity of the hydrothermal fluid (Roedder, 1984). Boiling is an important hydrothermal process, as it can cause rapid changes in fluid temperature and composition, and preferentially occurs in fluid conduits that are hydrologically well-connected to shallower depths (Hedenquist et al., 2000). Vein textures can provide evidence for the occurrence of boiling in fossil systems (Dong et al., 1995; Moncada et al., 2011).

The combination of structural data on the distribution, orientation and density of veins can therefore be integrated with physiochemical data from analysis of alteration minerals, fluid inclusions, and vein textures to reconstruct the location of fluid flow paths (Fig. 1). The comparison of fluid flow paths with caldera- and tectonic-related structures and lithologies can then be used to characterise the volcano-tectonic controls of calderas on hydrothermal fluid transport as shown in Chapter 4.

1.2.1. Study area and previous work

The 22.9 Ma Lake City caldera is the youngest caldera in the San Juan volcanic field of Colorado, U.S.A., and has exposures over a wide area and large depth range (~1,300 m), including along the caldera margin. This provides an opportunity to detail an exhumed fossil hydrothermal system to examine the controls on fluid flow in caldera related settings. Previous work at Lake City caldera used mapping of alteration and veins (Slack, 1980; Larson and Taylor, 1986b; Hon, 1987), oxygen isotope ratios (Larson and Taylor, 1986a, 1986b, 1987), lead isotope ratios (Sanford, 1992), and radiometric dating (Bove et al., 2001) to constrain the hydrothermal fluid pathway. However, there are still significant gaps and uncertainties in our understanding of the Lake City hydrothermal system. These are outlined below, and addressed in this thesis.

Previous models of the hydrothermal system generally highlighted the importance of the caldera ring fault, intra-caldera landslide breccias, and faults in the resurgent dome in facilitating fluid flow, with a central resurgent pluton as the primary heat source (Larson and Taylor, 1986b; Sanford, 1992). Previous work has not addressed how major structures such as the ring faults facilitated fluid flow, nor why there is significant heterogeneity in the alteration and veining along these structures. Interpretations varied on how compartmentalised (in time and/or space) fluid flow was inside versus outside the ring fault (compare Larson and Taylor, 1986b and Sanford, 1992), and whether areas of acid alteration were formed from the near-surface portion of a meteoric-dominated system or due to various abundance of magmatic fluid input (compare Larson and Taylor, 1987 and Bove et al., 1990). Vein textures and fluid inclusions have not been previously investigated at Lake City, nor has fluid inclusion microthermometry been used to quantify the temperature and salinity of the hydrothermal fluids and their variability across the caldera. Previous conceptual models have also not addressed how the contrasting magma types (Kennedy et al., 2016) may have affected the hydrothermal system, nor how the hydrothermal system evolved over time. As such, this thesis builds on previous work at Lake City caldera (e.g. Slack, 1980; Larson and Taylor, 1986; Hon, 1987; Sanford, 1992; Bove et al., 2001) by characterising fluid pathways in greater detail, down to the outcrop scale, and quantifying the variation in the fluid conditions across the caldera.

1.3. THESIS FORMAT

This thesis has been written so that each chapter represents a published and/or publishable stand-alone body of work. As such, the individual chapters contain the necessary background information, negating the need for extensive literature review above. Despite the self-contained nature of each chapter, the results from each still build on each other, so that a natural progression can be followed towards a full conceptual model of the Lake City caldera hydrothermal system. Following the findings on Lake City Caldera, the conclusion discusses the applications to other examples worldwide. Figure 1 is a simplified conceptual cartoon of hydrothermal fluid flow in a caldera setting, based on the detailed model that is presented in Chapter 4. This shows how the individual chapters relate to each other and contribute to understanding hydrothermal fluid flow in caldera-related settings.

After the current introductory chapter, the second chapter focusses on field observations made at Lake City caldera (Fig. 1). The introduction to this chapter explains the potential structural controls on hydrothermal fluid flow in caldera settings, and emphasizes the gaps in our understanding of them. This chapter is focused on answering the questions of *what is the lithological and permeability architecture of a caldera margin, and what structural and lithological factors are favourable for the creation of permeable fluid pathways in caldera settings?* (Table 1). To this end, lithological data are presented characterising the deformed granite basement rocks adjacent to the margin of the caldera, the identification of which enables the structural margin to be distinguished from the topographic margin of the caldera. It is demonstrated that the width of deformation at the caldera margin is wider than previously thought, and that the orientation of the margin is influenced by pre-existing basement weaknesses. A qualitative conceptual model is formed, which attributes the enhancement of fluid permeability to favourable combinations of lithology, high density of discontinuities, and intersecting orientations of discontinuities (Fig 1). This work presented as Chapter two has been published in the peer-reviewed journal *Geosphere*, and is presented unchanged from its published form.

Chapter three presents data comparing for the first time the efficacy of high versus low spatial resolution SWIR reflectance spectroscopy techniques in approximating the composition of hydrothermal white micas. Short wave infrared reflectance spectroscopy emerged as a key technique that enabled the identification of minerals and their compositions in hundreds of samples across the caldera, a feat that would have been too costly and time consuming with most other techniques (e.g. X-ray diffraction or scanning electron microscope). This chapter grew out of the question (Table 1) of *how comparable are the results from low spatial resolution (e.g. TerraSpec) and high spatial resolution (e.g. Corescan) SWIR reflectance spectroscopy techniques, with regards to white mica composition?* The Corescan system is poorly established in the literature, so spectral proxies for the composition of white mica were compared as analysed using TerraSpec and Corescan. In turn these were compared to white mica Al/Si composition as determined by scanning electron microscope (SEM) energy-dispersive x-ray spectroscopy (EDS). White mica composition data are then contoured across the caldera using geostatistical methods, and compared with independent previously published alteration mineralogy and oxygen isotope data (Figure 1) to answer the question (Table 1) *how useful is variation in white mica*

composition for understanding fluid-rock interaction? Chapter three has been submitted for peer review to *Journal of Geochemical Exploration.*

Chapter four focusses on answering the questions (Table 1) *what are the magmatic and structural controls on the physiochemical conditions of the Lake City hydrothermal fluid, and how do these change throughout the evolution of the caldera system?* A suite of field and laboratory data, including SWIR reflectance spectroscopy, cathodoluminescence and petrography, and fluid inclusion microthermometry, is used to group alteration assemblages, determine fluid temperature and salinity, and boiling conditions. This work builds on earlier structural observations, and published work on the magmatic history of Lake City caldera to reveal contrasting hydrothermal expressions of the two distinct magma batches previously documented at Lake City caldera (Figure 1). One magma batch was waning by the time the hydrothermal system established, and had little magmatic fluid input, while the other magma batch exsolved significant amounts of high temperature magmatic fluid. A conceptual model is created that builds on the concepts explored in Chapter 1 but incorporated data from Chapters 2 and 3 and adds quantified fluid temperatures, paleodepths and compositions.

The fifth and final chapter summarises the key findings of Chapters two to four, and explores the question *how can we use these data from an ancient analogue to inform our understanding of modern caldera-related geothermal systems such as those in the Taupō Volcanic Zone of New Zealand?* There is an emphasis on implications for the Taupō Volcanic Zone (Figure 1), because better understanding the influence of calderas in this setting was part of the rationale for doing an analogue study at Lake City caldera. Comparisons are also made with Valles and Long Valley calderas, in the U.S.A., as the simpler and better-constrained tectonic settings of these systems allow similarities and differences with Lake City caldera to be emphasised. Finally, potential directions for future work are discussed, both to further refine our understanding of the Lake City system, and the regional-scale controls on fluid flow in the Taupō Volcanic Zone of New Zealand. This is followed by a description of the several electronic appendices, which contain data used in the Chapters. The appendices are located in electronic folders accompanying this thesis.

1.4. SCIENTIFIC CONTRIBUTIONS ARISING FROM THIS THESIS

At the time of submitting this thesis, Chapter 2 has been accepted for publication in the journal *Geosphere*, while Chapter 3 has been submitted for publication to the *Journal of Geochemical Exploration*. The contents of Chapter 2 and Chapter 4 have also been presented at conferences. The full list of contributions is listed below:

1.4.1. Peer-reviewed journal articles

Garden, T.O., Gravley, D.M., Kennedy, B.M., Deering, C., and Chambefort, I., 2017, Controls on hydrothermal fluid flow in caldera-hosted settings: Evidence from Lake City caldera, USA: *Geosphere,* v. 13, no. 6, doi:10.1130/GES01506.1.

Garden, T.O., Chambefort, I., Deering, C., Gravley, D.M., and Kennedy, B.M., *under review*, A comparison and application of reflectance spectroscopy of white mica at Lake City caldera, U.S.A.: Implications for geothermal and ore exploration: *Journal of Geochemical Exploration*

1.4.2. Conference abstracts

Garden, T.O., Deering, C., Gravley, D., Kennedy, B., and Chambefort, I., 2014, Controls on hydrothermal fluid transport at Lake City caldera, Colorado, U.S.A.: *Proceedings of the V International Workshop on Collapse Calderas, Taupō, New Zealand, 7-11 December 2014.*

Garden, T.O., Gravley, D., Kennedy, B., Chambefort, I., and Deering, C., 2015, Caldera margins and hydrothermal fluid flow: A case study from Lake City caldera, Colorado, U.S.A.: *Proceedings of the Geoscience Society of New Zealand Annual Conference, Wellington, New Zealand, 24-27 November 2015.*

Garden, T.O., Gravley, D., Kennedy, B., Chambefort, I., and Deering, C., 2016, Ring fault architecture from a hydrothermal perspective: *Proceedings of the VI International Workshop on Collapse Calderas, Hokkaido, Japan, 4-10 September 2016.*

Garden, T.O., Gravley, D.M., Chambefort, I., Deering, C.D., and Kennedy, B.M., 2017, Calderas and their volcano-tectonic controls on hydrothermal fluid flow: A case study from Lake City caldera, Colorado, U.S.A.: *Proceedings of the IAVCEI 2017 Scientific Assembly, Portland, U.S.A., 14-18 August 2017.*

1.5. ORIGINALITY

The material presented in this thesis has benefitted from discussions and contributions from my supervisors and other collaborators. Darren Gravley first formed the idea to study an ancient analogue caldera, and Ben Kennedy and Chad Deering were important in helping formulate how Lake City caldera specifically could be used for such a study. In Chapter 2, Cameron Windham assisted with field collection of scanline data, and with field sampling for Chapters 3 and 4. Josephine Hicks assisted with interpretation of the data in scanlines I1 and I2. Jonathan Davidson assisted with the kinematic interpretation of vein data. Discussions with all of my supervisors, particularly Darren Gravley and Ben Kennedy, helped form the structural ideas presented in this chapter. Guido Giordano, Eoghan Holohan, Shanaka de Silva and an anonymous reviewer provided useful feedback on the manuscript during the reviewing process for *Geosphere*. In Chapter 3, Cameron Windham assisted with field sampling. Jordan Lubbers and Carlo Prandix provided valuable assistance in cutting samples used in this chapter and Chapter 4. Corescan staff, particularly Brigette Martini and Kathryn Conroy performed collection of Corescan data and identification of minerals in spectra. Mark Simpson provided useful guidance on the acquisition and interpretation of TerraSpec data, and Isabelle Chambefort assisted with acquisition of EDS data. In Chapter 4, Mark Simpson and Isabelle Chambefort taught and assisted in fluid inclusion microthermometry. Isabelle Chambefort also assisted in geochemical interpretation of alteration assemblages and white mica composition data. Kerry Swanson, Mike Flaws, and Isabelle Chambefort assisted in collection of SEM data. Chad Deering provided the important first formulation of ideas and insights into how fluid inclusions and vein textures could be used to reconstruct fluid conditions at Lake City, and assisted with sampling strategy. In Chapter 5, discussions with all four of my supervisors, particularly Darren Gravley and Isabelle Chambefort, helped inform the ideas discussed in my implications for hydrothermal fluid flow in the Taupō Volcanic Zone.

All of my supervisors, Darren Gravley, Ben Kennedy, Chad Deering and Isabelle Chambefort engaged in scientific discussions and provided editorial assistance with all of the thesis chapters. Apart from the exceptions described above, all of the field and laboratory data collection, processing, interpretation and presentation of data, and writing constitute my own work.

1.6. REFERENCES CITED

Acocella, V., Di Lorenzo, R., Newhall, C., and Scandone, R., 2015, An overview of recent (1988 to 2014) caldera unrest: Knowledge and perspectives: Reviews of Geophysics, v. 53, p. 896–955, doi: 10.1002/2013RG000437.

Arnórsson, S., 1995, Geothermal systems in Iceland: Structure and conceptual models—I. High-temperature areas: Geothermics, v. 24, p. 561–602, doi: 10.1016/0375-6505(95)00025-9.

Bertrand, E.A., Caldwell, T.G., Bannister, S., Soengkono, S., Bennie, S.L., Hill, G.J., and Heise, W., 2015, Using array MT data to image the crustal resistivity structure of the southeastern Taupo Volcanic Zone, New Zealand: Journal of Volcanology and Geothermal Research, v. 305, p. 63–75, doi: 10.1016/j.jvolgeores.2015.09.020.

Bons, P.D., Elburg, M.A., and Gomez-Rivas, E., 2012, A review of the formation of tectonic veins and their microstructures: Journal of Structural Geology, v. 43, p. 33–62, doi: 10.1016/j.jsg.2012.07.005.

Bove, D.J., Hon, K., Budding, K.E., Slack, J.F., Snee, L.W., and Yeoman, R.A., 2001, Geochronology and geology of late Oligocene through Miocene volcanism and mineralization in the western San Juan Mountains, Colorado: U.S. Geological Survey Professional Paper 1642.

Bove, D.J., Rye, R.O., and Hon, K., 1990, Evolution of the Red Mountain alunite deposit, Lake City, Colorado: U.S. Geological Survey Open-File Report 90-0235.

Branney, M., and Acocella, V., 2015, Calderas, *in* Sigurdsson, H., Houghton, B., McNutt, S., Rymer, H., and Stix, J. eds., The Encyclopedia of Volcanoes, Elsevier Inc., p. 299–315, doi: 10.1016/B978-0-12-385938-9.00016-X.

Browne, P.R.L., 1978, Hydrothermal alteration in active geothermal fields: Annual Reviews in Earth and Planetary Sciences, v. 6, p. 229–250.

Chambefort, I., Wilson, C.J.N., Rowland, J. V, Gravley, D.M., Bignall, G., Alcaraz, S.A., Milicich, S.D., Villamor, P., and Rosenberg, M.D., 2017, The deep controls on high

enthalpy geothermal systems: A multi-disciplinary overview from New Zealand: Proceedings 39th New Zealand Geothermal Workshop, Rotorua, 22-24 November 2017.

Dong, G., Gregg, M., and Jaireth, S., 1995, Quartz textures in epithermal veins, Queensland - Classification, origin, and implication: Economic Geology, v. 90, p. 1841–1856.

Duex, T.W., and Henry, C.D., 1981, Calderas and mineralization: Volcanic geology and mineralization in the Chianti caldera complex, Trans-Pecos Texas: Austin, University of Texas, Bureau of Economic Geology Geological Circular 81-2.

Flodin, E.A., Aydin, A., Durlofsky, L.J., and Wen, X., 2002, Computing permeability of fault zones in eolian sandstone from outcrop measurements: AAPG Bulletin, v. 86, p. 1187–1200.

Fournier, R.O., 1989, Geochemistry and dynamics of the Yellowstone National Park hydrothermal system: Annual Reviews in Earth and Planetary Sciences, v. 17, p. 13–53.

Geyer, A., and Martí, J., 2014, A short review of our current understanding of the development of ring faults during collapse caldera formation: Frontiers in Earth Science, v. 2, p. 1–13, doi: 10.3389/feart.2014.00022.

Giggenbach, W.F., 1984, Mass transfer in hydrothermal alteration systems - A conceptual approach: Geochimica et Cosmochimica Acta, v. 48, p. 2693–2711, doi: 10.1016/0016-7037(84)90317-X.

Gravley, D.M., Deering, C.D., Leonard, G.S., and Rowland, J. V., 2016, Ignimbrite flare-ups and their drivers: A New Zealand perspective: Earth-Science Reviews, v. 162, p. 65–82, doi: 10.1016/j.earscirev.2016.09.007.

Guillou-Frottier, L., Burov, E.B., and Milési, J.-P., 2000, Genetic links between ash-flow calderas and associated ore deposits as revealed by large-scale thermo-mechanical modeling: Journal of Volcanology and Geothermal Research, v. 102, p. 339–361, doi: 10.1016/S0377-0273(00)00246-8.

Heap, M.J., and Kennedy, B.M., 2016, Exploring the scale-dependent permeability of fractured andesite: Earth and Planetary Science Letters, v. 447, p. 139–150, doi: 10.1016/j.epsl.2016.05.004.

Heap, M.J., Xu, T., and Chen, C., 2014, The influence of porosity and vesicle size on the brittle strength of volcanic rocks and magma: Bulletin of Volcanology, v. 76, p. 1–15, doi: 10.1007/s00445-014-0856-0.

Hedenquist, J.W., Arribas Jr., A., and Gonzalez-Urienm, E., 2000, Exploration for epithermal gold deposits: Reviews in Economic Geology, v. 13, p. 45–77.

Henley, R.W., and Ellis, A.J., 1983, Geothermal systems ancient and modern: A geochemical

review: Earth-Science Reviews, v. 19, p. 1–50, doi: 10.1016/0012-8252(83)90075-2.

Henry, C.D., Castor, S.B., Starkel, W.A., Ellis, B.S., Wolff, J.A., Laravie, J.A., McIntosh, W.C., and Heizler, M.T., 2017, Geology and evolution of the McDermitt caldera, northern Nevada and southeastern Oregon, western USA: Geosphere, v. 13, p. 1067–1112, doi: 10.1130/GES01454.1.

Hodgson, C.J., 1989, The structure of shear-related vein-type gold deposits: A review: Ore Geology Reviews, v. 4, p. 231–273.

Hon, K.A., 1987, Geologic and petrologic evolution of the Lake City caldera, San Juan Mountains, Colorado [Ph.D. thesis]: University of Colorado at Boulder, 244 p.

Hurwitz, S., and Lowenstern, J.B., 2014, Dynamics of the Yellowstone hydrothermal system: Reviews of Geophysics, 51, p. 1-37, doi: 10.1002/2014RG000452.

de Joussineau, G., and Aydin, A., 2007, The evolution of the damage zone with fault growth in sandstone and its multiscale characteristics: Journal of Geophysical Research, v. 112, p. B12401, doi: 10.1029/2006JB004711.

Kennedy, B., Stix, J., Hon, K., Deering, C., and Gelman, S., 2016, Magma storage, differentiation, and interaction at Lake City caldera, Colorado, USA: Geological Society of America Bulletin, v. 128, p. 764–776, doi: 10.1130/B31305.1.

Kissling, W.M., and Weir, G.J., 2005, The spatial distribution of the geothermal fields in the Taupo Volcanic Zone, New Zealand: Journal of Volcanology and Geothermal Research, v. 145, p. 136–150, doi: 10.1016/j.jvolgeores.2005.01.006.

Kokelaar, P., 2007, Friction melting, catastrophic dilation and breccia formation along caldera superfaults: Journal of the Geological Society of London, v. 164, p. 751–754.

Larson, P.B., and Taylor, H.P., 1986a, An oxygen-isotope study of water-rock interaction in the granite of Cataract Gulch, western San Juan Mountains, Colorado: Geological Society of America Bulletin, v. 97, p. 505–515.

Larson, P.B., and Taylor, H.P., 1986b, An oxygen isotope study of hydrothermal alteration in the Lake City caldera, San Juan Mountains, Colorado: Journal of Volcanology and Geothermal Research, v. 30, p. 47–82.

Larson, P.B., and Taylor, H.P., 1987, Solfataric alteration in the San Juan Mountains, Colorado: Oxygen isotope variations in a boiling hydrothermal environment: Economic Geology, v. 30, p. 1019–1036.

Lipman, P.W., 1992, Ash-flow calderas as structural controls of ore deposits - Recent work and future problems: US Geological Survey Bulletin 2012, p. L1–L12.

Lipman, P.W., 2000, Calderas, *in* Sigurdsson, H., Houghton, B.F., McNutt, S.R., Rymer, H., and Stix, J. eds., Encyclopedia of Volcanoes, San Diego, California, Academic Press, p. 643–662.

Micklethwaite, S., 2009, Mechanisms of faulting and permeability enhancement during epithermal mineralisation: Cracow goldfield, Australia: Journal of Structural Geology, v. 31, p. 288–300, doi: 10.1016/j.jsg.2008.11.016.

Miura, D., 1999, Arcuate pyroclastic conduits, ring faults, and coherent floor at Kumano caldera, southwest Honshu, Japan: Journal of Volcanology and Geothermal Research, v. 92, p. 271–294, doi: 10.1016/S0377-0273(99)00089-X.

Moncada, D., Mutchler, S., Nieto, A., Reynolds, T.J., Rimstidt, J.D., and Bodnar, R.J., 2011, Mineral textures and fluid inclusion petrography of the epithermal Ag–Au deposits at Guanajuato, Mexico: Application to exploration: Journal of Geochemical Exploration, v. 114, p. 20–35, doi: 10.1016/j.gexplo.2011.12.001.

Moore, J.N., Christenson, B.W., Allis, R.G., Browne, P.R.L., and Lutz, S.J., 2004, The mineralogical consequences and behavior of descending acid-sulfate waters: An example from the Karaha - Telaga Bodas geothermal system, Indonesia: The Canadian Mineralogist, v. 42, p. 1483–1499, doi: 10.2113/gscanmin.42.5.1483.

Moore, I., and Kokelaar, P., 1998, Tectonically controlled piecemeal caldera collapse: A case study of Glencoe volcano, Scotland: Geological Society of America Bulletin, v. 110, p. 1448–1466.

De Natale, G., Troise, C., and Pingue, F., 2001, A mechanical fluid-dynamical model for ground movements at Campi Flegrei caldera: Journal of Geodynamics, v. 32, p. 487–517, doi: 10.1016/S0264-3707(01)00045-X.

Norton, D.L., 1984, Theory of hydrothermal systems: Annual Reviews in Earth and Planetary Sciences, v. 12, p. 155–157.

Peters, S.G., 1993, Nomenclature, concepts and classification of oreshoots in vein deposits: Ore Geology Reviews, v. 8, p. 3–22, doi: 10.1016/0169-1368(93)90025-T.

Reed, M.H., 1997, Hydrothermal alteration and its relationship to ore fluid composition, *in* Barnes, H.L. ed., Geochemistry of Hydrothermal Ore Deposits, John Wiley and Sons, p. 303–365.

Roedder, E., 1984, Fluid Inclusions: Reviews in Mineralogy and Geochemistry, v. 12.

Rowland, J.V., and Sibson, R.H., 2004, Structural controls on hydrothermal flow in a segmented rift system, Taupo Volcanic Zone, New Zealand: Geofluids, v. 4, p. 259–283, doi: 10.1111/j.1468-8123.2004.00091.x.

Rowland, J.V., and Simmons, S.F., 2012, Hydrologic, magmatic, and tectonic controls on hydrothermal flow, Taupo Volcanic Zone, New Zealand: Implications for the formation of epithermal vein deposits: Economic Geology, v. 107, p. 427–457, doi: 10.2113/econgeo.107.3.427.

Rytuba, J.J., 1994, Evolution of volcanic and tectonic features in caldera settings and their importance in localization of ore deposits: Economic Geology, v. 89, p. 1687–1696, doi: 10.2113/gsecongeo.89.8.1687.

Sanford, R.F., 1992, Lead isotopic compositions and paleohydrology of caldera-related epithermal veins, Lake City, Colorado: Geological Society of America Bulletin, v. 104, p. 1236–1245.

Shannon, J., 1988, Geology of the Mount Aetna cauldron complex, Sawatch Range, Colorado [Ph.D. thesis]: Golden, Colorado, Colorado School of Mines, 434 p.

Sibson, R.H., 1996, Structural permeability of fluid-driven fault-fracture meshes: Journal of Structural Geology, v. 18, p. 1031–1042, doi: 10.1016/0191-8141(96)00032-6.

Slack, J.F., 1980, Multistage vein ores of the Lake City District, western San Juan Mountains, Colorado: Economic Geology, v. 75, p. 963–991.

Smith, R.L., and Bailey, R.A., 1968, Resurgent cauldrons: Geological Society of America Memoirs, v. 116, p. 613–662, doi: 10.1130/MEM116.

Soden, A.M., and Shipton, Z.K., 2013, Dilational fault zone architecture in a welded ignimbrite: The importance of mechanical stratigraphy: Journal of Structural Geology, v. 51, p. 156–166, doi: 10.1016/j.jsg.2013.02.001.

Stelling, P., Shevenell, L., Hinz, N., Coolbaugh, M., Melosh, G., and Cumming, W., 2016, Geothermal systems in volcanic arcs: Volcanic characteristics and surface manifestations as indicators of geothermal potential and favorability worldwide: Journal of Volcanology and Geothermal Research, v. 324, p. 57–72, doi: 10.1016/j.jvolgeores.2016.05.018.

Stix, J., Kennedy, B., Hannington, M., Gibson, H., Fiske, R., Mueller, W., and Franklin, J., 2003, Caldera-forming processes and the origin of submarine volcanogenic massive sulfide deposits: Geology, v. 31, p. 375–378.

Taylor, H.P., 1974, The application of oxygen and hydrogen isotope studies to problems of hydrothermal alteration and ore deposition: Economic Geology, v. 69, p. 843–883.

Villamor, P., Nicol, A., Seebeck, H., Rowland, J., Townsend, D., Massiot, C., Mcnamara, D.D., Milicich, S., Ries, W., and Alcaraz, S., 2017, Tectonic structure and permeability

in the Taupō Rift: New insights from analysis of LiDAR derived DEMs: Proceedings 39th New Zealand Geothermal Workshop, Rotorua, 22-24 November 2017.

Walker, R.J., Holdsworth, R.E., Armitage, P.J., and Faulkner, D.R., 2012, Fault zone permeability structure evolution in basalts: Geology, v. 41, p. 59–62, doi: 10.1130/G33508.1.

Wilson, C.J.N., and Rowland, J. V., 2016, The volcanic, magmatic and tectonic setting of the Taupo Volcanic Zone, New Zealand, reviewed from a geothermal perspective: Geothermics, v. 59, p. 168–187, doi: 10.1016/j.geothermics.2015.06.013.

Wood, C.P., 1994, Aspects of the geology of Waimangu, Waiotapu, Waikite and Reporoa geothermal systems, Taupo Volcanic Zone, New Zealand: Geothermics, v. 23, p. 401–421.

Wood, C.P., 1995, Calderas and Geothermal Systems in the Taupo Volcanic Zone, New Zealand, *in* Proceedings of the World Geothermal Congress, Florence, Italy, p. 1331–1336.

PREAMBLE

In Chapter 1, I summarised the importance of caldera-related hydrothermal systems, and the scientific context and knowledge gaps that led to the research questions being addressed in this thesis. Chapter 2 presents field based data on the architecture of the caldera margin, and structural and lithological controls on the distribution of veins and hydrothermal alteration at Lake City caldera.

Chapter 2 has been published in the journal *Geosphere*:
Garden, T.O., Gravley, D.M., Kennedy, B.M., Deering, C., and Chambefort, I., 2017, Controls on hydrothermal fluid flow in caldera-hosted settings: Evidence from Lake City caldera, USA: *Geosphere,* v. 13, no. 6, p. XXX-XXX, doi:10.1130/GES01506.1.

The chapter is presented in its published form, including the use of American English.

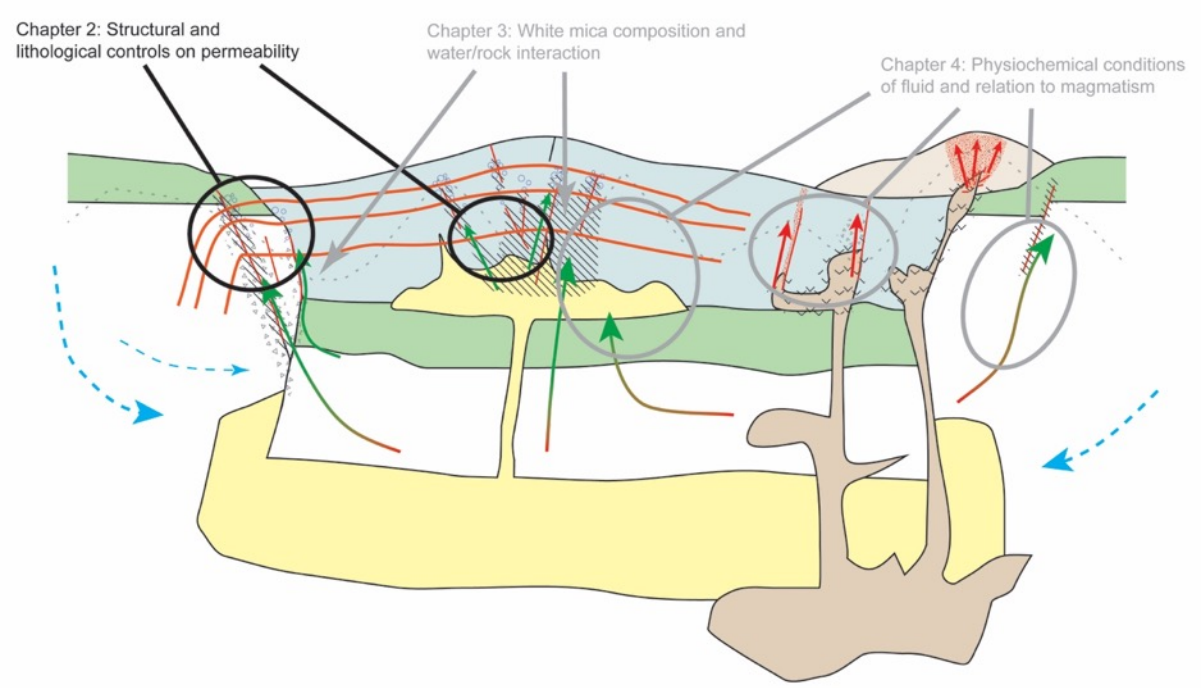

Simplified conceptual cartoon for hydrothermal fluid flow at Lake City caldera (cf. Chapter 4), showing the components of the model that are addressed in Chapter 2.

Chapter 2. Controls on hydrothermal fluid flow in caldera-hosted settings: Evidence from Lake City caldera, U.S.A.

2. Controls on hydrothermal fluid flow in caldera-hosted settings: Evidence from Lake City caldera, U.S.A.

2.1. ABSTRACT

Silicic caldera volcanoes are often associated with hydrothermal systems economically important for electricity generation and localization of ore deposits. Despite their potential importance, the poor exposure that is typical in caldera settings has limited the number of detailed studies of the relationship between caldera structures and fluid flow. We use field mapping, outcrop scale scanline transects, and petrographic analyses to characterize fault rocks, alteration, and veins in the well-exposed 22.9 Ma Lake City caldera fossil hydrothermal system. The caldera margin consists of relatively straight segments linked by more structurally complex intersections; these structural intricacies produce a zone of deformation that can reach >300 m wide. Structural analyses show that the wide (up to ~60 m) fault core of the ring fault contains abundant subparallel veins, with orientations similar to that of the caldera margin. Smaller displacement faults inside the caldera generally have narrow (<1 m), hydrothermally cemented fault cores with more variably oriented veins in the surrounding damage zone. These findings at Lake City illustrate that fluid flow is controlled by lithology and the location and displacement of faults, e.g. ring fault versus intracaldera fault. Fault connectivity is another key control. We propose a conceptual model where fluid flow in caldera hosted settings is influenced by: 1) the presence of favorable lithologies (proximity to magmatic intrusions and/or the presence of permeable lithologies), 2) a high density of faults and fractures, and 3) favorable orientations of faults and fractures that promote the formation of discontinuity intersections.

2.2. INTRODUCTION

Calderas have long been recognized as hosts for hydrothermal systems that can be economically important for geothermal power and the localization of ore deposits (e.g. Smith and Bailey, 1968; Rytuba, 1976; Duex and Henry, 1981; Stelling et al., 2016). In addition, characterizing hydrothermal activity in large, modern calderas worldwide (e.g. Yellowstone, U.S.A., Campi Flegrei, Italy, Taupō, New Zealand) has been important in understanding their restless behavior and associated hazards (Peltier et al., 2009; Rinaldi et al., 2010; Hurwitz and Lowenstern, 2014). These systems may be associated with the margin of a caldera, its

interior, adjacent regional-scale structures, or some combination thereof (Table 1). It is not well understood why some calderas host hydrothermal systems while others do not, or what factors promote fluid localization in certain parts of a caldera. In particular, caldera "ring faults" are commonly suggested to be important structures for localizing fluid flow (e.g. Duex and Henry, 1981; Wood, 1994; Guillou-Frottier et al., 2000; Stix et al., 2003; Kissling and Weir, 2005), yet no studies to date have focused on a thorough examination of their permeability structure.

Hydrothermal systems occur in a range of crustal settings. This paper is primarily focused on the upper ~2 km of a silicic caldera-related setting, where topography has less effect on reservoir fluid flow than in stratovolcano settings (Henley and Ellis, 1983). This corresponds with the mineralization and discharge zones of Rowland and Simmons (2012), which are above the feed zone that extends down to the brittle-ductile transition and the base of convection. It is in this upper portion of hydrothermal systems that discrete high-flux fluid conduits are important; the formation of these conduits strongly depends on the interplay of structure and lithology (Rowland and Simmons, 2012; Vignaroli et al., 2015). The location of fluid conduits is, thus, expected to be influenced by caldera-related structures and lithology.

Ring faults accommodate the bulk of caldera collapse and comprise part of the structural margin of a caldera. In this study, we use the term "structural margin" for the zone of deformation at the caldera margin and the term "ring fault" for the portion(s) of this with the highest strain, if present. Fault rocks (e.g. breccia, gouge, cataclasite, and pseudotachylyte) will generally form in, and be indicative of, the highest strain (i.e. ring fault) portions of the caldera margin. The topographic margin of a caldera is where the intra-caldera fill is juxtaposed against pre-caldera rocks or a significant scarp slope exists, but there is no evidence of faulting along this contact (Smith and Bailey, 1968; Spray, 1997; Lipman, 2000; Cole et al., 2005; Branney and Acocella, 2015). In many calderas, the contact between intra-caldera fill and basement can be located, but exposure is insufficient to ascertain whether this defines the topographic margin or the structural margin. In this study, we call this potentially ambiguous contact between intra and extracaldera rocks the "caldera margin discontinuity". Ring faults differ from other types of faults by: 1) a high strain rate; large displacements (>1 km for some calderas) are accommodated in a short period of time (i.e. during and/or immediately posteruption) (Spray, 1997), and 2) frequent modification by magmatism (e.g. dike intrusion into the fault) and/or landsliding soon after their creation (Branney and

Acocella, 2015). Well-exposed outcrops of ring faults are globally rare (Geyer and Martí, 2014), and work to date has focused on the volcanological aspects of unmineralized examples (e.g. Shannon, 1988; Moore and Kokelaar, 1998; Miura, 1999; Kokelaar, 2007).

Most faults, in general, can be broadly separated into a fault core that accommodates most displacement and consists of fault rocks such as gouge and cataclasite and a surrounding damage zone of highly fractured and deformed rock (Caine et al., 1996; Kim et al., 2004; Mitchell and Faulkner, 2009). Numerous studies have investigated the fault architecture, fault rocks, damage zones and resulting permeability structure in diverse fault styles and protoliths (e.g. Sibson, 1987; Wibberley and Shimamoto, 2002; Micarelli et al., 2006; Faulkner et al., 2010; Walker et al., 2012; Soden and Shipton, 2013). However, there have been no studies of the architecture and permeability of ring faults, despite the common association of hydrothermal fluid flow with caldera margins (Table 1).

Calderas are complex volcano-tectonic structures, and ring faults are not the only type of fault important in these settings. To understand controls on hydrothermal fluid flow in such settings other factors such as lithology, intra-caldera structures and regional structures must be considered as well as the architecture of the caldera margin. Resurgent uplift of the interior of a caldera often causes smaller-displacement normal faults to form on the crest of the resurgent dome (Smith and Bailey, 1968). Faults associated with regional tectonics are also common in caldera settings and accommodate caldera subsidence and/or resurgent uplift in some cases (Cole et al., 2005; Folkes et al., 2011). Hydrothermal fluid flow may be associated with any combination of ring faults, intra-caldera faults or regional faults in calderas worldwide (Table 1).

Table 1. The spatial relationship between components of a silicic caldera-forming volcano-tectonic system and the location of hydrothermal fluid flow

		Location of hydrothermal flow			
Caldera	**Reference(s)**	**Marginal**	**Intra-caldera**	**On Regional Structures**	**Quality of Constraints**
Bachelor/San Luis, U.SA.	Bethke et al., 1976		X		Good
Bonanza, U.S.A.	Pride and Hasenohr, 1983; Lipman et al., 2015	X	X		Good
Campi Flegrei, Italy	Allard et al., 1991	X	X		Poor
Cerro Aguas Calientes, Argentina	Petrinovic et al., 2010	X			Moderate
Citorek, Indonesia	Marcoux and Milési, 1994			X	Poor
Chacana, Ecuador	Beate et al., 2010	X	X	X	Moderate
Chegem, Russia	Lipman et al., 1993		X	X	Good
Chianti Mountains, U.S.A.	Duex and Henry, 1981	X	X		Moderate
Colli Albani, Italy	Giordano et al., 2014	X		X	Moderate
Creede, U.S.A.	Bethke, 2001	X			Excellent
Hamada, Japan	Matsuhisa et al., 1980		X		Good
Indio Muerto District, Chile	Gustafson et al., 2001	X			Poor
Infiernito, U.S.A.	Duex and Henry, 1981		X		Moderate
Ischia, Italy	Sbrana et al., 2010		X		Good
Karymshina, Russia	Leonov and Rogozin, 2010	X			Moderate
Lake City, U.S.A.	Larson and Taylor 1986b; Sanford et al., 1987	X	X		Good
La Pacana, Chile	Gardeweg and Ramirez, 1987		X		Poor
Long Valley, U.S.A.	Suemnicht and Varga, 1988; Sorey et al., 1991; Hildreth, 2017	X		X	Good
Los Azufres, Mexico	Ferrari et al., 1991		X		Poor
Luingo, Argentina	Guzmán and Petrinovic, 2010		X		Poor
Mangakino, N.Z.	Kissling and Weir, 2005		X		Good
McDermitt, U.S.A.	Rytuba, 1976; Castor and Henry, 2000	X			Good
Okataina, N.Z.	Wood, 1994; Rowland and Simmons, 2012; Caratori Tontini et al., 2016	X		X	Good
Onikobe, Japan	Klein et al., 1990		X		Poor
Pantelleria, Italy	Fulignati et al., 1997		X		Poor
Pongkor, Indonesia	Milési et al., 1999	X		X	Moderate
Porco, Bolivia	Cunningham et al., 1994	X	X	X	Good
Questa, U.S.A.	Lipman, 1992; Klemm et al., 2008	X	X	X	Good
Reporoa, N.Z.	Wood, 1994; Rowland and Simmons, 2012	X		X	Moderate
Rodalquilar/Lomilla,Spain	Arribas Jr. et al., 1995	X	X		Good
Rotorua, N.Z.	Wood, 1992; Milner et al., 2002	X			Good
Round Mountain, U.S.A.	Henry et al., 1997	X			Good
Silverton, U.S.A.	Lipman et al., 1976	X	X	X	Good
Snowdon, U.K.	Reedman et al., 1985	X	X		Good
Soledad, Bolivia	Redwood, 1987	X		X	Good
Summitville/Platoro, U.SA.	Bethke et al., 2005	X		X	Good
Taupō, N.Z.	Whiteford, 1992		X	X	Moderate
Toba, Indonesia	Hochstein and Sudarman, 1993	X		X	Poor
Valles, U.S.A.	Hulen and Nielson, 1986; Goff and Gardener, 1994	X	X		Excellent
Waihi, N.Z.	Smith et al., 2006			X	Poor
Whakamaru, N.Z.	Wood, 1995; Wallis et al., 2013	X	X	X	Poor
Xela, Guatemala	Bennati et al., 2011	X		X	Good
Yellowstone, U.S.A.	Fournier, 1989	X	X	X	Good
Zacatecas, Mexico	Ponce S. and Clark, 1988	X	X	X	Good

Note: The hydrothermal system in many of these systems is only briefly mentioned in volcanologically focused studies, so interpretation was necessary in order to classify some calderas.

Ignimbrites are the dominant lithology in most silicic calderas, and the intra-caldera facies of many ignimbrites are densely welded and have low intrinsic permeability (Heap et al., 2014a). Faults or horizons of more permeable lithologies (such as less consolidated breccias) are important for facilitating intra-caldera fluid circulation through voluminous, otherwise impermeable lithologies such as intra-caldera ignimbrites (Hulen and Nielson, 1986; Wood et al., 2001). Exhumed, well-exposed calderas are needed to study structure and lithology in detail, especially to put the outcrop scale in the context of the wider structural setting. Recently active calderas are too poorly exposed - even those that have been drilled for resource exploration - to allow effective integration of data from different scales. In this paper, we present and discuss new observations and mapping of the well-exposed Lake City caldera in the San Juan mountains of Colorado, U.S.A. We characterize outcrop-scale patterns of veins and lithology along the margin and compare them with structures from the interior of the caldera that have much smaller displacement. Integration of map and outcrop-scale data allows us to build a conceptual model of fluid flow localization from favorable combinations of lithology, fault and fracture density, and fault and fracture orientation. This model could aid in the prediction for where and how fluid flow (or mineralization) is localized at other calderas worldwide.

2.3. GEOLOGY OF LAKE CITY CALDERA

The ca. 22.9 Ma Lake City caldera (LCC) is the youngest caldera in the San Juan volcanic field (SJVF) in southwestern Colorado (Fig. 1), which is the largest erosional remnant of the Oligocene to Miocene Southern Rocky Mountains Volcanic Field (Lipman et al., 1970; Lipman and McIntosh, 2008). Lake City caldera postdates all other caldera-related eruptions in the SJVF by more than four million years, and it is nested within the older (ca. 28.2 Ma) Uncompahgre caldera (Bove et al., 2001). The basement lithology of LCC is the Precambrian Granite of Cataract Gulch, which is exposed along the western to southern caldera margin (Figs. 2a and 3a). The granite is coarse grained (2 - 8 mm) and mineralogically uniform where undeformed (Larsen and Cross, 1956; Larson and Taylor, 1986a). The granite is intruded by numerous Ordovician to Cambrian diabase dikes, which mostly have a west to northwest orientation (Lipman, 1976b). The rest of the LCC margin is bordered by the fill of the Uncompahgre caldera (Fig. 2a). The Uncompahgre caldera fill consists of welded intra caldera ignimbrite (Sapinero Mesa Tuff), landslide megabreccias of Uncompahgre caldera, and andesitic to dacitic lavas (Figs. 1 and 2a). The granite and Uncompahgre caldera fill are

variably included in the Lake City landslide breccias as blocks and are deformed at the LCC margins. The deformation of the granite is described in detail later in this paper.

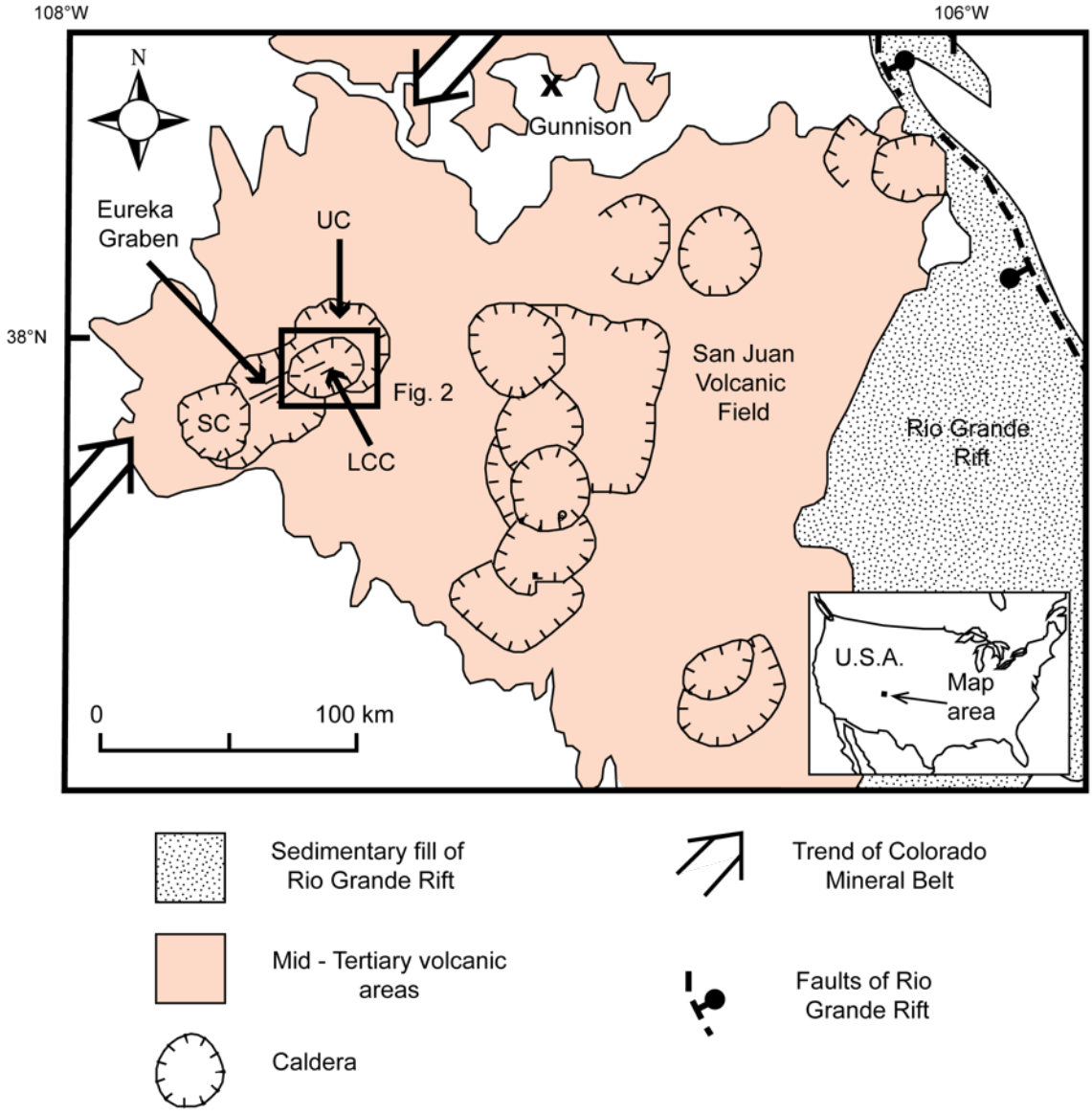

Figure 1: Location of Lake City caldera in the San Juan Volcanic Locus of the Southern Rocky Mountains Volcanic Field, highlighting major regional geologic features (modified from Lipman et al., 2015). Abbreviations: SC-Silverton caldera, UC-Uncompahgre caldera, LCC-Lake City caldera.

Lake City caldera was the source of the Sunshine Peak eruption, which produced a generally densely welded tuff (Figs. 2a and 3c) that is variably altered and, locally, lithic rich (Hon, 1987; Kennedy et al., 2016). Proximally, the tuff is closely associated with breccias (Figs. 2a and 3b) and megabreccias that formed from material collapsing from the over-steepened caldera walls during or following subsidence (Hon, 1987; Kennedy et al., 2016). The resulting caldera is oval shaped, within which ~260 km^3 of ignimbrite ponded up to a thickness of at least 1.5 km (Fig. 2a) (Hon, 1987).

Following caldera formation, magmatic activity continued with a series of domes and intrusions. Small "ring dike" intrusions were emplaced along the ring fault in places (Hon, 1987). These intrusions are highly altered and fractured (Fig. 3d). Dacitic lava domes and intrusions were emplaced along the caldera margin in the east of the caldera (Fig. 2a) and syenite (Fig. 3e) and monzonite resurgent intrusions in the center of the caldera (Fig. 2a) (Kennedy et al., 2012, 2016). Syenites, monzonites, and the domes are generally less affected by postemplacement alteration and deformation. The emplacement of the resurgent intrusion caused doming of the center of the caldera with a northeast – southwest oriented apical graben and inversion of displacement on the Alpine Gulch fault and parts of the reactivated ring fault. The largest displacements were approximately 1 km, near the intersection of the Alpine Gulch fault and the ring fault (Hon, 1987).

Mining in LCC has been less productive than in the Silverton, Uncompahgre, and San Juan calderas and nearby plutons (Slack, 1980). However, there is still evidence for widespread alteration and mineralization from hydrothermal fluids (Hon, 1987). Alteration and veining are generally most intense in the center of the caldera, at Red Mountain on the eastern edge of the caldera, and in discontinuous zones near the caldera margin (Larson and Taylor, 1986a, 1986b; Hon, 1987; Sanford, 1992). Oxygen-isotope data show that the basement granite is progressively more altered closer to the margin of the LCC (Fig. 2b) (Larson and Taylor, 1986a). Meteoric water is the principal source of hydrothermal fluid in shallow systems such as Lake City. Almost all meteoric water has a $\delta^{18}O$ composition less than 0‰ (Vienna standard mean ocean water [VSMOW]); hence, the more fluid-rock interaction that occurs, the lower the resultant $\delta^{18}O$ composition of the rock (Taylor, 1974). Thus, the $\delta^{18}O$ composition of alkali feldspar in the granite varies from more than +7‰ away from the caldera margin to less than +1‰ close to the western and southwestern portions of the caldera margin (Fig. 2b) (Larson and Taylor, 1986a, 1986b). The other areas of lowest whole-rock $\delta^{18}O$ (from +3‰ to a minimum of -1.8‰) are in the center of the caldera inside and near the resurgent intrusions (Fig. 2b) (Larson and Taylor, 1986b). Within the caldera most veins and faults have a northeast orientation, which is related to the adjacent northeast-trending Eureka graben formed by resurgence of the Uncompahgre-San Juan caldera (Fig. 2a) (Hon, 1987). This northeast orientation is also similar to the orientation of the Colorado Mineral Belt, a 500-km-long belt of plutons and mining districts stretching from the Four

Corners area in southwestern Colorado to an area near Boulder (Fig. 1). The Colorado Mineral Belt passes through the Lake City area and is related to Precambrian basement weaknesses that cut across the younger geologic grain of Colorado (Chapin, 2012). The Uncompahgre caldera, Colorado Mineral Belt, Eureka Graben, Lake City caldera, and its apical graben trend northeast – southwest (Figs. 1 and 2). This may reflect underlying basement structures, some of which may have been reactivated during caldera collapse and resurgence. However, most faults of the apical graben were probably new structures formed during resurgent doming due to their short trace lengths and restriction to the Lake City caldera fill (Hon, 1987).

The timing of mineralization is complex in the SJVF, and the Lake City area is no exception. Some mineralization in the larger Uncompahgre-San Juan caldera is older than the collapse of LCC. This includes the Golden Fleece vein and early stages of the Ute-Hidden Treasure system, adjacent to the caldera on the eastern and northern sides, respectively, and probably related to resurgence of Uncompahgre caldera (Fig. 2a) (Lipman et al., 1976; Hon et al., 1985; Bove et al., 2001). Mineralization at Red Mountain and late stages of the Ute-Hidden Treasure system are close in age to the formation of LCC at 22.9 Ma (Bove et al., 2001). Some mineralization outside the southern margin, at the Black Wonder mine, is younger than the caldera at 16.5 Ma, as is some mineralization to the west in the nearby Silverton caldera (Lipman et al., 1976; Bove et al., 2001; Fig. 2a).

The veins, alteration, and mineralization at LCC leave a record of hydrothermal fluid flow inside and outside the caldera. The diversity of well-exposed structures (ring fault, intra-caldera normal faults, and faults outside the caldera) and lithologies make this an ideal setting to build a conceptual model of the factors that promote fluid flow in calderas, particularly at their margins.

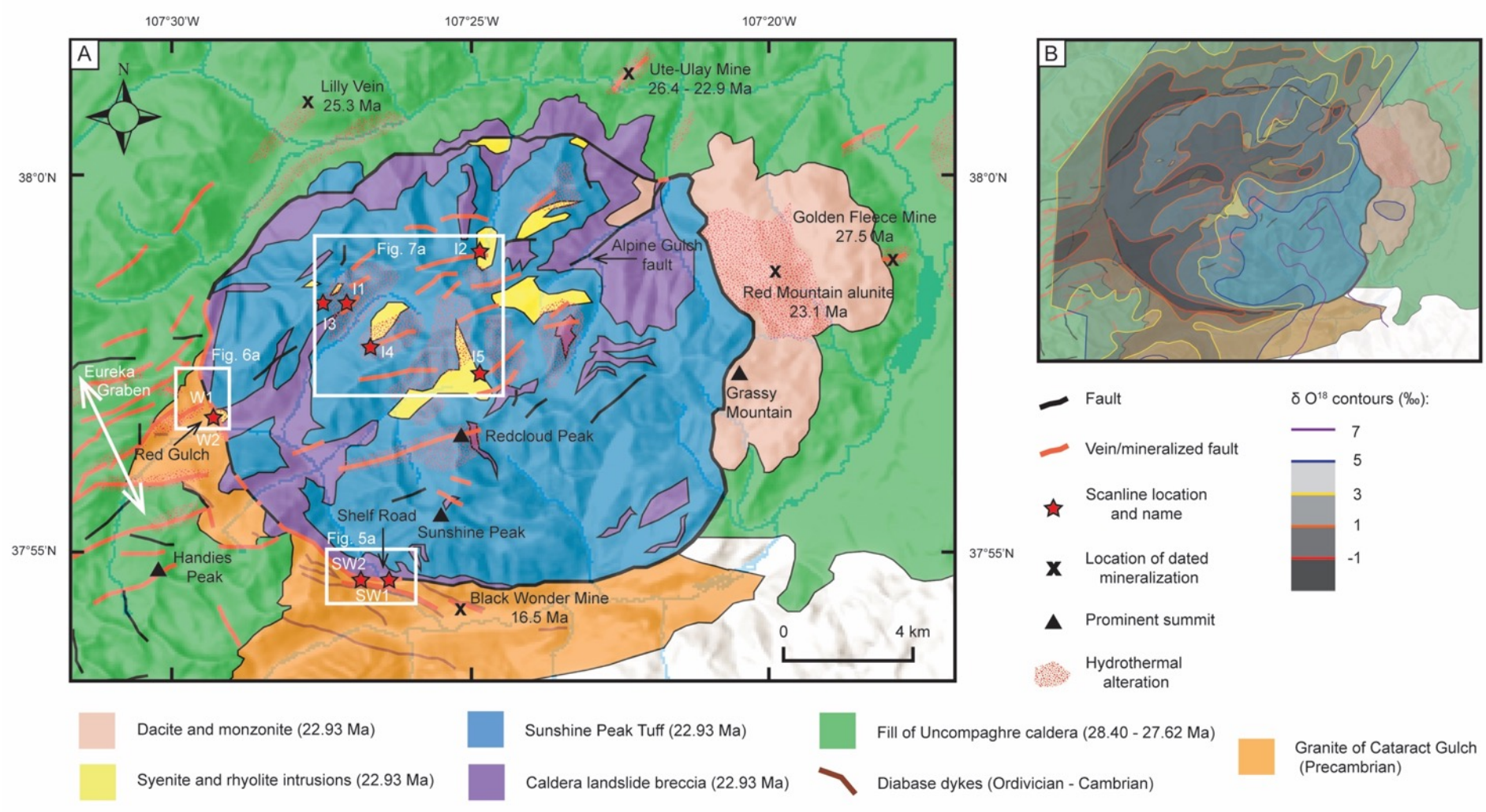

Figure 2: A: Simplified geologic map of Lake City caldera, based on the maps of Hon (1987) and Lipman (1976). Ages are from Bove et al. (2001). B: $\delta^{18}O$ contours from Larson and Taylor, 1986b, overlaid on the simplified geology of Lake City caldera.

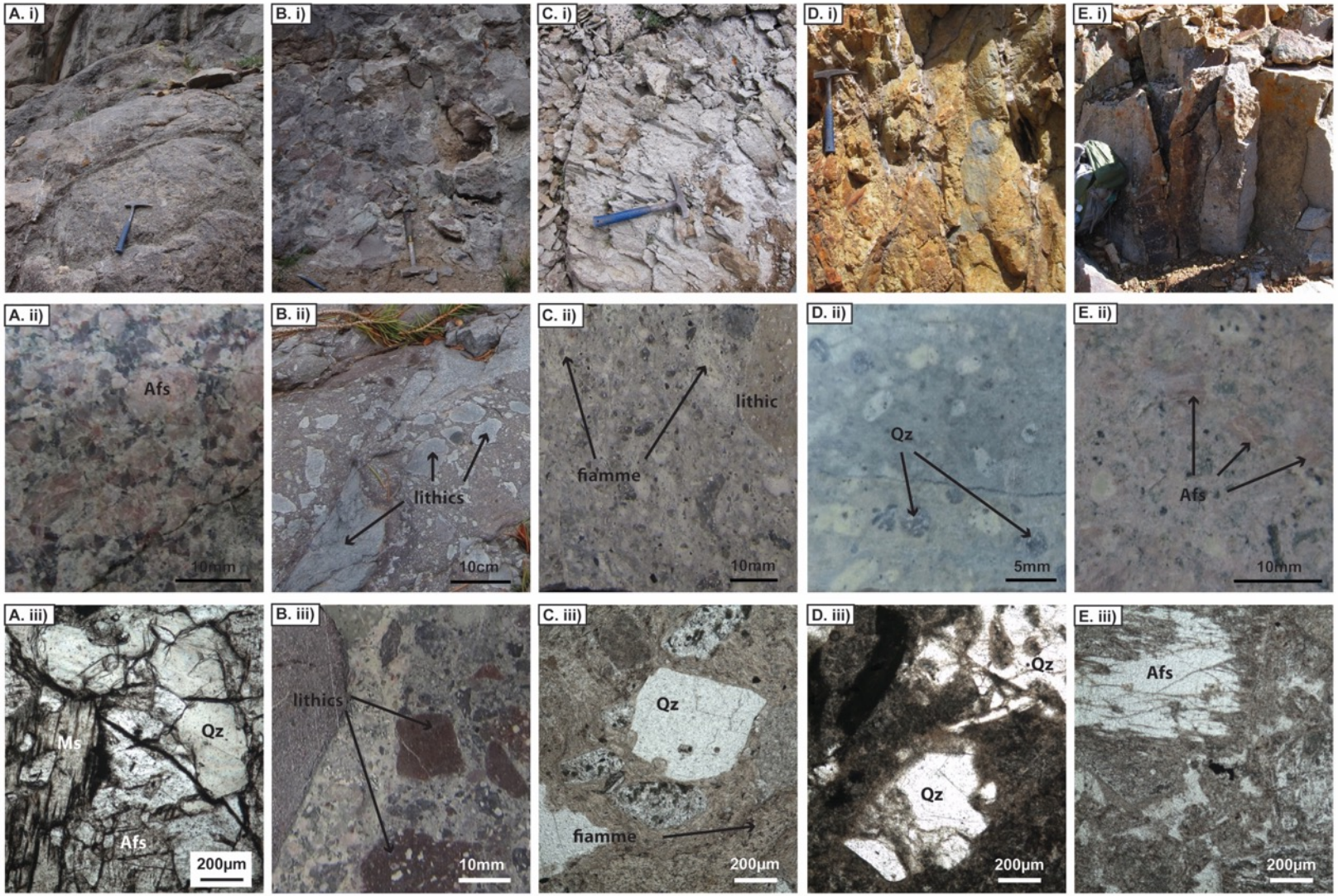

Figure 3: Five of the main rock types of Lake City caldera examined in this study. Photos in first row are outcrop scale (hammer or backpack for scale), photos in second row are hand sample scale, and photos in third row are thin section photomicrographs, except for b which is hand-sample scale. Column a) granite, b) intra-caldera breccia, c) Sunshine Peak tuff, d) rhyolite "ring-dyke" and e) syenite. (Abbreviations: Afs-alkali feldspar, Ms-muscovite, Qz-quartz).

2.4. METHODS

2.4.1. Field Mapping

Lithological, structural and vein mapping was focused on two areas of the caldera margin – known locally as "Shelf Road" in the southwest corner and "Red Gulch" on the western side (Fig. 2). Identification of fine-grained, granite-derived fault rocks was aided by thin-section petrography. Mapping revealed the caldera margin architecture and its relationship to hydrothermal veins in greater detail than the pioneering maps of Peter Lipman (1976b) and Ken Hon (1987).

2.4.2. Scanline Surveys

Transects (or "scanlines") were made across key structures with good exposure, following the methodology of Manda and Mabee (2010). Nine scanline surveys were made - two in the Shelf Road area on the caldera margin (SW2 and SW1), two at Red Gulch on the caldera margin (W1 and W2), and five inside the caldera (Appendix A). Of the scanlines inside the caldera, four (I3, I4, I5, and I1) were in Sunshine Peak Tuff, while one (I2) was in the syenite (Fig. 2). Scanline locations were chosen that had good (near 100%) exposure across and adjacent to major structures. The scanlines varied in length from 5 m to 64 m, depending on the available exposure, and all veins with a trace length of >0.2 m were measured. This cutoff was chosen because surface iron-oxide staining adjacent to veins obscures the location of some veins with a trace length of less than 0.2 m. It was therefore not considered possible to accurately record the location and orientation of all veins with such a short trace length. The orientation and location of every intersecting vein were recorded. Non-mineralized fractures were not recorded, as these do not record the presence of hydrothermal fluids. Veins that have an orientation subparallel to the scanline will be intersected less often than features that have an orthogonal orientation, therefore subparallel structures are underrepresented in scanline data. To account for this the Terzaghi (1965) correction was applied, using the software Stereonet 9 (Allmendinger et al., 2012; Cardozo and Allmendinger, 2013). For the correction we used the average orientation of each scanline and a "maximum correlation" (weighting) factor of 2. Stereonet 9 was also used to plot and analyze structural data, perform kamb contouring of poles to planes (Kamb, 1959), and calculate the circular variance of scanline strike data (e.g. Allmendinger et al., 2012; Cardozo and Allmendinger, 2013). Circular variance is a measure of the spread of the strikes of veins. It is a value between 0 (very well clustered) and 1 (very poorly clustered).

2.5. RESULTS

We describe the detailed distribution of fault rock facies (Table 2), subsidence structures and veins in two areas where the caldera margin is well exposed. Additionally, we present four scanlines in these two areas of the margin, and five additional scanlines from inside the caldera (Table 3) across faults where the entirety of the fault core is replaced or cemented by vein material. All veins that were recorded on scanlines, and most that were mapped, contain predominantly quartz with varying but always lesser amounts of calcite, adularia and pyrite. Euhedral "comb" quartz grains, with relict "vugs" of open space in the center of the vein, are common. Most veins appear to be extensional (mode I) and syntaxial (inward growing, see Bons et al., 2012), though unequivocal kinematic indicators are rare. Alteration is generally propylitic on the western caldera margin and propylitic or phyllic in the interior and is usually more pervasive in a "halo" around veins. The halos vary in width from several millimeters to several meters.

2.5.1. Facies and detailed mapping around the caldera margin discontinuity

2.5.1.1. Unbrecciated granite

The granite is phaneritic with mostly 2 to 8 mm crystals of quartz, alkali feldspar and plagioclase with minor muscovite and biotite (Fig. 3e). Near the caldera margin the granite is commonly deformed and brecciated (see below). The granite is altered near the southwest caldera margin and in the Eureka Graben (Fig. 2). The granite mostly alters to illite, calcite and quartz.

2.5.1.2. Granite fault rocks

Field mapping revealed previously unrecognized brecciated and cataclastic granite (Fig. 4 and Table 2) in some locations near the Lake City caldera margin (Figs. 5a and 5b). These fault rocks have been divided into four "facies" (facies A to D), reflecting progressively higher levels of brecciation and shearing (Fig. 4, Table 2). The fault rocks are named according to the classification scheme of Woodcock and Mort (2008). Not all four facies are present at every location, and they all exhibit a degree of alteration and host hydrothermal veins - an indication of their coherent nature. Table 2 describes the fault rocks and their distribution in more detail, and they are shown in Figure 4.

Table 2: Description of granite and granite-derived fault rock facies identified at the margins of Lake City caldera

Granite Fault Rock Facies	Rock name (Woodcock and Mort, 2008)	Description	Distribution
Un-brecciated	Granite	Phaneritic, with mostly 2 – 8 mm crystals of quartz, alkali feldspar and plagioclase, with minor muscovite and biotite (Fig. 3a). Alters mostly to illite, calcite and quartz.	To west, southwest and south of caldera. Granite is altered near the southwest caldera margin and in the Eureka Graben (Fig. 2). Commonly deformed and brecciated near the caldera margin.
Facies A	Crackle to mosaic breccia	Characterized by small micro-faults and shear zones, and consists of monomict, clast-supported granitic crackle to mosaic breccias with large angular clasts more than 20 cm across (Figs. 4ai and 4aii). Rare outcrops exhibit a 'jigsaw fit' texture. The breccia matrix consists of angular crystal fragments and fine dark clay-sized material. At the microscopic scale individual crystals are highly fractured at the margins of micro-faults or breccia clasts (Fig. 4aiii).	Near caldera margin discontinuity in the 'Shelf Road' area at the southwestern margin of the caldera.
Facies B	Chaotic breccia	Consists of monomict granitic chaotic breccias that are less coarse than facies A breccias (Fig. 4b). Most clasts are between 3 and 20 cm across. Matrix comprises a higher proportion of the breccias of facies A, hence they are mostly matrix supported. Clasts are mostly angular to subangular. The breccia matrix consists of angular crystal fragments and fine dark clay-sized material (Fig. 4biii).	Widespread (compared to other fault rock facies) near the caldera margin, and other major caldera-related structures in granite. At 'Shelf Road' and 'Red Gulch' areas on western and southwestern margins.
Facies C	Protocataclasite	Consists of small granite clasts less than 10 mm across in a matrix that consists of comminuted angular crystals and fine clay-sized material (Fig. 4c). The matrix is volumetrically dominant and is of similar grain size as the matrix of facies A and B breccias. A fabric is present at some locations, observable at the outcrop scale and rarely at the hand sample and thin section scale. The fabric is identified by alternations of coarser and finer grained layers (Fig. 4ci). Hydrothermal clay alteration and/or silicification is present in some locations.	Near caldera margin and other major caldera-related structures in granite at 'Shelf Road' and 'Red Gulch' areas on western and southwestern margins.
Facies D	Mesocataclasite and ultracataclasite	Few grains are visible to the naked eye. In thin section the rock can be seen to consist of small (<50 μm) angular crystal fragments in a dark colored clay-sized matrix (Fig. 4diii). At the hand sample scale, a foliation is observable in some locations as irregular layers of differing color, from light grey to black (Fig. 4dii).	Only found in a ~2 m thick band in the 'Red Gulch' area on the western margin of the caldera (Fig. 4di).

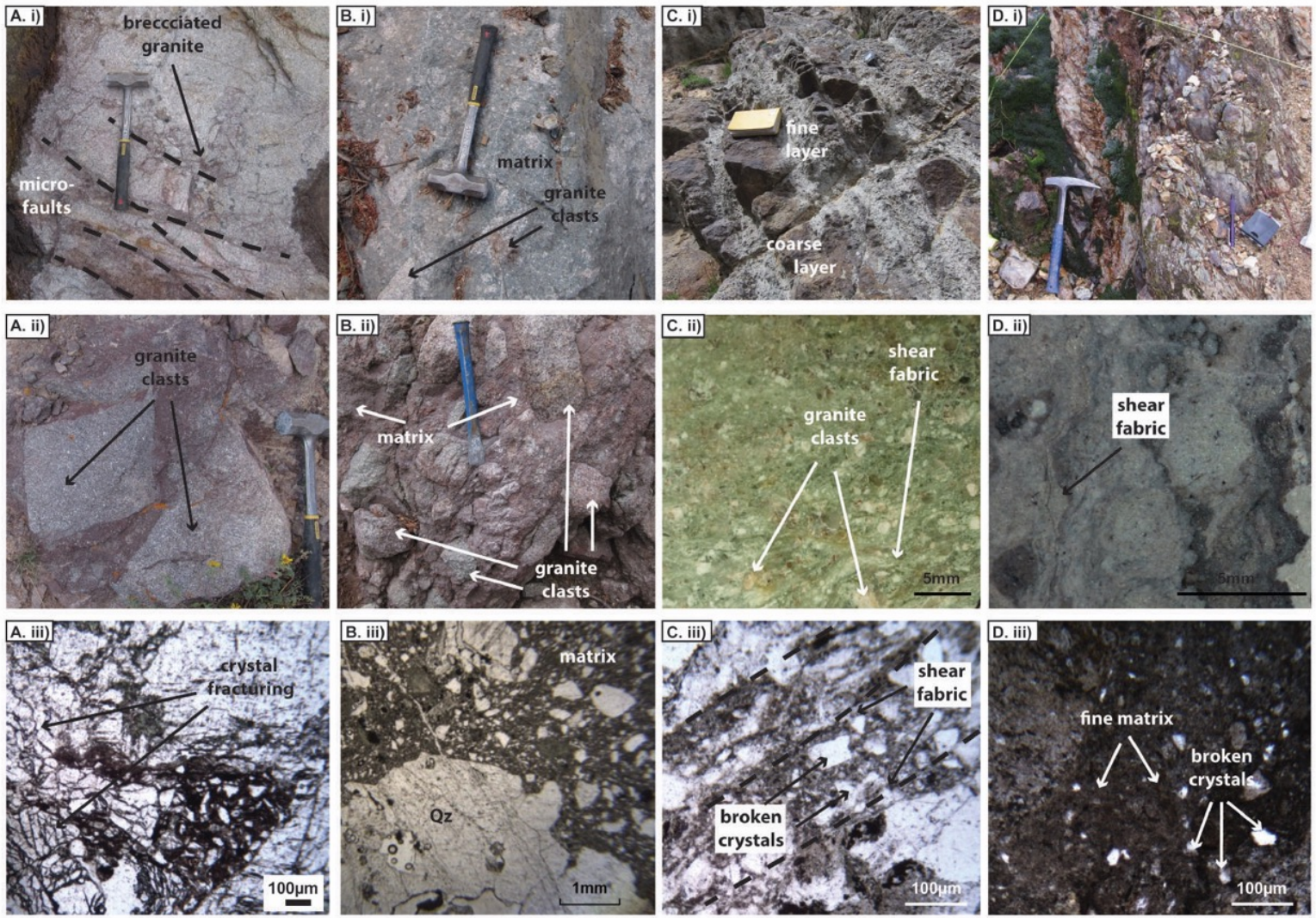

Figure 4: The four facies of granite fault rock identified in this study. Photos in top row are outcrop scale (hammer or notebook for scale), photos in second row are outcrop or hand sample scale, and photos in third row are thin-section photomicrographs. Column a) is facies A; b) is facies B; c) is facies C; and d) is facies D. These facies are described in Table 2. (Abbreviation: Qz-quartz).

2.5.2. Southwest Caldera Margin

In the vicinity of the Shelf Road, intra-caldera rocks of the Lower Sunshine Peak Tuff and associated landslide breccias are in contact with the basement lithologies, which consist of Proterozoic granite and diabase dykes that have been interpreted to be Ordovician (Lipman, 1976b) (Fig. 5d). Some small pegmatite dykes are also present. The caldera margin had previously been mapped as simple and arcuate in this area; however, our field mapping (Fig. 5a) has revealed two largely straight segments with a distinct corner between them with overshooting fault zones and a splaying and reconnecting fault segment. A large fault and vein structure (Fig. 5c) links this corner on the caldera margin with a diabase dyke in the granite basement. Veins and breccias suggest that the margin of this dyke may be a continuation of the ring fault where it continues roughly subparallel to the caldera margin to the SE.

Granite breccias (facies A and B; see Table 2) are found close to the caldera margin discontinuity at most locations where this margin is sufficiently exposed. There is a general progression towards coarser clast sizes farther from the margin. Veins (predominantly quartz and calcite) are generally more common in the granite basement than in the intra-caldera rocks (Fig. 5d) and generally decrease in density away from the caldera margin discontinuity. Veins crosscut all fault rock facies, and no veins were found in the granite more than ~2 km from the caldera margin discontinuity (Fig. 5a). The orientation of veins outside the caldera is variable but with a maximum in the NE direction.

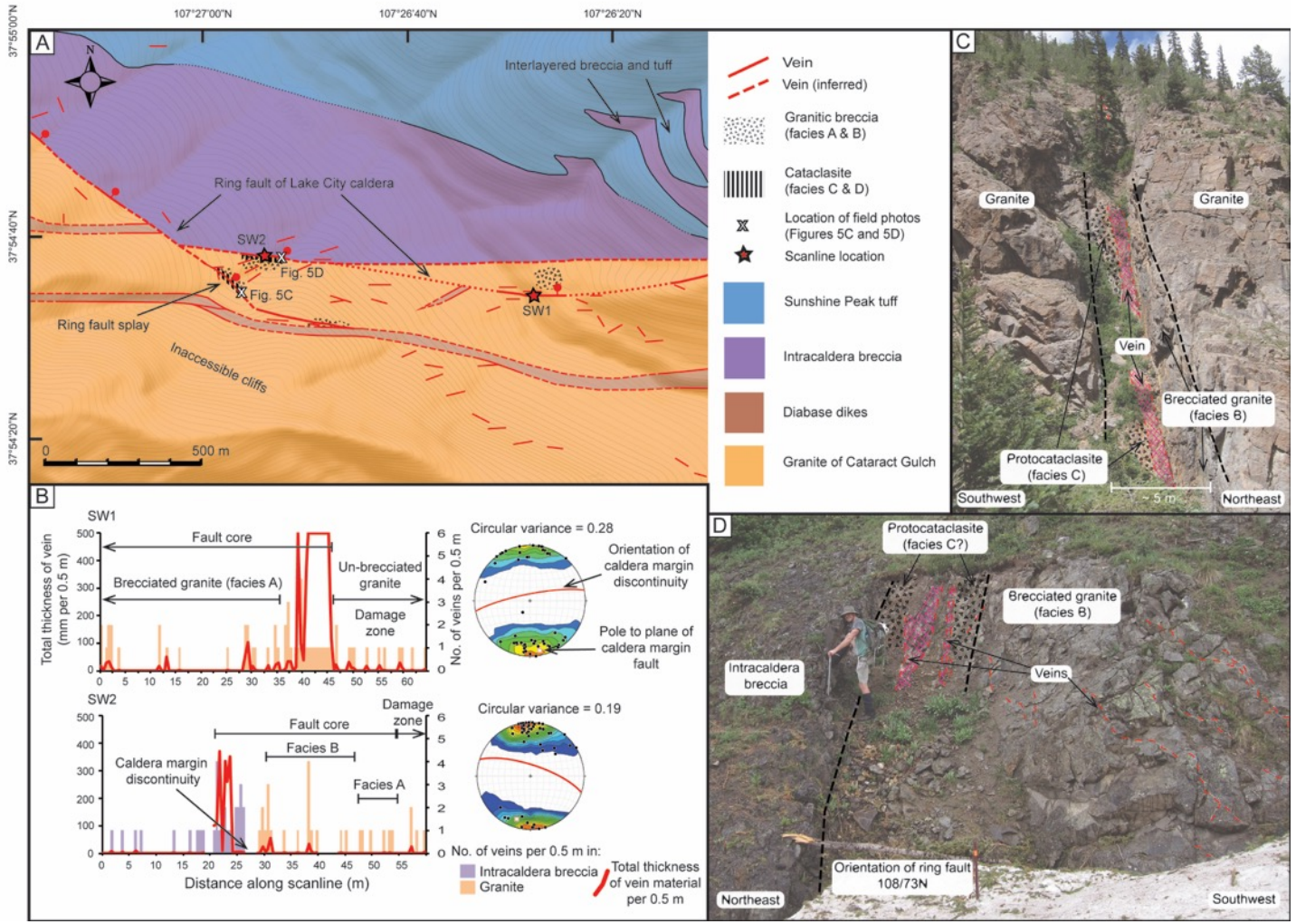

Figure 5: A: Geologic map of the 'Shelf Road' area in the southwestern corner of Lake City caldera. Field data are primarily from this study, with Sunshine Peak Tuff - Intra-caldera contact from Hon, 1987. B: Scanline data from scanlines on the southwestern margin of Lake City caldera. Charts on left show the vein density and thickness of veins per half meter. Kamb-contoured stereonet plots show pole to plane vein orientations and the orientation of the caldera margin. Stereonet contour intervals correspond to a point density of two times the standard deviation (2σ) of the number of points expected to fall within a given area if the points had a random orientation (see Kamb, 1959). Vein density columns are color coded according to the lithology in which the veins are hosted: purple is intracaldera collapse breccia, and orange is granite. Location of SW1: 37.90981°N, 107.44116°W, location of SW2: 37.91076°N, 107.44827°W. C: Field photo looking northwest of altered fault zone in granite outside of caldera margin. D: Field photo, looking southeast, of the steeply inward-dipping discontinuity at the caldera margin. Caldera-collapse breccia composed of predominantly andesite clasts on left, brecciated granite on right. Note the lack of small subsidiary veins in the intra-caldera breccia compared to the granite. Subsidiary veins in granite are subparallel to ring fault. Wavy appearance is due to three-dimensional irregularities of outcrop surface

2.5.2.1. Scanlines at southwestern corner around Shelf Road: SW1 and SW2

Near the Shelf Road in the southwestern corner of the caldera, the caldera margin orientation changes from approximately east-west to northwest-southeast (Fig. 5a). The veins in scanlines SW2 and SW1 have orientations well clustered around the east-west orientation of the caldera margin (Table 3). The orientation of veins measured in these scanlines (Fig. 5b) is much less variable than the orientation of surrounding mapped veins in the granite (Fig. 5a). In both scanlines, vein density is highest near the main caldera-related structure (Fig. 5b and Table 3). In scanline SW2, we interpret the intra-caldera breccia in the ~5 m adjacent to the caldera margin discontinuity as fault core. It has a higher proportion of matrix and finer clast size than the rest of the intracaldera breccia at this location. These breccias are therefore consistent with a landslide origin for intracaldera breccias that have undergone some dynamic textural modification by faulting, as described by Hon, (1987) and Kennedy et al., (2016). Most veins on scanlines SW1 and SW2 have a euhedral comb texture indicating the quartz minerals grew from the vein wall inward towards the vein (syntaxial) into open space, with no evidence of shearing or offset (Fig. 6). These are interpreted as extensional (type I) veins (cf. Bons et al., 2012) and have an east-west orientation on average, though there is significant variability in vein strike.

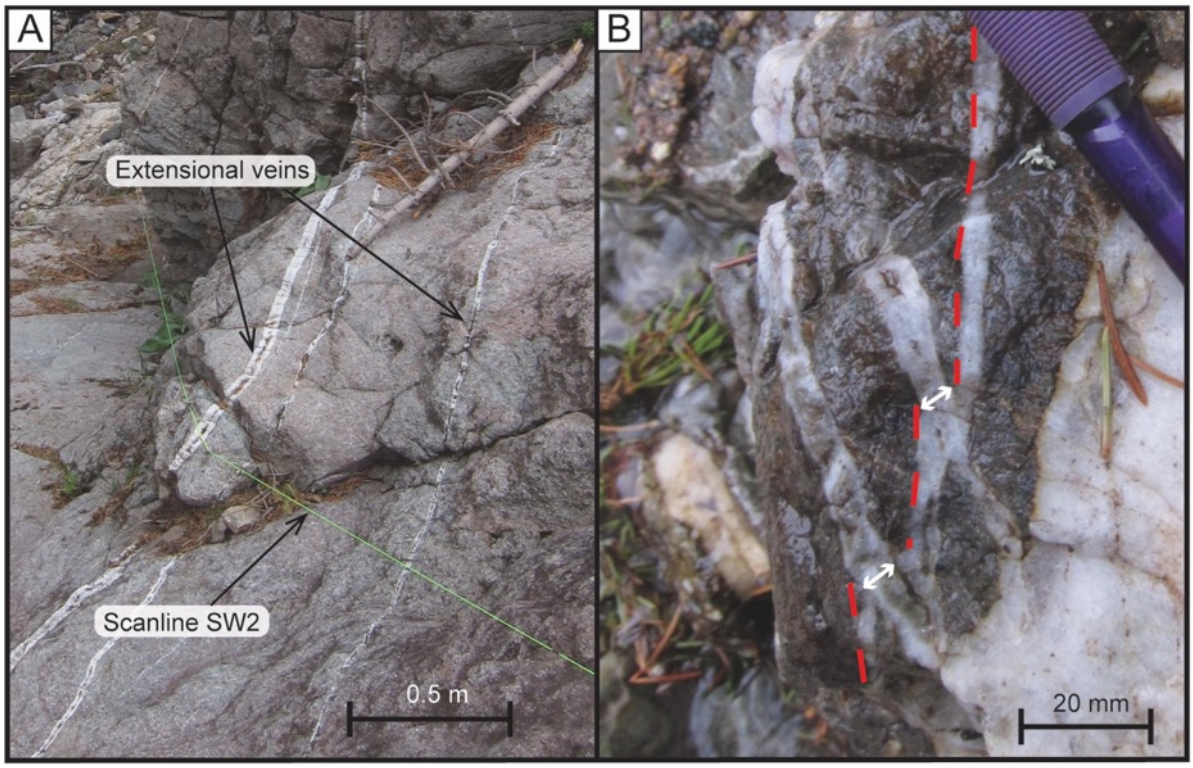

Figure 6: A: Field photo looking north at the location of scanline SW2, showing subparallel veins in granite that are interpreted as extensional veins. Green line is the trace of scanline SW2. B: Field photo looking downwards (up is to the east) at the location of scanline SW2, showing two veins crosscutting another vein with extensional displacement.

Table 3: Description of scanlines and the orientation and density of veins measured. See Appendix A for original scanline logs.

Location	Scanline	Orientation (trend/plunge)	Length (m)	Rock type	Circular variance	Vein density	Notes
Southwestern margin	SW1	000/09	64.3	Granite and granite-derived fault rocks	0.28	Higher in 7 to 10 m north of caldera-related structure. Low for the rest of the scanline.	Across caldera-related fault in granite.
	SW2	048/40	60.0	Granite, granite derived fault rocks, and intra-caldera breccia	0.19	Higher in first 7 to 10 m outside caldera margin discontinuity. Low (0 – 1 veins per meter) for the rest of the scanline.	Across caldera margin discontinuity.
Western margin	W1	280/17	10.0	Rhyolitic ring dyke	0.28	No increase near ring dike margin. Higher near subsidiary veins from 6.5 to 9 m.	Scanline starts at ring dike margin.
	W2	260/30	11.0	Rhyolitic ring dyke	0.58	Higher in 4 m near ring dike margin (up to 6 veins per 0.5 m). Low for rest of scanline (≤2 veins per 0.5 m).	Scanline starts at ring dike margin.
Intra-caldera	I1	094/00	22.0	Welded Sunshine Peak tuff	0.17	Higher vein density coincident with maximum vein thickness.	Across normal fault with ~120 m vertical displacement (from bedding offset)
	I2	289/04	15.5	Syenite	0.14	Low vein density (≤2 veins per 0.5 m) for most of scanline, except near a subsidiary vein at 4 to 6 m.	
	I3	080/26	10.0	Welded Sunshine Peak tuff	0.37	Higher vein density coincident with maximum vein thickness.	Across fault with ~70 m of apparent right-lateral strike-slip displacement
	I4	297/40	15.0	Welded Sunshine Peak tuff	0.48	Low for most of its length.	
	I5	101/00	5.7	Welded Sunshine Peak tuff	0.71	High vein density (up to 6 veins per 0.5 m) adjacent to maximum vein thickness, however orientations of subsidiary veins are very different to that of the fault.	

2.5.3. Western Caldera Margin

The western caldera margin discontinuity at Red Gulch (Fig. 7a), consists of intra-caldera rocks of the lower and middle Sunshine Peak Tuff and associated landslide breccias in contact with basement granite overlain by intracaldera rocks of the Uncompahgre caldera. The basement granite is intruded by small gabbro and pegmatite dykes. The caldera margin zone here has a generally north-south orientation and contains clastic rocks, veins, and a porphyritic rhyolitic "ring dike" intrusion (Fig. 7d). Most of the clastic rocks consist of monomict granitic breccias (facies B), with one area where the clasts are dominantly andesite. We interpret a thin (2 m wide) north-south trending zone of meso- to ultracataclasite (facies D) and discontinuous veins to represent the highest strain portion of the ring fault of the caldera (Fig. 4d). The breccias become finer towards this cataclasite zone and grade into protocataclasite (facies C) with a shear fabric (Figs. 4c and 7c). A short distance (20 – 30 m) away inside the caldera, the breccias are dominated by andesite and tuff clasts, as is common for most of the intra-caldera landslide breccias (Lipman, 1976a). The contact between the granite-dominated breccias (fault rock facies B) and the landslide breccias is sharp, and it crosscuts the fabric of facies C slightly to the north (Fig. 7a). We interpret this as an erosional boundary formed by destruction of fault rocks from landsliding of the fault scarp into the caldera. Outside the caldera and near the cataclasite zone, the granite is deformed (facies C) and contains a shear fabric in places. Most of the veins at Red Gulch are close to the caldera margin or outside of it, and veins cross-cut all fault rock facies. Veins of variable orientation pervade the "ring dike", while outside of the caldera, the majority of large veins have a northeast orientation. The latter observation is consistent with the location of this site within the northeast-trending Eureka Graben.

2.5.3.1. Scanlines at western caldera margin: W1 and W2

Exposures at Red Gulch on the western edge of the caldera indicate that the caldera margin is oriented approximately north-south and cuts across the Eureka Graben, in which many faults and veins are oriented northeast-southwest, as in the rest of Lake City caldera (Figs. 2 and 7a). The scanlines show that most veins within 10 m of the caldera margin have a north-south orientation, rather than following the regional northeast-southwest trend, and vein thickness is greatest near the ring dike margin (Fig. 7b and Table 3). Veins on scanlines W1 and W2 are interpreted as syntaxial, extensional quartz veins. Large (>10 mm) vugs of open space are

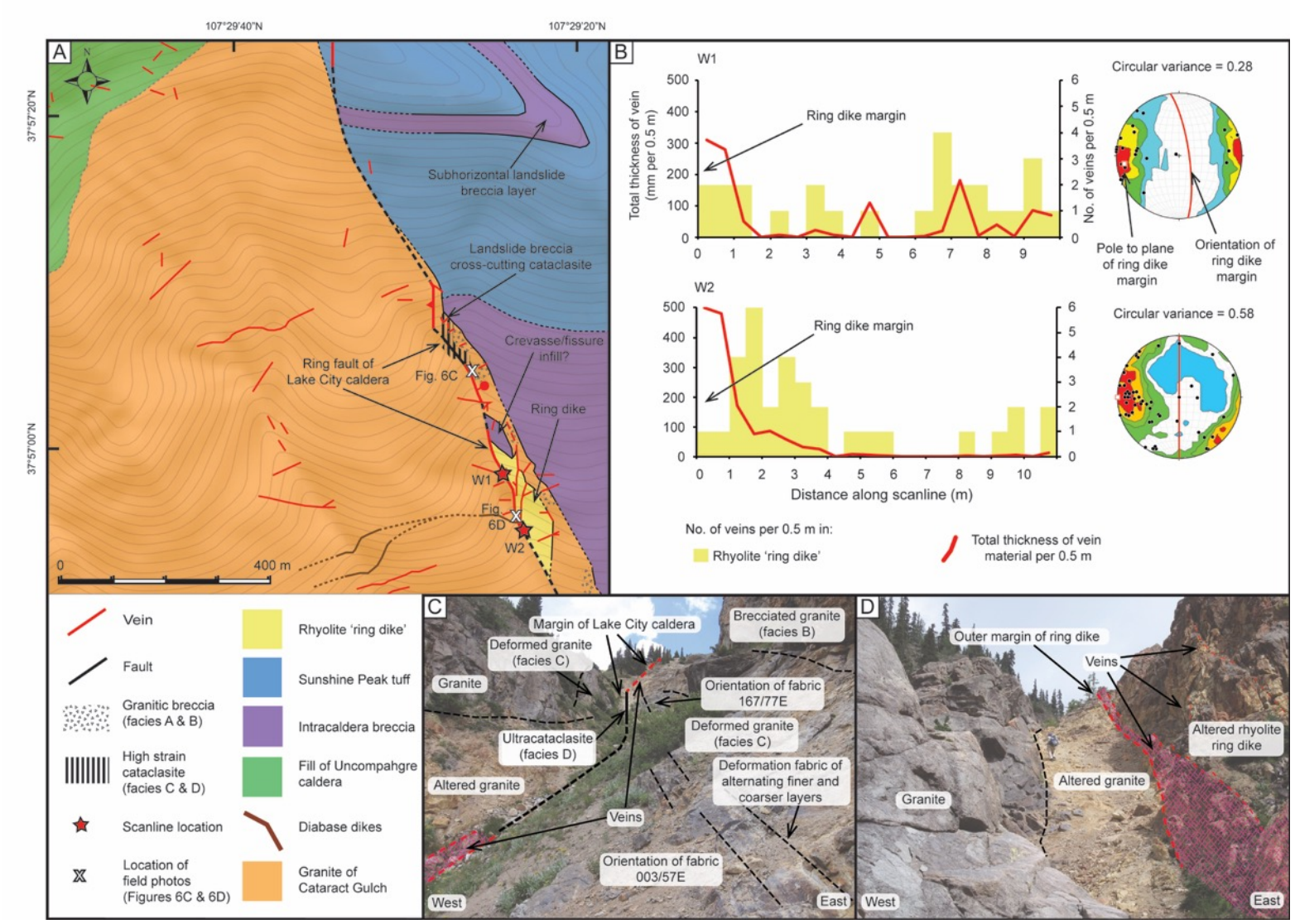

Figure 7: A: Geologic map of the 'Red Gulch' area on the western margin of Lake City caldera. Field data are from this study. B: Scanline data from scanlines on the western ring dike margin of Lake City caldera. Charts on left show the vein density and thickness of veins per half meter. Kamb-contoured stereonet plots show pole to plane vein orientations and the orientation of the ring dike margin. Stereonet contour intervals correspond to a point density of two times the standard deviation (2σ) of the number of points expected to fall within a given area if the points had a random orientation (see Kamb, 1959). Vein density columns are colored yellow due to their intrusive rhyolite lithology. Location of W1: 37.94878°N, 107.49133°W, location of W2: 37.9479°N, 107.49083°W. C: Field photo looking northwest of part of the western margin of Lake City caldera showing the distribution of deformed rocks, altered granite and unbrecciated granite. D: Field photo looking northwest of the altered rhyolite ring dike, altered granite and undeformed granite on the western margin of Lake City caldera.

common in the center of veins, especially in scanline W2. No shear or hybrid veins were identified.

2.5.4. Caldera Interior

The intra-caldera mapping focused on areas of veins and hydrothermal alteration. Identification of cataclastic rocks or facies was difficult due to the smaller sizes of fault cores, intense silicification, and presence of hydrothermal vein breccias. The interior of the caldera is dominated by smaller-displacement normal faults associated with intrusion and uplift and parallel to regional trends (Fig. 8a). More limited exposure across key structures in the caldera interior allowed focus on shorter scanlines (Fig. 8b). In general, less vein calcite was identified in veins in the interior of the caldera than at the southwestern margin. However, bladed calcite replaced by quartz is quite widespread.

2.5.4.1. Scanlines inside the Caldera: I1 to I5

Five scanlines were made across mineralized northeast-southwest-oriented faults inside the caldera (Fig. 8a). Most mapped faults inside the caldera have the same orientation (Fig. 2). From bedding offset, the total displacement of some of the faults in scanlines I1 and I3 can be constrained (Table 3). There is no obvious bedding to measure displacement for the other faults, so displacement is unconstrained. However, their trace length is shorter than the faults in scanlines I1 or I3 (Fig. 8a); therefore displacement is probably less than 120 m. The circular variance and vein density patterns for the intra-caldera scanlines are summarized in Table 3. In general, the major veins that the intra-caldera scanlines transected are smaller in total width compared to the scanlines near the caldera margin (Figs. 5b and 6b). Veins in two of the scanlines have well-clustered northeast-southwest orientations, while the others are less clustered (Table 3).

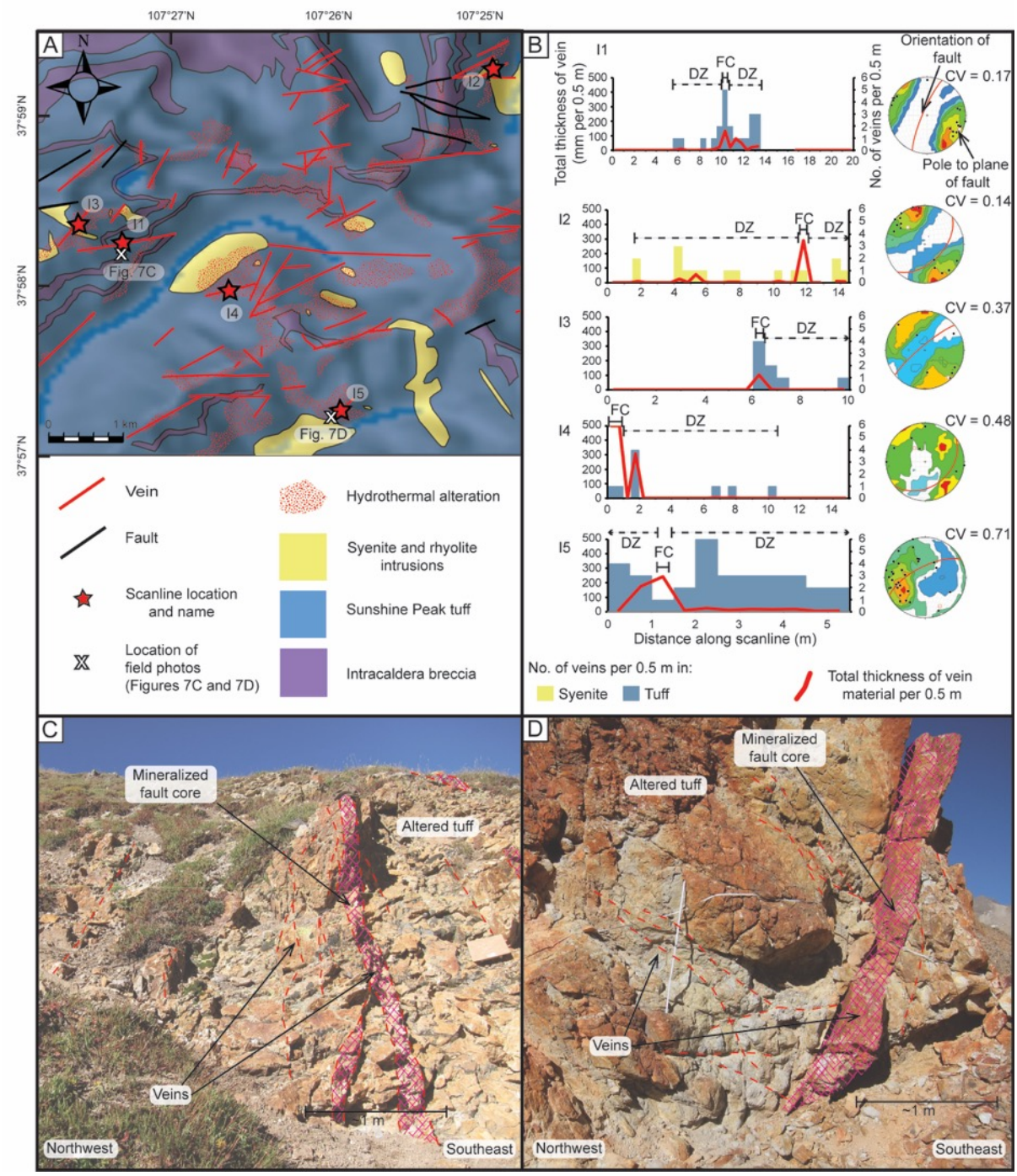

Figure 8: A: Map of part of the interior of Lake City caldera, showing the location of mineralized and unmineralized faults, and scanline locations. Map modified from Hon (1987). B: Scanline data from scanlines inside Lake City caldera. Charts on left show the vein density and thickness of veins per half meter. Kamb-contoured stereonet plots show pole to plane vein orientations and the orientation of the fault on the scanline. Stereonet contour intervals correspond to a point density of two times the standard deviation (2σ) of the number of points expected to fall within a given area if the points had a random orientation (see Kamb, 1959). Vein density columns are color coded according to the lithology in which the veins are hosted: yellow is syenite and blue is tuff. Abbreviations: CV-circular variance; FC-fault core; and DZ-damage zone. C: Field photo looking northeast of the mineralized fault and surrounding veins at scanline I1. D: Field photo looking northeast of the mineralized fault and surrounding veins at scanline I5.

In summary, a wider zone of deformation (up to ~300 m) than previously mapped has been identified at the southwest corner of Lake City caldera, with at least one large inward-dipping

mineralized fault extending into the granite basement outside of the caldera fill (Figs. 5a and 5b). A sheared preexisting dike, subparallel to the caldera margin, may also have accommodated some caldera-related deformation. At the western caldera margin, there is evidence for the destruction of fault rocks at moderate to high stratigraphic levels (Fig. 7a). Deformed granite fault rocks are present at both southwest and western segments of the ring fault (Fig. 4 and Table 2), and veins are associated with the caldera margin in both. At the southwestern margin, veins are more common in the granite outside the caldera than in the intra-caldera breccia (Fig. 5a). Outcrop-scale scanline surveys (Table 3) in both the west and southwest indicate that the orientation of veins near the caldera margin is similar to the orientation of the caldera margin itself (Figs. 5b, 7b and 9a). Veins surrounding smaller-displacement faults in the center of the caldera generally show orientations that are more variable and are not necessarily similar to the orientation of the faults they are associated with (Figs. 8b and 9a). The width of veins is generally larger near the caldera margin discontinuity than inside the caldera and surrounding smaller intra-caldera faults (Fig. 9b). Figure 9 provides a comparative summary of scanline data from the three parts of the caldera studied. The average thickness of vein per 0.5 m (Fig. 9b) is calculated by using only the first 4 m of each scanline away from the relevant major structural discontinuity, so that the shorter intra-caldera scanlines can be compared with those on the margin.

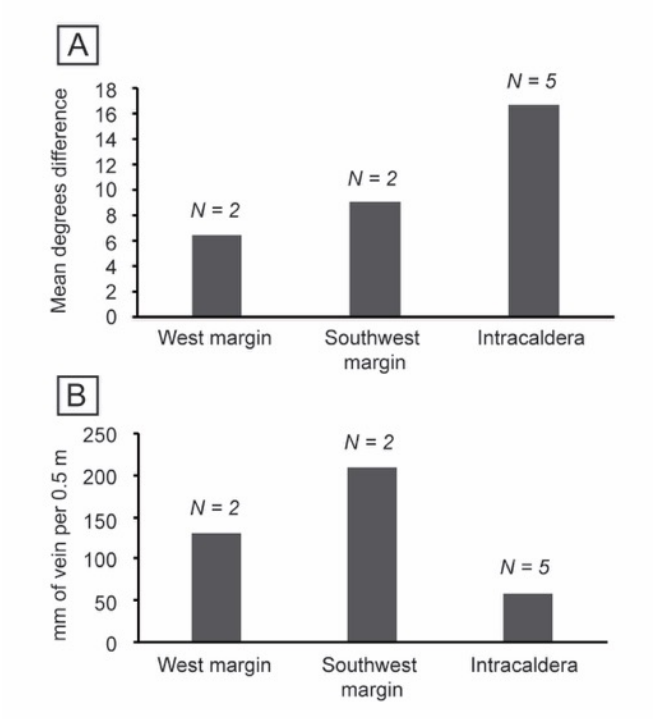

Figure 9: Summary of scanline data, comparing locations both within and along the margins of the Lake City caldera. *N* refers to the number of scanlines at each location. A: The difference in orientation between the mean strike of all veins, and the strike of the largest vein/fault for each scanline, averaged for each location. B: The mean thickness of vein material in the first 4 m away from the largest discontinuity, for each location. Only the first 4 m are used so that shorter intra-caldera scanlines can be compared with those on the margin. The major discontinuity is the ring fault splay in SW1, the caldera margin discontinuity for SW2, the ring dike margin in W1 and W2, and intra-caldera fault in scanlines I1 to I5.

2.6. DISCUSSION

The hazard and resource potential of calderas has led to intensive research on the mechanisms of caldera formation and the geometry of the resulting structures. Because a large caldera-forming eruption has never been observed, analogue and numerical models are useful tools to investigate the variables that control the diverse caldera morphologies. For any model, it is important to validate results by comparing them with actual field examples, and detailed lithological and structural mapping of well-exposed calderas can provide valuable comparative data. The first section of this discussion focuses on the interpretation of the geology of Lake City caldera, its controls, and comparisons with analogue models and other global examples. One of the important applications of understanding caldera structure is being able to predict the resource potential of calderas. As such, the second section of this discussion focuses on the potential relationship between structure, lithology and fluid flow at the Lake City caldera and how this compares with other calderas.

2.6.1. Structure and Lithology of Lake City Caldera

At Lake City, the caldera margin is a structurally complex zone of deformation, and we, therefore, prefer to describe it as a caldera margin discontinuity instead of a simpler ring fault, *sensu stricto*. We use the general term caldera margin discontinuity to describe the interface between intra- and extra-caldera rocks where it is ambiguous if the interface is structural (i.e. ring fault) or topographic, or if it varies between these along its length.

Detailed mapping in the Shelf Road area southwest of the caldera shows that the orientation of the caldera margin changes abruptly as a corner rather than gradual curve. This suggests that the structural margin of Lake City caldera may have a more polygonal shape rather than ellipsoidal as the previously mapped outline would suggest. In modern calderas, the most obvious morphological feature is often the topographic margin of the caldera, which often has a rounded perimeter and is located outboard of the structural ring fault margin (Lipman, 2000a). The topographic margin is created by shedding of material off the walls of the structural margin, the same process that has been inferred to be responsible for the widespread intra-caldera breccia units in Lake City caldera and other calderas worldwide (Lipman, 1976a; Hon, 1987; Lipman, 2000). The structural margin of a modern caldera is difficult to identify because it is usually buried by the sediment that was shed during creation of the topographic margin. It may be more rectilinear or polygonal than the topographic

margin, because the fault orientations accommodating the caldera collapse tend to follow pre-existing planar weaknesses in the crust (Branney and Acocella, 2015). Some examples of calderas where the structural margin has been inferred to be polygonal are Rotorua, Okataina, Taupō (New Zealand), Cerro Galán (Argentina), Colli Albani (Italy), Deception Island (Antarctica), and Sakurae (Japan) (Spinks et al., 2005; Giordano et al., 2006; Komuro et al., 2006; Folkes et al., 2011; Ashwell et al., 2013; Martí et al., 2013). Caldera subsidence experiments also indicate polygonal faults may form even in the absence of structural weakness, and can propagate beyond their intersecting corners (Kennedy et al., 2004; Holohan et al., 2013). In the southwest corner of Lake City caldera, a fault-vein structure splays off the caldera margin at the corner and continues southeastward until it meets a highly mineralized diabase dike (Fig. 5a). The dike contains abundant quartz veins. We interpret breccias at its northern margin as chaotic fault breccia, according to the classification scheme of Woodcock and Mort (2008). Additionally, we interpret that the NW-SE-trending fault that splays off the caldera accommodated some caldera-related displacement. The margin of the dike probably acted as a preexisting weakness at a favorable orientation to accommodate slip, as it is subparallel to the east-west portion of the caldera margin. This shows that the caldera displacement was not all focused on just one ring fault but a more distributed area of deformation (or fault zone *sensu* Childs et al., 2009) at least ~300 m wide (Fig. 5a). The fault zone width of ~300 m for a displacement of ~ 1.5 km is consistent with the (extrapolated) data of Childs et al. (2009). We suggest that the sub-parallel orientation of pre-caldera dikes and sections of the caldera margin reveal a common regional structural control.

In the west and southwest of the caldera and closest to the discontinuity, four "facies" of deformed granite with variations in clastic textures can be identified (Fig. 4 and Table 2). These clastic rocks show a decrease in grain size from facies A to D, with facies C and D exhibiting a clear fabric. We suggest that the decrease in grain size and formation of a fabric is due to increasing amounts of strain and deformation. These rocks are found only near the margin of Lake City caldera, and we interpret that these fault rocks formed by movement along the caldera structural margin. Not every facies is present at every location, due to variable fault core development and due to the destruction of fault cores by gravitational collapse of the margin during caldera formation. There is evidence for the latter at the western caldera margin, where well-developed foliated granitic protocataclasite is abruptly cross-cut by polymict andesite and tuff dominated breccia that we interpret was formed by landsliding (Fig. 7a). There are also large portions of the caldera margin where intracaldera

landslide breccia is juxtaposed against granite country rock without any fault rocks in between; presumably the fault rocks have been destroyed by gravitational collapse. At Red Gulch, there is a small area of andesite and Sapinero Mesa tuff (from Uncompahgre caldera)-dominated breccia among the granite derived fault rocks (Fig. 7a). This breccia does not have any kind of fabric, and was intruded by the ring dyke on its southern end. The origin of this andesite and tuff breccia is not clear. It is not likely to be fault derived because its composition varies markedly with the surrounding granitic breccias, and it has no fabric. Our preferred explanation is that it is the remains of an extensional "crevasse" on the margin of Lake City caldera, which formed after the formation of the granitic fault rocks and was infilled with blocks of the andesites and Sapinero Mesa tuff above the granite. Similar megabreccia-filled crevasses have been identified at Glencoe caldera (Moore and Kokelaar, 1998).

Due to the NW-SE extension direction inside the caldera indicated by numerous NE-trending normal faults, it could be expected that the northern, northwest and southeast sections of the ring fault, which are oriented approximately NE-SW, would be favorably oriented for the creation of extensional fractures and veins. There are, however, very few veins and/or alteration along these sections, despite similar amounts of exposure as along the much more mineralized western and southwestern sections (Fig. 2, Hon, 1987). The southeast part of the caldera margin is a similar distance from the resurgent pluton as the western and southwestern portions, but in contrast, it is across strike from the predominant northeast trend. Our data indicate that fluid flow in the resurgent dome may have been enhanced in the along-strike direction (with respect to the NE-SW-trending normal faults), utilizing abundant intersecting structures, and comparatively inhibited across strike towards the southeast part of the caldera. Permeability of the northern and northwestern margins may have been inhibited (compared to the western and southwestern portions) due to the lack of fault intersections (Fig. 2). Additionally, reactivation of an outward-dipping ring fault in this section of the caldera during resurgence may inhibit permeability in a manner similar to that proposed for Colli Albani caldera in Italy (Giordano et al., 2006). However, we do not have any data on the dip direction of this portion of the ring fault; so this inference is purely speculative.

The prolonged history of mineralization in the vicinity of Lake City caldera (Fig. 2) makes precise age control difficult to establish for the veins studied. Field relationships indicate that the veins inside the caldera and along the structures of the caldera margin are younger than

caldera subsidence. These relationships are that veins crosscut (and therefore postdate) the fault rocks of the ring fault and ring dikes and mineralize faults in the central resurgent dome. The small veins in the granite outside the caldera, beyond the major structural margin faults, could possibly be older than subsidence, but we consider this unlikely because they are only found within ~2 km of the caldera margin. $^{40}Ar/^{39}Ar$ dating (Bove et al., 2001) identified two episodes of mineralization after subsidence of Lake City caldera. The first episode is the same age as (or within error of) caldera collapse and resurgence and is represented by dated mineralization at Ute-Ulay mine (22.9 Ma) and at Red Mountain (23.1 Ma) (Fig. 2, Bove et al., 2001). The second is several million years younger, represented by dated mineralization at the Black Wonder mine (16.5 Ma), ~800 m outside the calderas southern margin (Fig. 2). This hydrothermal episode may have been driven by heat from small rhyolite intrusions of similar age (Bove et al., 2001). We have not been able to definitively correlate the veins in this study with either of these two ages, due to the lack of a distinctive mineralogy. However, it is clear that hydrothermal fluids have utilized caldera structures, and the spatial association with resurgent intrusion suggests strongly that the majority of the mineralization is associated with resurgence. We cannot preclude the possibility that some of the mineralization is younger, and previous research in the SJVF has shown that caldera structures often control the location of hydrothermal systems that are millions of years younger (Lipman et al., 1976; Lipman, 1992).

Mapping and scanlines show that vein orientations near the caldera margin (Figs. 5b and 7b) tend to be well-clustered around the structural margin orientation (apart from scanline W2 which is more variable, see Table 3), while veins farther away from the caldera margin mostly follow the regional northeast trend (Fig 8b). The majority of veins near the caldera margin are in a four to ten-meter-wide zone of increased vein density. The veins in the ring dike at Red Gulch may have formed by extensional reactivation and then infilling of dike-parallel shear fractures related to emplacement along the caldera margin (Fig. 7b). The veins near the southwestern caldera margin are most abundant in the highest strain fault rocks. The veins in these fault rocks follow a trend parallel to that of the caldera margin (E-W), rather than the regional NE-SW trend, showing that the structures related to caldera collapse are the primary control on fluid flow in this part of the caldera. The intense alteration, increased vein density, and hydrothermal oxygen isotope signature of the caldera margin (Larson and Taylor, 1986b) are consistent with a high degree of fluid-rock interaction along the discontinuity. Where the caldera margin cuts across the regional northeast-trending structural

grain, as at the western side of Lake City caldera (Fig. 7a), it creates additional fault and fracture intersections and potential for higher permeability (cf. Caine et al., 1996; Heap and Kennedy, 2016).

Scanlines across smaller faults inside the caldera do not always show such a clustering of orientations (e.g. circular variances of 0.48 and 0.71 for scanlines I4 and I5; see Table 3) or vein density close to the fault (Fig. 8b). Unlike scanlines SW1 and SW2, the fault cores of the faults sampled by intracaldera scanlines are thin (all one meter or less across) and almost entirely replaced or cemented by vein material (mostly quartz). The majority of veins sampled on the intra-caldera scanlines are therefore in the damage zone of the faults, rather than the fault core as in scanlines SW1 and SW2. This is possibly why vein orientations are more variable on intracaldera scanlines. In the damage zone around the faults, fluids may have utilized preexisting, variably oriented, fractures formed during cooling and structural doming of the tuff and syenite.

The limited vein kinematic data available suggest that the southwestern caldera margin may have been subject to N-S extension when the hydrothermal system was active (Fig. 6). This contrasts with the NW-SE extension on the resurgent dome, forming NE-SW-trending normal faults (Figs. 2 and 8) and the E-W-extension direction suggested by numerous dilational veins on the western margin (Fig. 7). It has been suggested that Lake City caldera formed during the onset of regional E-W extension in the western United States, which formed the Rio Grande rift and Basin and Range system (Bove et al., 2001); however, there is no geologic evidence for regional extension prior to 21 Ma (Ingersoll, 2001). The range in orientations of extensional veins at Lake City caldera suggests that the stress field at the time of hydrothermal activity was variable. The regional stress cannot be determined without more widespread and robust vein kinematic data and age control, i.e. whether veins in the southwestern, western and central caldera were contemporaneous. It can be concluded that spatial and/or temporal perturbations in the stress field were important in facilitating vein formation. The variable stress field at Lake City caldera may have been due to a complex interplay between regional stress, resurgent uplift, and extension in the apical graben in the center and on top of the resurgent dome.

Lithology has an important influence on fluid flow in hydrothermal systems (Wood et al., 2001; Rosenberg et al., 2009; Bignall et al., 2010; Farquharson et al., 2015). The physical

properties of rocks can determine whether a lithology promotes or hinders fluid flow, and whether fluid flow is along discontinuities or distributed through the rock matrix (Bignall et al., 2010; Heap and Kennedy, 2015; Siratovich et al., 2016). Rocks that have high strength deform brittlely to form discrete fractures that increase permeability (Rowland and Simmons, 2012). Repeated fracturing can sustain permeability after fractures seal due to mineralization. Low strength rocks are generally only able to sustain fluid flow if they have a high enough intrinsic permeability, unless the processes of alteration and/or silicification increase the rock strength to a high enough level that it can fracture (Henneberger and Browne, 1988; Rowland and Simmons, 2012). In most modern geothermal systems, fluid permeability is predominantly facilitated by fractures rather than matrix or intergranular flow (Grindley, 1970; Cas et al., 2011; Rowland and Simmons, 2012; Vignaroli et al., 2015; Siratovich et al., 2016). Rock strength testing has not been conducted on the lithologies at Lake City caldera; however, qualitatively one can observe that the intra-caldera breccias are more porous and weaker than the granite, welded tuff, intrusive rhyolite, and syenite. This is one of the reasons why at the map scale of tens to hundreds of meters there are fewer veins in the intra-caldera breccia near the caldera margin than the adjacent granite (Fig. 5a). In strong rock types near the caldera margin, such as the granite, the deformation associated with ring fault displacement will be important for creating fractures and facilitating fluid flow through the otherwise impermeable rock.

2.6.2. Implications for Fluid Flow

Lake City caldera and its structural margin are not uniformly altered or mineralized (Fig. 2). Understanding why some areas were subject to hydrothermal fluid flow and not others is what is important for better exploiting caldera-hosted geothermal and mineral resources. From this study at Lake City caldera we have identified three main factors that influence fluid flow: 1) The spatial relationship of lithologies inside and adjacent to the caldera; 2) the density of discontinuities (faults and fractures); and 3) the orientation of discontinuities. Favorable combinations of these factors promote fluid flow. Table 1 shows that hydrothermal fluids can be hosted in a variety of caldera related settings. We suggest that the favorable combination of the three factors promote hydrothermal fluid flow, and these can occur in any part of a caldera.

2.6.2.1. Spatial relationship of lithologies

The arrangement of lithologies inside and near the caldera has important implications for hydrothermal fluid flow. A key requirement for any geothermal system is a heat source. In the Lake City system, the caldera-related magmatism was the heat source (Larson and Taylor, 1986b). The areas near the syenite and monzonite intrusions were, therefore, near a heat source, and are generally altered and contain mineralized faults (Figs. 2 and 8a). Similarly, parts of the ring fault containing rhyolite are always associated with alteration whereas many parts of the ring fault without intrusions are unaffected by alteration (Fig. 2). Little alteration, or veining, is visible in the southeast part of the caldera interior where no intrusive rocks are exposed, and there is no evidence of structural pathways.

The arrangement of lithologies is also important for fluid flow localization. If the caldera margin discontinuity consists of undeformed, welded intracaldera tuff in contact with undeformed country rock, then the margin may not exhibit higher permeability than most of the caldera fill. If the margin consists of poorly to moderately consolidated landslide breccias in contact with undeformed country rock, then fluid flow may be localized through the more porous breccias but be facilitated by matrix flow rather than through fractures or veins. Oxygen-isotope studies of the altered rocks at Lake City have found that the stratigraphically lower elevation intra-caldera landslide breccias have higher water-rock ratios than adjacent welded ignimbrite (Larson and Taylor, 1986b). This suggests that breccia layers were permeable fluid pathways. The brecciated granite facies near the caldera ring fault would also have likely been more permeable than the unbrecciated granite due to the increased porosity and the granulated matrix. The permeability structure of the caldera margin will in part depend on the extent to which these fault rocks are preserved near the ring fault. Lithology has been interpreted to be an important factor in other caldera-related geothermal systems worldwide despite there being few published examples. In the Taupō Volcanic Zone of New Zealand, primary lithology has been recognized as an important control on hydrothermal fluid flow in the Ohaaki and Mokai geothermal systems (Bignall et al., 2010; Rissmann et al., 2011). At Ohaaki, the location of lava domes influences the distribution of permeable zones due to both the primary lithologies formed during dome emplacement and the response of these lithologies to faulting, fracturing, and sealing by hydrothermal minerals (Grindley, 1970; Rissmann et al., 2011).

2.6.2.2. Density of discontinuities

Discontinuities (i.e. fractures and faults) may provide permeability through rock masses with low intrinsic intergranular permeability (Sagar and Runchal, 1982; Evans et al., 1997). An area of the caldera setting that has a higher density of these discontinuities will, therefore, be more conducive to hydrothermal fluid flow. At Lake City caldera, this occurs at two different scales. At the wider map scale, the center of the caldera is dissected by numerous small-displacement normal faults (Fig. 8a), with >3 faults/km^2, over most of the resurgent dome, up to ~10 faults/km^2. By comparison, the southeastern part of the caldera, between Sunshine Peak and Grassy Mountain, has <1 fault/km^2 and is the least altered part of the caldera (Fig. 2). The high density of faults (>3/km^2) in the center of the caldera meant that fluid could readily flow through the welded Sunshine Peak tuff. Individually each of these faults lacks a wide 'halo' of fractures around it (usually less than two meters wide), and many of these fractures (which are now infilled to form veins) are of variable orientations and unrelated to the damage zone of the fault itself (Figs. 8b and 9). This contrasts with the wide (>50 m) zone of veins in the fault core of the caldera margin fault (Fig. 5b). Because there are many faults (>3/km^2, compared to <1/km^2 in the least altered part of the caldera) inside the caldera, there is still good permeability through the rock mass, even though each individual fault is providing a narrow (<2 m) corridor for fluid flow. Resurgent domes with a high density of normal faults have been interpreted to be important for hydrothermal fluid circulation in other calderas, such as Creede (Goff and Gardener, 1994; Bethke, 2001) and Valles in the United States, and Snowdon in the United Kingdom (Reedman et al., 1985) (Table 1). In contrast to the interior of Lake City caldera, the caldera margin faults and ring dykes have wider zones of increased fracture and/or vein density up to >60 meters thick (Figs. 5b, 7b, and 9b). These large and highly veined zones are restricted to only a few areas along the caldera margin (e.g. Shelf Road and Red Gulch, Figs. 5 and 7) where a large halo of subsidiary fractures exhibits enhanced fluid flow.

2.6.2.3. Orientation of discontinuities

The orientation of faults and fractures is a third important factor in controlling hydrothermal fluid flow. Certain fault and fracture orientations are more likely to intersect and promote permeability in relation to the stress field (Jolie et al., 2015). Discontinuities that have a dilational tendency (greatest when perpendicular to σ_3) and/or are critically stressed (ratio of shear stress to normal stress is greater than the critical friction coefficient of the rock) are

generally most permeable (Barton et al., 1995; Jolie et al., 2015). The wide variety of orientations of extensional veins throughout Lake City caldera suggests that the orientation of principal stresses may be variable and difficult to predict in resurgent calderas. Additionally, fault and fracture networks that contain higher numbers of intersecting discontinuities, i.e. that have a higher connectivity, will be more permeable than those that do not (Johnston and Lowell, 1961; de Dreuzy et al., 2001; Faulds et al., 2011). The creation of discontinuity intersections is dependent on both the density and orientation of discontinuities (Faulds et al., 2011; Jafari and Babadagli, 2012; Rowland and Simmons, 2012). In Lake City, regional structure (NE-SW) interacts with subsidence and resurgent structures during postcollapse magmatism. On the western side of the caldera (Fig. 5b), the margin is almost perpendicular to the prevailing NE trend of the Eureka Graben (see also Fig. 2) and rhyolite intrusion occurs along the ring fault. At the outcrop scale, the "halo" of smaller veins near the margin of the ring dike closely matches the N-S orientation of the caldera margin itself (Fig. 7b), so that fracture intersections would be enhanced with the variably oriented veins outside the caldera. The southwestern portion of the caldera contains fault and/or vein intersections between the ring fault, splays off the ring fault, and mineralized pre-existing dykes (Fig. 5a), but no intrusions are present. These intersections provide an additional range of structural orientations (NW-SE intersecting with E-W) associated with the ring fault, and the veins are evidence for the large volumes of fluid they transported. The sudden change in orientation at this corner in the southwestern part of the caldera is more likely to produce fault and fracture intersections than if the orientation changed gradually as a more classic subcircular ring fault. Inside the caldera, resurgent structures are typically subparallel (as are reactivated regional structures); however, slight differences in orientation and the high density (>3 faults/km^2) of faults still produce intersections (Fig. 8). Favorable discontinuity orientations are therefore any that form an intersecting "mesh". Along the caldera margin, this is most likely at ring fault corners or where the ring fault intersects regional structural grain (e.g. the N-S-oriented Lake City margin intersecting the NE-SW Eureka Graben). Fault intersections between pre-existing regional faults that accommodated caldera collapse and resurgence have been interpreted to be important in localizing hydrothermal fluid flow in Long Valley caldera (Suemnicht and Varga, 1988), similar in principal to interactions interpreted in this study along the southwestern and western margin of Lake City caldera. Rytuba (1994) also emphasized the importance of intersections between caldera and regional structures in localizing ore deposits. The difference in the orientation of veins in large caldera margin faults versus the damage zone of smaller intra-caldera faults may also affect permeability

anisotropy. The veins surrounding a small intra-caldera fault have variable orientations (Fig. 8b), which may mean the fault is equally permeable in all directions. However, on the caldera structural margin where most veins are parallel to the ring fault (Figs. 5b and 7b), permeability may be higher in the along-fault direction than across the fault. This is because fluid pathways will be more tortuous in the across fault direction, and more tortuous fracture networks result in lower permeability (Heap and Kennedy, 2015).

2.6.2.4. Compartmentalization of fluid flow

Faults are not usually effective conduits for fluid flow along their entire length, and fluid flow is compartmentalized to specific portions of a fault. In non-caldera settings, causes of this compartmentalization include differing sizes of fault cores and damage zones, intersections with other faults, and other structural complexities such as accommodation zones (Caine et al., 1996; Rowland and Sibson, 2004; Rowland and Simmons, 2012; Vignaroli et al., 2013; Maffucci et al., 2015). The compartmentalization occurs on a variety of scales. In the Taupō Volcanic Zone (TVZ) of New Zealand, the Paeroa fault system has discrete geothermal systems (Waikite, Te Kopia, and Orakeikorako) along its length separated by several kilometers (Kissling et al., 2015). The geothermal systems are sited where structural factors are particularly favorable for permeability; at Orakeikorako, there is a high density of small normal faults linking the larger Paeroa and Whakaheke faults; while Te Kopia is sited where the deformation zone associated with the Paeroa fault is particularly wide, due to extension of the fault footwall (Rowland and Sibson, 2004; Rowland and Simmons, 2012). Similar compartmentalization of geothermal fluid flow occurs along the normal fault systems of the Dixie Valley in Nevada. Extensive geothermal drilling has revealed complex patterns of faults and fractures that result in similarly complex permeability pathways in what had previously been assumed to be a large, simple normal fault (Blackwell et al., 2009). The Lake City caldera margin is not altered and mineralized along its entire length; fluid flow was focused in discrete areas tens to thousands of meters apart (Figs. 2, 5a, and 7a). This compartmentalization may be due to similar factors as those discussed above for tectonic faults. However, caldera margins may be even more likely to have large differences in permeability along their length due to added complexities that are not as common in non-caldera related settings. These added complexities include large scale landsliding and destruction of fault rocks (due to the large displacement accommodated in a short amount of time) and common modification of the structural margin by

syndeformational and postdeformational magmatism. Therefore, the heterogeneous nature of calderas and their margins requires a conceptual framework that identifies the character and spatial relationship of factors that enhance fluid flow.

2.6.2.5. Conceptual model of fluid flow at Lake City

The parts of Lake City caldera that are most altered can be shown to have combinations of the three important factors: 1) favorable lithologies, 2) high densities of faults and fractures (e.g. >3 faults/km^2 in the center versus <1 fault/km^2 in the southeastern part), and 3) favorable orientations and/or intersections of faults and fractures (e.g. ring fault cross-cutting regional structural grain). Hydrothermal fluid flow in the center of the caldera is aided by the close proximity to the syenite pluton heat source and a high density of small-displacement normal faults. The southwestern corner of the caldera has a high density of faults due to the structural complexities of accommodating caldera displacement at the caldera corner, and these complexities create fault intersections that enhance permeability. The western margin of the caldera is close to a heat source in the ring dyke, and cuts across the northeast-trending Eureka Graben, creating fault intersections that are highly permeable. Figure 10 is a conceptual cartoon of a caldera that shows how these factors may interact to explain why some areas of a caldera promote fluid flow while others do not. It must be emphasized that these three factors are not the only important variables. While these factors are important at Lake City, other factors may be as important in other systems worldwide. A similar general model for hydrothermal fluid flow in caldera settings has been proposed by Rytuba (1994), who emphasized extra-caldera deformation, intersections with regional structures, and high structural complexity as favorable for the localization of ore deposits. Our conceptual model for Lake City caldera is similar to that proposed by Larson and Taylor (1986b); their model comprised a convecting hydrothermal system that utilized the ring fault and permeable breccias to transport fluid from depth to the shallow resurgent dome. However, we recognize a wider zone of caldera margin deformation and emphasize the importance of discontinuity intersections and destruction of fault rocks during subsequent gravitational collapse events to explain the discontinuous nature of veins and alteration along the caldera margin. This study has also added a quantitative understanding of the width of the fluid transport corridor around smaller-displacement (<150 m) faults, which is usually less than five meters (Fig. 8b), versus the caldera margin, which is more than 50 m across (Fig. 5b).

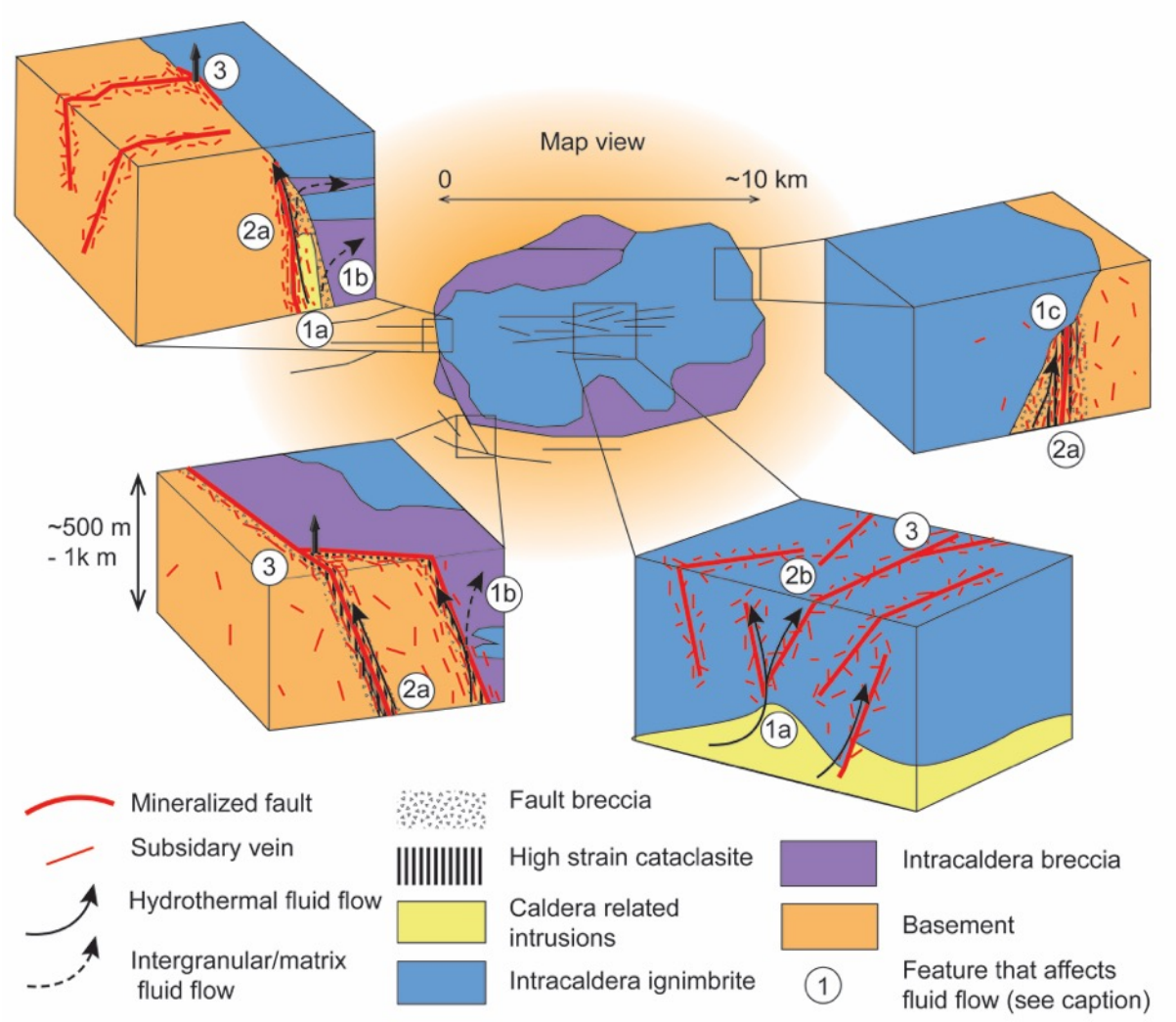

Figure 10: Conceptual model of hydrothermal fluid flow in caldera hosted settings, and how fluid flow is influenced by lithology, density of discontinuities, and orientation of discontinuities. Numbers refer to features that affect fluid flow related to the main three factors of (1) lithology, (2) density of discontinuities, and (3) orientation of discontinuities. 1a-Intrusive rocks as heat sources for hydrothermal fluids. 1b-Intra-caldera breccias with high matrix permeability. 1c-Degradation of caldera margin, destroying permeable ring fault zone. 2a-Permeable fault rocks and fractures related to caldera structural margin. 2b-High density of small-displacement normal faults. 3-Permeable fault and fracture intersections.

2.7. CONCLUSIONS

Detailed field work at Lake City caldera revealed evidence for fossil fluid pathways at Lake City. Evidence for fluid pathways is spatially highly variable and dependent on three key geological factors: 1) favorable lithologies, such as permeable horizons and proximity to intrusion heat sources, 2) a high density of faults and fractures, and 3) favorable fault and fracture orientations that enhance the likelihood of permeable fault and fracture intersections.

The caldera interior has favorable conditions for fluid flow due to proximity to large shallow resurgent intrusions (Fig. 8a). Permeable lithologies such as breccias are present but less common than near the caldera margins. Along the caldera margin, rhyolite ring dykes locally

provide a source of heat, and widespread landslide and fault breccias are favorable sites for porous fluid flow (Figs. 5 and 10). Coherent fault rocks on the structural margin also supported abundant fractures (Fig. 5b). The ring fault itself has been destroyed in certain areas due to subsidence and related landsliding (e.g. Fig. 7a). Parts of the caldera margin that have been subject to more landsliding may have less fracture-controlled permeability through landslide breccias than areas where the structural margin and associated fault rocks are still intact (Fig. 10).

A density of >3 faults/km^2 is important in the center of the caldera and at the southwestern margin. The center of the caldera has a high density of small-displacement (<150 m) faults (Fig. 8a), which individually have narrower zones of veining than along the caldera margin (Fig. 8b). The high density of faults in the caldera center allows for fault intersections to occur, even though most faults have a northeast orientation (Fig. 8a). The southwestern caldera margin consists of joined rectilinear segments. Newly identified structures in granite basement outside the caldera reveal a ~300 m zone of deformation, wider than previously thought. The outer faults utilize pre-existing dyke-related weaknesses to accommodate caldera subsidence (Fig. 5a). Transects across the ring fault show it has a high vein density in the fault core (Fig. 5b). Fractures in the granite accommodated fluid flow outside of the caldera margin discontinuity.

The orientation of veins close to the caldera margin discontinuity generally matches that of the main ring fault (Figs. 9a and 10). This is the case even in areas where there is a strong regional structural grain almost perpendicular to the ring fault (Figs. 7 and 10). At the western caldera margin, the intersection of the regional northeast trending structural grain with the north trending faults and fractures of the caldera structural margin favors the creation of permeable intersections (Fig. 7a). The structural complexities of the corner created at joined rectilinear segments at the southwestern margin also favor permeable intersections (Fig. 5a). The combination of a high density of faults and slight differences in orientation allow the creation of fault intersections in the caldera center, even though there is a strong preferred northeast orientation (Fig. 8a).

Consistent with accounts at other calderas (Table 1), our results show that both caldera margins and resurgent intrusions in caldera centers provide areas for favorable fluid flow. We establish that at Lake City the proximity to the intrusion and high density of small faults

favors fluid flow within the caldera, whereas the brecciated lithologies, structural density, and structural intersections favor fluid flow at the margins.

2.8. ACKNOWLEDGEMENTS

We acknowledge Jim Cole for useful feedback on the manuscript; Cameron Windham, Jordan Lubbers, Matthew Hoffman, and Annie Waterbury for help with field work; Patrick Kelley and Cionnaith O'Dubhaigh for logistical help in Lake City; Josephine Hicks for help with scanline data entry and interpretation; and Jonathan Davidson for help with kinematic interpretation. Thomas Garden benefited from a GNS Science Ph.D. Scholarship from the Geothermal Resources of New Zealand Project Water-Rock Interactions, and funding from the Mercury Energy sponsored Source to Surface Program at the University of Canterbury, and the University of Canterbury Department of Geological Sciences Mason Trust fund. Reviews from Guido Giordano, Eoghan Holohan, an anonymous reviewer, and the Editor Shanaka de Silva greatly improved the manuscript.

2.9. REFERENCES CITED

Allard, P., Maiorani, A., Tedesco, D., Cortecci, G., and Turi, B., 1991, Isotopic study of the origin of sulfur and carbon in Solfatara fumaroles, Campi Flegrei caldera: Journal of Volcanology and Geothermal Research, v. 48, p. 139–159, doi: 10.1016/0377-0273(91)90039-3.

Allmendinger, R.W., Cardozo, N., and Fisher, D., 2012, Structural Geology Algorithms: Vectors and Tensors: New York, Cambridge University Press, 302 p.

Arribas, A., Jr., Cunningham, C.G., Rytuba, J.J., Rye, R.O., Kelly, W.C., Podwysocki, M.H., McKee, E.H., and Tosdal, R.M., 1995, Geology, geochronology, fluid inclusions, and isotope geochemistry of the Rodalquilar gold alunite deposit, Spain: Economic Geology, v. 90, p. 795–822, doi: 10.2113/gsecongeo.90.4.795.

Ashwell, P.A., Kennedy, B.M., Gravley, D.M., von Aulock, F.W., and Cole, J.W., 2013, Insights into caldera and regional structures and magma body distribution from lava domes at Rotorua Caldera, New Zealand: Journal of Volcanology and Geothermal Research, v. 258, p. 187–202, doi: 10.1016/j.jvolgeores.2013.04.014.

Barton, C. a., Zoback, M.D., and Moos, D., 1995, Fluid flow along potentially active faults in crystalline rock: Geology, v. 23, p. 683.

Beate, B., Inguaggiato, S., Villares, F., Benitez, S., and Hidalgo, S., 2010, The Cachiyacu geothermal prospect, Chacana caldera, Ecuador: Proceedings World Geothermal Congress 2010, Bali, Indonesia, 9 p.

Bennati, L., Finizola, A., Walker, J.A., Lopez, D.L., Higuera-Diaz, I.C., Schütze, C., Barahona, F., Cartagena, R., Conde, V., Funes, R., and Rios, C., 2011, Fluid circulation in a complex volcano-tectonic setting, inferred from self-potential and soil CO_2 flux surveys: The Santa María–Cerro Quemado–Zunil volcanoes and Xela caldera (Northwestern Guatemala): Journal of Volcanology and Geothermal Research, v. 199, p. 216–229, doi: 10.1016/j.jvolgeores.2010.11.008.

Bethke, P.M., 2001, Preliminary scientific results of the Creede caldera continental scientific drilling program: U.S. Geological Survey Open-File Report 94–260–A, 16 p.

Bethke, P.M., Barton, P.B., Lanphere, M.A., and Steven, T.A., 1976, Environment of ore deposition in the Creede mining district, San Juan Mountains, Colorado: II. Age of mineralization: Economic Geology, v. 71, p. 1006–1011, doi: 10.2113/gsecongeo.71.6.1006.

Bethke, P.M., Rye, R.O., Stoffregen, R.E., and Vikre, P.G., 2005, Evolution of the magmatic-hydrothermal acid-sulfate system at Summitville, Colorado: Integration of geological, stable-isotope, and fluid-inclusion evidence: Chemical Geology, v. 215, p. 281–315, doi: 10.1016/j.chemgeo.2004.06.041.

Bignall, G., Rae, A.J., and Rosenberg, M.D., 2010, Rationale for targeting fault versus formation-hosted permeability in high-temperature geothermal systems of the Taupō Volcanic Zone, New Zealand: Proceedings World Geothermal Congress 2010, Bali, Indonesia.

Blackwell, D.D., Smith, R.P., Waibel, A., Richards, M.C., and Stepp, P., 2009, Why Basin and Range systems are hard to find II: Structural model of the producing geothermal system in Dixie Valley, Nevada: Geothermal Resources Council Transactions, v. 33, p. 441–446.

Bons, P.D., Elburg, M.A., and Gomez-Rivas, E., 2012, A review of the formation of tectonic veins and their microstructures: Journal of Structural Geology, v. 43, p. 33–62, doi: 10.1016/j.jsg.2012.07.005.

Bove, D.J., Hon, K., Budding, K.E., Slack, J.F., Snee, L.W., and Yeoman, R.A., 2001,

Geochronology and geology of late Oligocene through Miocene volcanism and mineralization in the western San Juan Mountains, Colorado: U.S. Geological Survey Professional Paper 1642, 30 p.

Branney, M., and Acocella, V., 2015, Calderas, *in* Sigurdsson, H., ed., The Encyclopedia of Volcanoes (second edition): London, Elsevier Inc., p. 299-315.

Caine, J.S., Evans, J.P., and Forster, C.B., 1996, Fault zone architecture and permeability structure: Geology, v. 24, p. 1025–1028.

Caratori Tontini, F., de Ronde, C.E.J., Scott, B.J., Soengkono, S., Stagpoole, V., Timm, C., and Tivey, M., 2016, Interpretation of gravity and magnetic anomalies at Lake Rotomahana: Geological and hydrothermal implications: Journal of Volcanology and Geothermal Research, v. 314, p. 84–94, doi: 10.1016/j.jvolgeores.2015.07.002.

Cardozo, N., and Allmendinger, R.W., 2013, Spherical projections with OSXStereonet: Computers and Geosciences, v. 51, p. 193–205, doi: 10.1016/j.cageo.2012.07.021.

Cas, R., Giordano, G., Balsamo, F., Esposito, A., and Lo Mastro, S., 2011, Hydrothermal breccia textures and processes: Lisca Bianca Islet, Panarea Volcano, Aeolian Islands, Italy: Economic Geology, v. 106, p. 437–450, doi: 10.2113/econgeo.106.3.437.

Castor, S.B., and Henry, C.D., 2000, Geology, geochemistry, and origin of volcanic rock-hosted uranium deposits in northwestern Nevada and southeastern Oregon, USA: Ore Geology Reviews, v. 16, p. 1–40, doi: 10.1016/S0169-1368(99)00021-9.

Chapin, C.E., 2012, Origin of the Colorado Mineral Belt: Geosphere, v. 8, p. 28–43, doi: 10.1130/GES00694.1.

Childs, C., Manzocchi, T., Walsh, J.J., Bonson, C.G., Nicol, A., and Schöpfer, M.P.J., 2009, A geo- metric model of fault zone and fault rock thickness variations: Journal of Structural Geology, v. 31, p. 117–127, doi: 10.1016/j.jsg.2008.08.009.

Cole, J., Milner, D., and Spinks, K., 2005, Calderas and caldera structures: A review: Earth-Science Reviews, v. 69, p. 1–26, doi: 10.1016/j.earscirev.2004.06.004.

Cunningham, C.G., Aparicio, H., Murillo S, F.M., Jiménez, N., Lizeca, J.L., McKee, E.H., Ericksen, G.E., and Tavera, F., 1994, Relationship between the Porco, Bolivia, Ag-Zn-Pb-Sn deposit and the Porco caldera: Economic Geology, v. 89, p. 1833–1841, doi: 10.2113/gsecongeo.89.8.1833.

de Dreuzy, J.-R., Davy, P., and Bour, O., 2001, Hydraulic properties of two-dimensional random fracture networks following a power law length distribution: 1. Effective connectivity: Water Resources Research, v. 37, p. 2065–2078, doi: 10.1029/2001WR900011.

Duex, T.W., and Henry, C.D., 1981, Calderas and mineralization: Volcanic geology and mineralization in the Chianti caldera complex, Trans-Pecos Texas: Bureau of Economic Geology, The University of Texas at Austin Geological Circular 81–2, 14 p.

Evans, J.P., Forster, C.B., and Goddard, J. V., 1997, Permeability of fault-related rocks, and implications for hydraulic structure of fault zones: Journal of Structural Geology, v. 19, p. 1393–1404, doi: 10.1016/S0191-8141(97)00057-6.

Farquharson, J., Heap, M.J., Varley, N.R., Baud, P., and Reuschlé, T., 2015, Permeability and porosity relationships of edifice-forming andesites: A combined field and laboratory study: Journal of Volcanology and Geothermal Research, v. 297, p. 52–68, doi: 10.1016/j.jvolgeores.2015.03.016.

Faulds, J.E., Hinz, N.H., Coolbaugh, M.F., Cashman, P.H., Kratt, C., Dering, G., Edwards, J., Mayhew, B., and Mclachlan, H., 2011, Assessment of favorable structural settings of geothermal systems in the Great Basin, western USA: Geothermal Resources Council Transactions, v. 35, p. 777–783.

Faulkner, D.R., Jackson, C.A.L., Lunn, R.J., Schlische, R.W., Shipton, Z.K., Wibberley, C.A.J., and Withjack, M.O., 2010, A review of recent developments concerning the structure, mechanics and fluid flow properties of fault zones: Journal of Structural Geology, v. 32, p. 1557–1575, doi: 10.1016/j.jsg.2010.06.009.

Ferrari, L., Gardufio, V.H., Pasquar, G., and Tibaldi, A., 1991, Geology of Los Azufres caldera, Mexico, and its relationships with regional tectonics: Journal of Volcanology and Geothermal Research, v. 47, p. 129–148.

Folkes, C.B., Wright, H.M., Cas, R.A.F., de Silva, S.L., Lesti, C., and Viramonte, J.G., 2011, A re-appraisal of the stratigraphy and volcanology of the Cerro Galán volcanic system, NW Argentina: Bulletin of Volcanology, v. 73, p. 1427–1454, doi: 10.1007/s00445-011-0459-y.

Fournier, R.O., 1989, Geochemistry and Dynamics of the Yellowstone National Park Hydrothermal System: Annual Reviews in Earth and Planetary Sciences, v. 17, p. 13–

53.

Fulignati, P., Malf, G., and Sbrana, A., 1997, The Pantelleria caldera geothermal system: Data from the hydrothermal minerals: Journal of Volcanology and Geothermal Research, v. 75, p. 251-270.

Gardeweg, M., and Ramirez, C.F., 1987, La Pacana caldera and the Atana Ignimbrite - A major ash-flow and resurgent caldera complex in the Andes of northern Chile: Bulletin of Volcanology, v. 49, p. 547-566.

Geyer, A., and Martí, J., 2014, A short review of our current understanding of the development of ring faults during collapse caldera formation: Frontiers in Earth Science, v. 2, p. 1–13, doi: 10.3389/feart.2014.00022.

Giordano, G., De Benedetti, A.A., Diana, A., Diano, G., Gaudioso, F., Marasco, F., Miceli, M., Mollo, S., Cas, R.A.F., and Funiciello, R., 2006, The Colli Albani mafic caldera (Roma, Italy): Stratigraphy, structure and petrology: Journal of Volcanology and Geothermal Research, v. 155, p. 49–80, doi: 10.1016/j.jvolgeores.2006.02.009.

Giordano, G., De Benedetti, A.A., Bonamico, A., Ramazzotti, P., and Mattei, M., 2014, Incorporating surface indicators of reservoir permeability into reservoir volume calculations : Application to the Colli Albani caldera and the Central Italy Geothermal Province: Earth Science Reviews, v. 128, p. 75–92, doi: 10.1016/j.earscirev.2013.10.010.

Goff, F., and Gardener, J.N., 1994, Evolution of a mineralized geothermal system, Valles caldera, New Mexico: Economic Geology, v. 89, p. 1803–1832.

Grindley, G.W., 1970, Subsurface structures and relation to steam production in the Broadlands geothermal field, New Zealand: Geothermics, v. 2, p. 248–261, doi: 10.1016/0375-6505(70)90024-6.

Guillou-Frottier, L., Burov, E.B., and Milési, J.-P., 2000, Genetic links between ash-flow calderas and associated ore deposits as revealed by large-scale thermo-mechanical modeling: Journal of Volcanology and Geothermal Research, v. 102, p. 339–361, doi: 10.1016/S0377-0273(00)00246-8.

Gustafson, L.B., Orquera, W., McWilliams, M., Castro, M., Olivares, O., Rojas, G., Maluenda, J., and Mendez, M., 2001, Multiple centers of mineralization in the Indio Muerto district, El Salvador, Chile: Economic Geology, v. 96, p. 325–350, doi:

10.2113/gsecongeo.96.2.325.

Guzmán, S., and Petrinovic, I., 2010, The Luingo caldera: The south-easternmost collapse caldera in the Altiplano-Puna plateau, NW Argentina: Journal of Volcanology and Geothermal Research, v. 194, p. 174–188, doi: 10.1016/j.jvolgeores.2010.05.009.

Heap, M.J., Baud, P., Meredith, P.G., Vinciguerra, S., and Reuschlé, T., 2014, The permeability and elastic moduli of tuff from Campi Flegrei, Italy: Implications for ground deformation modelling: Solid Earth, v. 5, p. 25–44, doi: 10.5194/se-5-25-2014.

Heap, M.J., and Kennedy, B.M., 2016, Exploring the scale-dependent permeability of fractured andesite: Earth and Planetary Science Letters, v. 447, p. 139–150, doi: 10.1016/j.epsl.2016.05.004.

Henley, R.W., and Ellis, A.J., 1983, Geothermal systems ancient and modern: A geochemical review: Earth Science Reviews, v. 19, p. 1–50, doi: 10.1016/0012-8252(83)90075-2.

Henneberger, R.C., and Browne, P.R.L., 1988, Hydrothermal alteration and evolution of the Ohakuri hydrothermal system, Taupō volcanic zone, New Zealand: Journal of Volcanology and Geothermal Research, v. 34, p. 211–231, doi: 10.1016/0377-0273(88)90034-0.

Henry, C.D., Elson, H.B., McIntosh, W.C., Heizler, M.T., and Castor, S.B., 1997, Brief duration of hydrothermal activity at Round Mountain, Nevada, determined from ^{40}Ar/^{39}Ar geochronology: Economic Geology, v. 92, p. 807–826, doi: 10.2113/gsecongeo.92.7-8.807.

Hildreth, W., 2017, Fluid-driven uplift at Long Valley Caldera, California: Geologic perspectives: Journal of Volcanology and Geothermal Research, v. 341, p. 269-286 doi: 10.1016/j.jvolgeores.2017.06.010.

Hochstein, M.P., and Sudarman, S., 1993, Geothermal resources of Sumatra: Geothermics, v. 22, p. 181–200.

Holohan, E.P., Walter, T.R., Schöpfer, M.P.J., Walsh, J.J., van Wyk de Vries, B., and Troll, V.R., 2013, Origins of oblique-slip faulting during caldera subsidence: Journal of Geophysical Research: Solid Earth, v. 118, p. 1778–1794, doi: 10.1002/jgrb.50057.

Hon, K.A., 1987, Geologic and petrologic evolution of the Lake City caldera, San Juan Mountains, Colorado [Ph.D. thesis]: University of Colorado at Boulder, 244 p.

Hon, K., Ludwig, K.R., Simmons, K.R., Slack, J.F., and Grauch, R.I., 1985, U-Pb isochron age and Pb isotope systematics of the Golden Fleece vein - Implications for the relationship of mineralization to the Lake City caldera, western San Juan Mountains, Colorado: Economic Geology, v. 80, p. 410–417.

Hulen, J.B., and Nielson, D.L., 1986, Hydrothermal alteration in the Baca geothermal system, Redondo Dome, Valles caldera, New Mexico: Journal of Geophysical Research, v. 91, p. 1867–1886.

Hurwitz, S., and Lowenstern, J.B., 2014, Dynamics of the Yellowstone hydrothermal system: Reviews of Geophysics, v. 51, p. 1-37, doi: 10.1002/2014RG000452.

Ingersoll, R. V, 2001, Structural and stratigraphic evolution of the Rio Grande Rift, northern New Mexico and southern Colorado: International Geology Review, v. 43, p. 867–891.

Jafari, A., and Babadagli, T., 2012, Estimation of equivalent fracture network permeability using fractal and statistical network properties: Journal of Petroleum Science and Engineering, v. 92–93, p. 110–123, doi: 10.1016/j.petrol.2012.06.007.

Johnston, W.P., and Lowell, J.D., 1961, Geology and origin of mineralized breccia pipes in Copper Basin, Arizona: Economic Geology, v. 56, p. 916–940.

Jolie, E., Moeck, I., and Faulds, J.E., 2015, Quantitative structural-geological exploration of fault-controlled geothermal systems - A case study from the Basin-and-Range Province, Nevada (USA): Geothermics, v. 54, p. 54–67, doi: 10.1016/j.geothermics.2014.10.003.

Kamb, W.B., 1959, Ice petrofabric observations from Blue Glacier, Washington, in relation to theory and experiment: Journal of Geophysical Research, v. 64, p. 1891–1909.

Kennedy, B., Stix, J., Vallance, J.W., Lavallée, Y., and Longpré, M.-A., 2004, Controls on caldera structure: Results from analogue sandbox modeling: Geological Society of America Bulletin, v. 116, p. 515, doi: 10.1130/B25228.1.

Kennedy, B., Wilcock, J., and Stix, J., 2012, Caldera resurgence during magma replenishment and rejuvenation at Valles and Lake City calderas: Bulletin of Volcanology, v. 74, p. 1833–1847, doi: 10.1007/s00445-012-0641-x.

Kennedy, B., Stix, J., Hon, K., Deering, C., and Gelman, S., 2015, Magma storage, differentiation, and interaction at Lake City caldera, Colorado, USA: Geological Society of America Bulletin, v. 128, p. 764–776, doi: 10.1130/B31305.1.

Kim, Y.S., Peacock, D.C.P., and Sanderson, D.J., 2004, Fault damage zones: Journal of Structural Geology, v. 26, p. 503–517, doi: 10.1016/j.jsg.2003.08.002.

Kissling, W.M., Rae, A.J., Villamor, P., and Ellis, S., 2015, Hydrothermal fluid flow in a structurally-controlled basin, Ngakuru graben, Taupō rift, New Zealand: Proceedings World Geothermal Congress 2015, Melbourne, Australia, 11 p.

Kissling, W.M., and Weir, G.J., 2005, The spatial distribution of the geothermal fields in the Taupō Volcanic Zone, New Zealand: Journal of Volcanology and Geothermal Research, v. 145, p. 136–150, doi: 10.1016/j.jvolgeores.2005.01.006.

Klein, C.W., McNitt, J.R., Sanyal, S.K., Abe, M., and Nakanishi, S., 1990, Corrosion vs. temperature: Field development options at Onikobe geothermal field, Miyagi Prefecture, Japan: Geothermal Resources Council Transactions, v. 14, p. 1493–1499, doi: 10.1080/09640560701402075.

Klemm, L.M., Pettke, T., and Heinrich, C.A., 2008, Fluid and source magma evolution of the Questa porphyry Mo deposit, New Mexico, USA: Mineralium Deposita, v. 43, p. 533–552, doi: 10.1007/s00126-008-0181-7.

Kokelaar, P., 2007, Friction melting, catastrophic dilation and breccia formation along caldera superfaults: Journal of the Geological Society of London, v. 164, p. 751-754.

Komuro, H., Aoyama, M., and Arayashiki, T., 2006, Collapse mechanism of the Paleogene Sakurae cauldron, SW Japan: Bulletin of Volcanology, v. 68, p. 631–640, doi: 10.1007/s00445-005-0036-3.

Larsen, E.S., and Cross, W., 1956, Geology and petrology of the San Juan region southwestern Colorado: U.S. Geological Survey Professional Paper 258, 303 p.

Larson, P.B., and Taylor, H.P., 1986a, An oxygen-isotope study of water-rock interaction in the granite of Cataract Gulch, western San Juan Mountains, Colorado: Geological Society of America Bulletin, v. 97, p. 505–515.

Larson, P.B., and Taylor, H.P., 1986b, An oxygen isotope study of hydrothermal alteration in the Lake City caldera, San Juan Mountains, Colorado: Journal of Volcanology and Geothermal Research, v. 30, p. 47–82.

Leonov, V.L., and Rogozin, A.N., 2010, Geologic development of the Karymshina caldera, Kamchatka, Russia, with special reference to its hydrothermal systems: Proceedings

World Geothermal Congress 2010, Bali, Indonesia, p. 25–29.

Lipman, P.W., 1976a, Caldera-collapse breccias in the western San Juan Mountains, Colorado: Geological Society of America Bulletin, v. 87, p. 1397-1410.

Lipman, P., 1976b, Geologic map of the Lake City caldera area, western San Juan Mountains, southwestern Colorado: U.S. Geological Survey Miscellaneous Investigations Series Map I-962, scale 1:48,000.

Lipman, P.W., 1992, Ash-flow calderas as structural controls of ore deposits - Recent work and future problems, *in* Thorman, C.H., ed., Application of Structural Geology to Mineral and Energy Resources of the Central and Western United States: U.S. Geological Survey Bulletin 2012, p. L1–L12.

Lipman, P.W., 2000, Calderas, *in* Sigurdsson, H., ed., Encyclopedia of Volcanoes: San Francisco, Academic Press, p. 643-662.

Lipman, P.W., and McIntosh, W.C., 2008, Eruptive and noneruptive calderas, northeastern San Juan Mountains, Colorado: Where did the ignimbrites come from? Geological Society of America Bulletin, v. 120, p. 771–795, doi: 10.1130/B26330.1.

Lipman, P.W., Steven, T.A., and Mehnert, H.H., 1970, Volcanic history of the San Juan Mountains, as indicated by potassium-argon dating: Geological Society of America Bulletin, v. 81, p. 2329–2352.

Lipman, P.W., Fisher, F.S., Mehnert, H.H., Naeser, C.W., Luedke, R.G., and Steven, T.A., 1976, Multiple Ages of Mid-Tertiary Mineralization and Alteration in the Western San Juan Mountains, Colorado: Economic Geology, v. 71, p. 571-588.

Lipman, P.W., Zimmerer, M.J., and Mcintosh, W.C., 2015, An ignimbrite caldera from the bottom up: Exhumed floor and fill of the resurgent Bonanza caldera, Southern Rocky Mountain volcanic field, Colorado: Geosphere, v. 11, p. 1902-1947, doi: 10.1130/GES01184.1.

Maffucci, R., Bigi, S., Corrado, S., Chiodi, A., Di Paolo, L., Giordano, G., and Invernizzi, C., 2015, Quality assessment of reservoirs by means of outcrop data and “discrete fracture network” models: The case history of Rosario de La Frontera (NW Argentina) geothermal system: Tectonophysics, v. 647, p. 112–131, doi: 10.1016/j.tecto.2015.02.016.

Manda, A.K., and Mabee, S.B., 2010, Comparison of three fracture sampling methods for layered rocks: International Journal of Rock Mechanics and Mining Sciences, v. 47, p. 218–226, doi: 10.1016/j.ijrmms.2009.12.004.

Marcoux, E., and Milési, J.-P., 1994, Epithermal gold deposits in West Java, Indonesia: Geology, age and crustal source: Journal of Geochemical Exploration, v. 50, p. 393–408, doi: 10.1016/0375-6742(94)90033-7.

Martí, J., Geyer, A., and Aguirre-Diaz, G., 2013, Origin and evolution of the Deception Island caldera (South Shetland Islands, Antarctica): Bulletin of Volcanology, v. 75, p. 732, doi: 10.1007/s00445-013-0732-3.

Matsuhisa, Y., Imaoka, T., and Murakami, N., 1980, Hydrothermal activity indicted by oxygen and hydrogen isotopes of rocks and minerals from a Paleogene cauldron, southwest Japan: Mining Geology Special Issue, p. 49–65.

Micarelli, L., Benedicto, A., and Wibberley, C.A.J., 2006, Structural evolution and permeability of normal fault zones in highly porous carbonate rocks: Journal of Structural Geology, v. 28, p. 1214–1227, doi: 10.1016/j.jsg.2006.03.036.

Milési, J.P., Marcoux, E., Sitorus, T., Simandjuntak, M., Leroy, J., and Bailly, L., 1999, Pongkor (west Java, Indonesia): A Pliocene supergene-enriched epithermal Au-Ag-Mn) deposit: Mineralium Deposita, v. 34, p. 131–149, doi: 10.1007/s001260050191.

Milner, D.M., Cole, J.W., and Wood, C.P., 2002, Asymmetric, multiple-block collapse at Rotorua Caldera, Taupō Volcanic Zone, New Zealand: Bulletin of Volcanology, v. 64, p. 134–149, doi: 10.1007/s00445-001-0191-0.

Mitchell, T.M., and Faulkner, D.R., 2009, The nature and origin of off-fault damage surrounding strike-slip fault zones with a wide range of displacements: A field study from the Atacama fault system, northern Chile: Journal of Structural Geology, v. 31, p. 802–816, doi: 10.1016/j.jsg.2009.05.002.

Miura, D., 1999, Arcuate pyroclastic conduits, ring faults, and coherent floor at Kumano caldera, southwest Honshu, Japan: Journal of Volcanology and Geothermal Research, v. 92, p. 271–294, doi: 10.1016/S0377-0273(99)00089-X.

Moore, I., and Kokelaar, P., 1998, Tectonically controlled piecemeal caldera collapse: A case study of Glencoe volcano, Scotland: Geological Society of America Bulletin, v. 110, p. 1448–1466.

Peltier, A., Hurst, T., Scott, B., and Cayol, V., 2009, Structures involved in the vertical deformation at Lake Taupō (New Zealand) between 1979 and 2007: New insights from numerical modelling: Journal of Volcanology and Geothermal Research, v. 181, p. 173–184, doi: 10.1016/j.jvolgeores.2009.01.017.

Petrinovic, I.A., Martí, J., Aguirre-Díaz, G.J., Guzmán, S., Geyer, A., and Paz, N.S., 2010, The Cerro Aguas Calientes caldera, NW Argentina: An example of a tectonically controlled, polygenetic collapse caldera, and its regional significance: Journal of Volcanology and Geothermal Research, v. 194, p. 15–26, doi: 10.1016/j.jvolgeores.2010.04.012.

Ponce S., B.F., and Clark, K.F., 1988, The Zacatecas mining district; a Tertiary caldera complex associated with precious and base metal mineralization: Economic Geology, v. 83, p. 1668–1682, doi: 10.2113/gsecongeo.83.8.1668.

Pride, D.E., and Hasenohr, E.J., 1983, Computer analysis of mineralization within evolving subvolcanic and caldera systems, Breckenridge and Bonanza Regions, Colorado Mineral Belt, U.S.A.: Journal of Geochemical Exploration, v. 19, p. 405–421, doi: 10.1016/0375-6742(83)90034-1.

Redwood, S.D., 1987, The Soledad Caldera, Bolivia: A Miocene caldera with associated epithermal Au-Ag-Cu-Pb-Zn mineralization: Geological Society of America Bulletin, v. 99, p. 395–404.

Reedman, A.J., Colman, T.B., Campbell, S.D.G., and Howells, M.F., 1985, Volcanogenic mineralization related to the Snowdon Volcanic Group (Ordovician), Gwynedd, North Wales: Journal of the Geological Society of London, v. 142, p. 875–888, doi: 10.1144/gsjgs.142.5.0875.

Rinaldi, A.P., Todesco, M., and Bonafede, M., 2010, Hydrothermal instability and ground displacement at the Campi Flegrei caldera: Physics of the Earth and Planetary Interiors, v. 178, p. 155–161, doi: 10.1016/j.pepi.2009.09.005.

Rissmann, C., Nicol, A., Cole, J., Kennedy, B., Fairley, J., Christenson, B., Leybourne, M., Milicich, S., Ring, U., and Gravley, D., 2011, Fluid flow associated with silicic lava domes and faults, Ohaaki hydrothermal field, New Zealand: Journal of Volcanology and Geothermal Research, v. 204, p. 12–26, doi: 10.1016/j.jvolgeores.2011.05.002.

Rosenberg, M.D., Bignall, G., and Rae, A.J., 2009, The geological framework of the

Wairakei–Tauhara Geothermal System, New Zealand: Geothermics, v. 38, p. 72–84, doi: 10.1016/j.geothermics.2009.01.001.

Rowland, J. V., and Sibson, R.H., 2004, Structural controls on hydrothermal flow in a segmented rift system, Taupō Volcanic Zone, New Zealand: Geofluids, v. 4, p. 259–283, doi: 10.1111/j.1468-8123.2004.00091.x.

Rowland, J. V., and Simmons, S.F., 2012, Hydrologic, Magmatic, and Tectonic Controls on Hydrothermal Flow, Taupō Volcanic Zone, New Zealand: Implications for the Formation of Epithermal Vein Deposits: Economic Geology, v. 107, p. 427–457, doi: 10.2113/econgeo.107.3.427.

Rytuba, J.J., 1976, Geology and ore deposits of the McDermitt caldera, Nevada-Oregon: U.S. Geological Survey Open-File Report 76-535, 9 p.

Rytuba, J.J., 1994, Evolution of volcanic and tectonic features in caldera settings and their importance in localization of ore deposits: Economic Geology, v. 89, p. 1687–1696, doi: 10.2113/gsecongeo.89.8.1687.

Sagar, B., and Runchal, A., 1982, Permeability of fractured rock: Effect of fracture size and data uncertainties: Water Resources Research, v. 18, p. 266–274.

Sanford, R.F., 1992, Lead isotopic compositions and paleohydrology of caldera-related epithermal veins, Lake City, Colorado: Geological Society of America Bulletin, v. 104, p. 1236–1245.

Sanford, R.F., Grauch, R.I., Hon, K., Bove, D.J., and Grauch, V.J.S., Korzeb, S.L., 1987, Mineral resources of the Redcloud Peak and Handies Peak Wilderness Study Areas, Hinsdale County, Colorado: U.S. Geological Survey Bulletin 1715-B, 35 p.

Sbrana, A., Fulignati, P., and Marianelli, P., 2010, Fast exhumation of a magmatic-hydrothermal system in a resurgent caldera environment. The example of Ischia Island (Italy): Proceedings of the World Geothermal Congress 2010, Bali, Indonesia, p. 646–647, doi:10.1144/0016-76492009-030.

Shannon, J., 1988, Geology of the Mount Aetna cauldron complex, Sawatch Range, Colorado [Ph.D. thesis]: Golden, Colorado, Colorado School of Mines, 434 p.

Sibson, R.H., 1987, Earthquake rupturing as a mineralizing agent in hydrothermal systems: Geology, v.15, p. 701–704, doi:10.1130/0091-7613(1987)15<701:ERAAMA>2.0.CO;2.

Siratovich, P.A., Heap, M.J., Villeneuve, M.C., Cole, J.W., Kennedy, B.M., Davidson, J., and Reuschlé, T., 2016, Mechanical behaviour of the Rotokawa Andesites (New Zealand): Insight into permeability evolution and stress-induced behaviour in an actively utilised geothermal reservoir: Geothermics, v. 64, p. 163–179, doi: 10.1016/j.geothermics.2016.05.005.

Slack, J.F., 1980, Multistage vein ores of the Lake City District, western San Juan Mountains, Colorado: Economic Geology, v. 75, p. 963-991

Smith, R.L., and Bailey, R.A., 1968, Resurgent Cauldrons: The Geological Society of America Memoirs, v. 116, p. 613-662

Smith, N., Cassidy, J., Locke, C. a., Mauk, J.L., and Christie, A.B., 2006, The role of regional-scale faults in controlling a trapdoor caldera, Coromandel Peninsula, New Zealand: Journal of Volcanology and Geothermal Research, v. 149, p. 312–328, doi: 10.1016/j.jvolgeores.2005.09.005.

Soden, A.M., and Shipton, Z.K., 2013, Dilational fault zone architecture in a welded ignimbrite: The importance of mechanical stratigraphy: Journal of Structural Geology, v. 51, p. 156–166, doi: 10.1016/j.jsg.2013.02.001.

Sorey, M.L., Suemnicht, G.A., Sturchio, N.C., and Nordquist, G.A., 1991, New evidence on the hydrothermal system in Long Valley caldera, California, from wells, fluid sampling, electrical geophysics, and age determinations of hot-spring deposits: Journal of Volcanology and Geothermal Research, v. 48, p. 229–263, doi: 10.1016/0377-0273(91)90045-2.

Spinks, K.D., Acocella, V., Cole, J.W., and Bassett, K.N., 2005, Structural control of volcanism and caldera development in the transtensional Taupō Volcanic Zone, New Zealand: Journal of Volcanology and Geothermal Research, v. 144, p. 7–22, doi: 10.1016/j.jvolgeores.2004.11.014.

Spray, J.G., 1997, Superfaults: Geology, v. 25, p. 579–582.

Stelling, P., Shevenell, L., Hinz, N., Coolbaugh, M., Melosh, G., and Cumming, W., 2016, Geothermal systems in volcanic arcs: Volcanic characteristics and surface manifestations as indicators of geothermal potential and favorability worldwide: Journal of Volcanology and Geothermal Research, v. 324, p. 57–72, doi: 10.1016/j.jvolgeores.2016.05.018.

Stix, J., Kennedy, B., Hannington, M., Gibson, H., Fiske, R., Mueller, W., and Franklin, J., 2003, Caldera-forming processes and the origin of submarine volcanogenic massive sulfide deposits: Geology, v. 31, p. 375–378.

Suemnicht, G.A., and Varga, R.J., 1988, Basement Structure and Implications for Hydrothermal Circulation Patterns in the Western Moat of Long Valley Caldera, California: Journal of Geophysical Research, v. 93, p. 13,191, doi: 10.1029/JB093iB11p13191.

Taylor, H.P., 1974, The application of oxygen and hydrogen isotope studies to problems of hydrothermal alteration and ore deposition: Economic Geology, v. 69, p. 843–883.

Terzaghi, R.D., 1965, Sources of Error in Joint Surveys: Géotechnique, v. 15, p. 287–304, doi: 10.1680/geot.1965.15.3.287.

Vignaroli, G., Pinton, A., De Benedetti, A.A., Giordano, G., Rossetti, F., Soligo, M., and Berardi, G., 2013, Structural compartmentalisation of a geothermal system, the Torre Alfina field (central Italy): Tectonophysics, v. 608, p. 482–498, doi: 10.1016/j.tecto.2013.08.040.

Vignaroli, G., Aldega, L., Balsamo, F., Billi, A., De Benedetti, A.A., De Filippis, L., Giordano, G., and Rossetti, F., 2015, A way to hydrothermal paroxysm, Colli Albani volcano, Italy: Bulletin of the Geological Society of America, v. 127, p. 672–687, doi: 10.1130/B31139.1.

Walker, R.J., Holdsworth, R.E., Armitage, P.J., and Faulkner, D.R., 2012, Fault zone permeability structure evolution in basalts: Geology, v. 41, p. 59–62, doi: 10.1130/G33508.1.

Wallis, I.C., Bardsley, C., Powell, T., Rowland, J. V., and Brien, J.M.O., 2013, A structural model for the Rotokawa geothermal field, New Zealand: Proceedings 35th New Zealand Geothermal Workshop 2013.

Whiteford, P.C., 1992, Evidence for geothermal areas beneath Lake Taupō from heat flow measurements: Proceedings 14th New Zealand Geothermal Workshop 1992, p. 185–188.

Wibberley, C.A.J., and Shimamoto, T., 2002, Internal structure and permeability of major strike-slip fault zones: The Median Tectonic Line in Mie Prefecture, Southwest Japan: Journal of Structural Geology, v. 25, p. 59–78, doi: 10.1016/S0191-8141(02)00014-7.

Wood, C.P., 1992, Geology of the Rotorua geothermal system: Geothermics, v. 21, p. 25–41, doi: 10.1016/0375-6505(92)90066-I.

Wood, C.P., 1994, Aspects of the geology of Waimangu, Waiotapu, Waikite and Reporoa geothermal systems, Taupō Volcanic Zone, New Zealand: Geothermics, v. 23, p. 401–421.

Wood, C.P., 1995, Calderas and geothermal systems in the Taupō Volcanic Zone, New Zealand: Proceedings World Geothermal Congress 1995, Florence, Italy, p. 1331–1336.

Wood, C.P., Brathwaite, R.L., and Rosenberg, M.D., 2001, Basement structure, lithology and permeability at Kawerau and Ohaaki geothermal fields, New Zealand: Geothermics, v. 30, p. 461–481, doi: 10.1016/S0375-6505(01)00003-7.

Woodcock, N.H., and Mort, K., 2008, Classification of fault breccias and related fault rocks: Geological Magazine, v. 145, p. 435–440, doi: 10.1017/S0016756808004883.

PREAMBLE

In the previous chapter I presented data from field mapping, scanline transects and petrographic analyses that suggest that permeability for hydrothermal fluids at Lake City caldera is enhanced where there are favourable combinations of permeable lithologies and densities and orientations of discontinuities that favour the formation of fault and fracture intersections. Estimation of the physiochemical conditions of the hydrothermal fluid can also be used to help reconstruct paleo-fluid pathways, and the evolution of the system through time. In the next chapter I explore the use of white mica composition as a tracer for changes in the physiochemical conditions of the fluid, and the application of reflectance spectroscopy as a tool to estimate white mica composition.

Chapter 3 has been submitted to *Journal of Geochemical Exploration*, and is currently under review. The chapter is presented in its submitted form, including the use of American English.

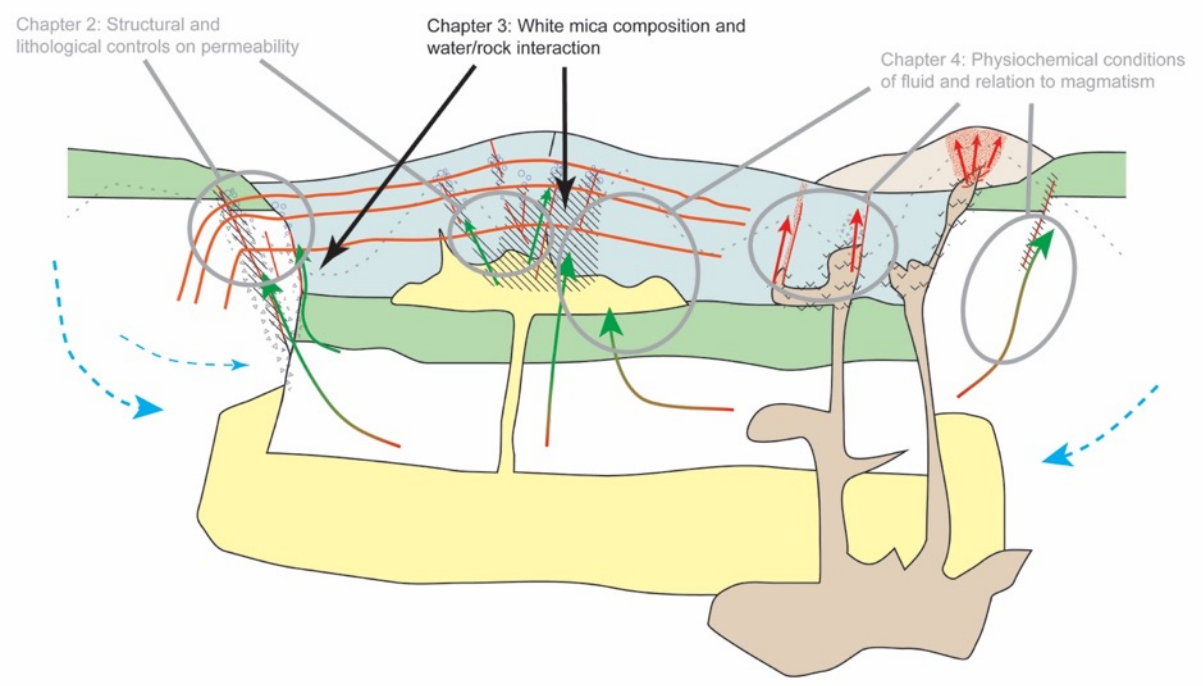

Simplified conceptual cartoon for hydrothermal fluid flow at Lake City caldera (cf. Chapter 4), showing the components of the model that are addressed in Chapter 3.

Chapter 3. A comparison and application of reflectance spectroscopy of white mica at Lake City caldera, U.S.A.: Implications for geothermal and ore exploration

3. A comparison and application of reflectance spectroscopy of white mica at Lake City Caldera, USA: implications for geothermal and ore exploration

3.1. ABSTRACT

Short wave infrared (SWIR) reflectance spectroscopy is a well-established tool for investigating alteration mineralogy and composition, with applications in ore and geothermal exploration. The composition (particularly aluminum content) of white mica varies according to the physiochemical conditions of formation, and correlates with the wavelength position of the 2200 nm AlOH absorption feature (λ_{AlOH}). The λ_{AlOH} parameter can therefore be used to track physiochemical gradients (e.g. pH, temperature, fluid/rock ratio), that may indicate fluid upflow zones. Currently there are a multitude of ground based SWIR spectrometers available, which mostly fall into one of two categories: 1) Portable, low spatial resolution systems (e.g. PIMA and TerraSpec), or 2) automated, high spatial resolution systems designed primarily for scanning lengths of drill core (e.g. Hylogger, Corescan and SisuCHEMA). In studying hydrothermal alteration, both of these types of systems may be used, however there is little published on how each performs specifically in analyzing λ_{AlOH}. In this study, we analyze 112 samples from the fossil hydrothermal system at Lake City caldera, Colorado, U.S.A. We use, as examples, a TerraSpec 4 and Corescan HCI-3 to compare results when measuring λ_{AlOH}. In addition, we analyze 16 samples with scanning electron microscope (SEM) energy-dispersive x-ray spectroscopy (EDS) to determine how the λ_{AlOH} measured for each technique compare with white mica composition. Corescan and TerraSpec results correlate well with each other but have small average differences (0.4 or 1.1 nm), the magnitude of which depend on how the data are processed. Both Corescan and TerraSpec λ_{AlOH} correlate well with white mica aluminum content, with the correlation slightly better for Corescan. High-Al white mica corresponds to short λ_{AlOH}. These results validate the accuracy and suitability of using the Corescan system, which is very poorly represented in the academic literature, to evaluate white mica composition. The spatial variability of λ_{AlOH} at Lake City caldera was evaluated with 327 samples using the Corescan HCI-3. High-Al white mica correlates with quartz-sericite-pyrite alteration and low $\delta^{18}O$ composition in the center of the caldera. However areas of distinctly low-Al white mica on the western caldera margin also have low $\delta^{18}O$ composition. These results suggest higher fluid/rock ratio, lower fluid pH, or higher temperature in the center of the caldera, however

more data are needed to determine the reason for the discrepancy between O-isotope and white mica composition data on the western caldera margin. Hand sample SWIR, particularly white mica λ_{AlOH}, provide an inexpensive and rapid analysis that can link low resolution satellite hyperspectral data and more detailed traditional methods such as petrography and fluid inclusion microthermometry.

3.2. INTRODUCTION

Short wave infrared (SWIR) reflectance spectroscopy has been widely used in mineral and geothermal exploration for rapid identification of alteration minerals and their composition, with little to no sample preparation (e.g. Herrmann et al., 2001; Yang et al., 2001; Jones et al., 2005; Yang et al., 2005; Simpson et al., 2009; Hosseinjani Zadeh et al., 2014). This contrasts with the more time consuming preparation and analysis required by other methods such as optical or electron microscopy and/or x-ray diffraction (XRD) (Yang et al., 2001; Mulder et al., 2013). The ease with which SWIR spectral reflectance data may be collected means many more samples may be analyzed in a given time compared to more traditional methods. This is important for delineating statistically robust patterns of alteration and mineralization, especially over large areas or long lengths of drill core, and makes SWIR reflectance spectroscopy a powerful tool for exploration (van Ruitenbeek et al., 2005). There are a variety of commercially available spectrometers currently used, such as the portable but lower spatial resolution systems produced by Integrated Spectronics Pty. Ltd (the PIMA instrument) and Analytical Spectral Devices Inc. (ASD) (Chang and Yang, 2012), and newer, higher resolution automated systems such as Corescan, HyLogger, and SisuCHEMA (Huntington et al., 2010; Dalm et al., 2017; Quigley and Yildirim, 2015) (Table 1). With many SWIR reflectance spectroscopy systems available it is important to be able to compare data among techniques and assess when the use of multiple techniques for exploration purposes is necessary.

The infrared response of minerals has long been used as an identification tool, particularly for clay minerals (Farmer, 1974; Van der Marel and Beutelspacher, 1976; Velde, 1978). Today the most widely used commercial SWIR reflectance spectrometers are portable low spatial resolution devices such as the ASD TerraSpec, which collects a spectrum from a circular window 25 mm in diameter. However, higher resolution, automated systems such as Corescan and HyLogger provide continuous coverage of higher resolution measurements

along a core or across a sample (Table 1). The Corescan system uses hyperspectral imaging to create a 0.5 mm resolution "photo" of the sample. Data can be displayed as a map, for example the white mica AlOH wavelength (λ_{AlOH}) can be compared with color photography and sample mineralogy (Fig. 1) (Quigley and Yildirim, 2015; Bellian et al., 2016). Corescan can also output a semi-quantitative mineral abundance, by counting how many 0.5 mm x 0.5 mm "pixels" detect a mineral. These high-resolution systems are intended for scanning lengths of drill core; however, in particular exploration settings, such as for geothermal, the availability of core material is often limited to nil. This study presents results obtained on hand samples.

Table 1: Comparison of exploration techniques

Technique	**Advantages**	**Disadvantages**
SWIR reflectance spectroscopy, low spatial resolution (e.g. TerraSpec)	Little to no sample preparation Can be used in the field (some instruments) Short analysis time	Large analysis window, therefore affected by overprinting and mixing of mineral spectra Can usually only identify two minerals per analysis Cannot identify many minerals, e.g. feldspars, quartz Can only indicate if a mineral is present or not, not how abundant it is.
SWIR reflectance spectroscopy, high spatial resolution (e.g. Corescan)	Can identify minerals at lower abundances than low resolution SWIR methods Allow imaging of textures and variations of mineralogy or composition at the sample scale Can provide semi-quantitative mineral abundances More analyses per sample, hence more statistical robustness	More time consuming and expensive than low-resolution methods Requires some preparation for use with hand samples Cannot identify some minerals, e.g. feldspars.
SWIR reflectance spectroscopy, aerial (aircraft, drone or satellite)	Wide aerial coverage No field work or sample collection needed	Low resolution

The white mica group of dioctahedral sheet silicates includes the minerals muscovite ($KAl_2[AlSi_3]O_{10}(OH)_2$), illite ($K_{0.65}Al_{2.0}[Al_{0.65}Si_{3.35}]O_{10}(OH)_2$), phengite

($KAl_{1.5}(Mg,Fe)_{0.5}[Al_{0.5}Si_{3.5}]O_{10}(OH)_2$), and paragonite ($NaAl_2[AlSi_3]O_{10}(OH)_2$) (Bailey, 1984). Muscovite and paragonite are end-members while illite and phengite are solid solutions. Fine-grained white mica is commonly called "sericite" during field exploration. White micas form in a variety of geological environments, and are common alteration products in many hydrothermal ore deposits and geothermal systems (Browne, 1978; Higashi, 1980; Parry et al., 1984). The aluminum, iron, magnesium and silicon content of hydrothermal white micas has long been known to vary according to the temperature, pressure, fluid composition and host-rock characteristics of the hydrothermal system (Velde, 1965; Higashi, 1980; Parry et al., 1984; Yang et al., 2011). Chemical variations in major elements are dominated by the Tschermak substitution, which is the coupled substitution in the octahedral (vi) site of Al^{3+} by Fe^{2+} and/or Mg^{2+}, and in the tetrahedral (iv) site of Al^{3+} by Si^{4+} (Duke, 1994). Short wave infrared reflectance spectroscopy is a useful tool for studying white mica because the wavelength position of the AlOH absorption feature between 2185 nm and 2235 nm (λ_{AlOH}) correlates with the white mica composition, particularly the Tschermak substitution, with shorter wavelengths correlating with higher aluminum content and lower iron and/or magnesium content (i.e. muscovitic compositions) (Duke, 1994; Beran, 2002; van Ruitenbeek et al., 2005; Yang et al., 2011; Doublier et al., 2010; Tappert et al., 2013). The link between the composition (and therefore λ_{AlOH}) of white mica and its physiochemical conditions of formation has led to it being used as an indicator of alteration intensity and/or rank . In ore deposits, λ_{AlOH} may systematically vary towards mineralization where mineralization correlates with rank or temperature of alteration and/or water/rock ratio (e.g. Jones et al., 2005; Yang et al., 2011; Harraden et al., 2013; Tappert et al., 2013). Due to the variety of physiochemical factors that affect white mica composition, there is no universal pattern of λ_{AlOH} variation correlating with a single variable such as temperature (Table 2; Swayze et al., 2014). However, shorter λ_{AlOH} (higher Al, more muscovitic composition) most commonly correlates with increased rank of alteration and/or increased fluid/rock interaction (e.g. Page and Wenk, 1979; Herrmann et al., 2001; Jones et al., 2005; Cohen, 2011; Harraden et al., 2013; Swayze et al., 2014; Chambefort et al., 2017, Table 2). The most notable exceptions to this pattern are in some volcanic hosted massive sulfide deposits with diverse lithologies (e.g. van Ruitenbeek et al., 2005; Yang et al., 2011, Table 2) and some active geothermal systems which show the opposite pattern or limited variability (e.g. Parry et al., 1984; Yang et al., 2000, Table 2). In summary, λ_{AlOH} can be a useful indicator of

hydrothermal mineralization and/or alteration facies and/or rank provided its interpretation is "calibrated" to the specific system of interest.

The aim of this study is to compare and assess the benefit of a multi-technique approach for field exploration. We compare data on the white mica λ_{AlOH} between reflectance spectroscopy techniques of different spatial resolutions, low resolution ASD TerraSpec and higher resolution Corescan, with white mica semi-quantitative chemistry data from scanning electron microscope with energy-dispersive x-ray spectroscopy (BSE-EDS). The data are collected from hydrothermally altered rocks inside and adjacent to Lake City caldera, Colorado, U.S.A. Lake City caldera was chosen for sampling because it is a well-studied fossil hydrothermal system that was explored for ore minerals (Sanford et al., 1987; Bove et al., 1990) and has spatially variable host rocks and mineral veining (Kennedy et al., and Garden et al. 2017). Advanced Spaceborne Thermal Emission and Reflection Radiometer (ASTER) SWIR satellite data have been interpreted and published for the Lake City area, and although some alteration zonation is apparent (e.g. dominated by white mica versus alunite), limited data are available in vegetated areas below the tree-line, and no compositional variation in white mica is reported (Rockwell, 2012). High topographic relief (>1,300 m) in the Lake City area also means sampling can cover a wide range of stratigraphic depths, which may relate to changing physiochemical conditions of formation. The variable nature of the host rocks and alteration allow measurement of a wide range of λ_{AlOH}.

Table 2: Comparison of previous studies on white mica composition in hydrothermal systems

Type and name of deposit or system	Host rocks					White mica aluminum composition and/or wavelength pattern										Reference
						Increasing Al towards higher:				Decreasing Al towards higher				No pattern	Complex pattern	
	Mafic	Inter.	Felsic	Sed.	Met.	Min.[1]	Acidity	Perm.[2]	Depth	Min.[1]	Acidity	Perm.[2]	Depth			
Active geothermal																
Broadlands - Ohaaki, N.Z.																Yang et al., 2001
Roosevelt Hot Springs, U.S.A.																Parry et al., 1984
Ngatamariki, N.Z.																Chambefort et al., 2017
Wairakei, N.Z.																Yang et al., 2000
Epithermal																
Cuprite, U.S.A.																Swayze et al., 2014
Favona, N.Z.																Simpson and Christie, 2016
Orogenic																
Elura, Australia																Sun et al., 2001
Macraes, N.Z.																Simpson et al., 2016
Reefton goldfield, N.Z.																Christie and Brathwaite, 2003
Porphyry																
Ann-Mason, U.S.A.																Cohen, 2011
Butte, U.S.A.																Page and Wenk, 1979

Type and name of deposit or system	Host rocks					White mica aluminum composition and/or wavelength pattern										Reference
						Increasing Al towards higher:				Decreasing Al towards higher				No	Complex	
	Mafic	Inter.	Felsic	Sed.	Met.	Min.[1]	Acidity	Perm.[2]	Depth	Min.[1]	Acidity	Perm.[2]	Depth	pattern	pattern	
Pebble, U.S.A.																Harraden et al., 2013
Tuwu, China																Yang et al., 2005
Tintic, U.S.A.																Parry et al., 1984
Volcanic hosted massive sulfide																
Glacier Creek, U.S.A.																Steeves et al., 2016
Hellyer, Australia																Yang et al., 2011
Highway-Reward, Australia																Herrmann et al., 2001
Panorama, Australia																Van Ruitenbeek et al., 2012
Western Tharsis, Australia																Herrmann et al., 2001
Other																
Olympic Dam, Australia																Tappert et al., 2013

Notes:

[1] Mineralization and/or rank of alteration

[2] Permeability

3.3. GEOLOGY AND HYDROTHERMAL SYSTEM OF LAKE CITY CALDERA

The 22.9 Ma Lake City caldera is the youngest caldera in the San Juan volcanic field (SJVF) of Colorado, U.S.A, and is the source of the Sunshine Peak tuff (SPT), which infills the caldera to a depth of at least 1.5 km (Bove et al., 2001). Widespread breccias are intercalated with the SPT inside the caldera. These breccias formed by gravitational collapse during caldera formation and are dominated by pre-caldera andesite and dacite lavas (Lipman, 1976a). A hydrothermal system formed soon after eruption, driven primarily by heat from resurgent syenite and monzonite plutons (Larson and Taylor, 1986b; Sanford, 1992). This formed quartz-dominated veins in the syenite and SPT of the central resurgent dome, along parts of the caldera margin, and the adjacent granite basement (Hon, 1987; Kennedy et al., 2012; Garden et al., 2017). This provides a unique window into an eroded hydrothermal system, and well-exposed alteration mineralogy. Widespread associated propylitic alteration is dominated by white mica, silica, chlorite and calcite, with widespread phyllic alteration (white mica, silica, pyrite) in the interior of the caldera and a smaller area of more intense argillic and advanced argillic alteration occurring at Red Mountain on the eastern caldera margin (Hon, 1987; Bove et al., 1990). Satellite SWIR data clearly define the acid alteration at Red Mountain, and shows a poorly defined area of dominantly sericite alteration without chlorite in the center of the caldera (Rockwell, 2012).

3.4. METHODS

3.4.1. Instruments

SWIR reflectance spectroscopy was undertaken using two systems: 1) an ASD TerraSpec 4 high-resolution portable field spectrometer at the GNS Science Wairakei Research Centre, New Zealand, and 2) a Corescan Hyperspectral Core Imager Mark III (HCI-3). The TerraSpec 4 has a 25-mm diameter analysis window, and a spectral resolution of 3 nm at 700 nm and 6 nm at longer wavelengths of 1400 to 2100 nm. The Corescan HCI-3 uses a 0.05 mm spatial resolution camera for visual sample imagery, and a 3.5 nm spectral resolution SWIR reflectance spectrometer with a 0.5 mm diameter analysis window. SEM work (BSE imaging and EDS) used a JEOL Neoscope 6000Plus SEM with EDS detector, at the GNS Science Wairakei Research Centre, New Zealand, and a JEOL JSM IT-300 SEM with an Oxford Aztec silicon drift detector EDS at the University of Canterbury, Christchurch, New Zealand.

3.4.2. Samples

Hand samples were collected from hydrothermal veins and adjacent altered rock inside Lake City caldera, on the margin, and in the surrounding granite basement. The rock types collected and analyzed include basement granite, welded tuff (Sunshine Peak Tuff), intra-caldera landslide breccia, syenite, and hydrothermal vein material. Most of the samples for Corescan analysis were slabs cut from hand samples. The Corescan HCI-3 was designed for logging lengths of drill core rather than hand samples, so the slabs were labelled and arranged in core trays for analysis. Representative areas of each slab, which were judged to show either the average or full range of texture and mineralogy, were cut into smaller thin-section sized blocks or "billets", 27 x 46 mm, which were used for TerraSpec analysis. A total of 327 samples (including the 112 above), from 173 locations, were measured with just Corescan in order to assess the spatial variation of λ_{AlOH} throughout Lake City caldera. After data reduction (see below) a total of 112 samples were compared between both TerraSpec and Corescan. Sixteen polished thin sections (30μm thick) were made for petrography and SEM analysis. See Appendix C for a list of all samples collected, their locations, and the analyses conducted on each.

3.4.3. Analytical Procedure

Corescan analyses produced continuous coverage of 0.5 x 0.5 mm "pixels" along a 40-mm wide strip of the sample slab, with the length analyzed depending on the size of the slab. Measurements were made using their standard operating parameters. For TerraSpec analyses, single measurements were taken on most billets, with multiple measurements made on samples where one measurement did not cover a satisfactory representative area. During TerraSpec measurements, calibration against a standard was conducted every ~60 minutes. The SEM BSE-EDS analysis was undertaken on thin sections, containing white mica crystals, with multiple individual EDS spectra measured in each area. Care was taken to avoid measuring extremely fine-grained areas or grains that could not be definitively identified as white mica by their composition, to reduce mixed signals from multiple minerals. Energy-dispersive x-ray spectroscopy data were quantified using standardless peak de-convolution, reported as oxide mass percent based on 24 oxygen.

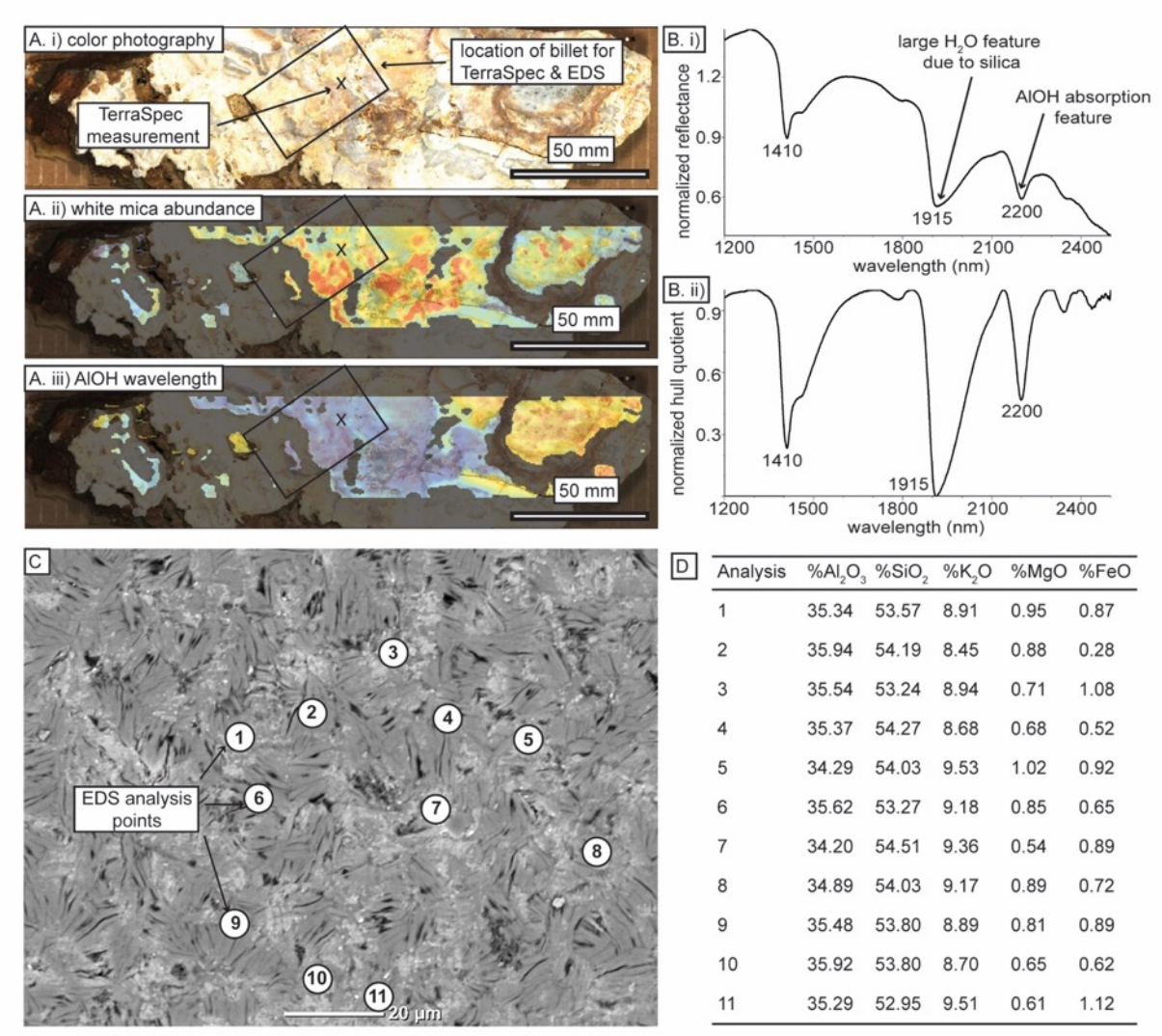

Analysis	%Al_2O_3	%SiO_2	%K_2O	%MgO	%FeO
1	35.34	53.57	8.91	0.95	0.87
2	35.94	54.19	8.45	0.88	0.28
3	35.54	53.24	8.94	0.71	1.08
4	35.37	54.27	8.68	0.68	0.52
5	34.29	54.03	9.53	1.02	0.92
6	35.62	53.27	9.18	0.85	0.65
7	34.20	54.51	9.36	0.54	0.89
8	34.89	54.03	9.17	0.89	0.72
9	35.48	53.80	8.89	0.81	0.89
10	35.92	53.80	8.70	0.65	0.62
11	35.29	52.95	9.51	0.61	1.12

Figure 1: Example of a comparison of the Corescan, TerraSpec and SEM BSE EDS methods for a single sample, LCBVRF091514-1B. A: Images of slab of hydrothermal vein and Corescan data. A. i) Visual imagery of sample, with area where thin section billet was cut from for TerraSpec and EDS. A. ii) Corescan data showing white mica abundance throughout the sample. Red = high abundance, blue = low abundance. A. iii) Corescan data showing the variation in AlOH wavelength throughout the sample. Blue = shorter wavelength, red = longer wavelength. B: TerraSpec spectra measured from the same sample. B. i) Uncorrected "raw" spectrum, with the wavelength of major absorption features labelled. The large H_2O feature is interpreted as being a result of aqueous fluid inclusions in quartz and silica. B. ii) Hull quotient corrected spectrum. C: SEM-BSE image of white mica from the same sample, showing location of EDS analysis points. Points shown are 11 of the 296 points analyzed on this sample, of which 223 were white mica analyses kept after data "cleaning". D: EDS oxide composition data from the 11 numbered points in panel B.

3.4.4. Data Reduction

For the TerraSpec data, mineral identification and calculation of λ_{AlOH} were made using 'The Spectral Geologist^{TM}' (TSG) software. Spectra that did not contain white mica or showed signs of strong mixing with other minerals were removed from the dataset. The numerical values of λ_{AlOH} were calculated using the Scalar function of TSG. The calculations were done on both the raw spectra and hull quotient corrected spectra (i.e. the background continuum removed). For the raw λ_{AlOH} the scalar parameters were set as follows: Spectral layer: reflectance; Center wavelength: 2204; Radius, 24; Smoothing: None; Profile type:

Wavelength at minimum. For the hull quotient λ_{AlOH} the parameters were the same but with the spectral layer: "Hull quot." (hull quotient). An index of the depth of the AlOH absorption feature compared to the H_2O feature is also sometimes used in mineral exploration. It has been considered as a measure of white mica "crystallinity" (Simpson et al., 2009; Dalm et al., 2017). This index was not compared in this study, as it is used less than λ_{AlOH}, and the TSG scalar is not directly comparable with the Corescan index. The high abundance of quartz and silica in the samples from Lake City, with their associated H_2O absorption features (due to fluid inclusions) also means crystallinity ratios based on the relative depth of the H_2O versus AlOH feature may not be accurate (Fig. 1). The mean of the λ_{AlOH} and the standard deviation were calculated for each sample. The mineral identification and calculation of λ_{AlOH} for the Corescan data was conducted by Corescan staff using their proprietary software.

For assessing the spatial variation in λ_{AlOH} with Corescan data, the mean λ_{AlOH} for each sampling location was calculated. Kriging of λ_{AlOH} was used to help objectively identify patterns in the spatial distribution of white mica compositions, and separate patterns from "noise", or variation at scales below the spacing of sampling. In contrast, contouring of the data without kriging would not reduce noise and would not elucidate patterns of broad spatial covariation beneath the noise. For the purposes of kriging, the sample location data were converted to the Universal Transverse Mercator (UTM) coordinate system, and a sample variogram produced using the software Surfer 12 by Golden Software (Fig. 2). The variogram shows that the λ_{AlOH} data are spatially auto-correlated at separation (lag) distances up to approximately 4000 m (Fig. 2). A spherical plus nugget variogram model was visually determined to have the most accurate shape, and was fitted using weighted least squares, following the procedure suggested by Oliver and Webster (2014). The resultant model has a nugget variance (y-intercept) of 12.45, a spatially correlated variance (scale) of 12.06, a sill of 24.51, and a range of 3750 m (Fig. 2). This variogram model was used for kriging the λ_{AlOH} data. Ordinary block kriging was used, with a 154 x 155 m block size.

Energy-dispersive x-ray spectroscopy (EDS) data were 'cleaned' by removing any analyses that showed signs of mineral mixing or were not white mica. Analyses were removed that identified more than 60% or less than 45% SiO_2. The EDS compositions were then averaged for each sample to allow comparison with Corescan and Terraspec data.

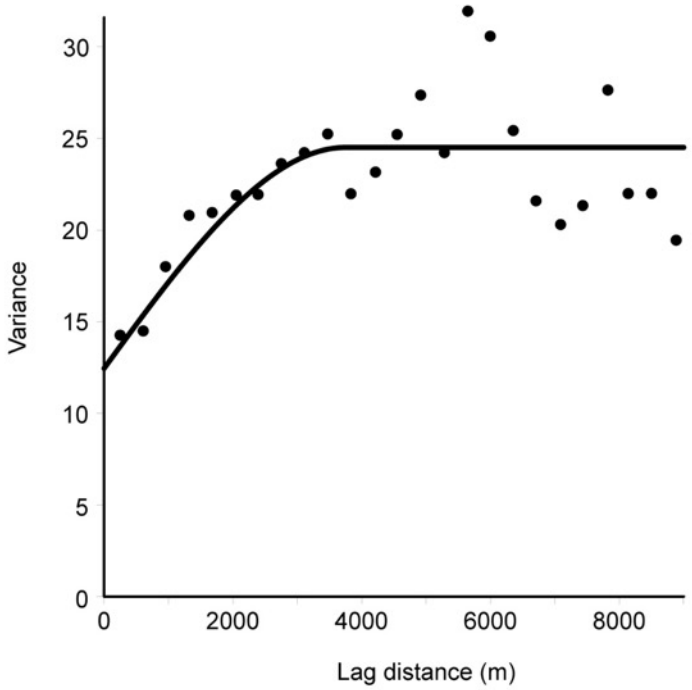

Figure 2: Sample/experimental variogram of λ_{AlOH} at Lake City caldera, computed from 159 sampling locations. The variogram has a total of 25 lags, with a lag width of 360 m, and a maximum lag distance of 9000 m. The solid line is the variogram model used for kriging. It is a spherical plus nugget model, with a nugget variance of 12.45, spatially correlated variance of 12.06, sill of 24.51 and range of 3750 m.

3.5. RESULTS

In this section we first compare how the TerraSpec and Corescan SWIR systems performed when measuring λ_{AlOH} on the same samples, and how the λ_{AlOH} measured by each system compares to the aluminum composition of white mica as determined by EDS. It was determined that the Corescan λ_{AlOH} was the most accurate in approximating white mica composition, so Corescan was used to assess the spatial variation in λ_{AlOH} at Lake City caldera.

3.5.1. AlOH wavelength: TerraSpec versus Corescan

Short wave infrared reflectance spectroscopy confirms the widespread abundance of and variation in white mica alteration at Lake City. Both the TerraSpec and Corescan methods detected a wide range of average λ_{AlOH}, from 2196 nm to 2217 nm for the raw (un-corrected) TerraSpec spectra (see Appendix D for all raw data), and 2194 nm to 2220 nm for Corescan. The raw and hull quotient TerraSpec values correlate well with each other (Fig. 2 and Table 2), however the hull wavelengths are consistently slightly lower than the raw (Fig. 3c and Table 2). Both the raw and hull quotient TerraSpec samples correlate with Corescan values,

though the correlation is slightly better for the raw spectra (Fig. 2, Table 2, and Appendix E). The raw TerraSpec wavelengths are on average slightly higher than Corescan, while the hull quotient TerraSpec values are slightly lower than Corescan (Table 2, Figs. 3a and 3b). Some outliers have large differences between the TerraSpec and Corescan λ_{AlOH} values, and between the TerraSpec raw and hull quotient (Figs. 2 and 3).

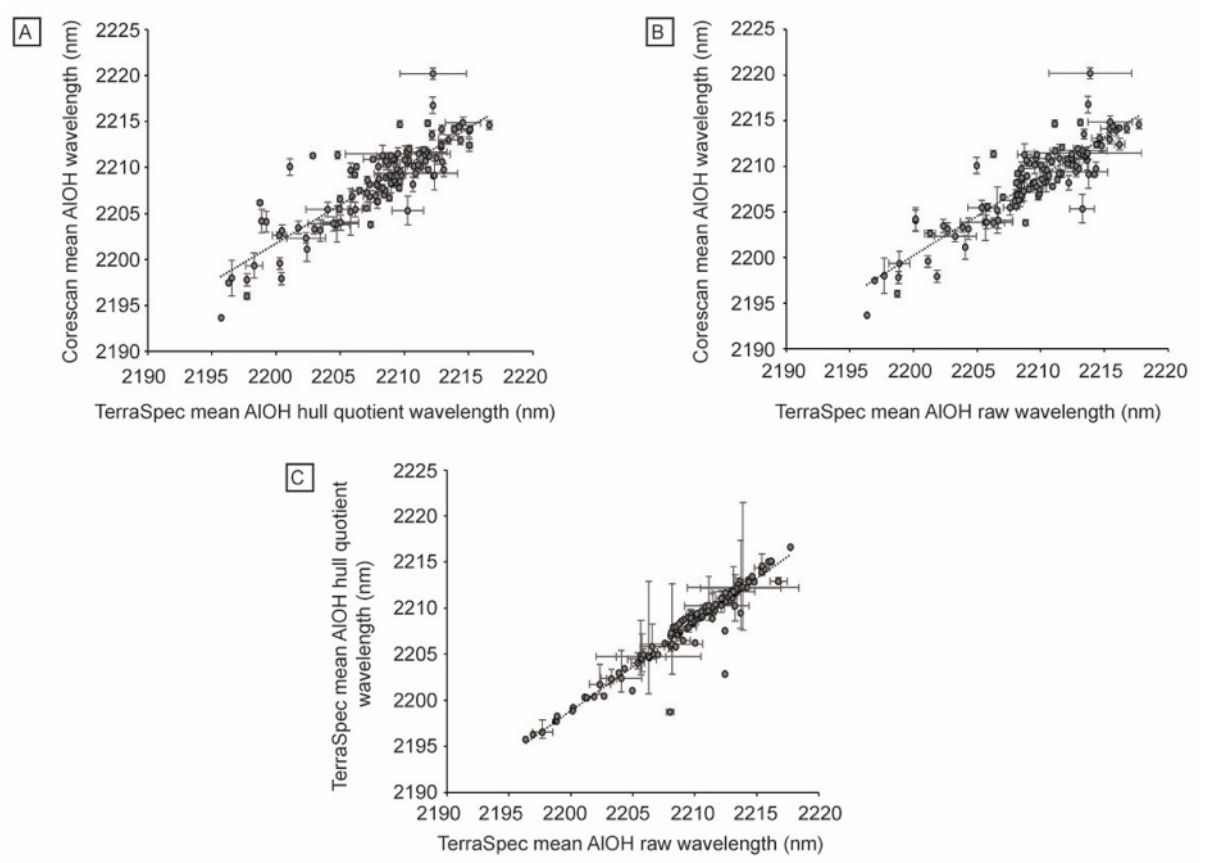

Figure 3: Comparison of the wavelength position of the AlOH absorption feature as determined by TerraSpec versus Corescan for the same sample. Error bars are 1 standard deviation from the mean. A: Corescan vs. hull quotient corrected TerraSpec. B: Corescan vs. raw (uncorrected) TerraSpec. C: Raw (uncorrected) TerraSpec vs. TerraSpec hull quotient corrected.

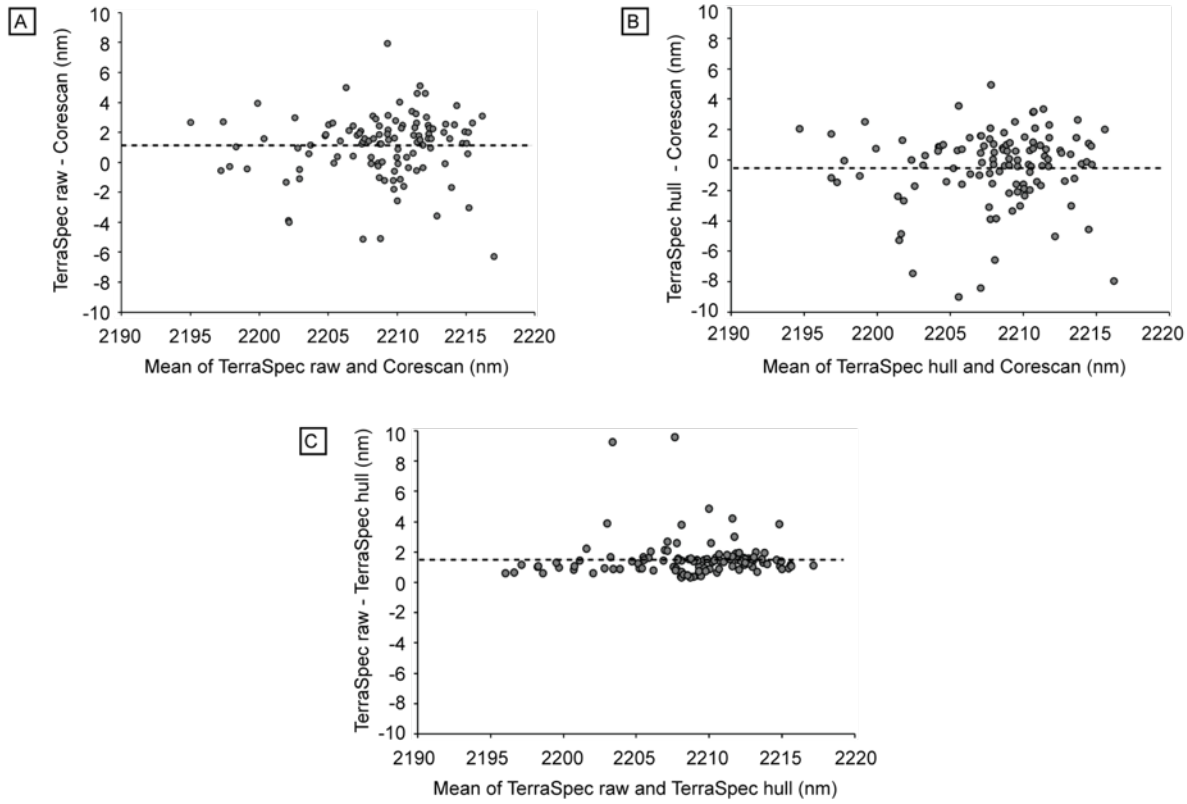

Figure 4: Tukey mean-difference plots of the white mica AlOH wavelength position, showing the difference between the two techniques versus their mean for each sample. The dashed line is the mean difference for each pairwise comparison of techniques. A) TerraSpec raw spectra versus hull quotient corrected. B) TerraSpec raw spectra versus Corescan. C) TerraSpec hull quotient corrected versus Corescan.

Table 3: Comparison of mean difference and Pearson correlation coefficient between SWIR techniques

	TerraSpec Hull			**Corescan**		
	Mean difference (nm)	**SD[1] (nm)**	**Correlation (R)**	**Mean difference (nm)**	**SD[1] (nm)**	**Correlation (R)**
TerraSpec Raw	1.5	1.3	0.96[2]	1.1	2.2	0.89[2]
TerraSpec Hull				-0.4	2.5	0.86[2]

[1] Standard deviation of differences

[2] $p < 0.01$

3.5.2. SWIR and EDS aluminum content

The EDS analysis measured a range of average white mica aluminum compositions at Lake City caldera, from 29.1% to 38.0% Al_2O_3, in a wide range of rock types (Table 3 and Appendix F). The averaged white mica Al_2O_3 content from EDS correlates well with both TerraSpec and Corescan λ_{AlOH} (Fig. 4). The correlation is best with Corescan (R = 0.92 (TerraSpec raw), 0.91 (TerraSpec hull quotient) and 0.94 (Corescan). White mica varies in

composition within each sample, however the number of EDS analyses per sample is sufficient that standard errors are generally low (Table 3).

Table 4: Aluminum content from EDS and wavelength position of the 2,200 nm AlOH absorption feature as measured by TerraSpec and Corescan.

			SEM BSE-EDS			TerraSpec		Corescan
Sample	**Rock type**	***n* =**	**Al_2O_3 mean**	**Al_2O_3 SD[1]**	**Al_2O_3 SE[2]**	**Raw AlOH mean (nm)**	**Hull AlOH mean (nm)**	**Mean AlOH (nm)**
LCG090814-2	Altered breccia	82	32.4	1.8	0.2	2209.6	2208.3	2207.8
LCGB091414-4B	Altered granite	63	31.3	1.0	0.1	2213.6	2212.9	2210.6
LCGVRF071614-4D	Altered granite	87	31.4	2.2	0.2	2214.2	2212.2	2209.1
LCIS091114-2A	Altered syenite	73	29.1	1.1	0.1	2213.0	2211.1	2211.5
LCIS091114-2B	Altered syenite	102	30.3	1.1	0.1	2212.7	2211.3	2210.1
LCT091014-1A	Altered tuff	105	31.0	2.5	0.2	2213.5	2212.5	2211.0
LCRF082514-1C	Cataclasite	148	30.0	1.8	0.1	2215.7	2214.3	2214.4
LCRF090814-1A	Cataclasite	33	31.8	1.9	0.3	2212.4	2207.6	2210.9
LCG090714-2A	Vein and altered granite	65	33.9	1.1	0.1	2206.6	2205.8	2205.2
LCGV081114-2C	Vein and altered granite	47	29.1	4.7	0.7	2212.5	2210.8	2210.1
LCGV082514-2A	Vein and altered granite	78	34.9	0.9	0.1	2203.3	2202.3	2202.3
LCGV090714-3A	Vein and altered granite	91	31.9	2.5	0.3	2213.0	2211.8	2209.7
LCGV091314-1A	Vein and altered granite	96	30.5	2.3	0.2	2214.8	2212.8	2212.2
LCTV090314-1A	Vein and altered tuff	175	35.2	1.0	0.1	2201.1	2200.3	2199.6
LCTV072314-1*	Vein and altered tuff	58	38.0	0.6	0.1	2196.3	2195.7	2193.7
LCBVRF091514-1B	Vein	222	34.3	2.7	0.2	2200.2	2198.9	2204.2

[1] Standard deviation

[2] Standard error

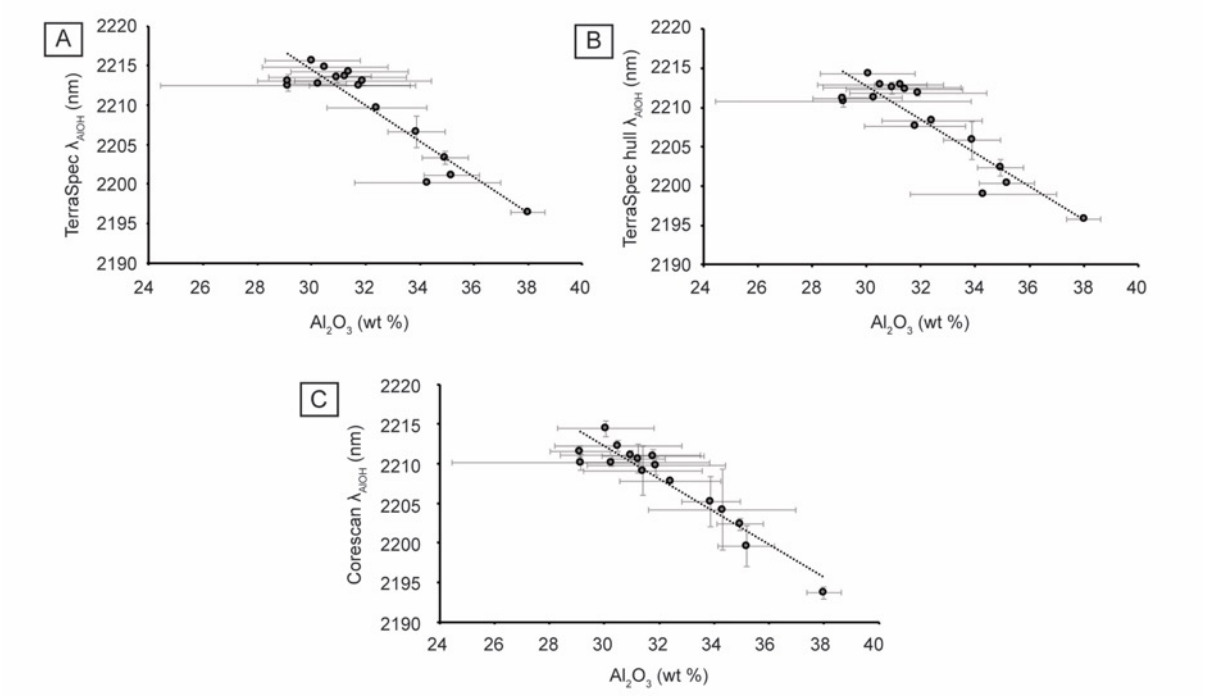

Figure 5: Comparison of the wavelength position of the AlOH absorption feature versus white mica aluminum content, reported as oxide mass percent. A: Raw TerraSpec vs. aluminum B: TerraSpec 'hull quotient' vs. aluminum C: Corescan vs. aluminum.

3.5.3. Spatial variation of AlOH wavelength

The λ_{AlOH}, and hence white mica composition, varies throughout the caldera (Fig. 5a and Appendix G). There is significant small-scale heterogeneity, or 'noise' in the spatial distribution of λ_{AlOH}, which is reflected in the high 'nugget' value of the λ_{AlOH} variograms (Fig. 2). However, the data do still show spatial self-correlation up to a separation distance of ~3 km (Fig. 2), and broad patterns are evident in the kriged data (Fig. 6). White mica are generally more muscovitic (low λ_{AlOH}, high Al by EDS) in the center of the caldera, near the syenite resurgent intrusions. White mica is also muscovitic near the quartz monzonite intrusion at the junction of the Alpine Gulch fault and the caldera margin. White mica is distinctly phengitic (high λ_{AlOH}, low Al, High Fe) along parts of the southwestern and western caldera margin, where sampling extends into (but is not confined to) the granite basement. In the kriged data, there is a distinct NE – SW trending zone of lower λ_{AlOH} from the center of the caldera to the western margin (Fig. 5b). This zone is only defined by two locations on the western caldera margin, so more data would be needed to confirm if this feature is accurate, however we note the trend parallel to faults and veins in this area. The variation in λ_{AlOH} with elevation is presented in Chapter 4 (section 4.5.2).

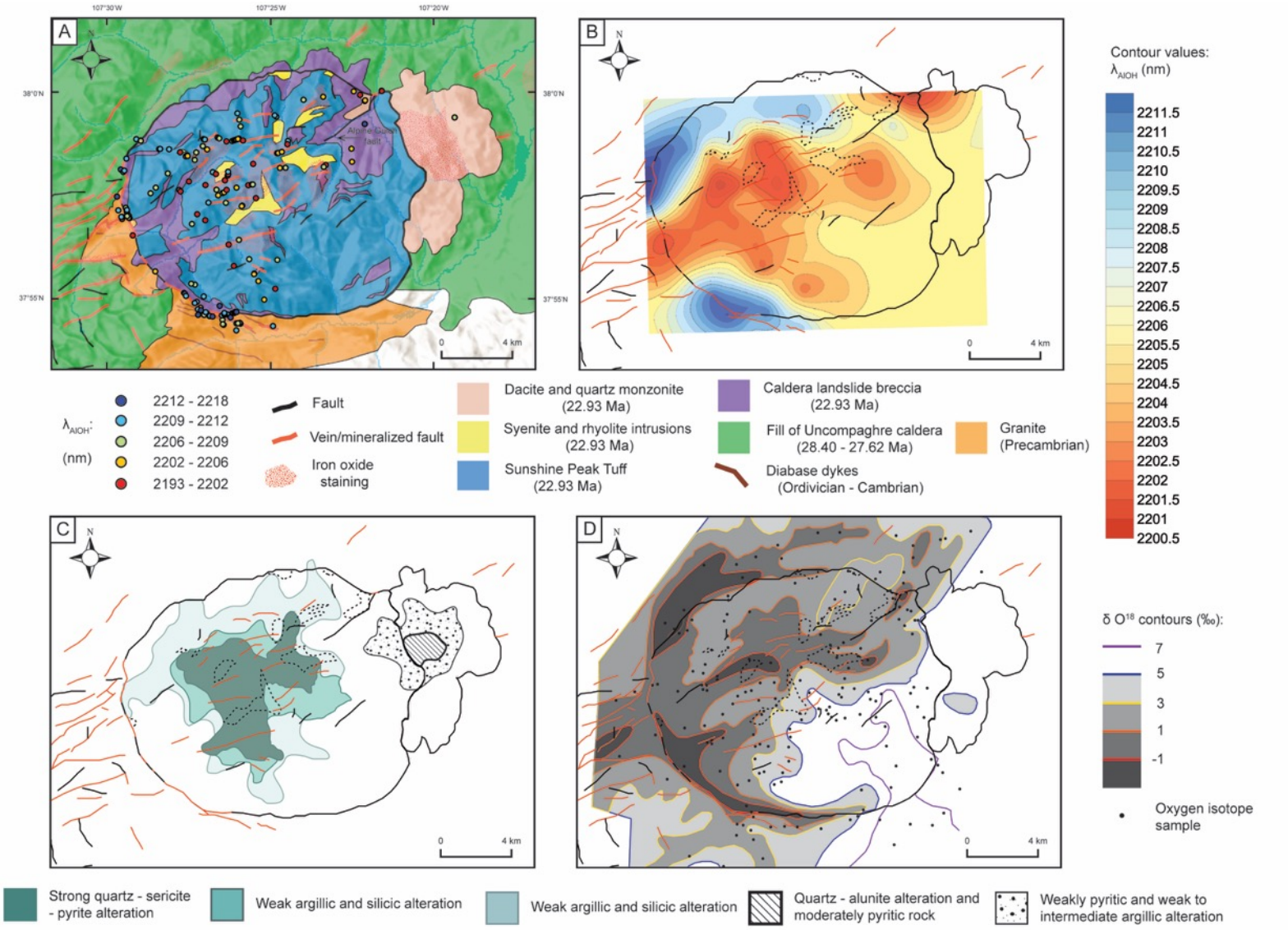

Figure 6: A: Simplified geological map of Lake City caldera (modified from Lipman, 1976b; Hon, 1987; Kennedy et al., 2016) showing the average λ_{AlOH} of white mica for locations analyzed with the Corescan HCI-3. B: The λ_{AlOH} of white mica modelled by kriging and overlaid on a simplified map of Lake City caldera showing major structures and magmatic intrusions (dashed lines). C: The alteration zones mapped by Hon (1987), overlaid on a simplified map of Lake City caldera showing major structures and magmatic intrusions (dashed lines). D: Oxygen isotope values from Larson and Taylor (1986a and 1986b), overlaid on a simplified map of Lake City caldera showing major structures and magmatic intrusions (dashed lines).

The areas of muscovitic alteration in the center of the caldera correlate with quartz – sericite – pyrite alteration as mapped by Hon (1987), and also with low $\delta^{18}O$ composition (Larson and Taylor, 1986b, 1986a) (Figs. 5c and 5d). The distinct area of muscovitic white mica on the northeastern margin, at the intersection with the Alpine Gulch fault, correlates well with an area of low $\delta^{18}O$ composition (Fig. 5d). The oxygen isotope data also show a broad area of low $\delta^{18}O$ composition extending from the center of the caldera to the western margin, which correlates with muscovitic λ_{AlOH} data (Figs. 5b and 5d). However, the muscovitic compositions do not always correlate with low $\delta^{18}O$ composition; on the southwestern and northwestern margins the white mica composition is distinctly phengitic, while the $\delta^{18}O$ composition is distinctly low (Figs. 5b and 5d).

3.6. DISCUSSION

This study shows that Corescan technique correlates well with the more established TerraSpec technique for determining λ_{AlOH} of white micas. Both techniques correlate well with the semi-quantitative aluminum content of the white mica as determined by SEM BSE-EDS, and confirm that λ_{AlOH} is a reliable indicator of white mica compositional variation (Duke, 1994; Yang et al., 2011). TerraSpec data that has been processed by removing the 'hull' produces a slightly worse correlation with both the Corescan λ_{AlOH} and aluminum content, though the correlation is still significant (Fig. 2). By contrast, the mean-difference analysis (Fig. 3) shows that the hull quotient data have closer average values to Corescan than the raw reflectance. Care must therefore be taken when choosing whether to use hull quotient or raw reflectance data. Our results would suggest that raw reflectance would more accurately reflect variations in aluminum content, however hull quotient may be more readily integrated with other SWIR datasets such as Corescan. The good correlation between TerraSpec and Corescan shows that both techniques are effective exploration tools for investigating white mica composition. For analysis of hand samples, TerraSpec involves less sample preparation, is quicker, and less costly than Corescan. It may be the more practical technique if only the average λ_{AlOH} of a sample is required, to be compared with other locations and/or for the recognition of broad patterns. However, the Corescan technique has several advantages (Table 1) such as: 1) Continuous coverage and imaging, so that sub-sample scale changes in λ_{AlOH} can be detected, and the location of low or high λ_{AlOH} zones can be more tightly constrained in a drill hole; 2) The wavelength can be compared with a greater variety of mineralogical and textural information, which may not be possible for

TerraSpec without laborious petrological description; 3) Minerals, especially those with a poor SWIR response, can be detected at much lower abundances due to the finer spatial resolution; 4) More minerals may be detected for the same sample area, so that a more complete suite of the primary and alteration mineralogy can be determined, and 5) Semi-quantitative mineral abundances can be calculated by counting how many 0.5 x 0.5 mm pixels detect a mineral. As an example of the advantages of Corescan in detecting more minerals, of the 165 samples that were analysed with both TerraSpec and Corescan for this study, TerraSpec detected white mica in 126 of them, while Corescan did in 158 samples. Corescan detected white mica in 31 samples that TerraSpec did not (i.e. detected it in 25% more samples), while TerraSpec detected white mica in only one sample that Corescan did not.

Although both the TerraSpec and Corescan λ_{AlOH} correlate with aluminum content, the correlation is better for the Corescan data (R^2 = 0.83 for Corescan vs. 0.75 or 0.72 for TerraSpec). This is most likely because the higher spatial resolution and continuous coverage of Corescan over a sample means the Corescan values are subject to less error, because the sample size is much larger, and there is less mixing of mineral spectra. This is evident in the smaller size of the Corescan error bars in Figure 2.

3.6.1. Limitations of this study

A potential limitation of this study is that the Corescan data have been collected from hand sample slabs that are larger than most samples used for the TerraSpec and EDS data; this will always apply to some extent because Corescan data form continuous coverage of small pixels over a sample. In this study, we chose visually representative parts of each sample to process further for TerraSpec and EDS analysis. Despite this, figure 1 shows that at the sample scale there can still be significant λ_{AlOH} variations, without any obvious visual clues, so this is a realistic example of how the discrete TerraSpec analyses will inevitably miss out on some compositional and mineralogical variation compared to Corescan.

The white mica composition data are from EDS, not electron microprobe. Although we realize that EDS is clearly not ideal to analyze precisely mineral composition, it is cheaper and faster to use than electron microprobe. Thus the oxide mass percent cannot be interpreted as the true chemical composition, as the data are re-calculated to total 100% (i.e. unable to account for water by difference). As the focus of this study is on relative differences in aluminum content, rather than absolute values, this approach is justified. This study shows

that there is still a good correlation between λ_{AlOH} and aluminum content as measured by EDS. If many spot measurements are made and averaged per sample, then EDS is accurate enough for exploration purposes, and importantly a wealth of information on alteration mineralogy and texture can be gathered at the same time.

3.6.2. Implications for ore and geothermal exploration

TerraSpec, Corescan and EDS analyses measured a range of phengitic and muscovitic white mica compositions not previously reported at Lake City caldera. This study shows that there is a small difference between the λ_{AlOH} as measured by TerraSpec and Corescan, with AlOH wavelength vary from 2196 to 2217 for SWIR TerraSpec and 2194 to 2220 with Corescan. If the relative change in λ_{AlOH} is being investigated, then the raw TerraSpec, hull quotient TerraSpec and Corescan data should show the same or similar patterns. In some settings, it may be advantageous to use multiple SWIR techniques, such as Corescan on drill core and TerraSpec in the field. If such methods are being integrated, it is recommended that there should be some overlap in sampling, so that the average difference between results can be taken into account. As an example, based on the data from this study, raw TerraSpec data should be decreased by 1.1 nm if being integrated with Corescan data, or hull quotient TerraSpec data should be increased by 0.4 nm.

The good correlation of both TerraSpec and Corescan data with aluminum content agrees with previous work that has shown λ_{AlOH} is correlated with white mica composition (e.g.Yang et al., 2011; van Ruitenbeek et al., 2005; Tappert et al., 2013). The Corescan system is poorly represented in the academic literature, so this study provides a valuable validation of its efficacy in estimating white mica composition.

Areas or conduits of high fluid flux are the part of a hydrothermal system where ore deposits are formed, and geothermal fluid extracted (Sibson, 1996; Rowland and Simmons, 2012). Towards a fluid conduit, the fluid/rock ratio will increase, pH will generally decrease (due to decreasing acid neutralization), and temperature may increase (Giggenbach, 1984). Therefore, fluid temperature, pH, and fluid/rock ratio are all important variables that can vector to areas favorable for geothermal upflow and/or ore mineralization (Parry et al., 1984; van Ruitenbeek et al., 2005; Cohen, 2011; Yang et al., 2011)

The spatial variation in λ_{AlOH} at Lake City caldera shows a broad pattern of muscovitic compositions in the central resurgent dome and northeastern caldera margin, and phengitic compositions along parts of the southwestern and western caldera margins (Figs. 5a and 5b). This suggests that different parts of the Lake City fossil hydrothermal system had significantly different physiochemical and/or temperature conditions. The muscovitic white mica in the center of the caldera correlates well with the locations of quartz – sericite – pyrite alteration and low $\delta^{18}O$ composition (Fig 5) (Larson and Taylor, 1986b; Hon, 1987). This would suggest that the high Al white muscovitic mica correlates with higher temperature, lower pH or higher fluid/rock ratio. However, on the southwestern and northwestern margins low Al phengitic white mica correlates with low $\delta^{18}O$ composition (Fig. 5). Previous work on other systems shows that there can be no single interpretation of the cause of differences in white mica composition (Swayze et al., 2014). Further work characterizing and comparing the alteration mineralogy in the center of the caldera and the northwestern/southwestern margins is needed to determine the reason for the opposite λ_{AlOH} and $\delta^{18}O$ correlations in these parts of the caldera. However, overall the patterns shown by these two independent methods are quite similar, showing that SWIR reflectance spectroscopy and λ_{AlOH} is a useful additional low-cost tool for investigating hydrothermal alteration. The interpreted controls on white mica composition are revisited later in this thesis in Chapter 4 (e.g. Section 4.6.4) where integration with further alteration mineralogy and fluid inclusion microthermometry data allow more robust interpretations to be made.

The hand sample based SWIR reflectance spectroscopy conducted in this study adds significant detail to the satellite SWIR work of Rockwell (2012), which shows a subtle change in alteration mineralogy between the margins of the caldera and the center. The presence or absence of sericite as determined by Rockwell (2012) is valuable data but cannot be used to tightly constrain physiochemical conditions, as white mica forms in diverse environments. Integration of with λ_{AlOH} with other, independent, datasets may allow the cause of the change in white mica composition to be determined and "calibrated" for the system of interest. This can constrain physiochemical conditions and gradients with more detail than exploration mineralogy techniques alone.

3.7. ACKNOWLEDGEMENTS:

We acknowledge Cameron Windham, Matthew Hoffman and Annie Waterbury for help with field work; Patrick Kelley and Cionnaith O'Dubhaigh for logistical help in Lake City; and Carlo Prandi and Jordan Lubbers for help with sample processing. We thank Corescan staff, particularly Brigette Martini and Kathyrn Conroy, for assistance with Corescan data acquisition and analysis, and Mark Simpson for assistance with TerraSpec data acquisition and analysis. Thomas Garden benefited from a GNS Science PhD Scholarship from the Geothermal Resources of New Zealand Project Water-Rock Interactions, and funding from the Mercury Energy sponsored Source to Surface Program at the University of Canterbury, and the University of Canterbury Department of Geological Sciences Mason Trust fund.

3.8. REFERENCES CITED

Bailey, S.W., 1984, Classification and structures of the micas: Reviews in Mineralogy and Geochemistry, v. 13, p. 1–12.

Bellian, J.A., Martini, B., Canter, L., Carey, R., Katz, D., Curnow, J., Jung, M., and Guisinger, M., 2016, Hyperspectral core imaging: Spanning the gap from plug to log to reservoir scale, *in* Proceedings of the AAPG Annual Convention and Exhibition, Calgary, Alberta, Canada, June 19-22, 2016,.

Beran, A., 2002, Infrared spectroscopy of micas: Reviews in Mineralogy and Geochemistry, v. 46, p. 351–369.

Bove, D.J., Hon, K., Budding, K.E., Slack, J.F., Snee, L.W., and Yeoman, R.A., 2001, Geochronology and geology of late Oligocene through Miocene volcanism and mineralization in the western San Juan Mountains, Colorado: U.S. Geological Survey Professional Paper 1642.

Bove, D.J., Rye, R.O., and Hon, K., 1990, Evolution of the Red Mountain alunite deposit, Lake City, Colorado: U.S. Geological Survey Open-File Report 90-0235.

Browne, P.R.L., 1978, Hydrothermal alteration in active geothermal fields: Annual Reviews in Earth and Planetary Sciences, v. 6, p. 229–250.

Chambefort, I., Lewis, B., Simpson, M.P., Bignall, G., Rae, A.J., and Ganefianto, N., 2017, Ngatamariki geothermal system: Magmatic to epithermal transition in the Taupo Volcanic Zone, New Zealand: Economic Geology, v. 112, p. 319–346, doi: 10.2113/econgeo.112.2.319.

Chang, Z., and Yang, Z., 2012, Evaluation of inter-instrument variations among short

wavelength Infrared (SWIR) devices: Economic Geology, v. 107, p. 1479–1488, doi: 10.2113/econgeo.107.7.1479.

Christie, A.B., and Brathwaite, R.L., 2003, Hydrothermal alteration in metasedimentary rock-hosted orogenic gold deposits, Reefton goldfield, South Island, New Zealand: Mineralium Deposita, v. 38, p. 87–107, doi: 10.1007/s00126-002-0280-9.

Cohen, J.F., 2011, Mineralogy and geochemistry of hydrothermal alteration at the Ann-Mason porphyry copper deposit, Nevada: Comparison of large-scale ore exploration techniques to mineral chemistry [MS thesis]: Corvallis, Oregon, Oregon State University, 580 p.

Dalm, M., Buxton, M.W.N., and van Ruitenbeek, F.J.A., 2017, Discriminating ore and waste in a porphyry copper deposit using short-wavelength infrared (SWIR) hyperspectral imagery: Minerals Engineering, v. 105, p. 10–18, doi: 10.1016/j.mineng.2016.12.013.

Doublier, M.P., Roache, T., and Potel, S., 2010, Short-wavelength infrared spectroscopy: A new petrological tool in low-grade to very low-grade pelites: Geology, v. 38, p. 1031–1034, doi: 10.1130/G31272.1.

Duke, E.F., 1994, Near infrared spectra of muscovite, Tschemak substitution and metamorphic reaction progress: Implications for remote sensing: Geology, v. 22, p. 621–624, doi: 10.1130/0091-7613(1994)022<0621.

Farmer, V.C., ed., 1974, The Infrared Spectra of Minerals, London, Mineralogical Society of Great Britain and Ireland, 539 p.

Garden, T.O., Gravley, D.M., Kennedy, B.M., Deering, C., and Chambefort, I., 2017, Controls on hydrothermal fluid flow in caldera-hosted settings: Evidence from Lake City caldera, USA: Geosphere, v. 13, p. 1–24, doi: 10.1130/GES01506.1.

Giggenbach, W.F., 1984, Mass transfer in hydrothermal alteration systems - A conceptual approach: Geochimica et Cosmochimica Acta, v. 48, p. 2693–2711, doi: 10.1016/0016-7037(84)90317-X.

Harraden, C.L., McNulty, B.A., Gregory, M.J., and Lang, J.R., 2013, Shortwave infrared spectral analysis of hydrothermal alteration associated with the Pebble porphyry copper-gold-molybdenum deposit, Iliamna, Alaska: Economic Geology, v. 108, p. 483–494, doi: 10.2113/econgeo.108.3.483.

Herrmann, W., Blake, M., Doyle, M., Huston, D., Kamprad, J., Merry, N., and Pontual, S., 2001, Short wavelength infrared (SWIR) spectral analysis of hydrothermal alteration zones associated with base metal sulfide deposits at Rosebery and Western Tharsis, Tasmania, and Highway-Reward, Queensland: Economic Geology, v. 96, p. 939–955,

doi: 10.2113/gsecongeo.96.5.939.

Higashi, S., 1980, Mineralogical studies of hydrothermal dioctahedral mica minerals: Memoirs of the Faculty of Science, Kochi University. Series E. Geology, v. 1, p. 1–39.

Hon, K.A., 1987, Geologic and petrologic evolution of the Lake City caldera, San Juan Mountains, Colorado [Ph.D. thesis]: University of Colorado at Boulder, 244 p.

Hosseinjani Zadeh, M., Tangestani, M.H., Velasco Roldan, F., and Yusta, I., 2014, Spectral characteristics of minerals in alteration zones associated with porphyry copper deposits in the middle part of Kerman copper belt, SE Iran: Ore Geology Reviews, v. 62, p. 191–198, doi: 10.1016/j.oregeorev.2014.03.013.

Huntington, J., Whitbourn, L., Mason, P., Berman, M., Schodlok, M.C., and Engineering, R., 2010, HyLogging - Voluminous industrial-scale reflectance spectroscopy of the earth's subsurface: Art, Science and Applications of Reflectance Spectroscopy Symposium, p. 23–25.

Jones, S., Herrmann, W., and Gemmell, J.B., 2005, Short wavelength infrared spectral characteristics of the HW horizon: Implications for exploration in the Myra Falls volcanic-hosted massive sulfide camp, Vancouver Island, British Columbia, Canada: Economic Geology, v. 100, p. 273–294, doi: 10.2113/gsecongeo.100.2.273.

Kennedy, B., Stix, J., Hon, K., Deering, C., and Gelman, S., 2016, Magma storage, differentiation, and interaction at Lake City caldera, Colorado, USA: Geological Society of America Bulletin, v. 128, p. 764–776, doi: 10.1130/B31305.1.

Larson, P.B., and Taylor, H.P., 1986, An oxygen isotope study of hydrothermal alteration in the Lake City caldera, San Juan Mountains, Colorado: Journal of Volcanology and Geothermal Research, v. 30, p. 47–82.

Lipman, P.W., 1976a, Caldera-collapse breccias in the western San Juan Mountains, Colorado: Geological Society of America Bulletin, v. 87, p. 1397–1410.

Lipman, P., 1976b, Geologic map of the Lake City caldera area, western San Juan Mountains, southwestern Colorado: U.S. Geological Survey Miscellaneous Investigations Series Map I-962, scale 1:48,000.

Mulder, V.L., Plötze, M., de Bruin, S., Schaepman, M.E., Mavris, C., Kokaly, R.F., and Egli, M., 2013, Quantifying mineral abundances of complex mixtures by coupling spectral deconvolution of SWIR spectra (2.1-2.4 um) and regression tree analysis: Geoderma, v. 207–208, p. 279–290, doi: 10.1016/j.geoderma.2013.05.011.

Oliver, M.A., and Webster, R., 2014, A tutorial guide to geostatistics: Computing and modelling variograms and kriging: Catena, v. 113, p. 56–69, doi:

10.1016/j.catena.2013.09.006.

Page, R., and Wenk, H.R., 1979, Phyllosilicate alteration of plagioclase studied by transmission electron microscopy: Geology, v. 7, p. 393–397, doi: 10.1130/0091-7613(1979)7<393:PAOPSB>2.0.CO;2.

Parry, W.T., Ballantyne, J.M., and Jacobs, D.C., 1984, Geochemistry of hydrothermal sericite from Roosevelt Hot Springs and the Tintic and Santa Rita porphyry copper systems: Economic Geology, v. 79, p. 72–86, doi: 10.2113/gsecongeo.79.1.72.

Quigley, M., and Yildirim, B.G., 2015, Mineral identification and domain characterisation using two automated hyperspectral core logging systems, Los Bronces Cu-Mo porphyry deposit, *in* Proceedings of the 13th SGA Biennial Meeting on Mineral Resources in a Sustainable World, Nancy, France, 24-27 August, p. 1443–1446.

Rockwell, B.W., 2012, Map of mineralogy, vegetation, and hydrothermal alteration type generated from ASTER satellite data, San Juan Mountains, Colorado: U.S. Geological Survey Scientific Investigations Map 3190.

Rowland, J. V., and Simmons, S.F., 2012, Hydrologic, magmatic, and tectonic controls on hydrothermal flow, Taupo Volcanic Zone, New Zealand: Implications for the formation of epithermal vein deposits: Economic Geology, v. 107, p. 427–457, doi: 10.2113/econgeo.107.3.427.

van Ruitenbeek, F.J.A., Cudahy, T., Hale, M., and van der Meer, F.D., 2005, Tracing fluid pathways in fossil hydrothermal systems with near-infrared spectroscopy: Geology, v. 33, p. 597–600, doi: 10.1130/G21375.1.

van Ruitenbeek, F.J.A., Cudahy, T.J., van der Meer, F.D., and Hale, M., 2012, Characterization of the hydrothermal systems associated with Archean VMS-mineralization at Panorama, Western Australia, using hyperspectral, geochemical and geothermometric data: Ore Geology Reviews, v. 45, p. 33–46, doi: 10.1016/j.oregeorev.2011.07.001.

Sanford, R.F., 1992, Lead isotopic compositions and paleohydrology of caldera-related epithermal veins, Lake City, Colorado: Geological Society of America Bulletin, v. 104, p. 1236–1245.

Sanford, R.F., Grauch, R.I., Hon, K., Bove, D.J., Grauch, V.J.S., and Korzeb, S.L., 1987, Mineral Resources of the Redcloud Peak and Handies Peak Wilderness Study Areas, Hinsdale County, Colorado: U.S. Geological Survey Bulletin 1715-B.

Sibson, R.H., 1996, Structural permeability of fluid-driven fault-fracture meshes: Journal of Structural Geology, v. 18, p. 1031–1042, doi: 10.1016/0191-8141(96)00032-6.

Simpson, M.P., and Christie, A.B., 2016, Exploration of New Zealand mineral deposits and geothermal systems using X-ray diffraction (XRD) and reflectance spectrometry (SWIR): A comparison of techniques: GNS Science Report 2016/61.

Simpson, M.P., MacKenzie, D.J., Craw, D., and Doyle, S., 2016, Short-wave infrared (SWIR) reflectance spectrometry studies of alteration at Frasers underground, Macraes gold mine, Otago, New Zealand, *in* Proceedings of the AusIMM New Zealand Branch Annual Conference 2016, p. 385–396.

Simpson, M.P., Rae, A.J., Ganefianto, N., and Sepulveda, F., 2009, Short wavelength infrared (SWIR) spectral characterisation of smectite, illite-smectite and illite for geothermal fields of the Taupo Volcanic Zone, New Zealand, *in* Proceedings of the New Zealand Geothermal Worshop 2009, p. 1–4.

Steeves, N.J., Hannington, M.D., Gemmell, J.B., Green, D., and McVeigh, G., 2016, The Glacier Creek Cu-Zn VMS deposit, Southeast Alaska: An addition to the Alexander Triassic metallogenic belt: Economic Geology, v. 111, p. 151–178, doi: 10.2113/econgeo.111.1.151.

Sun, Y., Seccombe, P.K., and Yang, K., 2001, Application of short-wave infrared spectroscopy to define alteration zones associated with the Elura zinc-lead-silver deposit, NSW, Australia: Journal of Geochemical Exploration, v. 73, p. 11–26, doi: 10.1016/S0375-6742(01)00167-4.

Swayze, G.A., Clark, R.N., Goetz, A.F.H., Livo, K.E., Breit, G.N., Kruse, F.A., Sutley, S.J., Snee, L.W., Lowers, H.A., Post, J.L., Stoffregen, R.E., and Ashley, R.P., 2014, Mapping advanced argillic alteration at Cuprite, Nevada, using imaging spectroscopy: Economic Geology, v. 109, p. 1179–1221, doi: 10.2113/econgeo.109.5.1179.

Tappert, M.C., Rivard, B., Giles, D., Tappert, R., and Mauger, A., 2013, The mineral chemistry, near-infrared, and mid-infrared reflectance spectroscopy of phengite from the Olympic Dam IOCG deposit, South Australia: Ore Geology Reviews, v. 53, p. 26–38, doi: 10.1016/j.oregeorev.2012.12.006.

Van der Marel, H.W., Beutelspacher, H., 1976, Atlas of Infrared Spectroscopy of Clay Minerals and their Admixtures, Amsterdam, Elsevier, 396 p.

Velde, B., 1965, Phengite micas: Synthesis, stability, and natural occurence: American Journal of Science, v. 263, p. 886–913, doi: 10.2475/ajs.263.10.886.

Velde, B., 1978, Infrared spectra of synthetic micas in the series muscovite-MgAl celadonite: American Mineralogist, v. 63, p. 343–349.

Yang, K., Browne, P.R.L., Huntington, J.F., and Walshe, J.L., 2001, Characterising the

hydrothermal alteration of the Broadlands-Ohaaki geothermal system, New Zealand, using short-wave infrared spectroscopy: Journal of Volcanology and Geothermal Research, v. 106, p. 53–65, doi: 10.1016/S0377-0273(00)00264-X.

Yang, K., Huntington, J.F., Browne, P.R.L., and Ma, C., 2000, An infrared spectral reflectance study of hydrothermal alteration minerals from the Te Mihi sector of the Wairakei geothermal system, New Zealand: Geothermics, v. 29, p. 377–392, doi: 10.1016/S0375-6505(00)00004-3.

Yang, K., Huntington, J.F., Gemmell, J.B., and Scott, K.M., 2011, Variations in composition and abundance of white mica in the hydrothermal alteration system at Hellyer, Tasmania, as revealed by infrared reflectance spectroscopy: Journal of Geochemical Exploration, v. 108, p. 143–156, doi: 10.1016/j.gexplo.2011.01.001.

Yang, K., Lian, C., Huntington, J.F., Peng, Q., and Wang, Q., 2005, Infrared spectral reflectance characterization of the hydrothermal alteration at the Tuwu Cu-Au deposit, Xinjiang, China: Mineralium Deposita, v. 40, p. 324–336, doi: 10.1007/s00126-005-0479-7.

PREAMBLE

The previous chapter shows how short wave infrared reflectance spectroscopy (in particular Corescan) and white mica composition can be used as tools to track physiochemical gradients in hydrothermal systems. In the next chapter these data are combined with alteration mineralogy, vein textures, and fluid inclusion microthermometry to constrain the physiochemical conditions of the Lake City caldera hydrothermal systems, its evolution, and the controls on fluid temperature and composition. A conceptual model is formed that incorporates these elements, as well as the lithological and structural controls discussed in Chapter 2.

I aim to submit Chapter 4 to *Geological Society of America Bulletin* or *Journal of Volcanology and Geothermal Research* for publication.

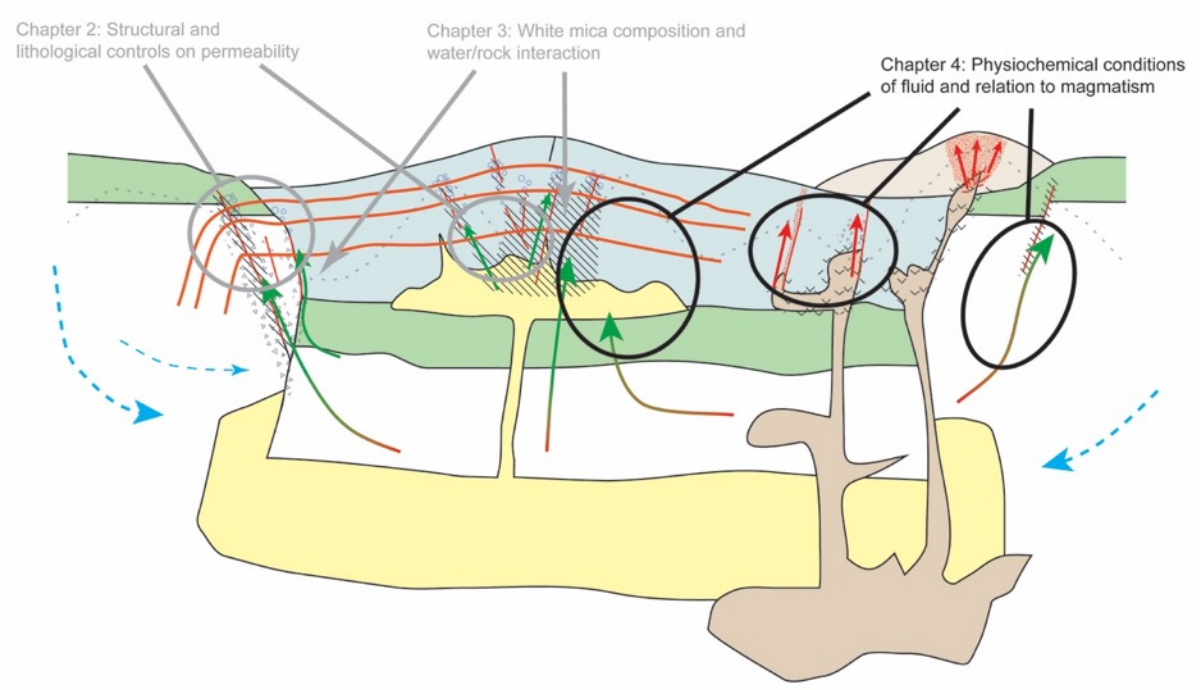

Simplified conceptual cartoon for hydrothermal fluid flow at Lake City caldera (cf. Fig. 4.23), showing the components of the model that are addressed in Chapter 4.

Chapter 4. Reconstruction of the fossil hydrothermal system at Lake City caldera, Colorado, U.S.A.

4. Reconstruction of the fossil hydrothermal system at Lake City caldera, Colorado, U.S.A.

4.1. ABSTRACT

Reconstruction of the physiochemical characteristics of fossil hydrothermal systems can help guide exploration for modern geothermal or mineral resources in similar settings. The 22.9 Ma Lake City caldera in Colorado, U.S.A. is well-exposed and contains an exhumed fossil shallow hydrothermal system. In this study, alteration mineralogy, short wave infrared reflectance spectroscopy, vein textures and fluid inclusions are used to characterise the temperature and composition, spatiotemporal variability, and structural controls of the hydrothermal system. The hydrothermal system was dominantly moderate temperature (up to ~290°C), low salinity (<3% NaCl equivalent) and neutral to weakly acidic pH. There is evidence for boiling in veins throughout the exposed depth range; however, boiling textures are most common at the highest elevations of the system, and in major fluid conduits. Phyllic alteration assemblages and muscovitic white mica compositions in the centre of the caldera indicate slightly more fluid-dominated conditions compared to those that formed propylitic alteration and phengitic white mica on the caldera margin. These contrasting alteration types reflect contrasting styles of permeability and fluid pathways in the more pervasively fractured and faulted resurgent dome compared to fewer, larger conduits in the granite of the caldera basement. Based on the lack of high-temperature, hypersaline fluid inclusions within the caldera centre, we interpret that the resurgent syenite intrusions (batch A magmas) provided little magmatic fluid input and had cooled significantly by the time the hydrothermal system had established. In contrast, in the eastern portion of the caldera, late distinct magma batches (batch B) provided high temperature (up to ~540°C) and hypersaline (up to ~65% NaCl eq.) magmatic fluid input above intrusions. Our conceptual hydrothermal model emphasizes the importance of discontinuity intersections in facilitating permeability in caldera settings. We also recognize the contrasting hydrothermal manifestations of a waning, degassed magma batch (batch A) and fresh, volatile-rich magma (batch B).

4.2. INTRODUCTION

Fossil hydrothermal systems allow integration of geochemical, lithological, and structural data from a field mapping scale to a fluid inclusion scale (e.g. Dilles and Einaudi, 1992). These data can provide a more complete picture to inform studies of active hydrothermal

systems where subsurface interpretations are constrained by integrating borehole geology and geophysical surveys. Here, we use the caldera-hosted fossil hydrothermal system at Lake City caldera Colorado U.S.A. to build a conceptual model, designed to inform the location of past or present fluid conduits in hydrothermal systems in caldera settings. Our conceptual model should facilitate data interpretation and guide exploration for geothermal or mineral resources in other caldera settings.

Calderas formed during silicic eruptions are important hosts for geothermal systems around the world, such as systems in the Taupō Volcanic Zone, New Zealand, Yellowstone, and Long Valley, U.S.A. (Fournier, 1989; Wilson and Rowland, 2016; Hildreth, 2017). The poor exposure and data available from drilling in modern systems (often from cuttings only) makes the influence of caldera related structure on hydrothermal fluid flow difficult to establish. Many exploited epithermal and porphyry ore deposits occur along silicic caldera structures (see Table 2.1), with chemical signatures in part controlled by volcanic topography. Hydrothermal systems can be broadly categorised into low relief systems dominated by meteoric-derived neutral chloride water, with a subordinate magmatic contribution, and higher relief systems with acidic magmatic fluid upflow in the core of the system and more laterally flowing chlorine fluids at the periphery (Henley and Ellis, 1983). The fossil, epithermal equivalents of these are generally classified adularia-sericite/low-sulfidation and acid-sulfate/high-sulfidation, respectively (White and Hedenquist, 1990; Giggenbach, 1997).

Chemical exchange between hydrothermal fluid and host rock forms hydrothermal alteration (Reed, 1997). The two end-member categories of shallow volcanic hydrothermal systems (hereafter referred to as adularia-sericite and acid-sulfate) have characteristic patterns of hydrothermal alteration due to differences in fluid chemistry, topography, magmatism and structure. Acid-sulfate systems typically contain a sub-vertical, upward-flaring core of silicic and advanced argillic alteration, formed by hydrolysis reactions between acidic, magma-derived fluid at high fluid/rock ratios (Hedenquist et al., 2000). Increasing acid neutralisation, and lower fluid/rock ratios outboard of this core produces zones of phyllic, argillic and then propylitic alteration (Reed, 1997). Acid-sulfate epithermal systems may have a spatial and/or genetic relationship to underlying higher temperature porphyry systems formed around magmatic intrusions (Hedenquist and Lowenstern, 1994). In contrast, adularia-sericite systems are characterised by neutral pH, low salinity fluids, and fluid flow often has a high

degree of structural control, using fault or fracture-controlled conduits towards the surface (Henley and Ellis, 1983; White and Hedenquist, 1990; Rowland and Simmons, 2012). These conduits are commonly surrounded by haloes of phyllic alteration, surrounded by widespread propylitic alteration (Hedenquist et al., 2000). Low temperature advanced argillic alteration may form in the near-surface environment due to condensation of CO_2 and H_2S-rich steam (Henley and Ellis, 1983; Hedenquist, 1986).

The classification of a fossil hydrothermal system is based upon alteration assemblages, fluid temperature, textural petrography, and vein data which are integrated to make a conceptual model that depicts the location of flow paths and favourable reservoir permeability conditions, to guide focussed exploration and resource development (White and Hedenquist, 1990; Cumming, 2009). Alteration mineral phase assemblages and compositions, and oxygen isotope compositions help to constrain the fluid composition and fluid/rock ratio (Reed, 1997; Taylor, 1997). Fluid temperature is estimated from mineral equilibria, and fluid inclusion microthermometry (Giggenbach, 1984; Roedder, 1984; Hedenquist et al., 2000). Textural petrography of fluid inclusions and vein textures can constrain the boiling history of the fossil system (Moncada et al., 2011), the fossil fluid pathways and the local pressure and temperature conditions. Structural, lithological, and mechanical data can be used to estimate matrix and fracture controlled permeability pathways in the reservoir.

Where geological constraints allow, these data can also be used to assess the temporal variation of the physiochemical conditions of a hydrothermal system, and the underlying causes for such changes (e.g. Henneberger and Browne, 1988; Goff and Gardener, 1994; Simmons and Brown, 2006; Klemm et al., 2008; Chambefort et al., 2017). An example is the Karaha - Telaga Bodas geothermal system in Indonesia. Distinct alteration assemblages, fluid inclusion microthermometry, modern geothermal fluid sampling, and dated igneous intrusion and volcanic flank collapse allow a detailed reconstruction of the evolution of the geothermal system (Moore et al., 2008; Moore, 2012). These data record a history where the geothermal system was initiated around a granodiorite intrusion, then catastrophically depressurised by ~1700 years later by a flank collapse, which caused the system to transition from liquid- to vapour-dominated (Moore et al., 2008). In ancient systems, it may be more difficult to determine such a detailed evolution, however the alteration assemblages, fluid inclusions and other geological evidence can still be used to determine relative timings of events.

The 22.9 Ma Lake City caldera is well-exposed and has a range of associated hydrothermal alteration and veins, over an exposed stratigraphic range of ~1,300 m. New petrographic, spectral, textural and fluid inclusion data are integrated with previous structural and geochemical studies to characterise the physiochemical conditions of the fossil hydrothermal system and their controls.

4.3. GEOLOGIC SETTING AND PREVIOUS WORK

The 22.9 Ma Lake City caldera (LCC) is the youngest of 15 Tertiary calderas in the San Juan volcanic field (SJVF) locus of the Southern Rocky Mountains volcanic field (SRMVF) (Fig. 1a) (Steven and Lipman, 1976; Bove et al., 2001; Kennedy et al., 2016). The LCC and the Silverton caldera (27.6 Ma) to the southwest are nested within the older Uncompahgre (28.2 Ma; Bove et al., 2001) and San Juan (28.4 Ma; Bove et al., 2001) calderas respectively, together forming a caldera cluster. The NE-SW trend of this cluster may be related to pre-existing Precambrian NE-SW trending shear zones that help control the "Colorado Mineral Belt" or "Colorado Lineament" (Chapin, 2012) (Fig. 1a). The geological history of the Lake City area is outlined below:

4.3.1. Basement

The oldest unit in the area is the Precambrian granite of Cataract Canyon that is adjacent to LCC along its southern, southwestern and western margin (Fig. 1b) (Lipman, 1976b). This granite is described in detail by Garden et al. (2017).

4.3.2. Uncompahgre caldera fill

Uncompahgre caldera erupted concurrently with the nearby San Juan caldera (~28.4 – 27.6 Ma) and together they formed a single coalesced topographic depression (Steven and Lipman, 1976). The fill of Uncompahgre – San Juan calderas consists of welded intra-caldera ignimbrite (Sapinero Mesa Tuff) and landslide breccia, overlain by a succession of intermediate to silicic lavas and volcaniclastic rocks (Lipman, 1976b; Steven and Lipman, 1976). The Sapinero Mesa Tuff contains plagioclase, sanidine and biotite. In the field it is distinguished from the Sunshine Peak Tuff of LCC by its comparatively crystal-poor texture and lack of quartz (Lipman, 1976b). The intra-caldera landslide breccias of Uncompahgre caldera contain mostly intermediate lavas, with clasts up to tens of metres across (Lipman, 1976a). Contemporaneous resurgence across the San Juan and Uncompahgre calderas formed

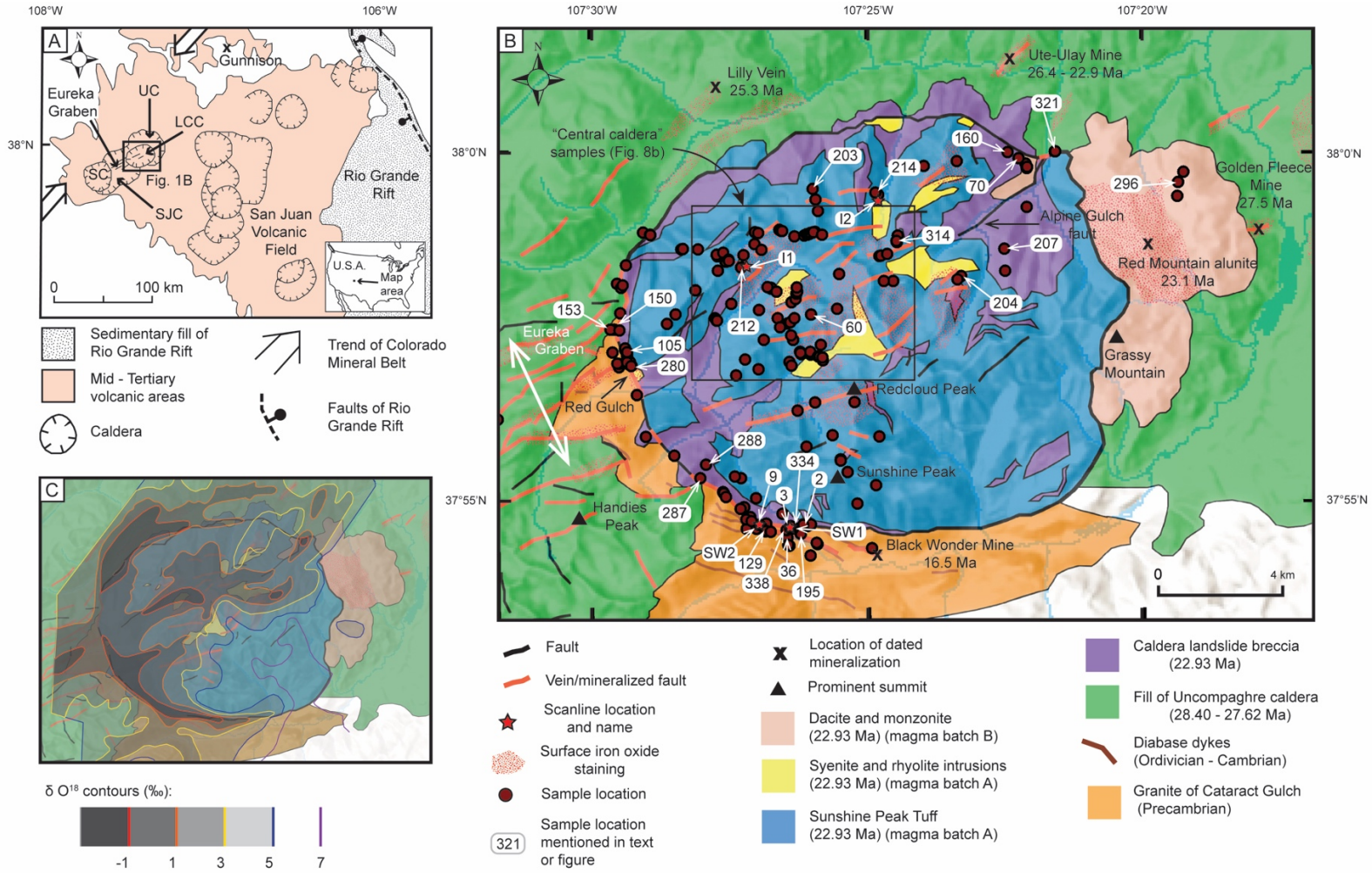

Figure 1: The simplified geology of Lake City caldera and the San Juan volcanic field. A: Location of Lake City caldera in the San Juan volcanic field locus of the Southern Rocky Mountain volcanic field, highlighting major regional geologic features (modified from Lipman et al., 2015). Abbreviations: LCC: Lake City caldera, SC: Silverton caldera, SJC: San Juan caldera, UC: Uncompahgre caldera. B: Simplified geological map of Lake City caldera showing the location of field sampling for this study and major geological and topographic features. Sample locations that are referenced in the text or figures are labelled (see Appendix H for all sample names and locations). Geology is modified from Lipman (1976b) and Hon (1987). Dates are from Bove et al. (2001). Magma batches refer to those defined by Kennedy et al. (2016). C: Whole-rock oxygen isotope compositions at Lake City caldera, from Larson and Taylor (1986b), overlaid on the simplified geology.

the Eureka Graben, an apical graben on top of the elongated resurgent dome (Steven and Lipman, 1976). This is expressed as a series of NE – SW trending normal faults between Silverton and Lake City calderas (Figs. 1a and 1b).

4.3.3. Lake City caldera fill

The caldera-forming eruption of Lake City caldera deposited the Sunshine Peak Tuff, and formed an oval caldera in plan view, 10 x 12 km across (Hon, 1987; Kennedy et al., 2016). The intra-caldera Sunshine Peak Tuff is moderately to densely welded, crystal-rich and lithic-rich. It contains three compositionally distinct members; upper, middle and lower, that are compositionally zoned upwards from rhyolite to trachyte (Hon 1987; Kennedy et al., 2016). The Lower Sunshine Peak Tuff is the most voluminous (200 - 250 km^3 dense rock equivalent [DRE]) and early-erupted unit and is mineralogically dominated by large (up to 10 mm) quartz and smaller sanidine (Kennedy et al., 2016). It is at least ~800 m thick, with the caldera floor below the tuff not exposed (Hon, 1987). The Middle Sunshine Peak Tuff contains mostly quartz, sanidine, plagioclase and biotite and is ~ 300 m thick (20 - 40 km^3 DRE). The Upper Sunshine Peak Tuff contains mostly sanidine, plagioclase and biotite and is at least 500 m thick (40 - 60 km^3 DRE) (Hon, 1987; Kennedy et al., 2016).

During caldera subsidence, gravitational collapse of over steepened caldera walls caused large scale landsliding, forming thick and widespread sequences of intra-caldera breccias (Lipman, 1976a) (Fig. 1b). These are most widespread in the lower stratigraphic levels of the caldera, intercalated with the Lower Sunshine Peak Tuff, however smaller layers are present at higher stratigraphic levels. The clasts of the intra-caldera landslide breccias consist mostly of Sapinero Mesa Tuff and the intermediate to silicic lavas infilling Uncompahgre caldera (Hon, 1987). Clasts of granite basement are uncommon but are present, close to the caldera margin. Clasts in the intra-caldera breccias are up to tens of metres across. The matrix of the breccias is often clay-sized, sometimes mixed with Sunshine Peak Tuff. Fault breccias and cataclasites are preserved at stratigraphically low levels in the southwest and western parts of the caldera margin, and are dominantly composed of deformed granite (Garden et al., 2017). Much of the margin of Lake City caldera comprises a single preserved caldera margin discontinuity. However, in the southwest of the caldera, collapse produced a zone of deformation at least 300 m wide, and utilized pre-existing weaknesses along the margin of the NW-SE trending mafic dykes that intrude the granite (Garden et al., 2017).

Magmatic resurgence caused intrusion of a syenite pluton into the Lake City caldera fill within 80,000 - 330,000 years of collapse (Bove et al., 2001; Kennedy et al., 2012). The Sunshine Peak tuff and syenite are related and were predominantly sourced from the same batch of magmas, called "batch A" by Kennedy et al. (2016). The pluton was emplaced in the central to northern part of the caldera and came from the same magma chambers that fed the Sunshine Peak Tuff (Kennedy et al., 2016). Related dykes were intruded into parts of the western and northern caldera margin, forming so-called "ring dykes". Some of the dykes are more silicic than the main pluton, due to assimilation of the silicic Lower Sunshine Peak Tuff (Hon, 1987). The syenite has a phaneritic to porphyritic texture and generally contains alkali feldspar, with minor quartz, plagioclase and biotite (Hon, 1987; Kennedy et al., 2016). Resurgence caused uplift over the pluton and parts of the caldera margin, forming a medial graben of NE-SW trending series of normal faults, many of which were mineralised by hydrothermal fluids, forming veins (Hon, 1987). These normal faults are aligned with the older NE-SW trending Eureka Graben, reflecting a common underlying structural control. Resurgence also caused uplift along the NE-SW trending Alpine Gulch Fault in the northeastern part of the caldera (Hon, 1987).

In the eastern part of the caldera a geochemically distinct batch of magmas, called "batch B", were emplaced concurrent with emplacement of the syenite pluton (Hon, 1987; Kennedy et al., 2016). The oldest of this suite were dacite lavas emplaced over the eastern caldera margin. Intrusions (smaller than the syenite pluton) were emplaced into the dacite lavas at Red Mountain and in Alpine Gulch. The intrusion at Alpine Gulch was emplaced at the intersection of the Alpine Gulch fault and the caldera margin. This intrusion is a porphyritic quartz monzonite, and contains phenocrysts of alkali feldspar with a groundmass of plagioclase, alkali feldspar, quartz, biotite and clinopyroxene (Hon, 1987). After quiescence at Lake City caldera, bimodal magmatism continued in the SJVF with the emplacement of several small silicic intrusions into the granite basement and Uncompahgre caldera fill at 18.8 Ma, and intermittent basaltic eruptions until 5 Ma (Lipman, 2000b; Bove et al., 2001). The Lake City caldera fill was exhumed by Quaternary glaciation, forming the present rugged ~1,300 m of topographic relief.

4.3.4. Mineralisation and previous work

The western San Juan Mountains have been a productive mining area from the late 19th Century to mid 20th Century, producing precious (silver and gold) and base (mostly lead,

copper and zinc) metals worth approximately US$8.5 billion at 1987 prices (Sanford et al., 1987). Most of the production has been from epithermal veins structurally associated with the Uncompahgre and Silverton calderas. The structural setting of vein deposits includes: intersecting faults in the Eureka Graben (e.g. Sunnyside Mine), faults and intrusions in the discontinuous ring fault system of Silverton caldera (e.g. Marcella Mine), and faults extending orthogonal from the northwestern margin of Silverton caldera (e.g. Argentine-Black Bear veins) (Lipman et al., 1976; Steven and Lipman, 1976; Doe et al., 1979). Although large economic ore deposits were not formed there is still widespread evidence for hydrothermal activity inside Lake City caldera (Slack, 1980; Hon, 1987; Sanford et al., 1987; Garden et al., 2017).

The timing of hydrothermal activity and mineralisation in the Lake City area is complex and covers at least an 11 Ma period from 27.5 Ma (Golden Fleece vein) to 16.5 Ma (Black Wonder vein) (Fig. 1b) (Bove et al., 2001). The oldest dated mineralisation near Lake City caldera is hosted in the Uncompahgre caldera fill (e.g. Ute-Ulay and Golden Fleece mines, Fig. 1b) and is related to resurgence of Uncompahgre caldera and the emplacement of 25 – 26 Ma monzonite intrusions (Lipman et al., 1976; Hon et al., 1985; Bove et al., 2001). Mineralisation at Red Mountain and late stages of mineralisation at Ute-Ulay mine are close in age to the formation of Lake City caldera at 22.9 Ma (Bove et al., 2001). Hydrothermal alteration and veins in the central to western parts of Lake City caldera, and along the caldera margin have not been dated but utilized structures formed during caldera collapse and resurgence as well as pre-existing discontinuities (Garden et al., 2017). Some mineralisation outside the southern caldera margin at the Black Wonder mine is younger than Lake City caldera, at 16.5 Ma (Bove et al., 2001). The majority of the mineralisation at the nearby Silverton caldera is five to ten million years younger than the formation of the caldera; some mineralisation is as young as ~10 Ma (Lipman et al., 1976).

Previous research on the fossil hydrothermal system at Lake City caldera have identified dominantly propylitic and quartz – sericite alteration in most of the caldera, with a distinct alunite – quartz – pyrite assemblage at Red Mountain on the eastern caldera margin (Hon, 1987; Sanford et al., 1987; Bove et al., 1990). Slack (1980) used field mapping and petrographic evidence to suggest that precious and base metal veins outside but near the northeastern Lake City caldera margin were formed as part of the hydrothermal systems active inside the caldera and at Red Mountain. Oxygen isotope studies identified areas of

highest water/rock ratios of alteration in the centre of the caldera, along the western caldera margin, and increasing alteration intensity in the granite basement towards the southwestern caldera margin (Fig. 1c) (Larson and Taylor, 1986a, 1986b). The fluid flow model developed by Larson and Taylor (1986b) emphasizes vertical and inward-directed flow from the granite basement and Uncompahgre caldera fill into Lake City caldera. Fluids utilized the caldera ring fault, megabreccias units and faults in the resurgent dome, with recharge from the Eureka Graben. The surface of the resurgent syenite intrusion was inferred to be 400°C (Larson and Taylor, 1986b). Conversely, Sanford (1992) used vein lead-isotope compositions to identify distinct isotopic signatures inside and outside of the caldera to suggest that hydrothermal fluid flow inside Lake City caldera was isolated from the Uncompahgre caldera fill and that the Lake City ring fault was a lateral barrier to fluid flow.

The well-constrained geology of Lake City caldera and its large topographic relief make this an ideal setting for using alteration mineralogy, vein textures, fluid inclusion microthermometry and structural geology to reconstruct the fluid conditions (depth, temperature, composition, pathways) of the fossil hydrothermal system.

4.4. METHODS

4.4.1. Sample collection and preparation

In total 471 hand samples of vein material and adjacent wall rock were collected from 322 separate field locations throughout Lake City caldera (see Fig. 1b and Appendix H for sample locations). Vein textures and mineralogy were recorded in the field, but no sample collected, from 62 additional locations. At each sampling location as many samples were collected as was necessary to represent the dominant vein textures and mineralogy of that location, although surface iron-oxide stains hindered identification of textures in the field at some locations. Sampling was most closely spaced in two areas at the western and southwestern margin, and in parts of the centre of the caldera. Fewer samples were collected in the eastern half of the caldera because exposure was poorer due to lower elevation and greater vegetation cover, and fewer veins. The Red Mountain area on the eastern caldera margin is dominated by advanced argillic acidic alteration. As the alteration is directly linked to the emplacement of the Red Mountain suite of intrusions and has been studied extensively by previous researchers (Bove and Hon, 1990; Bove et al., 1990; Bove and Hon, 1992), this area was not included in our sampling but is integrated in our general discussion on the Lake City caldera hydrothermal conceptual model. Samples were also collected along four scanline transects

across major veins or structures. These scanlines varied in length from 5 m to 62 m, depending on the available exposure, and the intersection points of all veins with a trace length of more than 0.2 m were recorded. Hand samples were cut into slabs, which were used for Corescan SWIR reflectance spectroscopy. Thin section-sized billets approximately 27 x 46 mm were cut from the larger slabs and thin sections prepared from the billets.

4.4.2. Textural classification methods

Alteration association and assemblages, relict primary mineralogy and vein textures were described in the field, on cut hand samples, and by thin section petrography. Vein textures were used to constrain whether the hydrothermal fluid was boiling. The textures were classified using criteria modified from Dong et al. (1995) and Moncada et al. (2011), which indicate whether a texture is formed primarily during intense boiling. Intense boiling (sometimes referred to as "flashing") involves the conversion of a large proportion of the fluid from liquid to steam, usually due to a sudden reduction in pressure (Moncada et al., 2011). This differs from "gentle boiling", which is when only a small proportion of the fluid is converted to steam, and characteristic boiling textures may not form (Moncada et al., 2011). The classifications used in this study are simplified from that of Moncada et al. (2011) and differ in that we do not consider crustiform banding to be necessarily indicative of intense boiling (Figure 2). Simple crustiform banding can form from a variety of factors, while complex crustiform banding usually involves pressure release and boiling (Dong et al., 1995). The distinction between simple and complex banding is considered too arbitrary and unreliable to use as a boiling indicator in this study. The formation of jigsaw or mosaic quartz has been attributed to recrystallisation of massive chalcedony or amorphous silica that formed during boiling (Dong et al., 1995; Moncada et al., 2011). However, we sometimes found it difficult to differentiate from silicified vein wall rock and therefore did not use it as an indicator for boiling. Most primary textures indicative of formation during intense boiling are commonly modified by later recrystallisation of calcite, chalcedony and/or amorphous silica to quartz. The relationship between primary growth textures and their recrystallised equivalents are summarized in Table 1. The bladed calcite (including bladed calcite replaced by quartz) and colloform textures are often identifiable in the field or hand sample. However, some other textures that are considered indicative of boiling, such as flamboyant or moss textures (Dong et al., 1995 and Moncada et al., 2011), are only readily identifiable under the microscope.

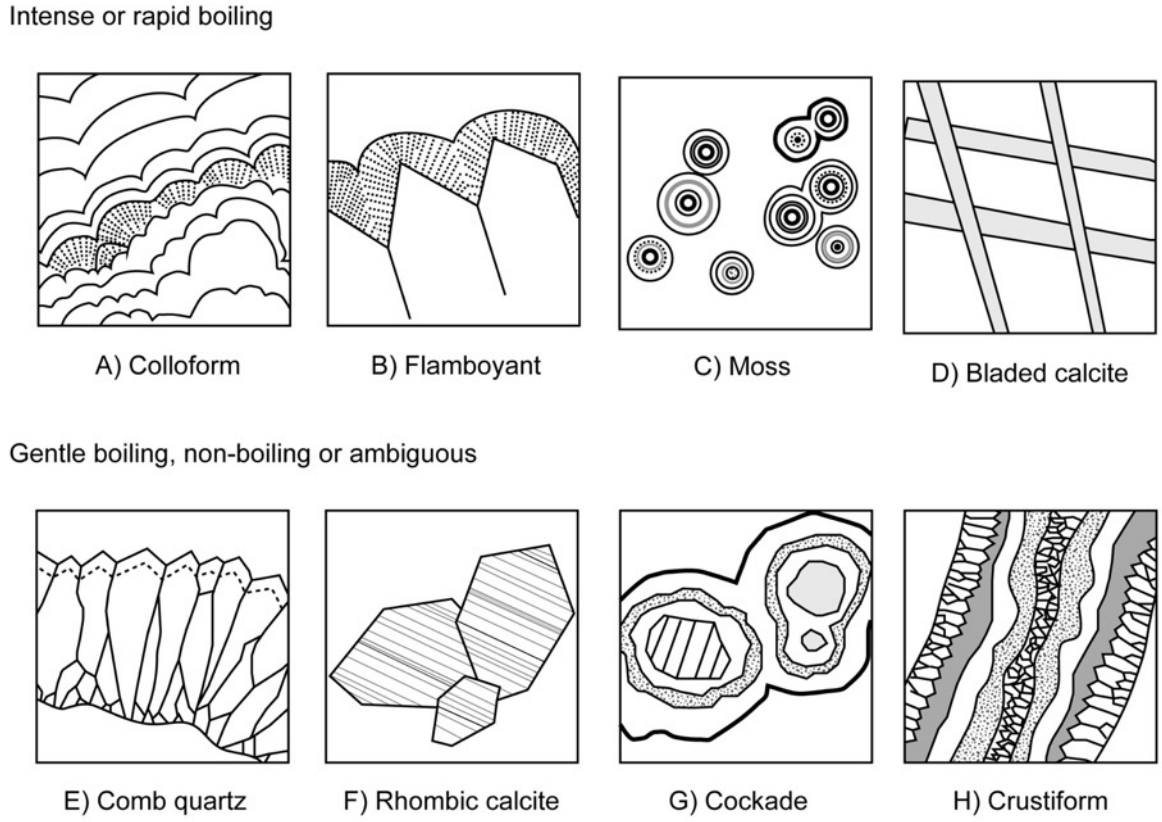

Figure 2: Summary of silica and calcite vein textures used in this study to distinguish between boiling and non-boiling or ambiguous fluid conditions (modified from Dong et al. (1995) and Moncada et al. (2011)). A) Colloform; B) Flamboyant; C) Moss; D) Bladed calcite (calcite is usually subsequently replaced by quartz); E) Comb quartz (includes zonal textures of Dong et al. (1995) and Moncada et al. (2011)); F) Rhombic (or "blocky") calcite; G) Cockade; H) Crustiform.

Table 1: Comparison of primary vein textures and their equivalents after recrystallisation of quartz.

Primary texture	**Texture(s) after re-crystallisation**	**Reference**
Colloform	Colloform-banded plumose	Moncada et al., 2011
	Colloform-banded jigsaw	
Flamboyant	Feathery	Adams, 1920; Sander and Black, 1988; Dong et al., 1995; Moncada et al., 2011
	Plumose	
Moss	Ghost sphere	Dong et al., 1995
Bladed calcite	Lattice bladed quartz	Dong et al., 1995
	Ghost bladed quartz	

4.4.3. Scanning electron microscope (SEM)

Scanning electron microscope work was undertaken on 100 μm and 30 μm polished thin sections. Backscatter secondary electron (BSE) imaging and energy-dispersive x-ray spectroscopy (EDS) used a JEOL Neoscope 6000Plus SEM with EDS detector, at the GNS

Science Wairakei Research Centre, New Zealand, and a JEOL JSM IT-300 SEM with an Oxford Aztec silicon drift detector EDS at the University of Canterbury, Christchurch, New Zealand. Cathodoluminescence (CL) imaging used a JEOL JSM 7000F SEM with a Gatan mono CL detector, at the University of Canterbury, Christchurch.

4.4.4. SWIR reflectance spectroscopy

SWIR reflectance spectroscopy used the Corescan Hyperspectral Core Imager Mark II (HCI-3). The Corescan HCI-3 uses a 0.05 mm spatial resolution camera for colour photography, and a 3.5 nm spectral resolution SWIR reflectance spectrometer with a 0.5 mm diameter analysis window. Corescan analyses were made on a total of 343 samples from 176 locations, mostly on hand sample slabs. Mineral identification and calculation of the wavelength position of the white mica AlOH absorption feature (λ_{AlOH}) for Corescan data was conducted by Corescan staff using proprietary software. Corescan was used as the method of choice over lower resolution TerraSpec for the reasons outlined in Chapter 3. The H_2O/AlOH ratio, sometimes called a crystallinity index, was not used in this study due to the high abundance of silica, which contains abundant H_2O fluid inclusions that interfere with the H_2O feature of other minerals such as interlayered smectite.

Semi-quantitative mineral abundances were obtained from the Corescan data and used to determine the mineralogy of each sample, and their spatial distribution of minerals. Mineral abundances were calculated by Corescan staff as the percentage of 0.5 x 0.5 mm "pixels" along each 0.5 mm high row of sample that contained a spectral signal for each mineral. Each pixel can contain spectral signals from more than one mineral; therefore the total mineral percentage per row is usually greater than 100%. This means only a semi-quantitative abundance is possible to evaluate relative differences. In this study, only presence or absence of a mineral species was judged valuable in each sample rather than their abundance. Therefore the maximum percentage value for each mineral in the sample was determined (see Appendix I). Very small maximum mineral percentages were common, so an arbitrary cut-off value of 3% was chosen for mineral occurrences. We cannot preclude the possibility that this approach may lead to "false negatives" where we erroneously conclude that minerals in low abundances are absent, however petrography has failed to identify any such cases. For locations where multiple samples were collected and analysed with Corescan, the maximum percentage value from all samples at that location was used. The λ_{AlOH} was used to

investigate the spatial variation in white mica composition, and contoured using kriging methods (see Chapter 3).

4.4.5. Fluid inclusion microthermometry

Fluid inclusions were identified by optical microscope in double-polished 100 μm thin sections of veins. Fluid inclusions may be classified by their timing of formation compared to the growth of the host crystal and have three main origins: primary, secondary or pseudosecondary (Roedder, 1984; Goldstein and Reynolds, 1994; Van den Kerkhof and Hein, 2001; Bodnar, 2003). Primary inclusions are formed during growth of the host crystal, while secondary inclusions form later, usually due to healing of micro-fractures. Pseudosecondary inclusions are trapped during healing of fractures that formed while the crystal was still growing (Roedder, 1984). In this study it was preferred to analyse primary fluid inclusions where possible, and the best criterion for determining primary origin is the relationship of fluid inclusions to the growth zonation of a crystal (Goldstein and Reynolds, 1994), although other criteria such as size, shape and isolation from other inclusions may be suggestive (see Roedder, 1984 for full criteria). In this study, crystal growth zones were identified by optical microscope where possible, and SEM cathodoluminescence (CL). Inclusions were considered primary if they obviously followed crystal growth zones. Inclusions were considered pseudo-secondary if a healed fracture or trail of inclusions clearly terminated abruptly at a specific crystal growth zone. Almost all fluid inclusions analysed were in comb-textured quartz (see Fig. 4). Fluid inclusions in quartz textures that show evidence for recrystallistion from amorphous silica or chalcedony, such as colloform or flamboyant, were avoided, as recrystallisation may significantly alter the inclusions (Sander and Black, 1988). Fluid inclusions were grouped into fluid inclusion assemblages (FIAs), which describe a group of fluid inclusions that were all trapped at the same time (Goldstein and Reynolds, 1994). All inclusions in a fluid inclusion assemblage are implied to have been trapped at approximately the same temperature and pressure, and have trapped fluid of approximately the same composition. A fluid inclusion assemblage therefore represents a "fluid event" in the history of the system (Goldstein and Reynolds, 1994; Bodnar, 2003). Fluid inclusion assemblage classifications are useful when it is difficult to determine the temporal classification (primary, secondary, pseudosecondary) of an inclusion or group of inclusions, which is often the case in reality (Roedder, 1984; Goldstein and Reynolds, 1994; Bodnar, 2003).

Fluid inclusion microthermometry was conducted on two phase liquid-dominated inclusions, to determine the homogenisation temperature (T_h). The melting temperature (T_m) of the frozen inclusions was used to determine the equivalent salt (NaCleq) content of the contained fluid, using the HokieFlincs_H2O-NaCl Excel spreadsheet and the equations used therein (Bodnar, 1983; Sterner et al., 1988; Bodnar, 1993; Bodnar and Vityk, 1994; Atkinson, 2002; Lecumberri-Sanchez et al., 2012; Steele-MacInnis et al., 2012). Pressure corrections were not made on homogenisation temperatures due to uncertainty in the depth/pressure of trapping. The effect of pressure is therefore assumed to be insignificant. The major assumptions made during microthermometry are as follows (from Roedder, 1984):

1. The fluid trapped when the inclusion was single homogenous phase.
2. The cavity in which the fluid is trapped did not change in volume after sealing.
3. Nothing is added or lost from the inclusion after sealing.
4. The effects of pressure are insignificant, or are known.
5. The origin of the inclusion is known.
6. The determinations of T_h are not only precise, but accurate.

Fluid inclusion microthermometry was conducted using a Linkam THMSG600 (precision ± 0.1 degrees C and an accuracy of ± 0.1 degrees for Tm and ± 1 degree for Th) heating and cooling stage, controlled by Linksys 32 DV software at the GNS Science Wairakei Research Centre, New Zealand, and Michigan Technological University, U.S.A. Stages were calibrated using the melting temperatures of synthetic CO_2 fluid inclusions (-56.6°C), deionised H_2O (0.0°C), and $K_2Cr_2O_7$ (398.0°C). In total 457 fluid inclusions were analysed, from 17 samples, of which 209 could be grouped into fluid inclusion assemblages.

4.5. RESULTS

4.5.1. Alteration associations

Petrographical descriptions from thin sections, backscatter SEM, and Corescan analysis show that most rocks inside and adjacent to Lake City caldera are altered to some degree. Several distinct associations of alteration minerals can be identified, as described below.

4.5.1.1. Propylitic

This association consists of quartz, chlorite and illite, with some calcite, epidote and adularia (Figs. 3a, 3b, 4a and 4b). It is the most widespread alteration association at Lake City caldera,

found throughout most of caldera except for above the resurgent pluton, and the area surrounding Red Mountain (Fig. 5). Parts of the granite basement, intra-caldera tuff, breccia and syenite all show propylitic alteration (Fig. 5). Satellite SWIR data show that propylitic alteration is common throughout the western San Juan Mountains (Rockwell, 2012). Veins hosted in propylitic-altered rock (Figs. 6c and 6d) are dominated by quartz/silica, ± calcite ± adularia.

4.5.1.2. Phyllic

Phyllic alteration consists of quartz/silica + white mica (mostly illite) ± pyrite (Figs. 3c, 3d, and 4c). This assemblage is widespread in the centre of the caldera above the resurgent pluton (Fig. 5) and in decimetre- to centimetre-wide "haloes" around some veins in areas of otherwise propylitic alteration (Fig. 6). It is analogous to the quartz – sericite – pyrite assemblage of Hon (1987). This association can be identified in the field by bleached rock, often with a thin red or yellow surface stain due to oxidation of pyrite (e.g. Fig. 6a). These surface stains form the large, distinctive areas of red rock in the centre of the caldera and around major veins, which are identifiable in satellite SWIR data (Rockwell, 2012). It is distinguished in SWIR hand sample data by an abundance of illite and lack of chlorite or epidote. Fig 5 shows the extent of the major phyllic alteration zone at the centre of the caldera, however "haloes" of phyllic alteration around major veins are not shown at the scale of this map. One of the largest of these haloes is associated with the ring dyke at Red Gulch on the western margin of the caldera and contains many veins (Fig. 6a). Veins hosted in phyllic-altered rocks are dominated by quartz/silica, ± pyrite ± illite. Textures indicative of replacement of bladed calcite by quartz are common.

4.5.1.3. Argillic

This association consists predominantly of montmorillonite (smectite) clay (Figs. 3e, 3f and 4d), indicating a low temperature argillic assemblage (Hedenquist et al., 2000). This association was only sampled in the east of the caldera in altered dacite lavas near Red Mountain (Fig. 5). The samples collected for this study are correlated with the argillic alteration surrounding Red Mountain that was mapped by Bove and Hon (1992). Veins have not been identified in this association, however the argillic alteration is most pervasive in linear ~1 – 10 m wide SE trending zones.

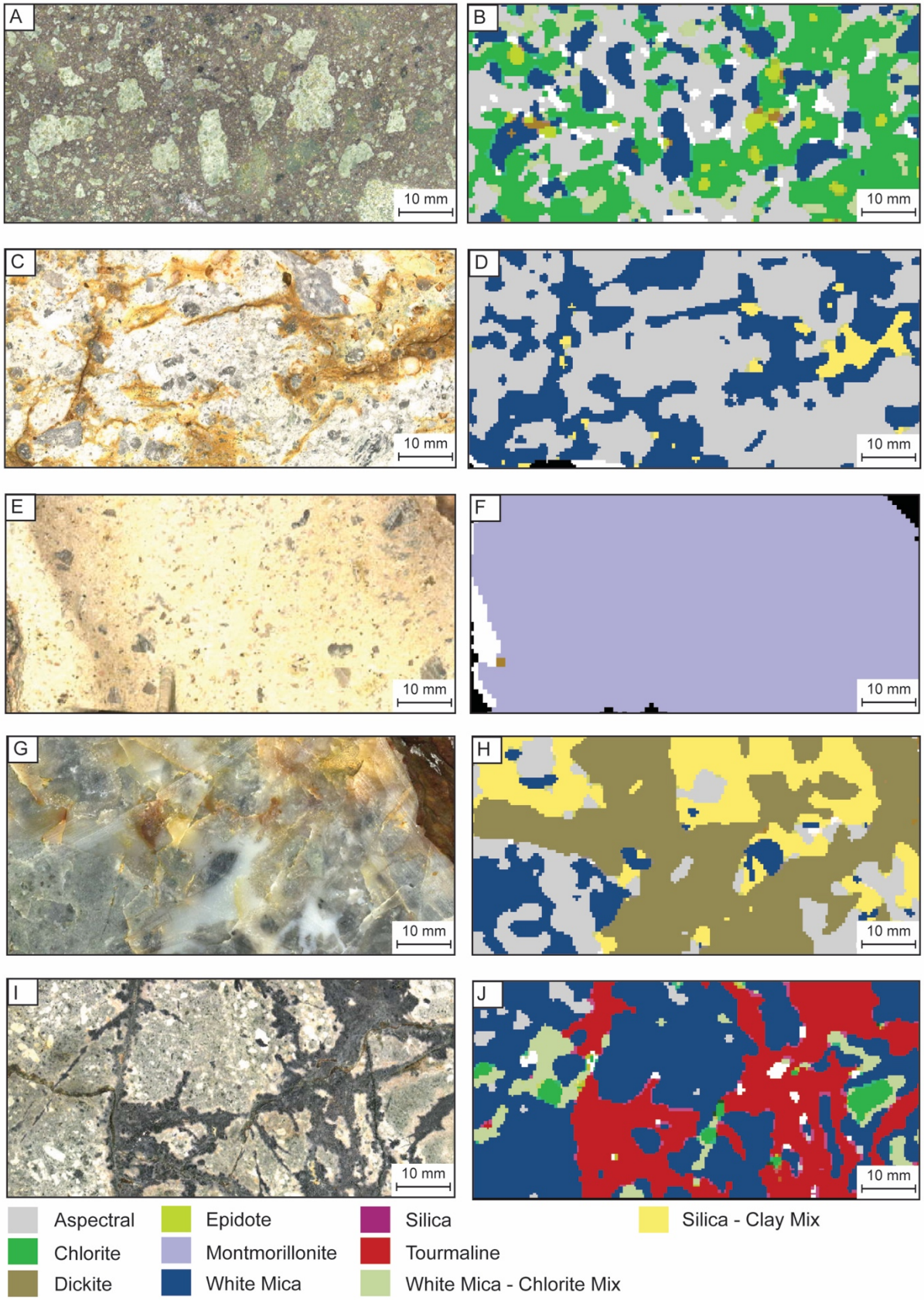

Figure 3: Examples of the alteration associations at Lake City caldera. Left column are hand sample images; right column Corescan mineral maps. A) Propylitic B) Phyllic; C) Argillic; D) Advanced argillic; E) "Porphyry-type". A and B are sample LCB090714-1A (location 9), C and D are sample LCT091014-1E (location 212), E and F are sample LCDLA082914-1 (location 296), G and H are sample LCTV090314-4A (location 207), I and J are sample LCTB080314-1A (location 70). See figure 1 for field locations.

4.5.1.4. Advanced argillic

Advanced argillic alteration is characterised by an abundance of kaolinite, dickite and/or alunite (Figs. 3g, 3h and 4e). This association was sampled at only one location (207 – see Fig. 1b) at a vein in tuff in the eastern half of the caldera, where it contained dickite, illite and quartz/silica. Satellite data show no major area advanced argillic alteration at this location (Rockwell, 2012), so the dickite alteration is probably very localized. We correlate this area of alteration as analogous to, but not contiguous with, the more widespread quartz-alunite alteration assemblage at Red Mountain (Fig. 7) (Bove and Hon, 1990, 1992).

4.5.1.5. "Porphyry type"

This association is used to describe the heterogeneous alteration and vein association inside and above the quartz monzonite intrusion of Alpine Gulch (Fig. 5). The quartz monzonite itself contains the alteration minerals chlorite and white mica (Fig. 5). Above the intrusion, in the tuff, is an area of breccia with clasts altered to white mica and chlorite, with a cement of almost entirely tourmaline (Figs. 3i, 3j and 4f). Veins inside and near the quartz monzonite contain quartz, carbonate, and the sulfides galena, sphalerite and chalcopyrite. Hon (1987) described this area as weak Cu-Mo porphyry-type mineralisation.

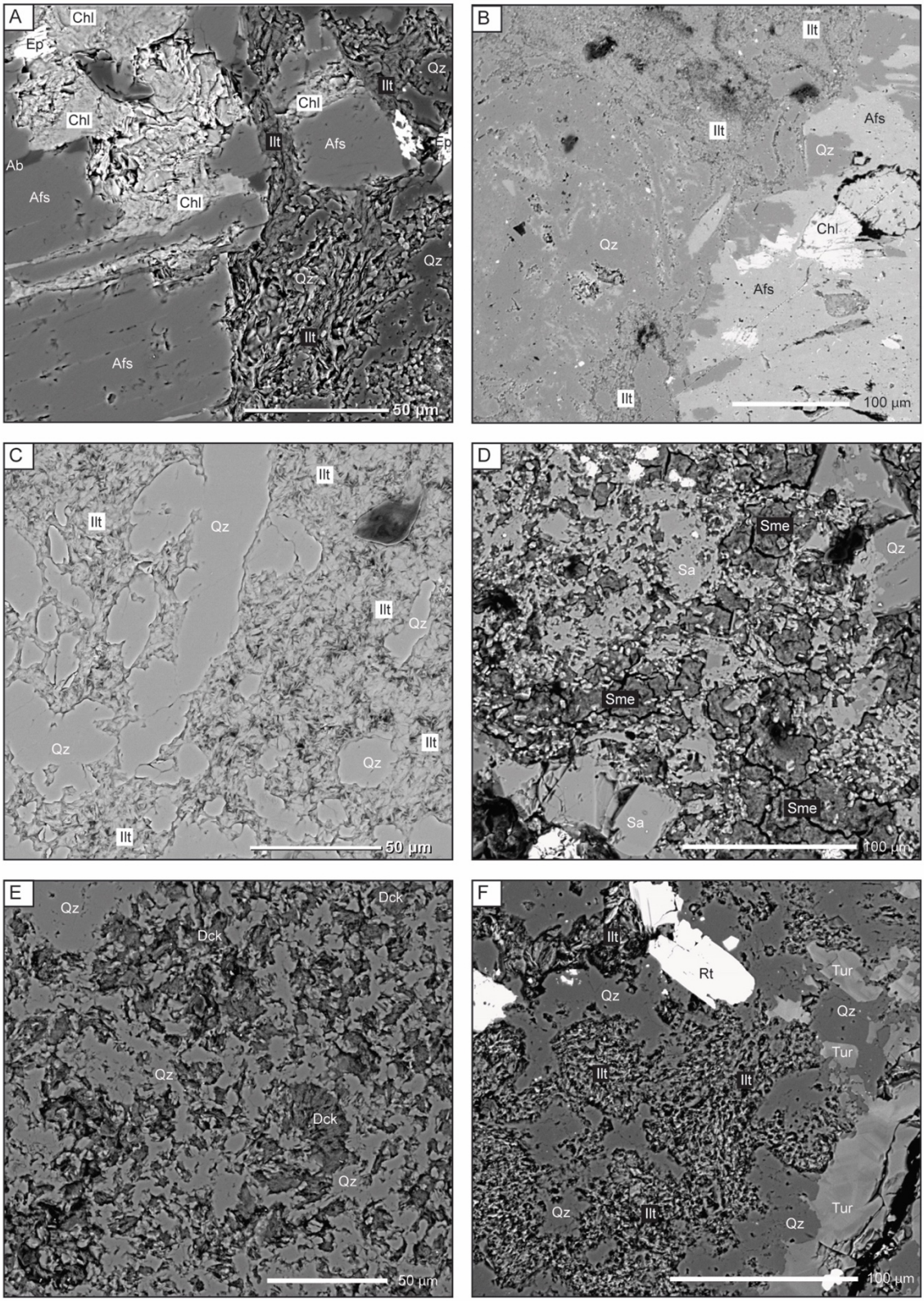

Figure 4: Backscatter SEM images of the alteration associations identified at Lake City caldera. A) Porpylitic altered granite; B) Sunshine Peak Tuff with weak propylitic alteration, showing chlorite which is restricted to crystals, absent from matrix in this sample; C) Sunshine Peak Tuff with phyllic alteration; D) Dacite lava with argillic alteration; E) Sunshine Peak Tuff with advanced argillic alteration; F) Matrix of tourmaline-rich breccia, hosted in intra-caldera landslide breccia above the quartz monzonite of Alpine Gulch. This is part of the"porphyry type" area of alteration and mineralisation. Abbreviations: Ab = albite; Afs = alkali feldspar; Chl = chlorite; Dck = dickite; Ep = epidote; Ilt = illite; Qz = quartz; Rt = rutile; Sa = sanidine; Sme = smectite; Tur = tourmaline. A = sample LCGB091414-4B (location 338), B = LCT091014-1A (location 212), C = LCTV090314-1A (location 204), D = LCDLA082914-1 (location 296), E = LCTV090314-4A (location 207), F = LCTB080314-1C (location 70). See figure 3 for field locations.

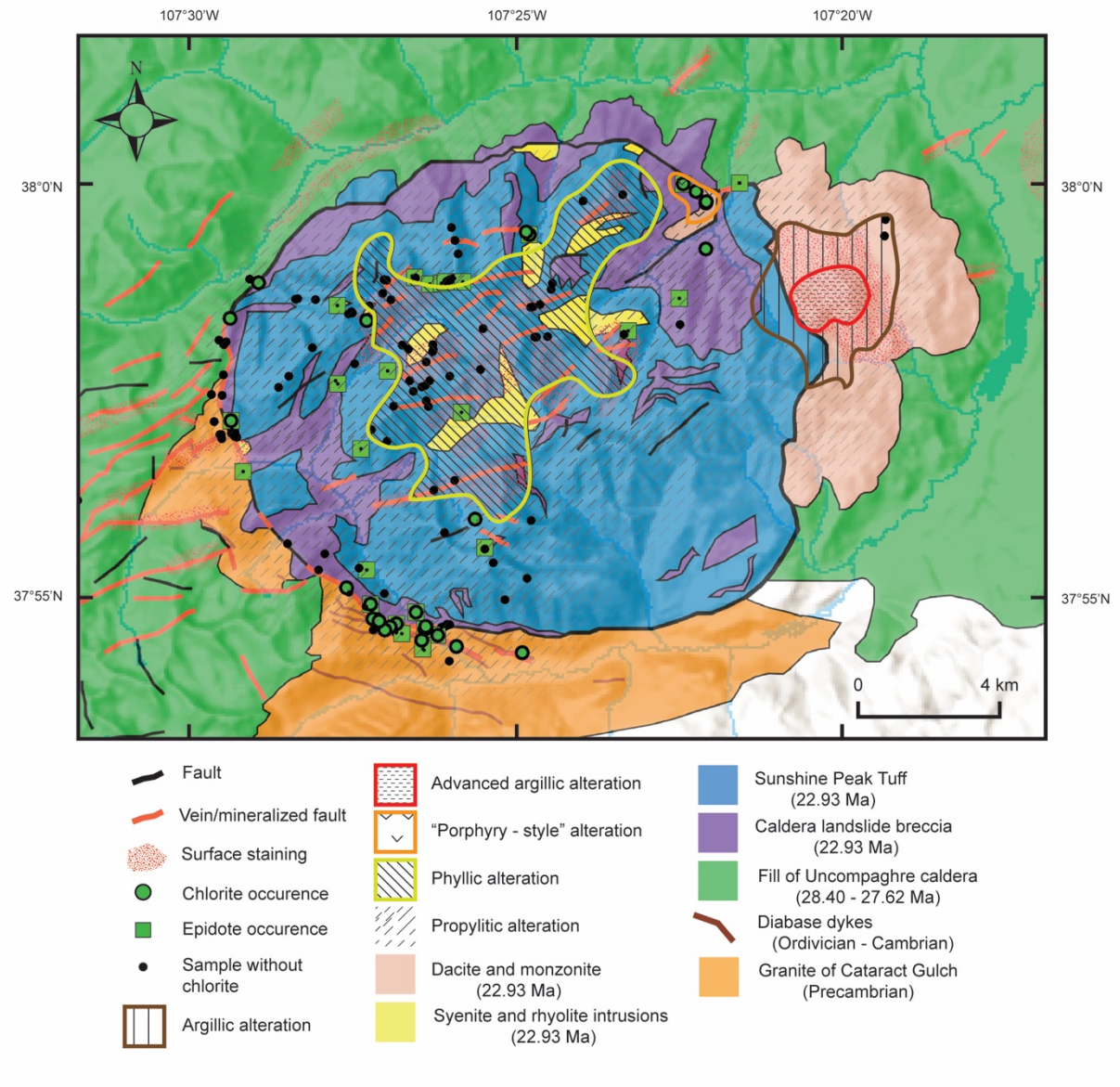

Figure 5: Map showing simplified geology of Lake City caldera (modified from Lipman, 1976 and Hon, 1987) and alteration associations. Associations are mapped based on mineralogy of samples collected for this study, augmented by geological data from Hon, 1987 and Bove and Hon, 1992; and ASTER satellite data from Rockwell, 2012. See text for descriptions of the mapped alteration associations.

Figure 6: Field photos of phyllic and propylitic alteration at Lake City caldera. A) Phyllic alteration halo in granite, outward from a large (up to 2 m wide) vein on the margin of a ring dyke on the western margin of the caldera. Note the abrupt transition to weak propylitic alteration. B) Phyllic alteration halo in intra-caldera welded tuff, outward from a series of veins up to 100 mm wide vein in the Cooper Creek catchment near the centre of the caldera. C) Vein hosted in propylitically altered diabase outside the southwestern caldera margin. Note the lack of a phyllic alteration halo. D) Small vein in propylitically altered granite outside the western caldera margin, with no phyllic alteration halo. A = location 280, B = location 212, C = location 3, D = location 150. See figure 3 for field locations.

4.5.2. Short wave infrared reflectance spectroscopy

The wavelength position of the 2200 nm AlOH absorption feature of white mica (referred to as λ_{AlOH}) varies considerably at Lake City caldera (see Appendix J), as does the white mica composition (see Chapter 3). Samples in the centre of the caldera, near the centre of the syenite resurgent pluton, generally have lower λ_{AlOH} values (down to <2201 nm), indicating muscovitic (high Al) compositions, than samples at the western and southwestern margin

(Fig. 7). The location near the intersection of the Alpine Gulch fault and northeastern ring fault has a distinctly low λ_{AlOH}, while samples near the quartz monzonite and northeastern most part of the syenite pluton have moderate to high λ_{AlOH}, indicating phengitic (lower Al, high Fe + Mg) compositions (Fig. 7). There is no significant correlation between elevation and λ_{AlOH} (Fig. 8) for all samples, nor for samples only in the centre of the caldera. Elevation is considered a proxy for paleodepth, because there has been negligible regional tilting at Lake City since caldera formation and resurgence (Hon, 1987). In the kriged data, there is a distinct NE – SW trending zone of lower λ_{AlOH} from the centre of the caldera to the western margin and Eureka Graben (Figs. 1b and 7). The extension of this zone to the western caldera margin is only defined by two low λ_{AlOH} values, so more data are needed to confirm if this feature is accurate. The area of low λ_{AlOH} in the centre of the caldera correlates somewhat with the large area of predominantly phyllic alteration (Fig. 7) and correlate well with low $\delta^{18}O$ ratio (Fig. 1c). However, on the northwestern and southwestern caldera margins, phengitic compositions (high λ_{AlOH}) correspond to areas of low $\delta^{18}O$ ratio (Figs.1c and 7).

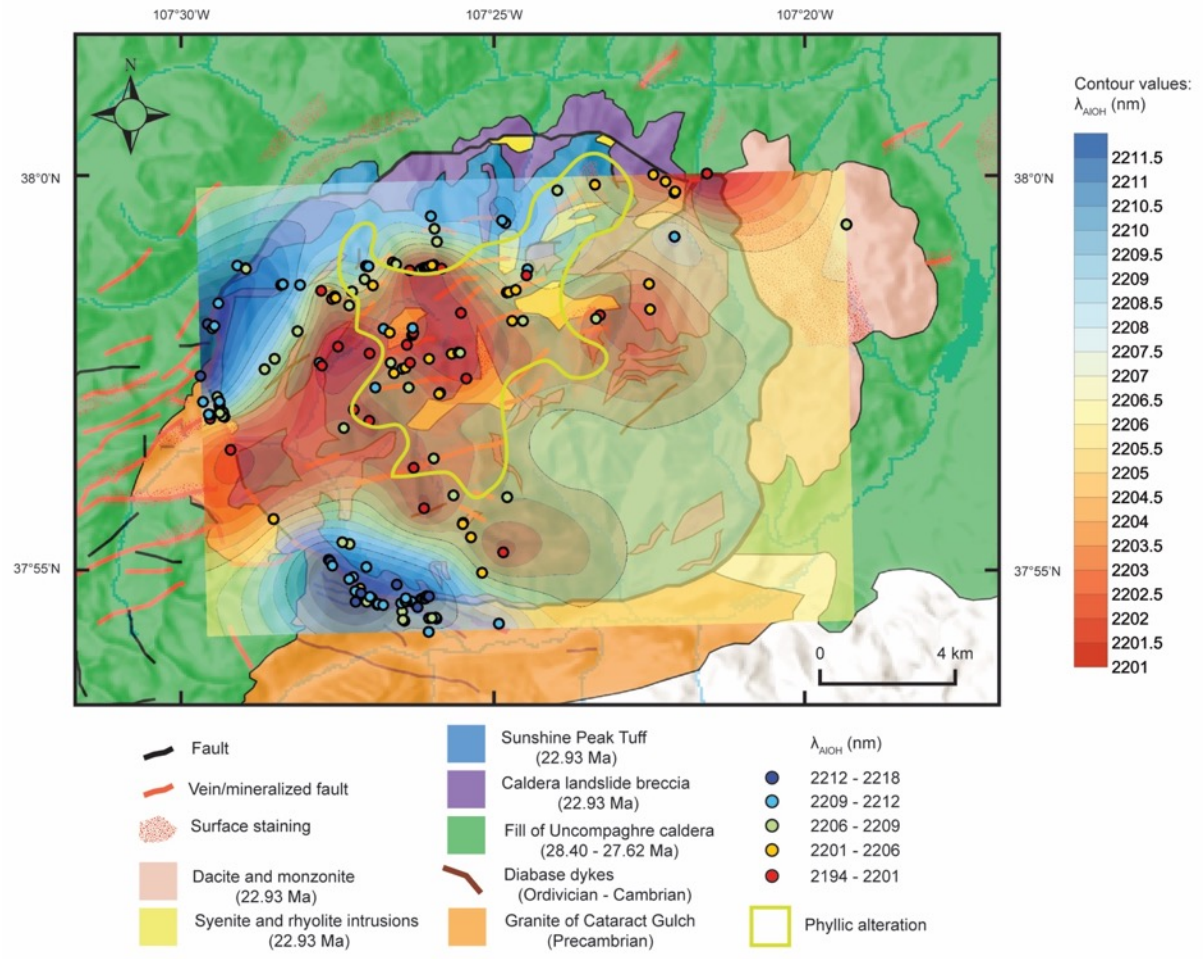

Figure 7: Map showing the wavelength position of the AlOH absorption feature (λ_{AlOH}) as measured by SWIR reflectance spectroscopy (Corescan HCI-3) on white micas. The contours are those of the kriged model, and are overlaid on the simplified geology of Lake City caldera (modified from Lipman, 1976 and Hon, 1987).

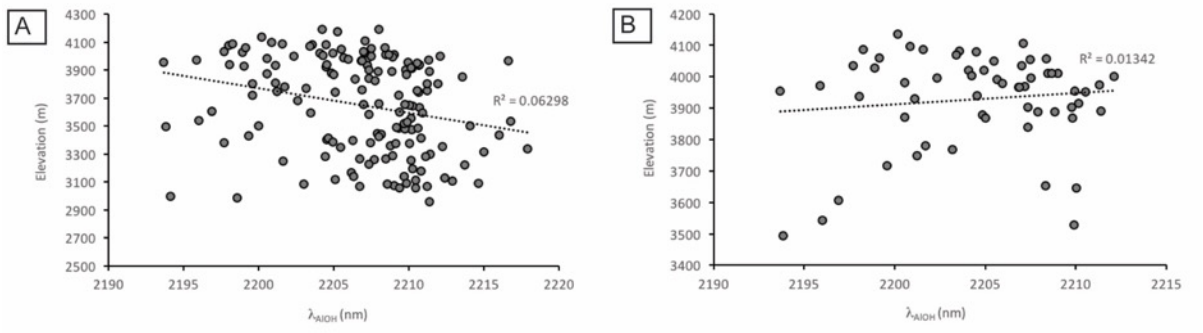

Figure 8: Comparison of the average wavelength of the AlOH absorption feature (λ_{AlOH}) of a location versus its elevation. A) Elevation versus λ_{AlOH} for all locations for which λ_{AlOH} data were acquired.B) Elevation versus λ_{AlOH} only for locations in the centre of the caldera, see Fig. 1b for the location of these sites. λ_{AlOH} data were acquired using a Corescan HCI-3.

4.5.3. Vein textures

A variety of vein textures are identified at Lake City caldera (Figs. 9 and 10). Textures that indicate intense boiling and those that do not (or are ambiguous), are both found throughout the caldera and at all elevation intervals (Fig. 11a and Appendix K). However, the proportion of locations that has boiling textures identified, compared to those that did not, increases with elevation (Fig. 12).

4.5.3.1. Centre of the caldera

In the centre of the caldera boiling textures are common in veins at higher elevation levels, and are usually found in veins on the high ridges above the resurgent pluton (Fig. 11a). Therefore there is a positive correlation between the proportion of locations with boiling textures identified and elevation for central locations (Fig. 12b). The boiling textures often comprise a majority of vein volume.

4.5.3.2. Western caldera margin

At the western caldera margin, inside and near Red Gulch, boiling textures are present but are mostly confined to the large veins along or very close to the caldera margin discontinuity (Fig. 11b). This includes veins along the margin of the ring dyke, and above it (Fig. 11b). If the boiling textures were formed during sudden "flashing" events due to a sudden pressure release, these results may imply that the caldera margin was more hydrologically well-connected to the surface and/or rest of the reservoir than surrounding smaller discontinuities. The only known occurrence of original bladed calcite (i.e. not replaced by quartz) at Lake City caldera is in one of the highest elevation veins along the western caldera margin discontinuity, which shows pervasive boiling textures. Boiling textures were not identified in the large NE-trending veins in the granite outside the caldera margin (Fig. 11b).

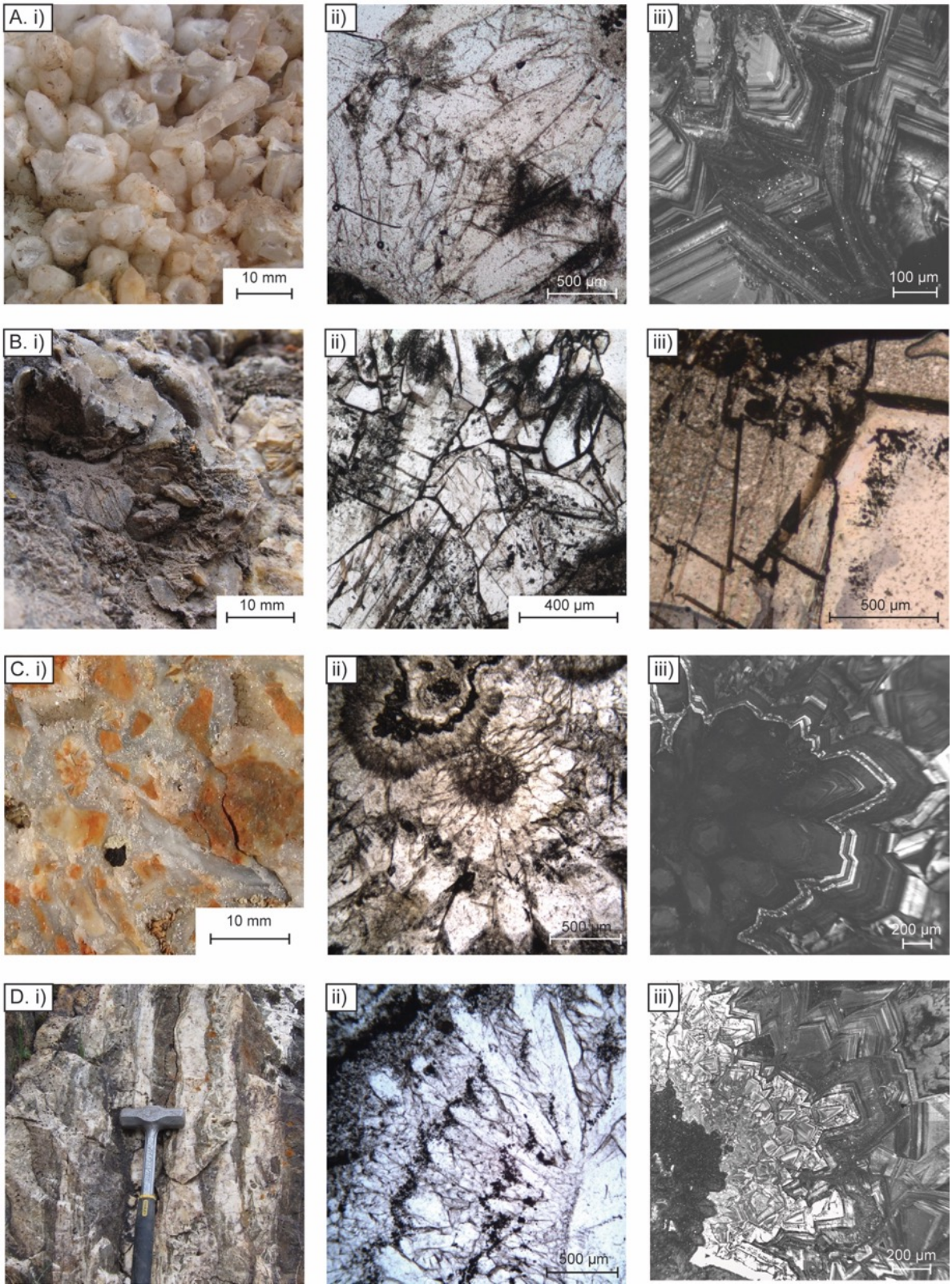

Figure 9: Examples from Lake City caldera of vein textures that are not considered indicative of intense boiling. Left column are field or hand sample photos; middle column are thin section photomicrographs; right column are cathodoluminescence SEM images, except for in row B, which is a photomicrograph. A) Comb quartz; B) Rhombic (or "blocky") calcite; C) Cockade; D) Crustiform banding. Samples and field locations: A. i) Location 2; ii) Sample LCIV082013-1D, location 280; iii) Sample LCUV081814-2B, location 153; B. i) Location 195; ii) Sample LCBVRF090714-1G, location 9; iii) Sample LCGV083114-2B, location 195; C. i) Location 207; ii) Sample LCBV082413-3A, location 288; iii) Sample LCTV090413-3, location 314; D. i) Location 36; ii) Sample LCIVRF082013-1B, location 280; iii) Sample LCBV082413-3A, location 288. See figure 3 for field locations.

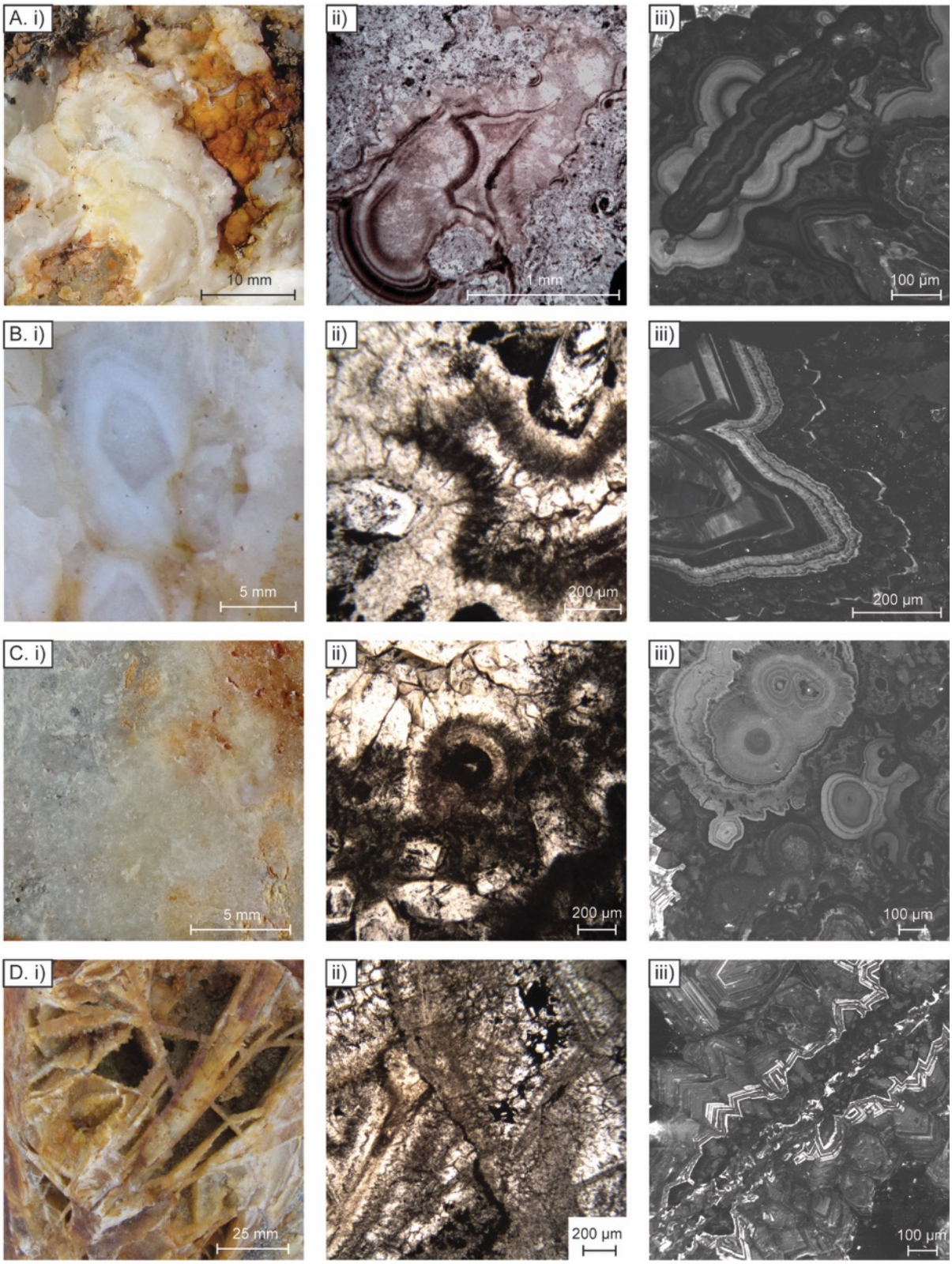

Figure 10: Examples from Lake City caldera of vein textures that are indicative of intense boiling. Left column are field or hand sample photos; middle column are thin section photomicrographs; right column are cathodoluminescence SEM images. A) Colloform; B) Flamboyant; C) Moss; D) Bladed calcite, or more commonly bladed quartz which has replaced calcite. Samples and field locations: A. i) Location 207; ii) Sample LCGV082514-2A, location 105; iii) Sample LCTV090413-3, location 314; B. i) Location 129; ii) Sample LCBV082413-3A, location 288; iii) Sample LCUV081814-2B, location 153; C. i) LCTV090413-3, location 314; Sample LCBV082413-3A, location 288; iii) Sample LCTV090413-3, location 314; D. i) Location 60; ii) Sample LCBV082413-3A, location 288; iii) Sample LCTV090413-3, location 314. See figure 3 for field locations.

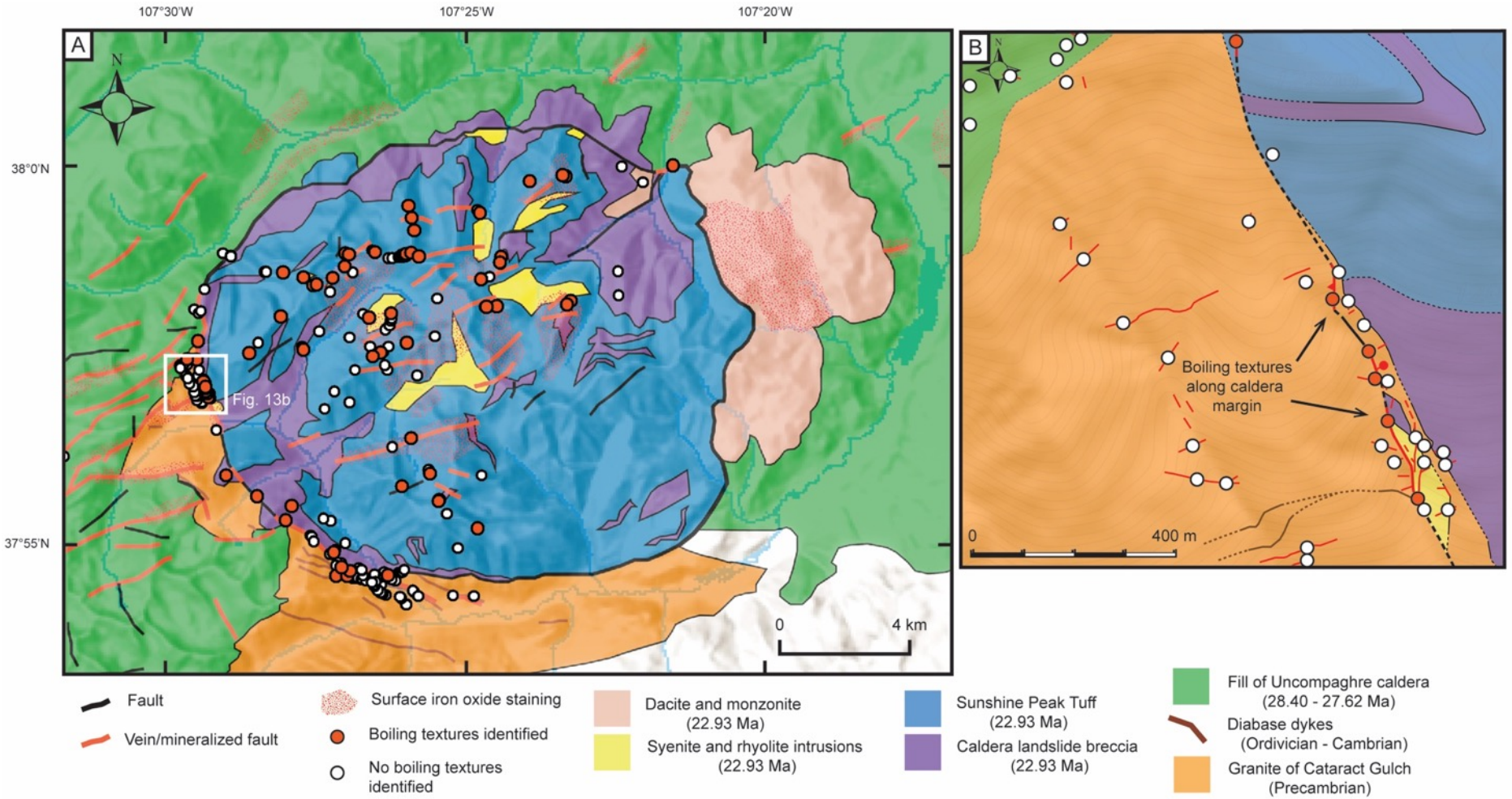

Figure 11: A: Map showing simplified geology of Lake City caldera (modified from Lipman, 1976 and Hon, 1987), and locations where boiling textures were identified (colloform quartz/silica and/or bladed calcite/quartz) versus locations where no such textures were identified (for location data see Appendix K). B: Map of part of the western margin of the caldera (modified from Garden et al., in press), showing the location of boiling textures. Note how boiling textures are restricted to the caldera margin, which cuts across the NE-SW structural grain outside the caldera.

4.5.3.3. Southwest caldera margin

Evidence for boiling is not widespread in veins at the southwestern caldera margin, in the vicinity of the Shelf Road. Where present they are often confined to major veins in the ring fault zone rather than smaller subsidiary veins (Fig. 11a). They are usually not a large proportion of the volume of these veins, but rather are confined to discrete layers within the vein. This is interpreted as infrequent, episodic, intense boiling events. Blocky or rhombic calcite (Fig. 9b) is more abundant in veins at the southwest caldera margin than in other parts of the caldera. It usually formed after the quartz precipitation phase, as evidenced by cross-cutting calcite veinlets or rhombic calcite infilling after comb quartz (Fig. 9b). The largest comb quartz crystals at Lake City caldera were identified at the southwest caldera margin (Fig. 9a).

4.5.3.4. Other parts of Lake City caldera

Veins inside and above the northeastern parts of the syenite pluton at Owl Gulch and "T Mountain" have boiling textures (Fig. 11a). These textures were not identified in veins associated with the quartz monzonite intrusion of Alpine Gulch, however there is evidence for boiling based on fluid inclusion assemblages (see fluid inclusion section below). Boiling textures were not identified in veins on the southeastern side of the Alpine Gulch fault (e.g. location 207). There is evidence for boiling in some, but not all, veins at high elevations on Sunshine Peak. No quartz veins were sampled at Red Mountain for this study, however the system experienced large areas of steam-heated alteration, suggesting that boiling occurred deeper (Larson and Taylor, 1987; Bove et al., 1990).

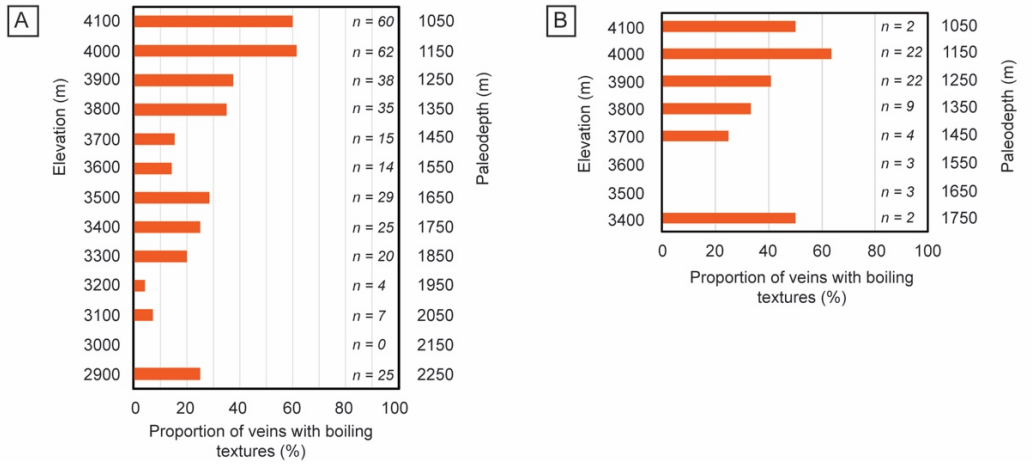

Figure 12: Comparisons of the proportion of veins with boiling textures identified with elevation, showing the greater prevalence of boiling textures at higher elevations/shallower paleodepths. The paleodepth is assuming a surface elevation of 5150 m, which is the maximum height of the resurgent dome as determined by Hon (1987) from the Lake City caldera stratigraphy. Note that these paleodepths are much larger than those determined in this study from fluid inclusion microthermometry (see fluid inclusions section below and Figure 22). The Lake City caldera area has been subject to

negligible regional tilting since the end of resurgence (Hon, 1987). A) Data for all veins throughout the caldera. B) Data for only veins in the centre of the caldera, in the resurgent dome.

4.5.4. Vein zoning

Samples were collected along four scanline transects across veins and adjacent country rock in order to evaluate how λ_{AlOH} for white mica changes on the scale of tens of metres around veins. These four scanlines were chosen so that the four major rock types at Lake City (granite basement, intra-caldera breccia, ignimbrite and syenite) could be systematically sampled and correlation between λ_{AlOH} and vein proximity could be analysed. The pattern is slightly different for each scanline, however in general λ_{AlOH} is lower in country rock closer to a major vein, and often lower or more variable in the vein itself than the country rock. Scanline SW1 (Fig. 13a) is across one of the major mineralised faults of the southwestern ring fault zone of the caldera, in deformed granite. The λ_{AlOH} has an average value of ~2211 - 2212 nm, and is most variable within the veined fault core, ranging from 2206 to 2212 nm (Fig. 13a).

Scanline SW2 (Fig. 13b) is across a series of large veins in deformed intra-caldera breccia adjacent to the caldera margin discontinuity. The λ_{AlOH} in the intra-caldera breccia 20 m away from the major vein is relatively low at 2205 nm, while inside and adjacent to the veins it is variable but still low at 2204 to 2207 nm. In the deformed granite outside the caldera margin discontinuity λ_{AlOH} gradually increases from 2205 nm to an apparent background level of 2210 nm in the 20 m away from the large veins (Fig. 13b). There is no phyllic alteration associated with this halo of decreased λ_{AlOH}.

Scanline I1 (Fig. 13c) is across a vein (mineralised fault) in the intra-caldera welded lower Sunshine Peak tuff. The vein has a distinct phyllic alteration halo 13 m across, in otherwise propylitically altered rock. The λ_{AlOH} shows a distinct trend of decreasing towards the vein, from a background of 2211 nm to 2203 nm inside the vein (Fig. 13c).

Scanline I2 (Fig. 13d) is across a vein/mineralised fault in the syenite resurgent pluton. Alteration is predominantly propylitic, with narrow zones of phyllic alteration. λ_{AlOH} is 2211 nm 11 m away from the main vein, while inside the vein, the two samples have variable λ_{AlOH}, at 2209 and 2212 nm (Fig. 13d).

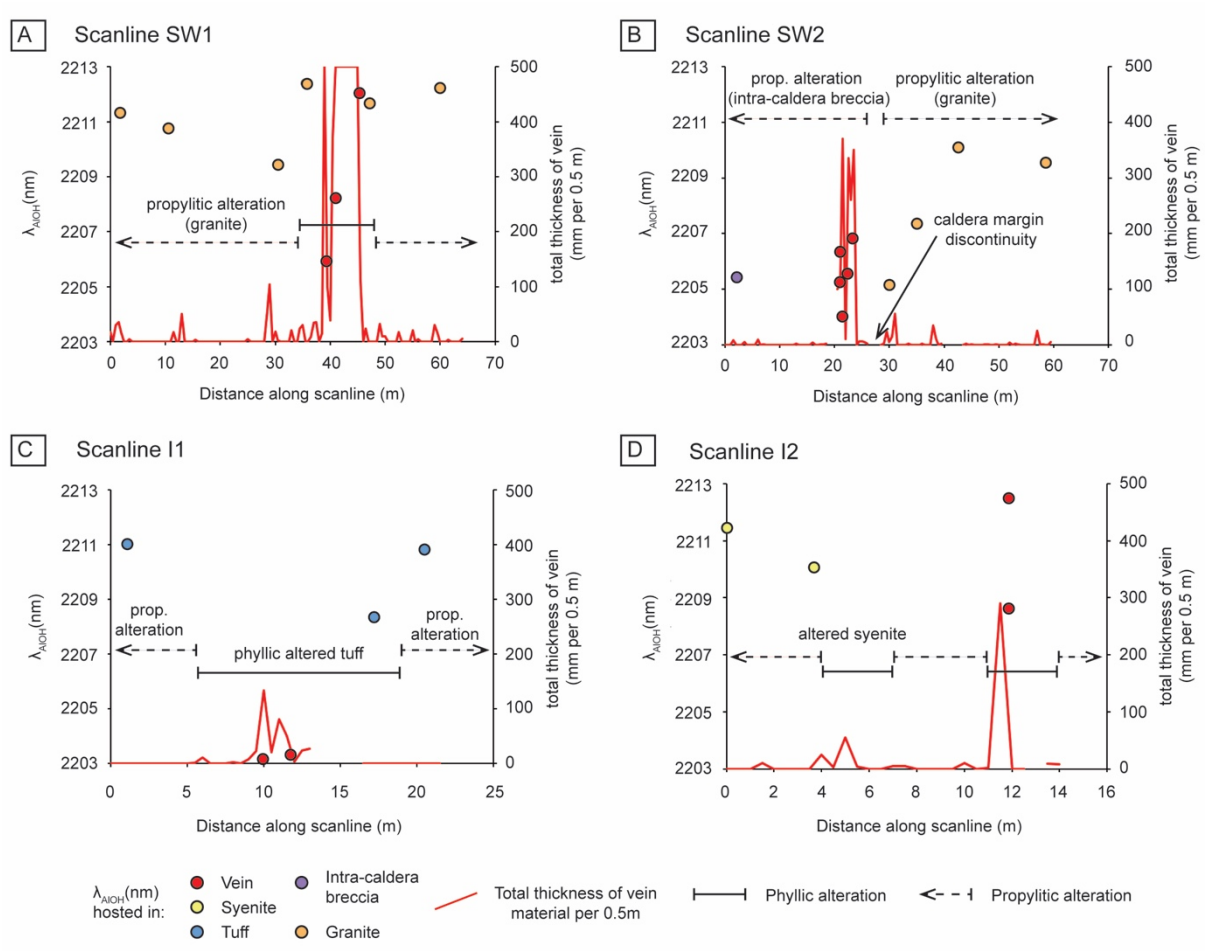

Figure 13: Scanline transects showing the average white mica λ_{AlOH} for samples collected, and the total amount of vein material per half meter. A) Scanline SW1 across a major mineralised fault in the ring fault zone of the southwestern caldera margin, B) Scanline SW2 across the southwestern caldera margin discontinuity, C) Scanline I1 across a mineralised fault in the welded tuff of the centre of the caldera, D) Scanline I2 across a mineralised fault in the syenite pluton.

4.5.5. Fluid inclusions and quartz zoning

Fluid inclusions at Lake City caldera are mostly aqueous liquid-rich (L+V), hosted in quartz, although vapour-rich and three-phase inclusions were identified in some samples (Fig.14, see Appendix L for all fluid inclusion data). Most samples have fluid inclusions with low salinity (<3 % NaCl equivalent), and homogenisation temperatures (T_h) typical of the epithermal environment (~170 – 260°C) (e.g. Figs. 15 and 16). Cathodoluminesence images show that hydrothermal comb textured quartz have well defined growth zones, sometimes with complex geometries (Figs. 15, 16, and 17). The position of fluid inclusions relative to the growth zones was used to define whether the inclusions are primary or secondary. Two samples (from locations 203 and 288) are described in more detail below, as examples, to show how fluid inclusions were related to crystal growth zones to determine their origin.

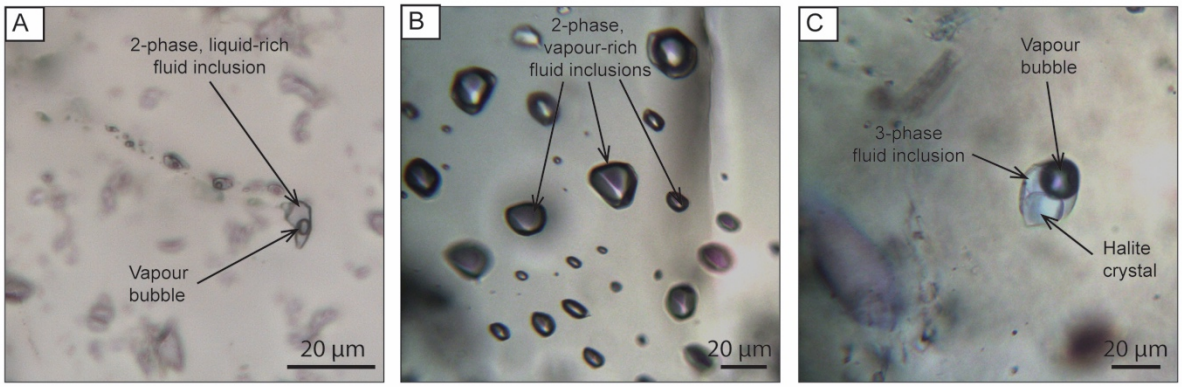

Figure 14: The three main types of fluid inclusions identified during this study. A) Two-phase, liquid-rich (L + V); B) Two-phase, vapour-rich (V + L); C) Three-phase, liquid-rich (L + V + crystal) with NaCl daughter crystal. Samples and locations: A: Sample LCBVRF082413-2A, location 287; B: Sample LCTV081914-1A, location 160; C: Sample LCTV081914-1A, location 160.

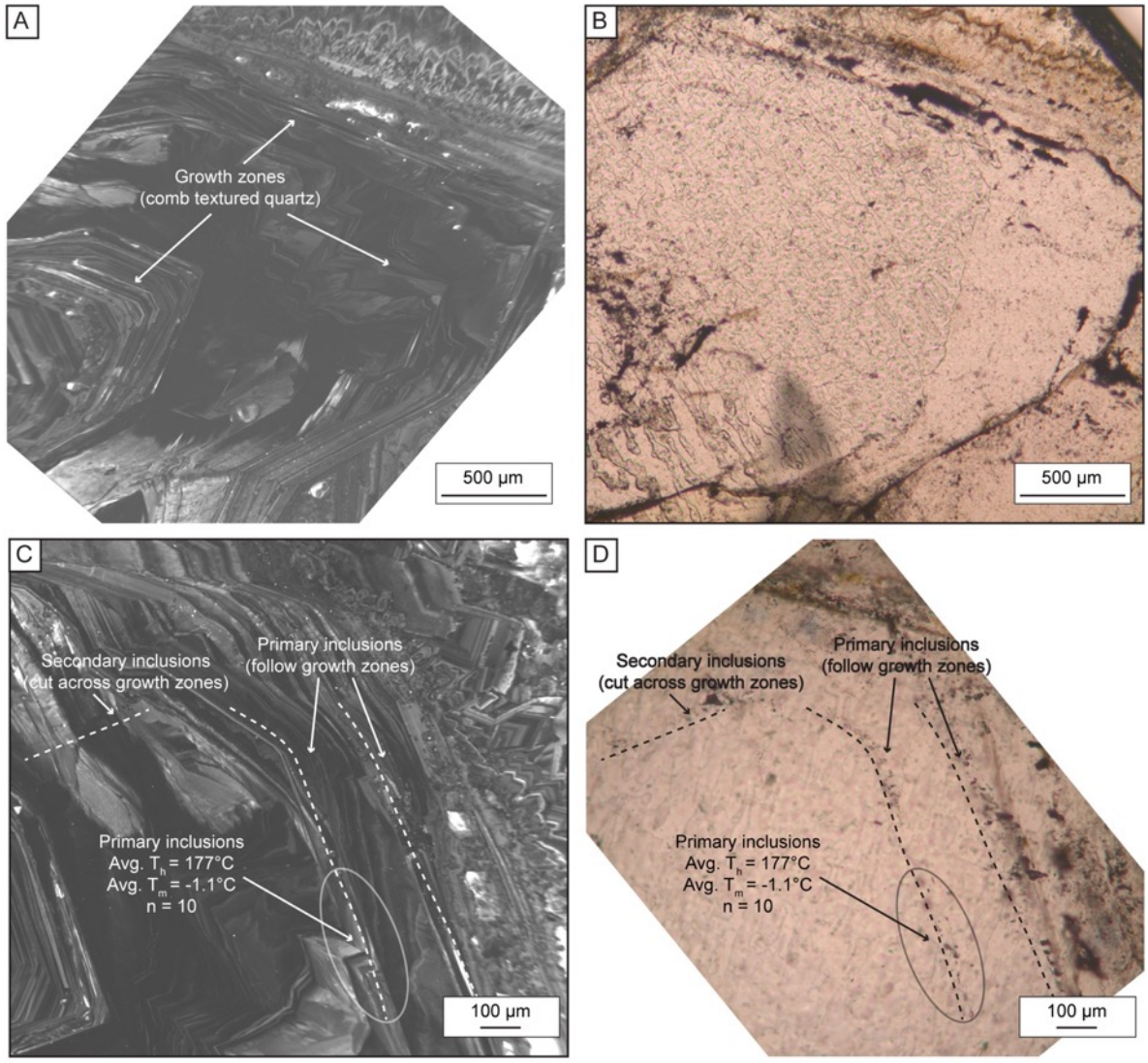

Figure 15: An example of how petrography and CL can be used to distinguish primary and secondary fluid inclusions. A) A large quartz crystal in sample LCTV090114-4C (location 203) with overlaid thin section photomicrograph (plane-polarised light) and CL image, showing intricate internal zoning visible by CL but not the optical microscope. B) Overlaid thin section photomicrograph (plane-polarised light) and CL image showing planes of primary fluid inclusions that follow the growth

zones visible in CL, and a plane of secondary inclusions that cut across growth zonation. Dashed lines indicate fluid inclusion trails.

The vein at location 203 (sample LCTV090114-4C) is dominated by comb quartz, which has intricate internal growth zoning (Figs. 15a and 15c). Some planes of fluid inclusions clearly cut across this zoning, and are hence interpreted as secondary (Figs. 15c and 15d), and were not analysed for microthermometry. Another group of fluid inclusions follows the geometry of the growth zoning, and are interpreted as primary (Figs. 15c and 15d). This fluid inclusion assemblage (assemblage A3, see Table 2) was used for microthermometry. The vein sampled at location 288 (sample LCBV082413-3A) contains a variety of quartz textures. Primary fluid inclusions are hosted by comb textured quartz, showing intricate growth zoning, and are in-between two layers with boiling textures (Figs. 16a and 16b). A group of probably pseudosecondary inclusions is identified as a plane which ends at a growth zone and does not continue to the edge of the crystal (Figs. 16d and 16e). Primary inclusions follow the growth zoning of the crystal (Fig. 16). Although no vapour-rich fluid inclusions were identified, the homogenisation temperatures are likely close to the boiling temperature, due to the close overgrowth of boiling textures.

Overall, there is no obvious trend in homogenisation temperature versus salinity (Fig. 18). This suggests that dilution from meteoric water was important in the hydrothermal system, as the classical boiling trend of higher NaCl content with decreasing temperature was not identified (cf. Hedenquist and Henley, 1985). The locations of all assemblages identified are shown in Figure 19. The lowest homogenisation temperatures (<204°C) are found at high elevations on the western caldera margin and at high elevations in the centre of the caldera (Figs. 19 and 20). High temperatures (>260°C) are found at the southwestern caldera margin, in the centre of the caldera, and at the intersection of the Alpine Gulch fault and the northeastern caldera margin (Fig. 19). One more significant sample is discussed in greater detail below, due to important insights it provides on the Lake City hydrothermal system. This sample (from location 160) shows evidence for two distinct generations of hydrothermal fluid and the only hypersaline fluid inclusions identified at Lake City caldera. The limitations of the fluid inclusion data collected in this study are then outlined.

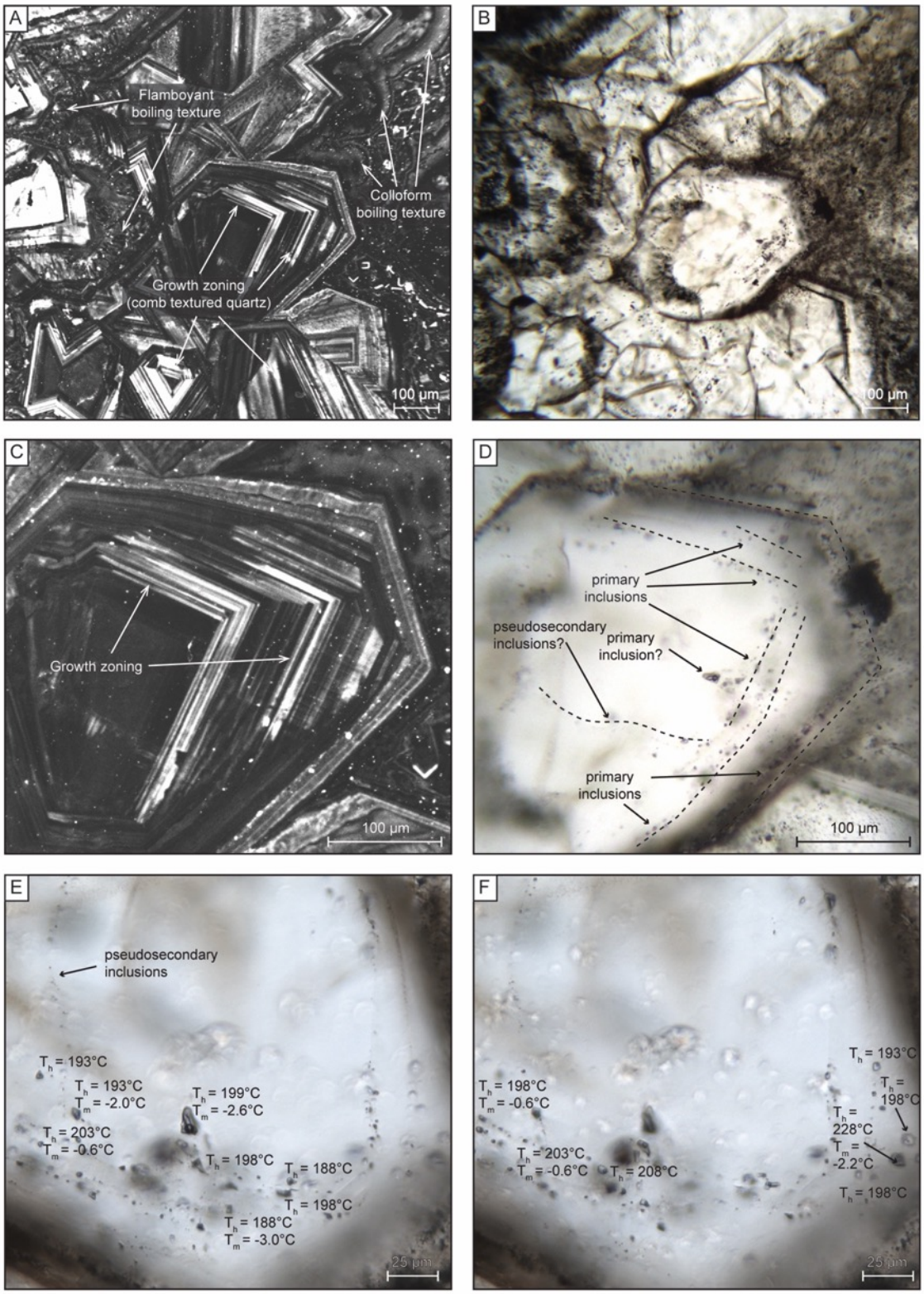

Figure 16: Example fluid inclusion analysis from sample LCBV082413-3A (location 288). A) Overlaid thin section photomicrograph (plane-polarised light) and CL image showing comb quartz with strong growth zoning visible in CL. The quartz is overgrown by colloform silica, indicating it formed before an intense boiling event. B) Overlaid thin section photomicrograph (plane-polarised light) and CL image showing primary fluid inclusion trails following growth zones, and a another trail that cuts across several growth zones before terminating at an outer growth zone, indicating a possible pseudosecondary origin. Dashed lines indicate fluid inclusion trails. A large (~20 µm) inclusion is of unsure origin, but possibly primary due to not belonging to an obvious trail of inclusions. C) and D) photomicrographs (plane-polarised light), showing microthermometry data for the primary fluid inclusion assemblage in this crystal. Note that most inclusions have values of T_h = ~190 – 200°C, with some outliers. T_m is variable from -3.0 to -0.6°C.

4.5.5.1. Hypersaline fluid inclusions and two distinct fluid generations

The vein sampled at location 160 (sample LCTV081914-1A) is near the Alpine Gulch quartz monzonite intrusion (350 m away laterally and ~150 m above) and ~1.6 km from the northeastern limit of the syenite resurgent pluton. It contains two distinct fluid inclusion assemblages, which can be distinguished from their relationship to quartz zoning, as well as fluid inclusion petrography and microthermometry. The first assemblage is identified in quartz and calcite, and the inclusions in quartz are mostly confined to a single growth zone, which is visible with CL imaging (Figs. 17a and 17b). This suggests that the fluid inclusion assemblage is primary. This assemblage has a T_h of ~208°C and T_m of -0.5°C (0.9% NaCl equivalent) (Fig. 17c). The assemblage contains numerous vapour-rich inclusions (Figs. 9b and 17c), which show that the fluid was boiling at the time of trapping. Microthermometry was conducted only on the most liquid-rich inclusions. The second fluid inclusion assemblage follows the path of a healed fracture in the quartz crystal, which is visible with CL imaging and cuts across growth zones (Figs. 17a and 17b). This suggests that it is of secondary origin. The inclusions in this assemblage have visible halite daughter crystals (Figs. 9c and 17d). Microthermometry results determined a T_h of ~488°C and T_m of ~540°C, from the melting of halite daughter crystals (64% NaCl equivalent) (Fig. 17d). This second hypersaline assemblage is unlike any other fluid inclusion assemblage identified at Lake City caldera, having a much higher temperature and salinity (Table 2).

4.5.5.2. Limitations of fluid inclusion data

The fluid inclusion data collected at Lake City provide important constraints on the hydrothermal fluid conditions but do have some limitations. Fluid inclusions were measured in comb textured quartz (Figs. 2 and 9a), because this texture contained the largest and least obviously modified inclusions. Comb quartz requires relatively stable, slow-changing conditions in open space for growth, and hence is generally not formed under conditions of intense boiling (Dong et al., 1995; Moncada et al., 2011). This means that most microthermometry data probably reflect temperatures below boiling, and this is supported by the paucity of vapour-rich inclusions that were identified, even in samples that contained textural evidence of boiling in the same vein. However, comb quartz that is near or rimmed by boiling textures (e.g. Fig. 16) was probably formed from fluid at a temperature close to boiling. When using the fluid inclusion microthermometry data to constrain the spatial variation in fluid temperature and composition, we are limited to only one or two assemblage

homogenisation temperatures for each field location (Fig. 19). This is because it is not practical to be able to fully assess the variation in homogenisation temperatures at each location, and hence temporal variation cannot be fully accounted for. This means the spatial variation in temperatures that is observed (Fig. 19) is only an approximation and may not reflect what the true variation was at one time. The CO_2 content of the fluid inclusions measured in this study is poorly constrained, but the absence of clathrates implies a low CO_2 content, and therefore assumed to be zero for the purposes of calculating NaCleq content. The presence of bladed calcite textures however (Fig. 12d) indicates that at least some CO_2 was present in the hydrothermal fluid. The presence of undetermined CO_2 content will affect the calculated NaCl data (Roedder, 1984; Hedenquist and Henley, 1985).

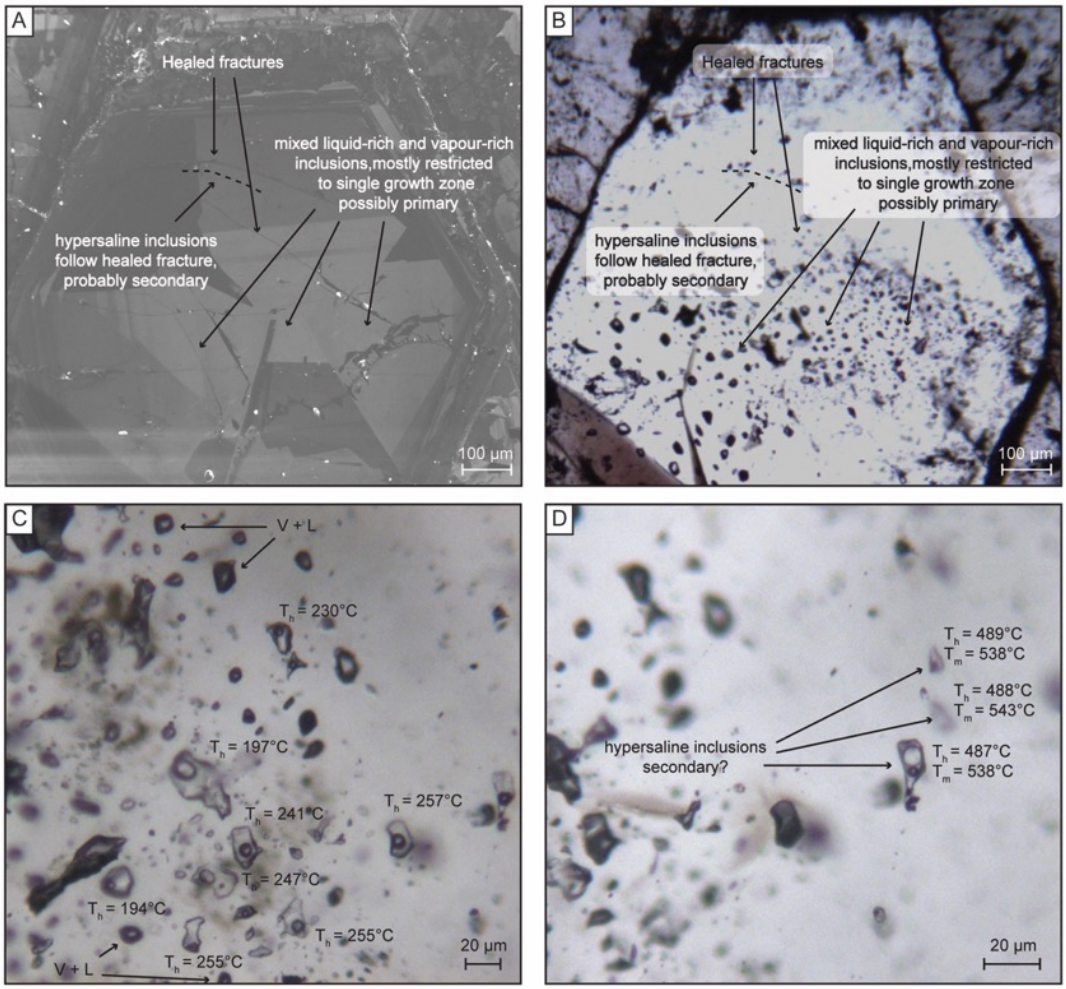

Figure 17: Example fluid inclusion analysis from sample LCTV081914-1A (location 160). A) Overlaid thin section photomicrograph (plane-polarised light) and CL image of a quartz crystal, showing abundant mixed vapour and liquid rich inclusions that are mostly confined to the higher luminescence parts of the crystal, and are therefore possibly primary. A short trail of hypersaline three-phase inclusions (dashed line) are possibly secondary. B) and C) Plane-polarised photomicrographs showing mixed liquid-rich and vapour-rich fluid inclusions, with microthermometry data. T_h is variable form 194 to 257°C, probably due to varying ratios of liquid to vapour at trapping. The lowest values (194 to 202°C) are considered to represent the true temperature of trapping (i.e. trapped liquid only). Freezing (T_m) data were not obtained for these inclusions, however a similar assemblage in another quartz crystal in the same sample (average T_h = 208°C) had a consistent T_m of -0.5°C, and an inclusion in calcite in the same sample had T_h = 202°C, T_m = -0.7°C. D) Plane-polarised photomicrograph showing microthermometry data for three three-phase hypersaline inclusions. T_m is the melting temperature of the halite daughter crystals. Note the high temperatures of T_h and T_m.

Table 2: Summary table of average fluid inclusion assemblage microthermometry data collected at Lake City caldera. Error values are standard deviations for the entire assemblage. See Appendix L for all fluid inclusion data.

Sample	Assemblage	Wpt.	Elev. (m)	Vein host rock	Th (°C)	Tm (°C)	NaCl (%)*	n (Th)	n (Tm)	Origin	Reason	Boiling?
LCTV090413-4B	B1	315	3872	Tspl	260 ± 3	-1.0 ± 0.14	1.74 ± 0.24	11	8	P	G	No
LCIVRF082013-1B	E	280	3395	Tspl (Tirh)	227 ± 6	-0.6 ± 0.05	1.05 ± 0.09	8	7	I		No
LCIVRF082013-1D	B	280	3395	Tspl (Tirh)	226 ± 6	-0.7 ± 0.08	1.22 ± 0.14	7	5	I		No
LCBV082413-3A	E	288	3446	Tspl (Tspb)	201 ± 11	-1.5 ± 1.26	2.57 ± 2.02	27	9	P + PS	G	Text.
LCTV081713-1A	C	272	3781	Tspl	268 ± 9	-1.8 ± 0.08	3.06 ± 0.13	11	5	I		Text.
LCTV081513-3	C	257	3907	Tspl	203 ± 7	-0.6 ± 0.04	1.05 ± 0.07	10	6	I?		Text.
LCTVRF091213-1B	A1_1	321	3000	Tspu	287 ± 11	-0.6 ± 0.07	1.05 ± 0.12	9	2	P	G	Text.
LCTVRF091213-1B	A1	321	3000	Tspu	267 ± 16	-0.6 ± 0.07	1.05 ± 0.12	35	2	P	G	Text.
LCBVRF082613-1	C_2	290	3837	Tspl (Tspb)	183 ± 7	-0.7	1.22	6	1	P	G	Text.
LCTBV090313-3	A	311	3868	Tspl	202 ± 9	-0.3	0.53	3	2	P?	II	No
LCBVRF090513-2C	A	317	3997	Tspm	233 ± 3	-0.3	0.53	3	3	P?	II	Text.
LCTV091813-1B	B	325	3768	Tspl	245 ± 6	N/A	N/A	3	0	P?	II	No
LCGVRF071614-3A	B	25	3104	Tspl/Granite	265 ± 6	-0.5 ± 0.05	0.88 ± 0.09	25	8	P	G	Text.
LCITV091114-1B	C	213	3640	Tspl/syenite	231 ± 7	-0.4 ± 0.04	0.70 ± 0.07	6	6	P?	II	VI + text.
LCGV083114-2B	H	195	3084	Granite	261 ± 11	-0.6 ± 0.05	1.05 ± 0.09	11	8	P?	II	No
LCGV083114-2B	G	195	3084	Granite	211 ± 13	-0.5 ± 0.04	0.88 ± 0.07	13	6	P	G	No
LCTV090114-4C	A3	203	3939	Tspl	177 ± 12	-1.1 ± 0.16	1.91 ± 0.27	10	8	P	G	Text.
LCUV081814-2B	C3	153	3969	Tsm	246 ± 2	N/A	N/A	2	0	P?	II	Text.
LCTV081914-1A	F	160	3411	Tspl (Tspb)	208 ± 8	-0.5	0.88	6	6	I		VI
LCTV081914-1A	C: FIA2	160	3411	Tspl (Tspb)	488 ± 1	540.0 ± 3	64.35 ± 0.33	3	3	S		No
Total:								209	95			

Note:
** Weight equivalent of NaCl*
Tspl = Lower Sunshine Peak Tuff
Tirh = Rhyolite ring dyke
Tspb = Lake City intra-caldera landslide breccia
Tspu = Upper Sunshine Peak Tuff
Tspm – Middle Sunshine Peak Tuff
P = primary
I = indeterminate
PS = pseudosecondary
G = fluid inclusions follow or are confined to crystal growth zones
II = fluid inclusions are large and/or isolated from other inclusions in crystal (suggestive of a primary origin (Roedder, 1984))
Text. = textural evidence for boiling in the same vein
VI = vapour-rich inclusions identified in the same or similar fluid inclusion assemblages

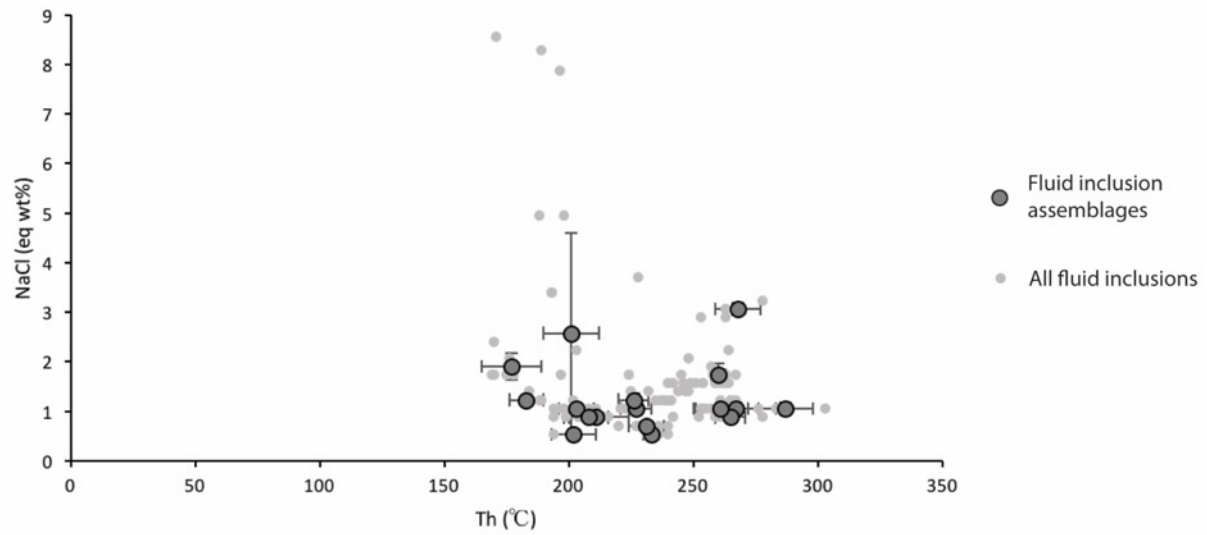

Figure 18: Graph of sailinty ($NaCl_{eq}$ wt. %) versus homogenisation temperature (°C) for fluid inclusion assemblages, and all fluid inclusions. Error bars are one standard deviation. The very high temperature and high salininy assemblage C: FIA2 from sample LCTV081914-1A is excluded from this plot.

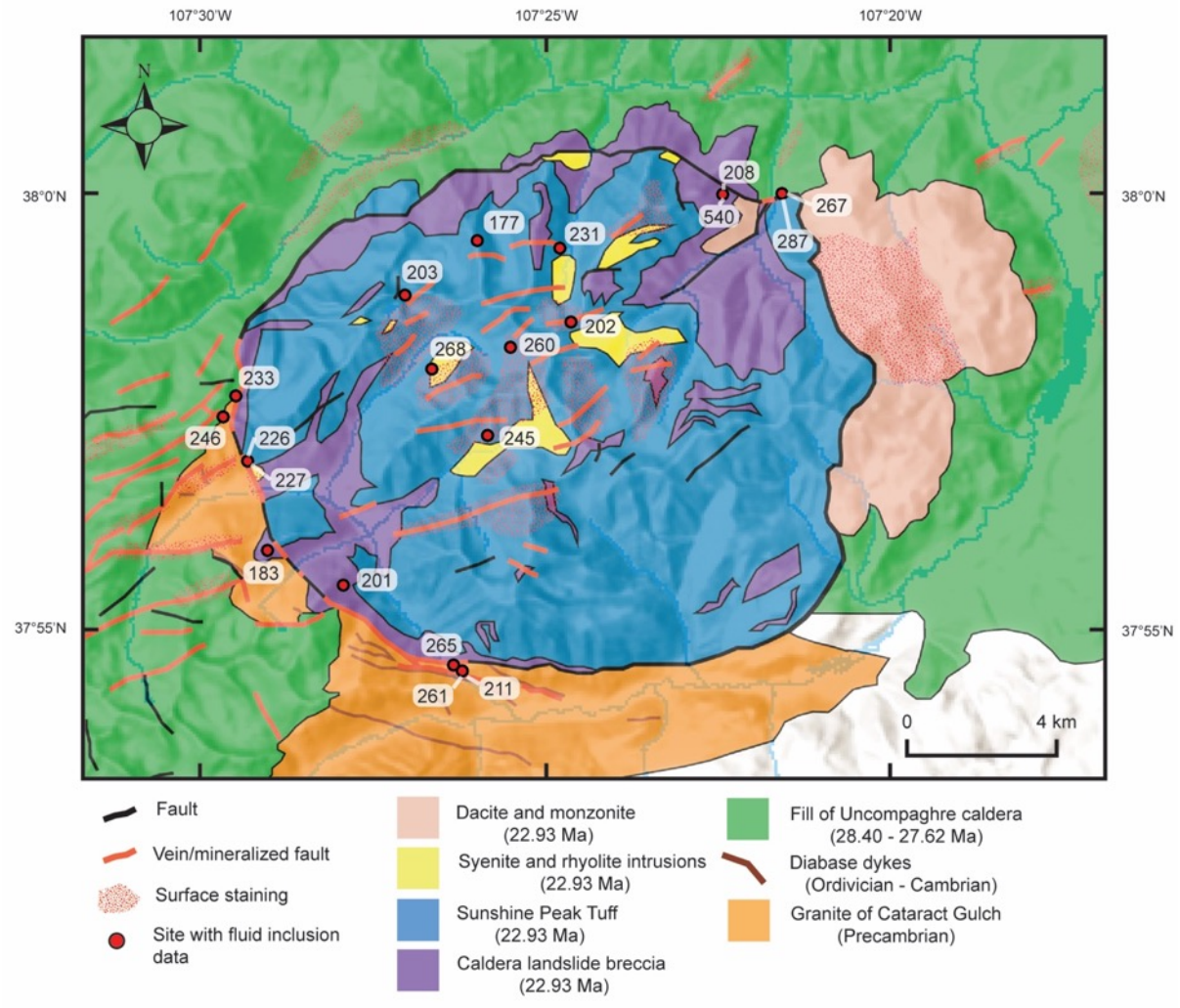

Figure 19: Map showing the location and average homogenisation temperature of fluid inclusion assemblages identified in this study.

4.6. DISCUSSION

Here we interpret the physiochemical processes responsible for the variation in alteration associations, fluid temperatures, boiling conditions and fluid-rock interaction at Lake City caldera. We discuss the significance of the three dominant alteration assemblages: advanced argillic, phyllic and propylitic, and the less widespread high-temperature "porphyry-type" and low-temperature argillic alteration. These physiochemical data are then used to construct a generalised conceptual model for the hydrothermal system at Lake City, and its magmatic and structural controls.

4.6.1. Mineral equilibria and significance of the hydrothermal assemblages.

There are three main hydrothermal assemblages at Lake City caldera: Propylitic, phyllic, advanced argillic. These assemblages are characteristic of the epithermal environment (Hedenquist et al., 2000) and dominantly reflect variable degrees of acid neutralisation by the country rock. Advanced argillic alteration reflects intense pervasive acid alteration in a fluid-dominated environment (Giggenbach, 1997). Progressively less fluid-dominated conditions form phyllic then propylitic stable assemblages representative of rock-dominated pH-neutral fluid conditions. The primary controlling factors on which of these alteration assemblages form are the acidity of the fluid and the amount of water/rock interaction. However, the presence or absence of certain mineral phases, as well as fluid inclusion microthermometry of adjacent veins, constrains the fluid temperature.

4.6.1.1. Advanced argillic association

Advanced argillic alteration is an important assemblage at Lake City caldera and has been well studied by previous researchers (Larson and Taylor, 1987; Bove et al., 1990; Bove and Hon, 1992). This study builds on this work by identifying a previously undocumented occurrence in Lake City caldera. Advanced argillic, quartz + alunite alteration occurs mostly at Red Mountain and has been interpreted as forming from a buoyant magmatic acid sulfate-bearing vapour plume, related to shallow dacite intrusions (Bove et al., 1990). During cooling, these shallow intrusions likely released acids such as H_2S, SO_2, HCl, and potentially HF, which mixed with groundwater and reacted with country rock to form secondary alumino-silicate minerals (alunite, dickite) and quartz. The alteration process involves hydrolysis reactions that neutralize the solutions and convert framework silicate minerals

(e.g., feldspars) to hydrothermal micas and clays, and in extreme cases alumino silicate and alumino-phosphate-sulfate phases. Bove et al. (1990) estimated (using oxygen and sulfur isotopes) the alunite deposition temperatures as ~400°C - 200°C, which is consistent with the presence of the high temperature acidic mineral topaz. Subsurface drilling encountered high temperature potassic alteration (characterised by hydrothermal biotite and alkali feldspar) beneath Red Mountain (Bove et al., 1990; Bove and Hon, 1992). The surface of Red Mountain was probably near the paleosurface at the time of hydrothermal activity, estimated as in the top ~300 m by Larson and Taylor (1987).

Advanced argillic alteration is locally pervasive as in the Red Mountain area, but can also occur highly focussed in veins. In the eastern part of the caldera (location 207), a previously unrecognised quartz + dickite + illite + pyrite advanced argillic assemblage was identified (Figs. 3g and 4e). This is also indicative of a fluid dominated, high water/rock ratio system, with the presence of dickite implying temperatures of >120°C - 200°C (Reyes, 1990; Hedenquist et al., 2000). This vein may have been a conduit for fluid derived from the source of the dacite and/or quartz monzonite intrusions. This shows that highly acidic fluid was not restricted only to the Red Mountain area, and may suggest that an intrusion exists at shallow depth under this location. The lack of boiling textures at this location (Fig. 11a) suggests that there was a greater liquid component to the hydrothermal fluid there compared to Red Mountain, which was vapour dominated (Larson and Taylor, 1987; Bove et al., 1990). White mica composition is poorly constrained for the advanced argillic alteration assemblage at Lake City caldera. Location 207 has a low to moderate λ_{AlOH} value (2203 nm), however further work characterising white mica composition at Red Mountain would be needed to determine how representative this is.

4.6.1.2. Phyllic association

Phyllic alteration has been previously recognised at Lake City caldera (Larson and Taylor, 1986b; Hon, 1987), however the temperature and salinity of veins hosted by this assemblage have not previously been quantified by fluid inclusion microthermometry. The geochemical and structural controls on the distribution of phyllic versus propylitic alteration have also not been well constrained by previous work. In this association, hydrolysis reactions (e.g. acid neutralisation) lead to the replacement of feldspar by white mica or clay. This is characteristic

of the phyllic assemblage, which consists of quartz + white mica + pyrite. The assemblage generally forms at higher fluid/rock ratios than propylitic alteration (Henley and Ellis, 1983; Giggenbach, 1984; Peters, 1993), and constraints from fluid inclusion data for Lake City caldera show that the trapped hydrothermal fluid was at 177°C - 268°C and had a salinity of <3.1% NaCl eq. Generally the areas of phyllic alteration correlate well with both low $\delta^{18}O$ composition (Larson and Taylor, 1986b) and low λ_{AlOH} (muscovitic white mica) (Figs. 1c and 7). The large area of pervasive phyllic alteration in the centre of the caldera probably reflects the high permeability and fluid flux in the resurgent dome, facilitated by a high density of faults and fractures formed during uplift (Garden et al., 2017). Phyllic alteration haloes formed due to acid neutralisation around certain major fluid conduits (Figs. 6a, 6b, 13c and 13d). On the caldera margin, these conduits were formed at structural intersections on the southwest corner of the caldera and the intersection of the Eureka Graben and the ring fault(s). Muscovitic (high Al) white mica formed in the halo of acid neutralisation around veins and in the centre of the caldera (Fig. 13c). The maximum fluid inclusion homogenisation temperatures of 268°C in the resurgent dome are much lower than the 400°C estimated by Larson and Taylor (1986b), who assumed that the syenite pluton was the heat source for the hydrothermal system. No hypersaline, high temperature, fluid inclusions were identified in the resurgent dome. This all suggests that the upper part of the syenite pluton had cooled significantly (to at least ~270°C) by the time the main hydrothermal system at Lake City had been established. The rhyolitic ring dyke on the western margin of the caldera is altered to a phyllic assemblage (Fig. 6a), however fluid inclusion temperatures of ~227°C for veins hosted in the ring dyke (location 280, Table 2, Fig. 19) suggest that the dyke had also cooled significantly before the start of hydrothermal activity. Similar temperatures (231°C) in a vein on the margin of the syenite intrusion of Owl Gulch (location 213, Table 2, Fig. 19), show that this part of the syenite pluton had also cooled.

Textural evidence suggests boiling was widespread in phyllic-hosted veins, particularly in the centre of the caldera and at shallower levels (Figs. 11 and 12). On the western caldera margin boiling was mostly confined to the caldera margin, where it cuts across the Eureka Graben (Fig. 11b). This supports the interpretations of Chapter 2 that discontinuity intersections are key controls on permeability at Lake City caldera (Garden et al., 2017). Fitting boiling per depth (BPD) curves to the assemblages identified in the phyllic-dominated centre of the caldera allows estimation of the paleo-depth of samples beneath the water table at the time of

trapping. Not all assemblages can be adequately fitted to a single curve, but a maximum and lower limit can be determined (Fig. 20). The fluid inclusion data are consistent with paleo-depths of ~200 to 700 m, corresponding to a paleosurface elevation of ~4000 – 4500 m. These estimates are significantly lower in elevation (by ~650 to 1500 m) than the paleosurface estimated by Hon (1987) using the stratigraphic thickness of the three members of the Sunshine Peak Tuff. In general, simple fitting of BPD curves, although common practice (e.g. Moore et al., 1997; Simpson et al., 2016), underestimates paleodepth. This is because the curves of Haas (1971) do not take into account the progressive decreasing density of the hydrothermal fluid with height, due to the presence of a vapour phase from boiling (i.e. steam bubbles in the water column) (Canet et al., 2011; Cruz-Pérez et al., 2016). The resulting under-estimation can be as much as 50% (Canet et al., 2011; Cruz-Pérez et al., 2016). Not accounting for the presence of CO_2 in the hydrothermal fluid will also result in underestimation of the paleodepth (Hedenquist and Henley, 1985). Despite these uncertainties, the magnitude of the difference in estimated paleodepths makes it unlikely to be due to these factors alone. Stratigraphic reconstructions suggest that the surface of the Lake City resurgent dome was probably topographically quite steep-sided (Hon, 1987), and was probably subject to some erosion during and/or after uplift.

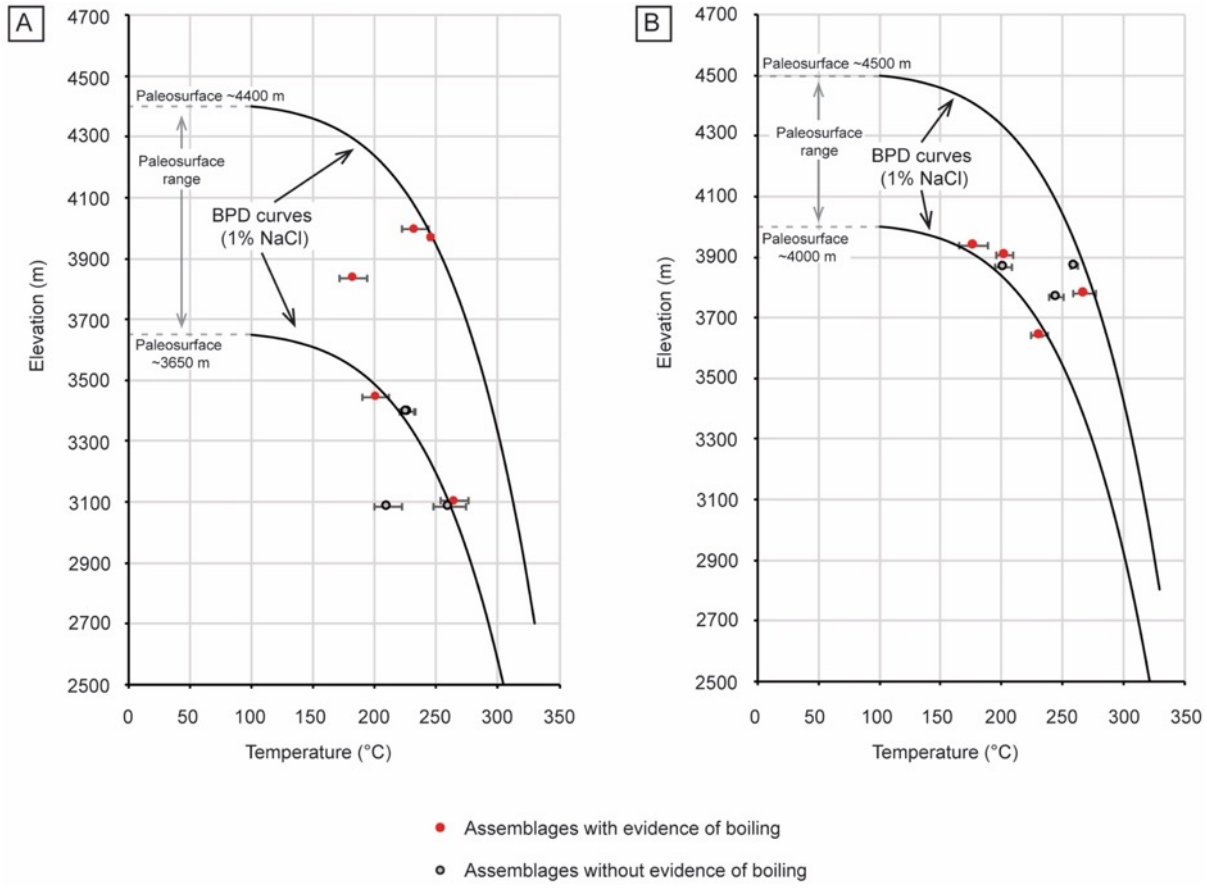

Figure 20: Average fluid inclusion assemblage homogenisation temperatures versus elevation, with fitted boiling per depth (BPD) curves (1% NaCl) from Haas (1971). Error bars are one standard deviation. A) Samples from near the western and southwestern margin of the caldera margin. The data are consistent with BPD curves that indicate a paleo-water table elevation of between 3650 and 4400 m. B) Samples in the centre of the caldera, within or above the syenite pluton. The data are consistent with BPD curves that indicate a paleo-water table elevation of between 4000 and 4500 m. Evidence for boiling includes fluid inclusion evidence (i.e. vapour dominated inclusions in the same or nearby crystals), or textural evidence of boiling in the same vein.

4.6.1.3. Propylitic association

In this study we constrain the temperature, salinity and boiling conditions of the propylitic alteration forming fluid at Lake City caldera for the first time, which complements previous oxygen isotope work (Larson and Taylor, 1986a, 1986b). The propylitic mineral assemblage of chlorite + illite + quartz ± calcite ± epidote ± adularia is widespread at Lake City, particularly at its periphery (Fig. 5). It is indicative of a low water/rock ratio and near neutral pH fluid in rock dominated equilibrium. Illite and epidote are stable at temperatures above ~220°C and 200°C respectively (Browne, 1978; Henley and Ellis, 1983; Reyes, 1990; Charles and Browne, 1991), which is in agreement with fluid inclusion assemblage homogenisation temperatures of 188°C - 265°C, and low fluid salinity (<3 wt% NaCl eq.). Some veins, particularly near the southwestern margin of the caldera (Figs. 6c and 6d), are hosted in propylitic alteration, without a phyllic halo, however white mica is slightly more

muscovitic closer to the veins, even where no transition to phyllic alteration is evident (e.g. Fig. 13b). This shows the usefulness of SWIR reflectance spectroscopy and λ_{AlOH} as a tool in systems where changes in alteration mineralogy are subtle. The area of propylitic alteration on the southwestern caldera margin correlates with low $\delta^{18}O$ values (Larson and Taylor, 1986b) but high λ_{AlOH} (phengitic white mica) (Figs. 1c and 7). This means $\delta^{18}O$ compositions are low in both the phyllic alteration zone and parts of the propylitic zone, while λ_{AlOH} is high in the propylitic zone and low in the phyllic zone. This discrepancy between the oxygen isotope and white mica composition data may be due to the southwest part of the caldera having a large, high temperature fluid flux (as evidenced by large veins and fluid inclusion microthermometry) but the fluid chemistry equilibrium is dominated by the country rock composition. Many modern high temperature geothermal systems contain huge volumes of fluid but the reservoir alteration is still a rock dominated propylitic assemblage, because acid neutralisation may have occurred at greater depths (Hedenquist et al., 2000). The rocks in these systems generally have low $\delta^{18}O$ compositions (Taylor, 1974). Similarly, at Lake City the rock-controlled chemistry of the propylitic fluid may have resulted in phengitic white mica composition, but the high fluid flux meant there was still oxygen isotope exchange.

Some veins in the propylitic zone of the southwestern caldera margin contain blocky or rhombic calcite, which usually infills the centre of the vein (e.g. Fig. 9b). This texture is distinct from the bladed calcite textures that are often related to CO_2 loss during boiling (Simmons and Christenson, 1994). The veins containing rhombic calcite are near what would have been the margins of the system. The non-bladed calcite was probably deposited during the heating of invading cooler waters due to the retrograde solubility of calcite. Late-stage vein calcite is a common feature of adularia-illite epithermal systems (Simmons and Christenson, 1994).

Textural evidence for boiling is present in some veins hosted in propylitic alteration. At the western and southwestern caldera margin, boiling textures tend to be restricted to discrete layers in major veins associated with caldera structures. Boiling is often characteristic of main upflow zones in geothermal systems, hence these veins were probably main upflow channels that were hydrologically connected to shallower depths (Hedenquist et al., 2000). The non-pervasive nature of boiling textures in these veins shows that boiling (or at least

intense “flashing” events) was episodic, and may have been related to near-surface depressurisation events such as hydrothermal eruptions or fault movement. As in the centre of the caldera, BPD curves may be fitted to fluid inclusion data on the caldera margin to estimate the paleodepth of veins sampled. The homogenisation temperatures on the western caldera margin are consistent with a paleosurface of ~3650 to 4400 m. This is similar to the paleosurface elevations estimated by Hon (1987) for this part of the caldera.

4.6.1.4. Other associations

Three more different assemblages are present in specific locations. Smectite-dominated (low-temperature argillic) alteration was only identified on the margin of the advanced argillic alteration at Red Mountain. In modern geothermal systems, smectite alteration persists under low temperature (<200°C) and neutral to slightly acidic pH conditions (Reed, 1997).

Above the quartz monzonite intrusion in Alpine Gulch is an area of tourmaline-cemented breccia, with chlorite, illite and quartz. In Philippine geothermal fields, Tourmaline is stable above 200°C (Reyes, 1990), while at Karaha-Telaga Bodas in Indonesia it is found above ~300°C in the biotite alteration zone, within ~300 m of an intrusion (Moore et al., 2008). The tourmaline in Alpine Gulch is related to high fluid temperatures near the quartz monzonite intrusion. This is supported by high temperature (~488°C) hypersaline fluid inclusions in veins near the tourmaline breccia, and the presence of magnetite veinlets in the intrusion (Hon, 1987). There is no widespread high temperature potassic alteration zone and it is likely that the B-rich fluid was very localised and associated with small volume, high temperature magmatic fluids. Geological evidence shows that the emplacement of the quartz monzonite was one of the last events of the Lake City caldera cycle (Hon, 1987), which is consistent with the observation that the hypersaline fluid inclusions are secondary in sample LCTV081914-1A (Fig. 18).

Near the quartz monzonite, at the intersection of the caldera margin and the Alpine Gulch fault (location 321), high temperature (287°C), low salinity fluid inclusions (<3 wt% $NaCl_{eq}$) were identified. This intersection is also the site of a distinct anomaly of high-Al white mica composition and low $\delta^{18}O$ composition (Figs. 1c, 8). Fitting a BPD curve to these data suggests a paleodepth of at least 900 m, corresponding with a paleosurface elevation of

~3900 m. This is higher than the expected paleosurface elevation of ~3400 m estimated by Hon (1987). This sample is near the dacite lavas of the eastern caldera margin, and near the quartz monzonite intrusion; both derived from "batch B" magmas (Kennedy et al., 2016). A pile of lavas at least ~500 m thick on top of the Upper Sunshine Peak Tuff at this location could be the most likely explanation for this discrepancy. These lavas could be sourced from either the Alpine Gulch quartz monzonite, or the dacite lavas of the Grassy Mountain and Red Mountain area, because both are from the same magma batch.

Outside near the northeastern caldera margin are several base and precious metal mineralised veins. The veins of the Ute-Ulay mine (Fig. 1b) are an example. The youngest mineralisation episode at this mine, called the barite-precious metal assemblage, is dated as the same age as Lake City caldera (Bove et al., 2001). Fluid inclusion data from this assemblage are similar to those measured in this study, with average homogenization temperatures of 226 - 272°C and salinities of 1.5 – 3.2 eq. wt% NaCl (Slack, 1980). There are also similarities in vein mineralogy, with base metal sulfides more abundant in veins in Alpine Gulch than the rest of the caldera. However the Lake City veins lack the barite abundant at Ute-Ulay. Veins in the barite-precious metal assemblage are surrounded by phyllic alteration haloes (Slack, 1980). The similarities in age and fluid inclusion microthermometry suggest that barite-precious metal assemblage veins in the vicinity of the Ute-Ulay mine represent the northeasternmost extension of the Lake City hydrothermal system.

4.6.2. Reconstruction of the fossil hydrothermal system

The integration of new and previously published data at Lake City caldera allows a generalised reconstruction of the physiochemical conditions of the fossil hydrothermal system and their relation to the structure and magmatism of the caldera (Fig. 21). The general configuration of the fossil hydrothermal system is summarised as follows. Neutral chloride fluid pervades the western margin, with phyllic haloes around major intersecting, boiling, fluid conduits. In the resurgent dome, more pervasive fracture- and fault-facilitated permeability and a less-neutralised fluid forms widespread phyllic alteration, at similar temperatures as on the western margin. Boiling is widespread on the many small fault-hosted fluid conduits. The flat-topped syenite intrusion in the caldera fill had cooled significantly, but the larger crystallising batch A magma chamber at depth below the caldera floor may have still provided a heat source. The ring dyke on the western caldera margin (part of

magma batch A) had also cooled significantly. The low-salinity, near neutral pH reservoir may have reached the vicinity of the Ute-Ulay mine. Areas with a high density of discontinuities of diverse orientations that enabled the formation of discontinuity intersections were key controls on permeability (Garden et al., 2017). This is illustrated by the high fluid temperatures at the intersection of the Alpine Gulch fault and the caldera margin, with concomitant high Al white micas and low $\delta^{18}O$ composition (Figs. 1c and 8), and by the presence of boiling textures and phyllic alteration halos around large intersecting veins in the southwestern and western caldera margin (e.g. Fig. 11b). These findings support the structural observations of Garden et al. (2017), who emphasised the importance of structural intersections. The general NE-SW trend of the hydrothermal system, from the Ute-Ulay mine in the northeast to the western caldera margin, shows that fault-related permeability (for both magma and hydrothermal fluid) was greater in the along-fault direction than across-fault.

The neutral chloride reservoir was punctuated by intrusions from batch B magmas at Alpine Gulch and Red Mountain. These resulted in an influx of high temperature, high boron magmatic fluid at the quartz monzonite of Alpine Gulch, and a vigorous buoyant, acidic, magmatic vapour plume at Red Mountain (Bove et al., 1990). The magma of batch A did not provide direct magmatic fluid input into the shallow hydrothermal system, as evidenced by the lack of advanced argillic alteration or high temperature fluid inclusions. This is probably because it was already degassed due to eruption of the Sunshine Peak tuff, and it was already waning by the time the hydrothermal system established. It is possible that the primary heat source for the hydrothermal system may have been the batch B trachyandesite magma. It is not well-constrained how local the effect of the batch B heat source was, however this magma which was demonstrably hotter (from fluid inclusion evidence) at shallow levels than the cooling batch A magma. The advanced argillic alteration at location 203 on the southeast side of Alpine Gulch (Figs. 3g, 3h, and 4e) suggests that a shallow intrusion may exist under this part of the caldera. Though speculative, this intrusion could reasonably be assumed to belong to batch B, because advanced argillic alteration is not associated with batch A intrusions anywhere else in the caldera. This would imply that the batch B intrusions are more extensive than their limited surface outcrops (at Alpine Gulch and Red Mountain) would suggest, and could comprise a primary heat source.

Using various lines of geological evidence, it is possible to determine a tentative relative timing of major events in the history of the magmatic-hydrothermal system. First, eruption of the Sunshine Peak tuff from the batch A magma chamber(s) caused subsidence and formation of Lake City caldera and its structural pathways (Kennedy et al., 2016). Rejuvenation of the batch A magma body caused resurgence, and the intrusion of a flat topped syenite pluton into the caldera fill, which cooled relatively quickly. The batch A intrusions have been overprinted by phyllic and propylitic alteration, formed from moderate temperature (<270°C), neutral chloride fluid. The magmatic replenishment by batch B magma, which drove resurgence (Kennedy et al., 2012, 2016), provided the heat source for hydrothermal convection, and may have also driven initiation of the Lake City hydrothermal system. Late batch B intrusions provided an influx of high temperature (up to 540°C) magmatic fluid at Red Mountain and Alpine Gulch, forming associated advanced argillic and porphyry style alteration.

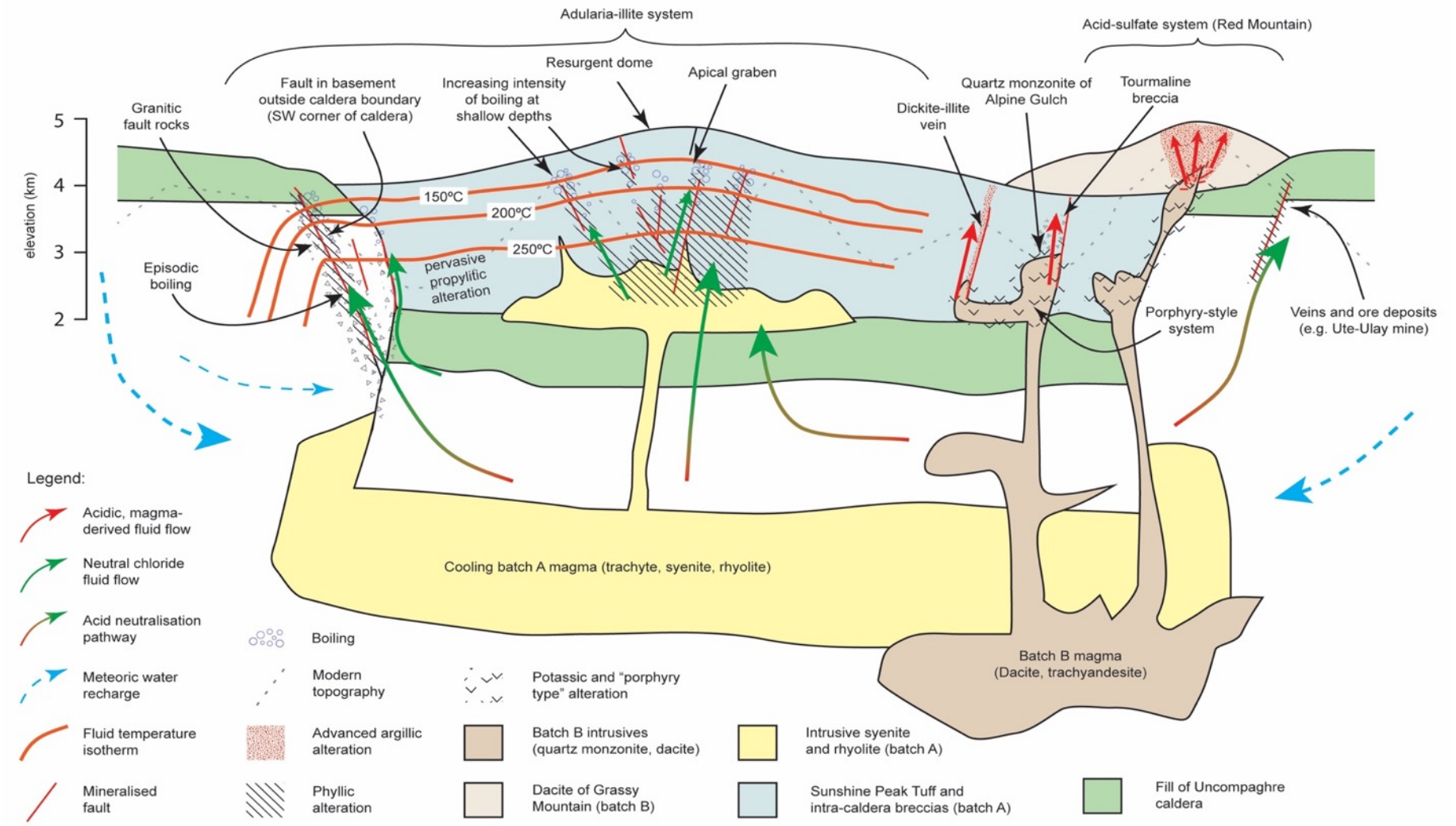

Figure 21: Conceptual model of the Lake City hydrothermal system. Schematic cross-section is taken on a kinked line from the Shelf Road area at the southwestern corner of the caldera, to the centre of the resurgent dome, to Red Mountain. Vertical scale is exaggerated. Propylitic alteration is not shown, but extends through virtually all of the Lake City caldera fill, and the basement within several kilometres of the caldera margin. Temperature contours end in eastern part of caldera because two generations of fluid were present here (neutral chloride then high temperature magmatic fluid. Alteration assemblages arbitrarily end at depth because data are not available in the caldera floor.

4.6.3. Formation of hydrothermal ore deposits

Small ore deposits have been mined from inside Lake City caldera in historic times, however by far the largest ore deposit formed during the Lake City hydrothermal cycle was the late stages of the mineralisation at Ute-Ulay Mine (Slack, 1980; Bove et al., 2001). This deposit is outside the Lake City caldera margin, in the fill of Uncompahgre caldera (Fig. 1b). The Uncompahgre and nearby Silverton calderas hosted much more economic mineralisation than Lake City caldera (Slack, 1980; Sanford et al., 1987): the reasons for this may be structural and magmatic. To form an ore deposit a geothermal system must contain dissolved metals in the hydrothermal fluid, often from an enriched source. This may be magma with a higher than average metal concentration or leached from metal-rich lithological units (cf. Hedenquist and Lowenstern, 1994). The fluid composition must also allow the transport of metals, for example as chloride or sulfur complexes (Henley and Ellis, 1983; Wilkinson et al., 2013). The fluid must be focussed and encounter a change in physiochemical conditions that encourages efficient and rapid (in time and/or space) precipitation of the metals out of solution (Sibson, 1987; Hedenquist et al., 2000). High fluid flux is necessary to concentrate the ore in the trap in high enough quantities to be economic to mine (Johnston and Lowell, 1961). All of these factors must occur together to form an ore deposit, thus not every geothermal system is favourable. Silverton caldera has a complex structure with multiple ring fault strands and radial structures, forming a high number of intersections (Steven and Lipman, 1976; Sanford et al., 1987; Bove et al., 2007). These structural complexities will tend to increase permeability for hydrothermal fluids, and the likelihood of creating high flux conduits that are concentrated enough to form a deposit. Both Silverton and Uncompahgre calderas are older than Lake City and therefore have a longer and more complex magmatic history. Repeated magmatic intrusive magmatic activity is favourable for the creation of ore deposits because a similarly long and complex hydrothermal history allows more time, or a greater chance, for the favourable conditions for ore deposition to come together.

4.6.4. Interpretation of variation in white mica composition

The variation in white mica composition has been used in many studies to help understand the physiochemical conditions of hydrothermal systems and/or act as a vector to ore mineralisation. However, there have been varying interpretations of what the primary physiochemical variable(s) are that control the variation in white mica composition (see Chapter 3, Table 3.2). In Chapter 3 it was concluded that more data was needed to

understand the controlling variables on white mica composition at Lake City caldera. However, in this Chapter it is shown that high-Al white mica (low λ_{AlOH}) broadly correlates with areas of widespread phyllic alteration, and fluid inclusion microthermometry data show that there is no obvious correlation between white mica composition and temperature. It is therefore most likely that fluid pH (i.e. the amount of neutralisation of acidic fluids) is the primary control on both white mica composition and phyllic alteration at Lake City caldera. There have been relatively fewer studies on white mica compositional variation in epithermal systems compared to other settings such as porphyry and volcanic hosted massive sulphide ore deposits (Table 3.2), so this is an important result that may help guide future use of white mica composition as a tool in understanding hydrothermal fluid flow in shallow hydrothermal systems.

4.7. CONCLUSIONS

A variety of geological evidence including alteration mineralogy, mineral composition, vein textures and fluid inclusion microthermometry, is used to characterise the physiochemical conditions of the fossil Lake City caldera hydrothermal system and their spatiotemporal variability. We show that a large, neutral chloride (adularia-illite) hydrothermal system was active at Lake City caldera during and after resurgence, and its NE-SW elongation is likely to have been controlled by the regional structural grain. Fluid of moderate temperature (up to 287°C) was neutralised at the periphery of the system, and likely associated with down cooling fluid. Permeability on the margins was facilitated by a low number of large, intersecting, episodically boiling conduits, formed at the intersection between regional and caldera margin structures (Fig. 11b). In the centre of the caldera fluid was at a similar temperature (up to 268°C) and produced more phyllic alteration due to more acidic conditions. This alteration was pervasive in the highly faulted and fractured resurgent dome (Fig. 5). Similarities in age and fluid inclusions at Ute-Ulay Mine suggest that the neutral chloride reservoir extended into the fill of Uncompahgre caldera on the northeast of the caldera. Late intrusions of “batch B” magmas provided high temperature magmatic fluid input into the hydrothermal system at Red Mountain and Alpine Gulch, as evidenced by high temperature advanced argillic and porphyry style alteration (Figs. 3 and 4), and high temperature (540°C), hypersaline (64% $NaCl_{eq}$) fluid inclusions (Fig. 17). The deeper source of the batch B magmas may have been the primary heat source for the hydrothermal system rather than the waning “batch A” syenite, which has no associated acidic alteration or high

temperature fluid inclusions. Even if the shallow syenite was not the primary heat source, the many faults and fractures it created during resurgent uplift were still an important structural control on fluid flow. This reconstruction shows how the diverse magmatism and structural inheritance of the caldera resulted in a hydrothermal expression that was a hybrid of the two end member adularia-sericite and acid-sulfate types of epithermal system.

4.8. REFERENCES CITED

Adams, S.F., 1920, A microscopic study of vein quartz: Economic Geology, v. 15, p. 623–664, doi: 10.2113/gsecongeo.15.8.623.

Atkinson, A.B., 2002, A Model for the PTX Properties of H_2O-NaCl [M.Sc. thesis]: Blacksburg, Virginia, Virginia Polytechnic Institute and State University, 126 p.

Bodnar, R.J., 1983, A method of calculating fluid inclusion volumes based on vapor bubble diameters and P-V-T-X properties of inclusion fluids: Economic Geology, v. 78, p. 535–542.

Bodnar, R.J., 2003, Introduction to fluid inclusions, *in* Samson, I., Anderson, A., and Marshall, D. eds., Fluid Inclusions: Analysis and Interpretation. Mineral. Assoc. Canada, Short Course 32, p. 1–8.

Bodnar, R.J., 1993, Revised equation and table for determining the freezing point depression of H_2O-NaCl solutions: Geochimica et Cosmochimica Acta, v. 57, p. 683–684.

Bodnar, R.J., and Vityk, M.O., 1994, Interpretation of microthermometric data for H_2O-NaCl fluid inclusions, *in* De Vivo, B. and Frezzotti, M.L. eds., Fluid Inclusions in Minerals, Methods and Applications, Blacksburg, VA, Virginia Tech, p. 117–130.

Bove, D.J., and Hon, K., 1990, Compositional changes induced by hydrothermal alteration at the Red Mountain alunite deposit, Lake City, Colorado: U.S. Geological Survey Bulletin 1936, 21 p.

Bove, D.J., and Hon, K., 1992, Geologic and Alteration Map and Drill-Core Logs of the Red Mountain area near Lake City, Hinsdale County: U.S. Geological Survey Miscellaneous Investigations Series Map I-2286, scale 1:12,000.

Bove, D.J., Hon, K., Budding, K.E., Slack, J.F., Snee, L.W., and Yeoman, R.A., 2001, Geochronology and geology of late Oligocene through Miocene volcanism and mineralization in the western San Juan Mountains, Colorado: U.S. Geological Survey Professional Paper 1642, 30 p.

Bove, D.J., Mast, M., Dalton, J., Wright, W., and Yager, D., 2007, Major styles of

mineralization and hydrothermal alteration and related solid- and aqueous-phase geochemical signatures: Geological Survey professional paper 1651, p. 161–230.

Bove, D.J., Rye, R.O., and Hon, K., 1990, Evolution of the Red Mountain alunite deposit, Lake City, Colorado: U.S. Geological Survey Open-File Report 90-0235, 30 p.

Browne, P.R.L., 1978, Hydrothermal alteration in active geothermal fields: Annual Reviews in Earth and Planetary Sciences, v. 6, p. 229–250.

Canet, C., Franco, S.I., Prol-Ledesma, R.M., González-Partida, E., and Villanueva-Estrada, R.E., 2011, A model of boiling for fluid inclusion studies: Application to the Bolanos Ag-Au-Pb-Zn epithermal deposit, Western Mexico: Journal of Geochemical Exploration, v. 110, p. 118–125, doi: 10.1016/j.gexplo.2011.04.005.

Chambefort, I., Lewis, B., Simpson, M.P., Bignall, G., Rae, A.J., and Ganefianto, N., 2017, Ngatamariki geothermal system: Magmatic to epithermal transition in the Taupo Volcanic Zone, New Zealand: Economic Geology, v. 112, p. 319–346, doi: 10.2113/econgeo.112.2.319.

Chapin, C.E., 2012, Origin of the Colorado Mineral Belt: Geosphere, v. 8, p. 28–43, doi: 10.1130/GES00694.1.

Charles, C., and Browne, P.R.L., 1991, Mixed-layer clay geothermometry in the Wairakei geothermal field, New Zealand: v. 39, p. 614–621.

Cruz-Pérez, M.A., Canet, C., Franco, S.I., Camprubí, A., González-Partida, E., and Rajabi, A., 2016, Boiling and depth calculations in active and fossil hydrothermal systems: A comparative approach based on fluid inclusion case studies from Mexico: Ore Geology Reviews, v. 72, p. 603–611, doi: 10.1016/j.oregeorev.2015.08.016.

Cumming, W., 2009, Geothermal resource conceptual models using surface exploration data: 34th Workshop on Geothermal Reservoir Engineering, Stanford, California, 9-11 February 2009.

Dilles, J.H., and Einaudi, M.T., 1992, Wall-rock alteration and hydrothermal flow paths about the Ann-Mason porphyry copper deposit, Nevada - a 6-km vertical reconstruction: Economic Geology, v. 87, p. 1963–2001, doi: 10.2113/gsecongeo.87.8.1963.

Doe, B.R., Steven, T.A., Delevaux, M.H., Stacey, J.S., Lipman, P.W., and Fisher, F.S., 1979, Genesis of ore deposits in the San Juan Volcanic Field, Southwestern Colorado - Lead isotope evidence: Economic Geology, v. 74, p. 1–26.

Dong, G., Gregg, M., and Jaireth, S., 1995, Quartz textures in epithermal veins, Queensland - Classification, origin, and implication: Economic Geology, v. 90, p. 1841–1856.

Fournier, R.O., 1989, Geochemistry and dynamics of the Yellowstone National Park

hydrothermal system: Annual Reviews in Earth and Planetary Sciences, v. 17, p. 13–53.

Garden, T.O., Gravley, D.M., Kennedy, B.M., Deering, C., and Chambefort, I., 2017, Controls on hydrothermal fluid flow in caldera-hosted settings: Evidence from Lake City caldera, USA: Geosphere, v. 13, p. 1–24, doi: 10.1130/GES01506.1.

Giggenbach, W.F., 1984, Mass transfer in hydrothermal alteration systems - A conceptual approach: Geochimica et Cosmochimica Acta, v. 48, p. 2693–2711, doi: 10.1016/0016-7037(84)90317-X.

Giggenbach, W.F., 1997, The origin and evolution of fluids in magmatic-hydrothermal systems, *in* Barnes, H.L. ed., Geochemistry of Hydrothermal Ore Deposits, John Wiley and Sons, p. 737–796.

Goff, F., and Gardener, J.N., 1994, Evolution of a mineralized geothermal system, Valles Caldera, New Mexico: Economic Geology, v. 89, p. 1803–1832.

Goldstein, R.H., and Reynolds, T.J., 1994, Systematics of fluid inclusions in diagenetic minerals: Society for Sedimentary Geology Short Course 31, 212 p.

Haas, J.L., 1971, The effect of salinity on the maximum thermal gradient of a hydrothermal system at hydrostatic pressure: Economic Geology, v. 66, p. 940–946, doi: 10.2113/gsecongeo.66.6.940.

Hedenquist, J.W., 1986, Geothermal systems in the Taupo volcanic zone: Their characteristics and relation to volcanism and mineralisation, in Smith, I.E.M., ed., Late Cenozoic volcanism in New Zealand: Royal Society of New Zealand Bulletin, v. 23, p. 134–168.

Hedenquist, J.W., Arribas Jr., A., and Gonzalez-Urienm, E., 2000, Exploration for epithermal gold deposits: Reviews in Economic Geology, v. 13, p. 45–77.

Hedenquist, W., and Henley, R.W., 1985, The importance of CO_2 on freezing point measurements of fluid inclusions: Evidence from active geothermal systems and implications for epithermal ore deposition: Economic Geology, v. 80, p. 1379–1406.

Hedenquist, J.W., and Lowenstern, J.B., 1994, The role of magmas in the formation of hydrothermal ore-deposits: Nature, v. 370, p. 519–527, doi: 10.1038/370519a0.

Henley, R.W., and Ellis, A.J., 1983, Geothermal systems ancient and modern: A geochemical review: Earth-Science Reviews, v. 19, p. 1–50, doi: 10.1016/0012-8252(83)90075-2.

Henneberger, R.C., and Browne, P.R.L., 1988, Hydrothermal alteration and evolution of the Ohakuri hydrothermal system, Taupo volcanic zone, New Zealand: Journal of Volcanology and Geothermal Research, v. 34, p. 211–231, doi: 10.1016/0377-0273(88)90034-0.

Hildreth, W., 2017, Fluid-driven uplift at Long Valley Caldera, California: Geologic perspectives: Journal of Volcanology and Geothermal Research, v. 341, p. 269–286, doi: 10.1016/j.jvolgeores.2017.06.010.

Hon, K.A., 1987, Geologic and petrologic evolution of the Lake City caldera, San Juan Mountains, Colorado [Ph.D. thesis]: University of Colorado at Boulder, 244 p.

Hon, K., Ludwig, K.R., Simmons, K.R., Slack, J.F., and Grauch, R.I., 1985, U-Pb isochron age and Pb isotope systematics of the Golden Fleece vein - Implications for the relationship of mineralization to the Lake City caldera, western San Juan Mountains, Colorado: Economic Geology, v. 80, p. 410–417.

Johnston, W.P., and Lowell, J.D., 1961, Geology and origin of mineralized breccia pipes in Copper Basin, Arizona: Economic Geology, v. 56, p. 916–940.

Kennedy, B., Stix, J., Hon, K., Deering, C., and Gelman, S., 2016, Magma storage, differentiation, and interaction at Lake City caldera, Colorado, USA: Geological Society of America Bulletin, v. 128, p. 764–776, doi: 10.1130/B31305.1.

Kennedy, B., Wilcock, J., and Stix, J., 2012, Caldera resurgence during magma replenishment and rejuvenation at Valles and Lake City calderas: Bulletin of Volcanology, v. 74, p. 1833–1847, doi: 10.1007/s00445-012-0641-x.

Van den Kerkhof, A.M., and Hein, U.F., 2001, Fluid inclusion petrography: Lithos, v. 55, p. 27–47, doi: 10.1016/S0024-4937(00)00037-2.

Klemm, L.M., Pettke, T., and Heinrich, C.A., 2008, Fluid and source magma evolution of the Questa porphyry Mo deposit, New Mexico, USA: Mineralium Deposita, v. 43, p. 533–552, doi: 10.1007/s00126-008-0181-7.

Larson, P.B., and Taylor, H.P., 1986a, An oxygen-isotope study of water-rock interaction in the granite of Cataract Gulch, western San Juan Mountains, Colorado: Geological Society of America Bulletin, v. 97, p. 505–515.

Larson, P.B., and Taylor, H.P., 1986b, An oxygen isotope study of hydrothermal alteration in the Lake City caldera, San Juan Mountains, Colorado: Journal of Volcanology and Geothermal Research, v. 30, p. 47–82.

Larson, P.B., and Taylor, H.P., 1987, Solfataric alteration in the San Juan Mountains, Colorado: Oxygen isotope variations in a boiling hydrothermal environment: Economic Geology, v. 30, p. 1019–1036.

Lecumberri-Sanchez, P., Steele-MacInnis, M., and Bodnar, R.J., 2012, A numerical model to estimate trapping conditions of fluid inclusions that homogenize by halite disappearance: Geochimica et Cosmochimica Acta, v. 92, p. 14–22, doi:

10.1016/j.gca.2012.05.044.

Lipman, P.W., 1976a, Caldera-collapse breccias in the western San Juan Mountains, Colorado: Geological Society of America Bulletin, v. 87, p. 1397–1410.

Lipman, P., 1976b, Geologic map of the Lake City caldera area, western San Juan Mountains, southwestern Colorado: U.S. Geological Survey Miscellaneous Investigations Series Map I-962, scale 1:48,000.

Lipman, P.W., 2000, The central San Juan caldera cluster: Regional volcanic framework, *in* Bethke, P.M. and Hay, R.L. eds., Ancient Lake Creede: Its Volcano-Tectonic Setting, History of Sedimentation, and Relation of Mineralization in the Creede Mining District: Geological Society of America Special Paper, Geological Society of America, v. 346, p. 9–69, doi: 10.1130/0-8137-2346-9.9.

Lipman, P.W., Fisher, F.S., Mehnert, H.H., Naeser, C.W., Luedke, R.G., and Steven, T.A., 1976, Multiple ages of mid-Tertiary mineralization and alteration in the Western San Juan Mountains, Colorado: Economic Geology, v. 71, p. 571–588.

Lipman, P.W., Zimmerer, M.J., and Mcintosh, W.C., 2015, An ignimbrite caldera from the bottom up: Exhumed floor and fill of the resurgent Bonanza caldera, Southern Rocky Mountain volcanic field, Colorado: Geosphere, v. 11, p. 1902–1947, doi: 10.1130/GES01184.1.

Moncada, D., Mutchler, S., Nieto, A., Reynolds, T.J., Rimstidt, J.D., and Bodnar, R.J., 2011, Mineral textures and fluid inclusion petrography of the epithermal Ag–Au deposits at Guanajuato, Mexico: Application to exploration: Journal of Geochemical Exploration, v. 114, p. 20–35, doi: 10.1016/j.gexplo.2011.12.001.

Moore, J.N., 2012, The evolution of a partially vapor-dominated geothermal system at Karaha-Telaga Bodas, Indonesia: Insights from mineral distributions and fluid inclusion measurements: Proceedings of the New Zealand Geothermal Worshop 2012, Auckland, New Zealand, 19-21 November 2012.

Moore, J.N., Allis, R.G., Nemcok, M., Powell, T.S., Bruton, C.J., Wannamaker, P.E., Raharjo, I.B., and Norman, D.I., 2008, The evolution of volcano-hosted geothermal systems based on deep wells from Karaha-Telaga Bodas, Indonesia: American Journal of Science, v. 308, p. 1–48, doi: 10.2475/01.2008.01.

Moore, J.N., Powell, T.S., Norman, D.I., and Johnson, G.W., 1997, Hydrothermal alteration and fluid-inclusion systematics of the reservoir rocks in Matalibong-25, Tiwi, Philippines, *in* Proceedings, Thirty-Second Workshop on Geothermal Reservoir Engineering, Stanford, California, 22-24 January 2007, p. 447–456.

Peters, S.G., 1993, Nomenclature, concepts and classification of oreshoots in vein deposits: Ore Geology Reviews, v. 8, p. 3–22, doi: 10.1016/0169-1368(93)90025-T.

Reed, M.H., 1997, Hydrothermal alteration and its relationship to ore fluid composition, *in* Barnes, H.L. ed., Geochemistry of Hydrothermal Ore Deposits, John Wiley and Sons, p. 303–365.

Reyes, A., 1990, Petrology of Philippine geothermal systems and the application of alteration mineralogy to their assessment: Journal of Volcanology and Geothermal Research, v. 43, p. 279–309.

Rockwell, B.W., 2012, Map of mineralogy, vegetation, and hydrothermal alteration type generated from ASTER satellite data, San Juan Mountains, Colorado: U.S. Geological Survey Scientific Investigations Map 3190.

Roedder, E., 1984, Fluid Inclusions: Reviews in Mineralogy and Geochemistry, v. 12, 646 p.

Rowland, J. V., and Simmons, S.F., 2012, Hydrologic, Magmatic, and Tectonic Controls on Hydrothermal Flow, Taupō Volcanic Zone, New Zealand: Implications for the Formation of Epithermal Vein Deposits: Economic Geology, v. 107, p. 427–457, doi: 10.2113/econgeo.107.3.427.

Sander, M. V., and Black, J.E., 1988, Crystallization and recrystallization of growth-zoned vein quartz crystals from epithermal systems - Implications for fluid inclusion studies: Economic Geology, v. 83, p. 1052–1060.

Sanford, R.F., 1992, Lead isotopic compositions and paleohydrology of caldera-related epithermal veins, Lake City, Colorado: Geological Society of America Bulletin, v. 104, p. 1236–1245.

Sanford, R.F., Grauch, R.I., Hon, K., Bove, D.J., Grauch, V.J.S., and Korzeb, S.L., 1987, Mineral resources of the Redcloud Peak and Handies Peak Wilderness Study Areas, Hinsdale County, Colorado: U.S. Geological Survey Bulletin 1715-B, 37 p.

Sibson, R.H., 1987, Earthquake rupturing as a mineralizing agent in hydrothermal systems: Geology, v.15, p. 701–704, doi:10.1130/0091-7613(1987)15<701:ERAAMA>2.0.CO;2.

Simmons, S.F., and Brown, K.L., 2006, Gold in magmatic hydrothermal solutions and the rapid formation of a giant ore deposit: Science, v. 314, p. 288–291, doi: 10.1126/science.1132866.

Simmons, S.F., and Christenson, B.W., 1994, Origins of calcite in a boiling geothermal system: American Journal of Science, v. 294, p. 361–400, doi: 10.2475/ajs.294.3.361.

Simpson, M.P., Stevens, M.R., Mauk, J.L., Harris, M.C., and Stuart, A.G.J., 2016,

Exploration and geology of the Karangahake and Rahu epithermal gold – silver deposits, Hauraki Goldfield, *in* Mineral Deposits of New Zealand - Exploration and Research, AusIMM Monograph 31, p. 283–292.

Slack, J.F., 1980, Multistage vein ores of the Lake City District, western San Juan Mountains, Colorado: Economic Geology, v. 75, p. 963–991.

Steele-MacInnis, M., Lecumberri-Sanchez, P., and Bodnar, R.J., 2012, HokieFlincs_H_2O-NaCl: A Microsoft Excel spreadsheet for interpreting microthermometric data from fluid inclusions based on the PVTX properties of H_2O–NaCl: Computers & Geosciences, v. 49, p. 334–337, doi: 10.1016/j.cageo.2012.01.022.

Sterner, S.M., Hall, D.L., and Bodnar, R.J., 1988, Synthetic fluid inclusions. V. Solubility relations in the system NaCl-KCl-H_2O under vapor-saturated conditions: Geochimica et Cosmochimica Acta, v. 52, p. 989–1005, doi: 10.1016/0016-7037(88)90254-2.

Steven, T.A., and Lipman, P.W., 1976, Calderas of the San Juan Volcanic Field, southwestern Colorado: U.S. Geological Survey Professional Paper 958, 35 p.

Taylor, H.P., 1997, Oxygen and hydrogen isotope relationships in hydrothermal mineral deposits, *in* Barnes, H.L. ed., Geochemistry of Hydrothermal Ore Deposits, John Wiley and Sons, p. 229–302.

Taylor, H.P., 1974, The application of oxygen and hydrogen isotope studies to problems of hydrothermal alteration and ore deposition: Economic Geology, v. 69, p. 843–883.

White, N.C., and Hedenquist, J.W., 1990, Epithermal environments and styles of mineralization: Variations and their causes, and guidelines for exploration: Journal of Geochemical Exploration, v. 36, p. 445–474, doi: 10.1016/0375-6742(90)90063-G.

Wilkinson, J.J., Simmons, S.F., and Stoffell, B., 2013, How metalliferous brines line Mexican epithermal veins with silver: Scientific Reports, v. 3, p. 2057, doi: 10.1038/srep02057.

Wilson, C.J.N., and Rowland, J. V., 2016, The volcanic, magmatic and tectonic setting of the Taupo Volcanic Zone, New Zealand, reviewed from a geothermal perspective: Geothermics, v. 59, p. 168–187, doi: 10.1016/j.geothermics.2015.06.013.

Chapter 5. Conclusions and implications for hydrothermal fluid flow in caldera-related settings

5. Conclusions and implications for hydrothermal fluid flow in active caldera-related settings

5.1. INTRODUCTION

The main conclusions of this research at Lake City caldera are summarised in the bullet points below. A selection of these key findings are then discussed and compared with other calderas worldwide, with an emphasis on the Taupō Volcanic Zone (TVZ) of New Zealand. I then discuss how this work can inform our ability to understand and possibly predict the location of permeable fluid conduits in caldera settings to benefit geothermal utilisation.

- At Lake City caldera, the zone of deformation at the structural margin is wider than previously thought (up to ~300 m), and is partly controlled by pre-existing discontinuities. The structural margin is only rarely preserved at the present levels of exposure/erosion due to gravitational collapse of the ring fault scarps.

- The Lake City caldera margin is characterised by a very heterogeneous permeability architecture, due to varying amounts of gravitational collapse, intersections with regional structures, variable host lithologies, and potential inversion of fault displacement during resurgence. Vein concentration indicates that permeability was highest on structurally complex parts of the caldera margin, such as where it is oriented across the regional structural grain, at fault intersections/orientation changes, and where fault rocks of the structural margin are preserved. Permeability is also high in other parts of the caldera system where there are similarly favourable combinations of permeable lithologies, a high density of discontinuities, and discontinuity orientations that promote the formation of intersections.

- High spatial resolution SWIR reflectance spectroscopy methods (i.e. Corescan) are more accurate than low spatial resolution methods (i.e. TerraSpec) at detecting changes in white mica composition. The differences are small enough, however, that both are accurate enough for most practical purposes. The main advantage of Corescan-type methods is the ability to detect minerals at low abundances, and textural information.

- At Lake City, changes in white mica composition are likely correlated to the water-rock ratio, and thus the pH of the hydrothermal fluid without drastic changes in temperatures. High-Al (muscovitic) white mica forms under conditions of lower pH or higher water-rock interaction. Muscovitic white mica compositions correlate with zones of phyllic (quartz-sericite-pyrite) alteration. Muscovitic white mica also correlates with low $\delta^{18}O$ ratio in the centre of the caldera, however on the western margin neutral-pH fluid in equilibrium with the country rock forms low-Al white mica, but high $\delta^{18}O$.

- The two distinct magma batches at Lake City have distinct styles of alteration associated with them. Batch A magmas were the source of the caldera-forming ignimbrite and resurgent syenite. The lack of high temperature and saline fluid inclusions, and a lack of acid alteration near the syenite suggest that batch A magmas provided little magmatic fluid input into the hydrothermal reservoir. Phyllic alteration formed in the resurgent dome, while fully neutralised fluid formed propylitic alteration on the western caldera margin. Our interpretation is that the upper parts of the resurgent syenite pluton (part of magma batch A) had already cooled significantly by the time the main neutral chloride hydrothermal system had established, contrary to previous interpretations of the syenite as a high temperature heat source for the hydrothermal system (Larson and Taylor, 1986). Batch B magmas exsolved high temperature (up to ~540°C) fluid into the hydrothermal system at Red Mountain and Alpine Gulch, and may have been a major source of heat for the neutral chloride portions of the hydrothermal system.

One of the main aims of this thesis is to improve our understanding of hydrothermal fluid flow in active caldera-related geothermal systems and what controls high permeability areas versus low permeability. To address this aim three key findings from Lake City caldera are compared and discussed with other modern calderas worldwide. These are that:

1) The structural margin of the caldera is wider than a single ring fault, and may have a polygonal component controlled by pre-existing discontinuities;

2) Permeability on the margin and the interior of the caldera was favoured where discontinuity intersections were formed, such as where the caldera margin cuts across regional structural grain;

3) Distinct magma batches at Lake City had distinct hydrothermal manifestations, meaning that end-member neutral chloride/adularia-illite and acid-sulfate systems formed in the same caldera system.

In this chapter, I apply the specific findings from Lake City caldera to the Taupō Volcanic Zone of New Zealand, Valles caldera, U.S.A., and Long Valley caldera, U.S.A. These modern analogues all host geothermal systems and have diverse regional settings that let us explore how universal the findings at Lake City are to other settings.

5.2. IMPLICATIONS FOR HYDROTHERMAL CIRCULATION IN NEW ZEALAND CALDERA-RELATED GEOTHERMAL SYSTEMS

The Taupō Volcanic Zone (TVZ) is a NE-SW trending rifting-arc in the North Island of New Zealand (Fig. 1). It is the southernmost portion of the much larger Tonga-Kermadec arc system (Wilson and Rowland, 2016). The TVZ is one of the most productive areas of Quaternary silicic volcanism and geothermal activity in the world, and the central silicic portion has produced at least 25 caldera-forming eruptions, and hosts 23 active geothermal systems (Fig. 1b) (Houghton et al., 1995; Wilson et al., 1995; Wilson and Rowland, 2016). In this section I discuss the implications of my research at Lake City caldera for understanding and exploring the location of permeable fluid conduits in the TVZ. In addition to the key findings mentioned in the previous section I also discuss how the longevity and stability of geothermal systems in the TVZ compares to the Lake City area, and how intra-caldera landslide breccias may compare in the TVZ and Lake City caldera.

5.2.1. Caldera morphology

The abrupt southwestern corner of Lake City, and the sub-parallel trend of the southern margin to dykes in the granite basement, suggests that the structural margin had a more polygonal shape than previously recognised. The structural margin has been eroded due to gravitational collapse along most of its length, meaning that most of the exposed caldera margin discontinuity is a topographic margin. The structure of the TVZ is complex and has a large effect on the geometry and orientation of calderas (Spinks et al., 2005; Seebeck et al., 2010). For example, Rotorua caldera has a rounded topographic boundary, which extends far from and is superimposed upon the inferred polygonal structural margin (Milner et al., 2002; Spinks et al., 2005; Ashwell et al., 2013). This exemplifies how erosional processes can

significantly modify shallow caldera morphology, although how much of this modification occurs from widespread catastrophic landsliding during caldera collapse is unconstrained in the TVZ, and the association of domes and structural trends indicates that subsiding fault blocks may be rectilinear (Milner et al., 2002; Ashwell et al., 2013). Other examples of polygonal calderas in the TVZ are Taupō, and Okataina, which all have complex shapes, usually involving reactivation of regional faults during caldera collapse (Wilson, 2001; Spinks et al., 2005; Cole and Spinks, 2009). The newly defined Waiora caldera is also inferred to have a distinctly rectilinear shape (Rosenberg, 2017). An important consequence of polygonal and rectilinear caldera structure is the role that fault intersections may play in their permeability.

5.2.2. Influence of caldera structures and fault intersections on permeability

The Taupō Volcanic Zone has a very strong NE-SW "structural grain", due to the multitude of normal faults that accommodate intra-arc extension (Fig. 1b) (Davey et al., 1995; Villamor et al., 2001; Rowland and Sibson, 2004). Previous work has suggested that inferred N-S trending basement structures and NW-SE trending "accommodation zones" are important in controlling the location of geothermal plumes that have enhanced vertical permeability, due to the intersections they create with NE-SW trending normal faults (Rowland and Sibson, 2004; Wilson and Rowland, 2016). At Lake City, the caldera margin provides a similar means of creating permeable intersections where it cuts across the structural grain, and intersections in the caldera margins probably have the same effect in parts of the TVZ at shallow depth.

The thin, heavily faulted crust, active extension, and high magma production rate in the TVZ, makes magma intrusion and caldera formation an integral part of the tectonic process (Rowland et al., 2010). Regional intrusive, rifting, and caldera subsidence processes form a continuum where fault reactivation is common. Examples of reactivated regional structures to accommodate caldera subsidence occurred during the Whakamaru Group eruptions, especially along the Paeroa fault (Downs et al., 2014b; Rosenberg, 2017), during the paired Ohakuri-Mamaku eruptions, along the Horohoro fault (Gravley et al., 2007), during the Oruanui eruption, along the Waihi fault (Wilson, 2001), and re-activation of faults during eruptions from Okataina caldera (Seebeck and Nicol, 2009; Seebeck et al., 2010; Villamor et al., 2011). However, the parts of caldera margins that intersect the regional structural grain

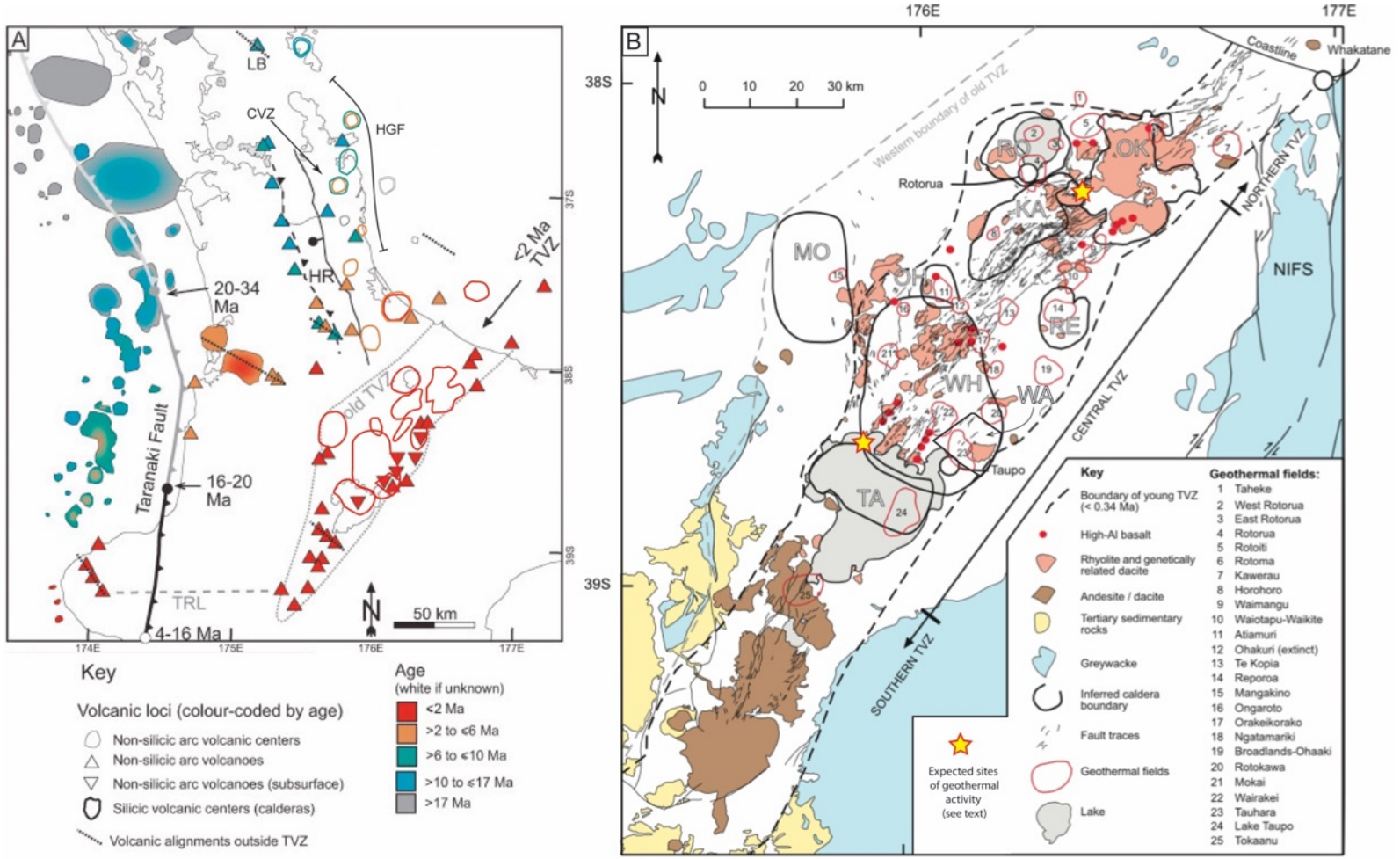

Figure 1: Simplified geology and regional setting of the Taupō Volcanic Zone and northern New Zealand, modified from Wilson and Rowland (2016). (A): Miocene to present arc volcanic centres and volcanoes, both silicic and non-silicic, and other major geological features. Depicted are: HR – Hauraki Rift, with border fault shonw by black line with ball on downthrown side, barbed dashed line shows approximate position of hanging wall flexure; HGF – Hauraki Goldfield; CVZ – Coromandel Volcanic Zone; LB – Little Barrier Volcano. (B): Geological map of the Taupō Volcanic Zone, from Wilson and Rowland (2016) and references therein. Calderas labelled are: Ka – Kapenga, MO – Mangakino, OH – Ohakuri, OK – Okataina, RE – Reporoa, RO – Rotorua, TA – Taupō, WA – Waiora, and WH – Whakamaru. Position of the Waiora caldera from Rosenberg (2017). Also depicted is the North Island Fault System (NIFS). Low resistivity zones were used to delimit the geothermal fields (<30 Ωm) (after Bibby et al., 1995). Major towns labelled. Expected sites of geothermal activity refer to favourable sites for exploration discussed in section 1.2.2.

are frequently obscured by intra-caldera fill or buried by younger volcanic and volcaniclastic deposits . The N-S trend of the poorly defined western and eastern margins of Whakamaru caldera has been suggested to relate to inferred N-S trending basement structures related to the Hauraki Rift (Wilson and Rowland, 2016 and references therein). The interaction of these deeper basement structures with caldera collapse structures is important because this allows connectivity between deep hot fluids and the complex caldera structures and lithologies. This connectivity could link the deep upflow of geothermal plumes (Bertrand et al., 2015; Heise et al., 2016) with shallow geothermal reservoirs.

The most unequivocal examples of the position of geothermal systems in the TVZ being strongly influenced by caldera structures include Lake Taupō geothermal system (Taupō caldera) (Bibby et al., 1995), Rotorua geothermal system (Rotorua caldera) (Wood, 1992) and Waimangu-Rotomahana geothermal system (Okataina caldera) (Wood, 1994). The Lake Taupō geothermal system is located over the approximate vent locations for most of the post-caldera-forming Oruanui eruptions (Wilson, 1993; Bibby et al., 1995; Barker et al., 2014). The Rotorua geothermal system is located on or near the southern edge of Rotorua caldera, though the exact location of the structural margin of the caldera is slightly uncertain (cf. Milner et al., 2002; Spinks et al., 2005; Ashwell et al., 2013). The Waimangu-Rotomahana geothermal system is on the southwestern corner of the structural margin of Okataina caldera (Wood, 1994). This location is where the caldera margin intersects regional NE-SW trending faults (Fig. 1b). This is exemplified by the 1886 Tarawera eruption, in which a NE trending basaltic fissure caused substantial phreatomagmatic and hydrothermal eruptions along strike of the geothermal system and greatly modified the near surface hydrology (Simmons et al., 1993; Caratori Tontini et al., 2016). The Rotoma geothermal system is located on the northeastern corner of the Okataina caldera (Simpson and Bignall, 2016), while the Tikitere geothermal system is located in a graben structure between Rotorua and Okataina calderas.

Other geothermal systems with spatial relationships to, and possible control from, caldera-related structures include Wai-o-Tapu near the northeastern margin of Reporoa caldera (Wood, 1994), and Atiamuri, Ohakuri (extinct), Orakei-Korako, and Rotokawa, which are all near the poorly defined east to northeast side of Whakamaru caldera (see Fig. 1b) (Rowland and Sibson, 2004). All of the above examples (except Lake Taupō) are geothermal systems that are associated with the part of the caldera margin that is oriented across, rather than parallel, to the regional structural trend. Fault intersections have been considered important

controls on permeability in the TVZ (Rowland and Sibson, 2004; Rowland and Simmons, 2012; Chambefort et al., 2017b; Villamor et al., 2017), and the formation of such intersections will likely be enhanced where caldera margins cut across regional rift faults. This is analogous to the situation at Lake City caldera, where fluid flow was focussed on the western and eastern margins, but not on the north and south.

The most notable exceptions to this pattern are the Lake Taupō and Wairakei-Tauhara geothermal systems, which are discussed below. The location of the Lake Taupō system over the source of most recent (post-Oruanui) eruptions from Taupō volcano (Wilson and Walker, 1985; Caldwell and Bibby, 1992; Barker et al., 2014) make it likely its location is controlled by the presence of a relatively shallow magmatic heat source. Recent volcanic conduits (such as from the 1.8 ka Taupo eruption) could potentially provide increased permeability (Caldwell and Bibby, 1992), and the NE-SW oriented linear pattern of young vents suggests some permeability control from regional faults or the eastern structural margin of the Oruanui caldera (Barker et al., 2014), though the structural geology of the system is very poorly constrained. Most magmas erupted since the 26.5 ka Oruanui caldera-forming eruption are geochemically distinct from the Oruanui magma system (Barker et al., 2014). This distinct post-Oruanui magma system probably drives the Lake Taupō geothermal system. The association of high-temperature geothermal activity with a younger, distinct magma batch has some similarities to the distinct post-caldera "batch B" magmas at Lake City, which released high temperature magmatic fluids into the Lake City hydrothermal system, and may have been the main heat source for the system (see Chapter 4).

The Wairakei-Tauhara geothermal system is located near the poorly defined southern margin of the Whakamaru caldera, and inside the newly recognised Waiora caldera, which shares its southeastern margin with the Whakamaru (Rosenberg, 2017). The geothermal system is also within a corridor of downsag subsidence extending to the northeast from Taupo caldera (Walker, 1984). The presence of the young (<60 ka), active geothermal system is at least partly attributed to the presence of a young magma system (called the "NE dome system"), which fed local effusive eruptions (Rosenberg, 2017). Permeability is focussed by basement fault structures, which were created or reactivated during the piecemeal Whakamaru and Waiora caldera collapse, and by "overprinting" NE-SW and E-W trending faults (Villamor et al., 2015; Rosenberg, 2017). The diversity of structural orientations will create multiple fault intersections that may enhance permeability.

Using the conclusions derived from Lake City caldera on the importance of fault intersections in facilitating permeability, and the importance of caldera margin faults cross-cutting the regional structural grain, two additional areas may be favourable sites for exploration. These are: 1) The western margin of Okataina caldera, in the vicinity of Lake Okareka and the northwestern side of Lake Tarawera, and 2) the northeastern margin of Taupō caldera, near Whangamata Bay (Fig. 1). These two sites exemplify the favourable map scale permeability characteristics discussed in this thesis. Location 1 is where the orientation of the Okataina caldera margin changes from approximately NW-SE to SSW-NNE, and is near the northeasternmost extension of Kapenga caldera (Fig. 1). The NW-SE oriented segment of the Okataina caldera margin intersects with the NE-SW trending Taupō Fault Belt. Overall, these structural complexities are expected to enhance permeability. Location 2 is at the northwestern corner of Taupō caldera, where the orientation of the caldera margin changes from NE-SW to NW-SE (Fig. 1). The NW-SE oriented segment intersects with the southern part of the NE-SW trending Taupō Fault Belt. Location 2 is also at the inferred southwestern corner of the Whakamaru caldera, where the orientation of its margin changes from approximately N-S to NW-SE (Fig. 1). The combination of a change in the orientation of the margin of two calderas, and intersections with regional faults are expected to favour permeability. Major geothermal activity has not been identified in either of these locations, however deep resistivity structure as delineated by magnetotelluric data indicates the presence of a deep conductive plume under Location 1, the western margin of Okataina caldera (Heise et al., 2010). Comparable data are not available for the northeastern margin of Taupō caldera. Further geophysics and exploration wells would be necessary to explore whether the local geological and fluid geochemical characteristics support the map scale inferences.

5.2.3. Stability and longevity of TVZ geothermal systems

In the Lake City area, the repeated formation of hydrothermal systems in the same location is well-documented (Lipman et al., 1976; Bove et al., 2001). Silverton and Uncompaghre calderas hosted hydrothermal systems soon after caldera collapse, and more than ten million years later. Even specific vein systems, such as that at Ute-Ulay Mine, have been rejuvenated after hiatuses of millions of years (Bove et al., 2001). Similarly, in some geothermal systems in the TVZ there is evidence for past hydrothermal activity, where independent geothermal

systems have been established at the same place in different times. The two most unequivocal examples of this are Kawerau and Ngatamariki, both of which have intrusions that were linked to the older system (Milicich et al., 2013; Chambefort et al., 2014). The link between specific local magmatism and geothermal activity in these systems suggests the existence of deep favourable permeability structures at these locations, which localises both magmatism and hydrothermal fluid flow.

The volcano-tectonic setting between the San Juan volcanic field (SJVF) and TVZ differs in that the TVZ is fundamentally linked to an extensional tectonic regime. The high rate of extension may explain the lack of structural resurgence in calderas of the TVZ (Kennedy et al., 2012), and active tectonics may also help maintain permeability along critically stressed structures. These data from both the SJVF and TVZ show how structures can maintain high permeability long after their initial formation, though the timescale is different between the SJVF (millions of years) and TVZ (up to hundreds of thousands of years) due at least in part to the relatively young age (~2 Ma) of the TVZ (Wilson and Rowland, 2016). The discontinuities with rejuvenated fluid flow can be pre-existing basement structures, caldera structures, or some combination thereof.

5.2.4. Intra-caldera landslide breccias in the TVZ

Widespread intra-caldera breccias formed by landsliding of the oversteepened caldera walls during subsidence are an important and distinctive feature of many calderas in the SJVF (including Lake City) and worldwide (e.g. Lipman, 1976; Branney and Kokelaar, 1994; Cornejo et al., 1997). These have been inferred to be potentially favourable fluid conduits in caldera systems, having a higher intrinsic permeability than surrounding welded intra-caldera ignimbrite (e.g. Larson and Taylor, 1986; Sanford, 1992). However, no widespread intra-caldera landslide breccias have been identified in the TVZ. The closest approximation are scattered occurrences of coarse lithic breccias (possibly lithic lag breccias) that have been reported in the Whakamaru caldera (Wilson et al., 1995). Coarse lag breccias occur proximal to vents from caldera-forming eruptions, such as Oruanui-derived breccias on the shores of Lake Taupo (Self, 1983), however these have an explosive origin, rather than forming from lansliding (Walker, 1985). Identification of intra-caldera landslide breccias is more difficult in the TVZ than at Lake City caldera due to the limited exposure and the nature of the lithologies of the central TVZ. It is possible that drill holes have misidentified landslide

breccia units in drill core or cuttings. Landslide breccias can be comprised of extremely coarse megabreccias, which by definition contain blocks with dimensions from metres to kilometres that would be difficult to distinguish from in situ rock. The distinction would be most difficult when the lithic clasts are composed of ignimbrite lithics similar in appearance to the intra-caldera ignimbrite. A systematic re-analysis of drill core, paying close attention to the orientation of primary deposition features (e.g. welded pumice fiamme) and occurrences of ignimbrites that are incongruous (in texture and/or composition) with the stratigraphy above and below, could help elucidate the presence of landslide deposits or lack thereof. Additionally, distinguishing landslide breccia facies from lithic lag breccia facies, which are associated with many TVZ calderas (Wilson et al., 1995; Wilson, 2001), may also be difficult without the spatial context that exposures in exhumed calderas provide.

The formation of landslide breccias requires large, oversteepened scarps, and therefore subsidence must occur rapidly enough that infilling by eruptive products cannot fill the accommodation space or buttress the scarp (Lipman, 1976a). Styles of collapse that involve distributed deformation over a large area at the caldera margin, such as downsag subsidence, may also not produce high enough scarps to catastrophically fail. Poor exposure and insufficient resolution of geophysical and drill-hole data makes the structure of calderas in the TVZ difficult to ascertain. The available data suggest that TVZ calderas may have a strong component of piecemeal-style subsidence, as has been shown for Rotorua and Whakamaru calderas (Milner et al., 2002; Rosenberg, 2017). The strong NE-SW structural grain controls the morphology of collapsed blocks, with collapse occurring predominantly along reactivated NE-SW trending faults. The reactivation of regional faults and/or accommodation zones during caldera formation also causes the polygonal structural margins that are characteristic of many TVZ calderas, such as Rotorua, Waiora, Taupō and Okataina (Cole and Spinks, 2009; Seebeck et al., 2010; Ashwell et al., 2013; Rosenberg, 2017). If subsidence occurs as a series of relatively small blocks, then it is probable that any landslide breccias that form could be confined to a single block, and not be as widespread as at Lake City.

The differing lithologies at Lake City and in the TVZ may also affect the formation of landslide breccias. At Lake City, most rock types are coherent, such as welded ignimbrite, voluminous andesitic to dacitic lavas, and granite basement. The high strength of these lithologies would make it easier for a high, oversteepend scarp to form, and make it possible

for large blocks (up to 100s of metres across) to stay coherent in the landslides themselves. By contrast, the lithologies in the TVZ are more variable, and weak poorly- to non-welded ignimbrites and other pyroclastics make up a large proportion of the volcanic fill (e.g. Rosenberg et al., 2009; Downs et al., 2014a). The effects of hydrothermal alteration, which are widespread in parts of the TVZ, can weaken or strengthen rocks, further increasing this variability (Wyering et al., 2014). Weak rocks are less likely to maintain a large, steep fault scarp, and will therefore probably fail before they can grow high enough to form widespread landslides on collapse. Less widespread, or lower volume landslide deposits will be less likely to be encountered by geothermal drilling. Some calderas in the TVZ (e.g. Rotorua and Okataina) have topographic boundaries that extend far from the inferred structural margin, and provide evidence that large scale erosional modification does occur in TVZ calderas (Spinks et al., 2005). No widespread breccias or megabreccias have been identified however, and it is likely that this erosion occurs more gradually than the catastrophic gravitational failure that occurred during collapse of Lake City caldera. If landslide breccias have been misidentified as in-situ rock, then this would lead to erroneous geological models of TVZ geothermal reservoirs. Inaccurately complex structural and stratigraphic relationships would have to be invoked in order to explain the presence of the units that comprise megabreccia blocks.

5.3. IMPLICATIONS FOR OTHER CALDERA-RELATED SYSTEMS WORLDWIDE

The conclusions regarding the volcano-tectonic controls on hydrothermal fluid flow at Lake City caldera can be applied to other calderas outside of New Zealand. The key conclusions that are addressed in these examples are that:

1) The structural margin of the caldera is wider than a single ring fault, and may have a polygonal component and controlled by pre-existing discontinuities;

2) Permeability on the margin and the interior of the caldera was favoured where discontinuity intersections were formed, such as where the caldera margin cuts across regional structural grain;

3) Distinct magma batches at Lake City had distinct hydrothermal manifestations, meaning that end-member neutral chloride/adularia-illite and acid-sulfate systems formed in the same caldera system.

As examples, I focus on the comparisons with, and implications for, the well-documented active geothermal systems at Valles and Long Valley calderas, U.S.A.

5.3.1. Valles caldera, New Mexico, U.S.A.

The 1.26 Ma Valles caldera is in the Jemez Mountains volcanic field (JMVF) of New Mexico, U.S.A. (Phillips et al., 2007), and hosts an active geothermal system (Fig. 2). The JMVF is located at the intersection of the western margin of the N-S trending extensional Rio Grande Rift, and the NE-SW trending Jemez Lineament (Fig. 2a), which is an alignment of Miocene to Holocene volcanic centres, localised along a reactivated Precambrian structure (Self et al., 1986; Goff and Janik, 2002). Similarities in the regional setting, size, and structure of Valles and Lake City calderas means they have been compared as volcanological analogues to each other (e.g. Kennedy et al., 2012).

The active geothermal reservoir is in the highly faulted resurgent dome of the caldera (Baca geothermal system) and near the combined margin of the resurgent dome and structural margin of the caldera (Sulphur Springs) (Goff and Gardener, 1994). At Sulphur Springs, NE-SW trending intra-caldera faults intersect the structural margin of the caldera (Hulen and Nielson, 1990). This is similar to the configuration of the adularia-illite portion of the Lake City hydrothermal system in the resurgent dome and along the western caldera margin. The Valles geothermal system consists predominantly of a ≤ 300°C liquid-dominated, near-neutral chloride reservoir, recharged by meteoric water (Goff and Gardener, 1994). Of the 24 geothermal wells drilled into the Valles geothermal system, all six of the most permeable wells (which include wells B-6, B-4 and B-13 on Fig. 2) are clustered within a 2 km^2 area of the resurgent dome (Hulen and Nielson, 1990). Fault intersections, between NE-SW trending apical graben faults and E-W trending faults, have been interpreted to be important controls favouring the maintenance of permeability in this area (Hulen and Nielson, 1990). The fluid and alteration is similar to that observed for the western, adularia-illite, part of the Lake City caldera system. In the near-surface portion of the Valles system, acid sulfate waters are present with associated advanced argillic alteration, due to condensation of steam into near-surface (<20 m depth) ground waters (Goff and Gardener, 1994). Such near-surface acid-sulfate alteration was not observed at Lake City, probably because this portion of the system was eroded away, as supported by fluid inclusion microthermometry that indicates erosion of

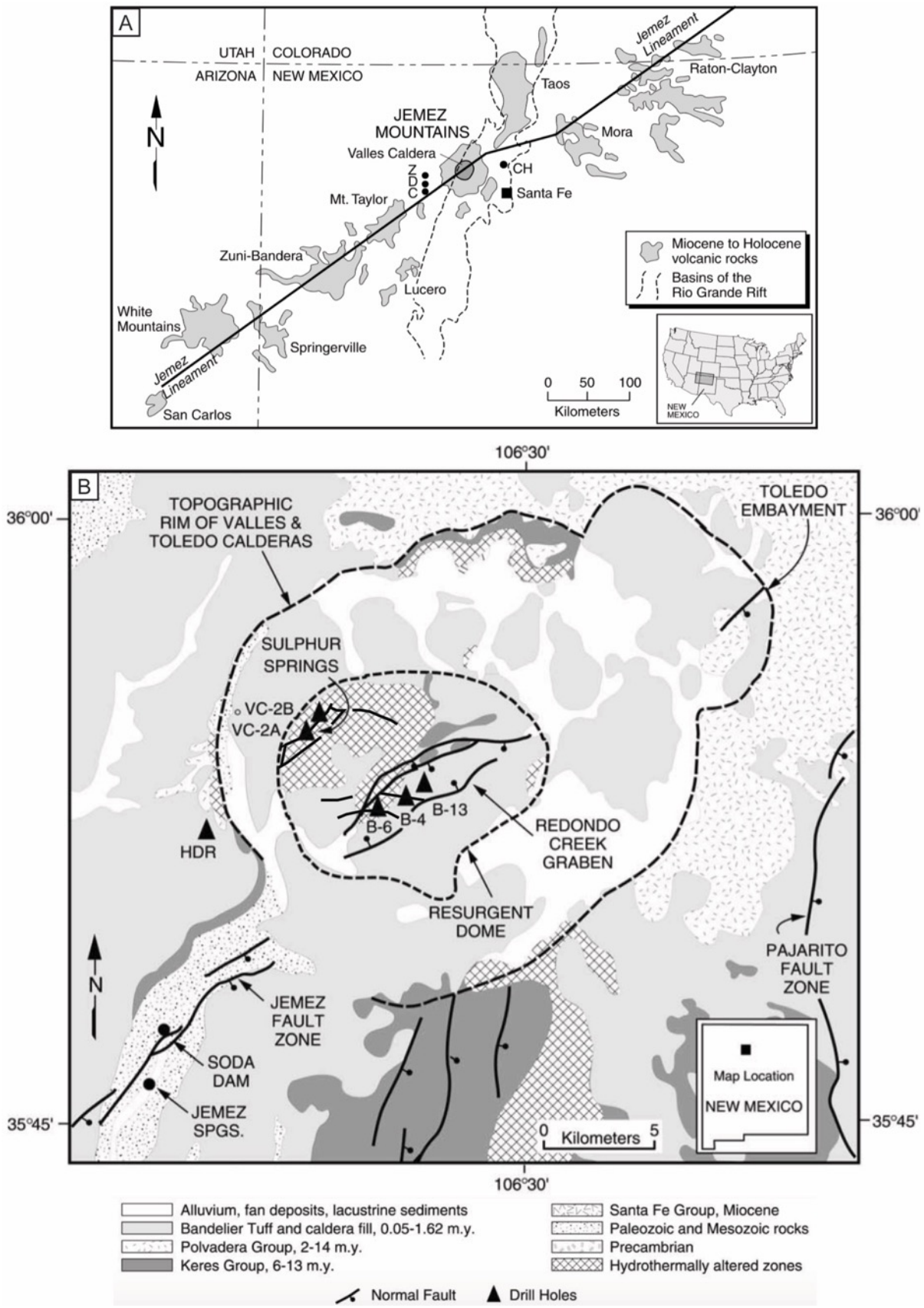

Figure 2: Regional setting and geology of Valles caldera, modified from Goff and Janik, 2002 and Hulen and Nielson, 1990. A: Location of the Jemez Mountains and Valles caldera with respect to other volcanic centres of the Jemez Lineament and the Rio Grande Rift. B: Map of Valles caldera showing general geology and structure, and the location of thermal features and geothermal wells.

at least ~200 m (Chapter 4, Fig. 24). At Valles, below the acid-sulfate zone, alteration is predominantly propylitic and phyllic, with phyllic alteration strongest in highly deformed (fractured, faulted and brecciated) zones with high fluid throughput (Goff and Gardener, 1994). This agrees well with observations at Lake City caldera, where phyllic alteration is common around veins (former conduits with high fluid throughput) and in the highly fractured and faulted resurgent dome.

At Valles, no major input of magmatic fluid into any part of the geothermal system has been detected, and advanced argillic alteration has not been identified below the shallow acid-sulfate zone (Goff and Gardener, 1994; Goff and Janik, 2002). Shallow subeconomic molybdenum mineralisation has been encountered during drilling at Sulphur Springs (Hulen et al., 1987), however further deep drilling has not identified any evidence of a larger intrusion- and/or magmatic-fluid related ore body (Goff and Gardener, 1994). This contrasts with Lake City caldera, which had significant input of magmatic fluid from "batch B" magmas in the east of the caldera. The Redondo Creek Rhyodacite at Valles formed from a distinct, hotter, more mafic magma batch than the bulk of the magma erupted during the caldera forming eruption (Kennedy et al., 2012). It has therefore been interpreted as an analogue to the batch B magmas at Lake City caldera (Kennedy et al., 2012). However, the distinctive acid alteration and high temperature fluid inclusions associated with batch B magmas at Lake City are lacking at Valles caldera. It is possible that episodes of high volume magmatic fluid exsolution were short-lived and highly localised, and evidence for them has been missed by drilling. The molybdenum mineralisation at Sulphur Creek, which is near the outcropping of Redondo Creek Rhyodacite, may be the near-surface expression of deeper exsolution of magmatic fluids (Hulen et al., 1987). However, this is not supported by available deep drilling data (Goff and Gardener, 1994), and clearly there was no magmatic fluid dominated system as large or intense as the Red Mountain system at Lake City caldera. Despite this geochemical difference between the history of the Valles and Lake City hydrothermal systems, there are remarkable similarities in the structural controls on permeability. Both are parts of NE-aligned volcanic clusters, with control from basement structures that localised permeability for magmas. Hydrothermal fluids in both systems were localised in areas of high permeability in the highly deformed resurgent dome and at areas of discontinuity intersection along the caldera margin.

In summary, the Valles geothermal system has a similar configuration to the adularia-illite portion of the Lake City hydrothermal system, probably reflecting similar permeability controls on the caldera margin and resurgent dome. The character of the structural margin of the caldera is not well constrained, however its NE-SW elongation and position along the Jemez Lineament at the intersection with the Rio Grande Rift (Fig. 2) implies that re-activation of regional structures was important in its formation. Permeability for hydrothermal fluids is highest where fault intersections form in the highly faulted resurgent dome, but geothermal upflow also occurs where intra-caldera faults intersect the structural margin at Sulphur Springs. These controls on permeability are similar to those identified at Lake City caldera. The presence of shallow molybdenum mineralisation at Sulphur Springs near where the distinct Redondo Creek rhyodacite magma batch was erupted suggests the younger magma batch may have exsolved magmatic fluid into the hydrothermal system, similar to the batch B magmas at Lake City caldera. However, any such input was likely much smaller than the Red Mountain system at Lake City.

5.3.2. Long Valley caldera, California, U.S.A.

The 0.76 Ma Long Valley caldera is in an active regional transtensional zone on the eastern margin of the Sierra Nevada mountains, at the transition to the Basin and Range system (Hildreth, 2004). The northwestern margin of the caldera is intersected by the younger (20 – 0.6 ka) Mono-Inyo craters chain, which follows the NNW trending structural grain, while the Mammoth Mountain (111 - 57 ka) dome system is located just outside southwest structural margin of the caldera (Fig. 3) (Hildreth, 2004). Surface hot springs and fumaroles are mostly located on the southern to eastern side of the resurgent dome of the caldera (Sorey et al., 1991). Resurgent uplift at Long Valley was predominantly caused by the post-caldera intrusion of multiple stacked rhyolite sills, with a cumulative thickness of up to >300 m in the centre of uplift (McConnell et al., 1995; Hildreth et al., 2017). This contrasts with the observed morphology of the Lake City resurgent intrusion, which predominantly consists of a single syenite pluton (Hon, 1987).

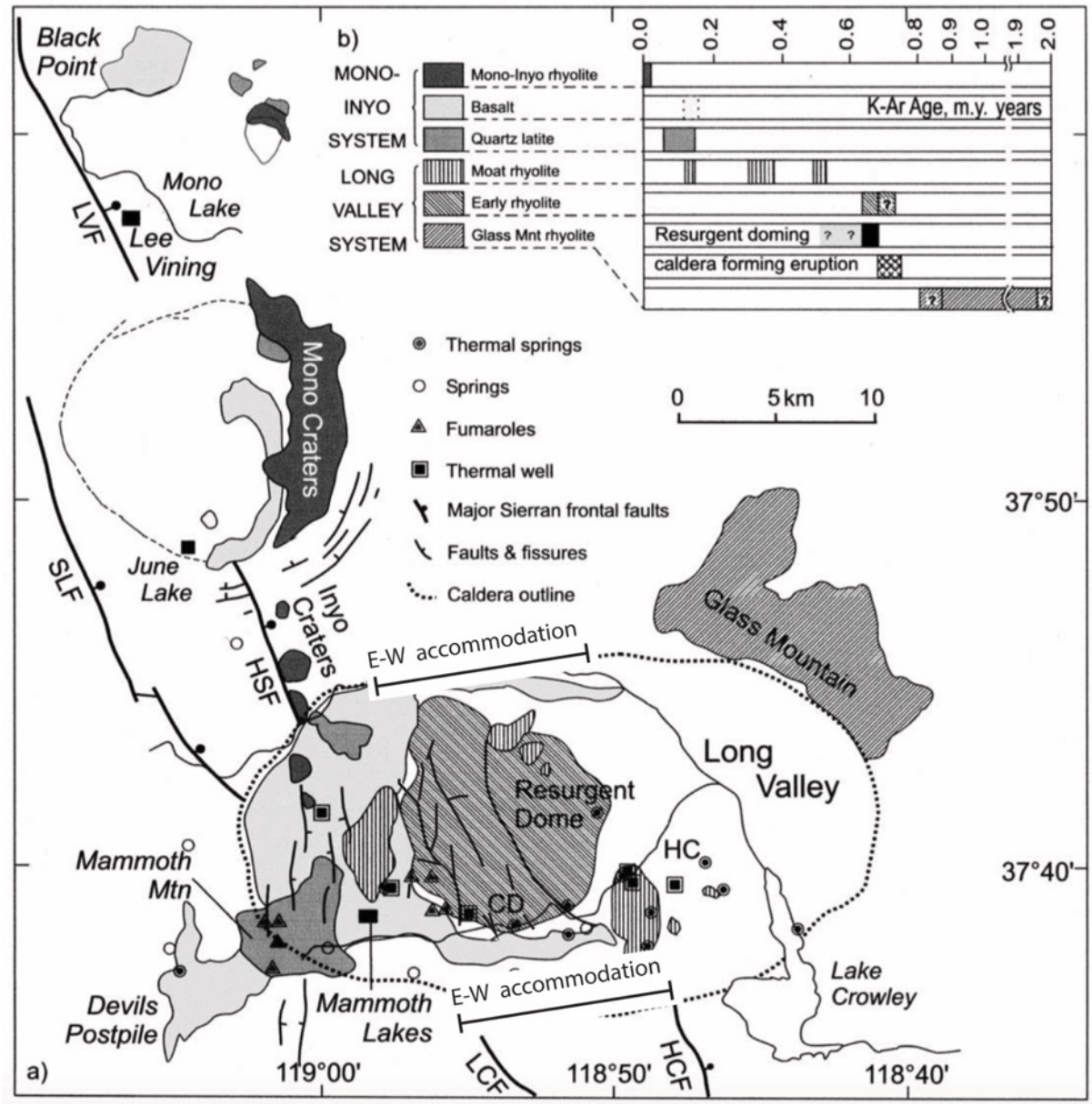

Figure 3: Simplified geologic map of Long Valley caldera, (modified from Fischer et al., 2003, and Hildreth, 2017) showing the distribution and age of post-caldera volcanic rocks, and the distribution of present-day hydrothermal activity at the surface. Abbreviations: LVF – Lee Vinig fault; HSF – Hartley Springs fault; SLF – Silver Lake fault; CD – Casa Diablo; HC – Hot Creek.

A geothermal power plant (Casa Diablo) is located on the southern flank of the resurgent dome (Fig. 3), however a 3 km deep borehole drilled from the crest of the resurgent dome only identified maximum temperatures of 103°C, typical of a near-normal geothermal gradient (Fischer et al., 2003; Hurwitz et al., 2010). Fluid inclusion evidence from this borehole suggests, that a high-temperature (250 – 350°C) hydrothermal system was active there in the past (Fischer et al., 2003). Current evidence suggests that the caldera-forming magma system is in terminal decline, though it has been locally re-energised by the

Mammoth Mountain magmatic system at their intersection on the western margin of the caldera (Hildreth, 2004, 2017). This part of the western margin of the caldera contains the highest enthalpy hydrothermal upflow at depth (Smith and Suemnicht, 1991), while the crystallising magma residue under the resurgent dome releases fluid that flows laterally to the permeable and tectonically reactivated discontinuities of the southern ring fault zone (Hildreth, 2017). Permeability in the modern geothermal system is thus facilitated by reactivated caldera margin structures on the southern and western margins (Suemnicht and Varga, 1988; Hildreth, 2017).

The importance of basement structures in controlling the emplacement of magma bodies, the morphology of caldera collapse, and hydrothermal fluid flow is shown well at both Lake City and Long Valley calderas. However, unlike Lake City caldera, Long Valley is elongate in an E-W direction, orthogonal to the major N-S basement structural grain (Fig. 3). Long Valley is located at an E-W bend or accommodation zone between N-S Sierra range front faults, the Hilton Creek fault and Hartley Springs fault (Fig. 3) (Suemnicht and Varga, 1988; Hildreth, 2004; Lucic et al., 2015). The second-order E-W faults and their associated structural complexities where they intersect the first-order N-S faults must have provided the most favourable permeability for magma accumulation and eruption. The western side of the resurgent dome contains a graben with several NW-SE trending normal faults, however the area of resurgent uplift is equant in shape, in contrast to the elongation of the caldera (Hildreth et al., 2017).

In summary, the location and morphology of Long Valley caldera is strongly controlled by regional structures, and it probably has a polygonal structural boundary at depth. Current geothermal fluid flow is focussed along the tectonically active southern margin, and structurally (and magmatically) complex southwestern corner of the caldera, similar in principal to the location of permeable pathways on the Lake City caldera margin. However, in contrast the resurgent dome at Long Valley caldera is no longer permeable enough for hydrothermal fluid flow, and was formed by the intrusion of stacked sills rather than a large pluton. The caldera magmatic system is in decline, similar to the batch A magma system at Lake City caldera, and is being partly sustained by interaction with younger distinct magma batches on the caldera margin. This is somewhat analogous to the role of batch B magmas at Lake City caldera.

5.4. IMPLICATIONS AND GUIDELINES FOR GEOTHERMAL EXPLORATION

The results from this thesis can be used to form general guidelines for geothermal exploration in caldera-related settings, in order to address the primary aim of helping understand and predict controls on hydrothermal fluid flow in modern caldera-related geothermal systems. This specifically relates to the research question posed in Chapter 1; *How can we use these data from an ancient analogue to inform our understanding of modern caldera-related geothermal systems such as those in the Taupō Volcanic Zone of New Zealand?* In keeping with the structure of the thesis, I will first discuss implications based on, the structural controls of permeability (Chapter 2), followed by, reflectance spectroscopy as an exploration tool (Chapter 3), and finally the physiochemical conditions of the hydrothermal fluid in caldera settings (Chapter 4).

Based on the data presented in this thesis, the best targets for fault and fracture hosted permeability in caldera-related settings are at fault intersections. Caldera margins may be good exploration targets, but drilling should aim for where the caldera margins change in orientation or intersect regional faults. This is supported by the location, frequency and dimensions of veins at Lake City caldera (Chapter 2), and is consistent with available data for Valles and Long Valley calderas, and some TVZ systems (see sections 5.2 and 5.3 above). The structural, rather than topographic margin of a caldera is expected to be a better exploration target, due to the preservation of potentially permeable fault rocks and damage zones. Distinguishing the structural margin from the topographic margin may be difficult, but may be achieved by identifying fault rocks in drill cuttings or core, and by targeting steep gravity contours in Bouger anomalies (Rymer and Brown, 1986; Stagpoole, 1994), rather than the surface expression of the caldera margin. Resurgent domes, if present, may also be good targets for geothermal exploration due to the high fault and fracture densities associated with the apical graben formed during resurgent uplift and/or reactivated regional faults that accommodate uplift.

Characterisation of the hydrothermal alteration encountered during drilling is an important part of the exploration process (Browne, 1970; Reyes, 1990). Short wave infrared reflectance spectroscopy is an effective tool for identifying many important alteration minerals, such as chlorite, white mica, epidote and more. The composition of white mica can be easily investigated and incorporated into any SWIR study of alteration, and can be a cheap and effective tool for tracing changes in fluid conditions (Chapter 3), especially when combined

with other techniques (e.g. Chapter 4). The wavelength of the AlOH absorption feature (λ_{AlOH} - the SWIR proxy for white mica composition) is generally related to the amount of water-rock interaction (Chapter 4), therefore λ_{AlOH} may correlate with the proportion of secondary versus primary minerals in a sample. If so, this would be a much faster method of approximating alteration index, which is used in geothermal engineering geology applications (e.g. Wyering et al., 2015). Classical studies of hydrothermal alteration in geothermal fields (e.g. Reyes, 1990; Moore et al., 1997) could be conducted more easily with SWIR reflectance spectroscopy as an additional mineral identification tool, and with white mica composition as an additional parameter to evaluate variance in water-rock interaction. Recent work at Ngatamariki in New Zealand is an example where white mica composition (as estimated by TerraSpec) has been used with a suite of other tools to characterise alteration (Chambefort et al., 2017a). Newer, high resolution SWIR systems such as Corescan have significant advantages over older, lower resolution systems such as TerraSpec that may justify their extra cost. These advantages include slightly greater accuracy, the ability to determine semi-quantitative mineral abundances, and the addition of textural information from imaging (Chapter 3). These could be best leveraged in an exploration campaign by using TerraSpec on drill cuttings, where much textural information is already lost, and Corescan on drill core, which requires a significant extra cost to extract.

The physiochemical characteristics of the geothermal fluid are of crucial importance in exploring and exploiting geothermal systems. For example, low pH acid-sulfate fluids must be avoided or neutralised if possible, due to their corrosive nature (Ellis, 1970; Reyes, 1990; Villaseñor and Vicedo, 2010). Reconstruction of the Lake City hydrothermal system shows that acid sulfate fluids were exsolved from the youngest magmas (‘batch B’) of the caldera magmatic cycle, which were compositionally distinct from the caldera-forming magmas (Chapter 4). Although high temperature, fluids such as these would be challenging to exploit due to their acidic nature. Near neutral fluids associated with the resurgent dome and western margin of the caldera would have been more amenable to development. This example shows how in caldera settings, areas near recent intrusions or underneath recent post-caldera volcanics may be poor exploration targets. However, exploitable reservoirs may be present on the margins of these acid-sulfate areas, where the fluids have been neutralised and there is good permeability.

Table 1: Conclusions of thesis.

Question	What answer can be provided?	Chapter
What is the lithological and permeability architecture of a caldera margin and what structural and lithological factors are favourable for the creation of permeable fluid pathways in caldera settings?	The Lake City caldera structural margin consists of fault rocks (from breccia to ultracataclasite) that define fault cores up to ~60 m wide. Faults and veins extend more than 300 m from the intra/extra-caldera interface (caldera margin discontinuity). Important factors for the creation of permeable fluid pathways are 1) the presence of favourable lithologies (proximity to magmatic intrusions and/or the presence of permeable lithologies), 2) a high density of faults and fractures, and 3) diverse orientations of faults and fractures that promote the formation of discontinuity intersections.	Chapter 2
How comparable are the results from low spatial resolution (e.g. TerraSpec) and high spatial resolution (e.g. Corescan) SWIR reflectance spectroscopy techniques, with regards to white mica composition?	The results from TerraSpec and Corescan correlate well with each other, but have small average differences (0.4 or 1.1 nm), the magnitude of which depend on data processing. Both Corescan and TerraSpec correlate well with white mica aluminium content, with the correlation slightly better for Corescan	Chapter 3
How useful is variation in white mica composition for understanding fluid-rock interaction?	High-Al white mica correlates with quartz-sericite-pyrite alteration and low $\delta^{18}O$ composition throughout most of the caldera. Higher Al white mica reflects higher amounts of water-rock interaction.	Chapter 3
What are the magmatic and structural controls on the physiochemical conditions of the Lake City hydrothermal fluid, and how do these change throughout the evolution of the caldera system?	The hydrothermal system was dominantly moderate temperature (up to ~290°C), low salinity (<3% NaCl equivalent) and neutral to weakly acidic pH. However, high temperature (up to ~540°C), hypersaline (up to ~65% NaCl eq.) magmatic fluid was exsolved from distinct "batch B" magmas in the east of the caldera. Fluid inclusion microthermometry indicates that the syenite resurgent intrusion was already significantly cooled by the time the hydrothermal system established, and that batch B magmas in the east of the caldera provided a later input of high temperature magmatic fluid.	Chapter 4

How can we use these data from an ancient analogue to inform our understanding of modern caldera-related geothermal systems such as those in the Taupō Volcanic Zone of New Zealand?	The location and geometry of calderas in the Taupō Volcanic Zone (TVZ) is strongly controlled by pre-existing regional structure, to an even greater degree than Lake City caldera. Data from geothermal systems in the TVZ is generally consistent with fluid flow being focused at fault intersections, which may be favoured where caldera margins cut across regional faults. Structural complexities such as these should be targets for exploration, while directly targeting the most recent post-caldera magmatic heat sources may encounter undesirable acid-sulfate fluids.	Chapter 5

5.5. FUTURE WORK

There are still questions and gaps that can be filled in our understanding of Lake City caldera and its hydrothermal system. In this section I suggest future work that could be done at Lake City and elsewhere to improve our understanding of calderas and their volcano-tectonic controls on hydrothermal fluid transport.

No kinematic indicators were identified in the fault rocks of the Lake City structural margin. However, detailed field work focussed on finding such indicators may have more success. Kinematic indicators could make it possible to determine if fault rocks were formed during inversion of displacement during resurgence, or only during subsidence. Analysis of microstructures in the granite on the margin of the caldera may also be a fruitful area of future research. Microstructural analysis of samples in a transect hundreds of metres out from the caldera margin may reveal that the width of deformation outside the caldera margin is further than the ~300 m proposed in this study. Any microscopic deformation will influence the rock permeability, particularly in crystalline granite, and hence fluid flow.

The long and complex history of hydrothermal activity in the western San Juan Volcanic Field makes the understanding of the timing of hydrothermal events in Lake City caldera uncertain. It is clear that structures related to caldera formation were important in localising fluid flow, however we do not know for sure if hydrothermal activity on the western margin, centre of the caldera, and eastern margin were concurrent. The currently available age data (Bove et al., 2001) do not have sufficient spatial coverage to fully understand the timing of

hydrothermal activity. Further radiometric dating of vein minerals (e.g. adularia) (as done by Lipman et al., 1976; Bove et al., 2001) at multiple locations in the caldera and outside its western margin could resolve some of these questions, or bring to light previously unknown complexities.

Further fluid inclusion work would also help further constrain our understanding of the Lake City hydrothermal system. Quantitative analysis of fluid inclusion composition, particularly CO_2 content using Raman spectroscopy, would reduce errors in determination of the depth of formation, and would also provide insight into the fluid composition. Increased spatial resolution of fluid inclusion microthermometry across the caldera would further refine the conceptual model presented here. Higher spatial resolution may enable anomalies in temperature or composition to be better defined and related to specific structures, which would further refine our understanding of the fluid pathways in the Lake City hydrothermal system.

While working with the semi-quantitative Corescan mineral abundance data, one difficulty was knowing whether the low abundances found in some samples for some minerals (e.g. 3% epidote) meant the mineral was actually present or were due to errors in interpretation of spectra. Resolving this question at Lake City would be helpful for future users of Corescan hyperspectral data elsewhere. In this study it was not possible to adequately resolve this question because Corescan abundances were calculated from slabs that are larger than thin sections. If the Corescan data were collected only from thin-section sized billets, or I worked with Corescan staff to isolate the data only from the thin-section sized area of interest, then detailed optical and SEM petrography could be compared with the Corescan data. Stitching of SEM images across an entire thin section and quantitative analysis with software such as ImageJ would allow a true abundance to be calculated that can be compared with the semi-quantitative Corescan abundance.

Spatial correlations between alteration assemblage, oxygen isotope composition and white mica composition (λ_{AlOH}) appear convincing visually (Chapter 3), however it would be useful to quantify this covariance and determine why they appear anti-correlated in parts of the caldera. A detailed geostatistical study of covariance between these data may allow some understanding of cause of these discrepancies, for example it appears visually that λ_{AlOH} may

be well correlated in the phyllic alteration zone but more poorly correlated in the propylitic zone. This would provide further physiochemical constraints, such as in the phyllic zone λ_{AlOH} may be a proxy for water-rock interaction, however in the propylitic zone temperature may be the primary control. This would aid workers in interpreting white mica composition data in other systems worldwide. Assistant Professor Snehamoy Chatterjee at Michigan Technological University has expressed interest in working with a student on continuing this aspect of my thesis, with input from myself.

A Ph.D. student at Michigan Technological University, Rachel Hetherington, is working with a selection of my Lake City samples to determine the rock strength and permeability of a suite of rock types at the caldera, with varying types of hydrothermal alteration. The goal for her project is to develop an alteration strength index (modified from Wyering et al., 2015) that can be estimated using hyperspectral data. The strength and permeability data would also be useful for quantifying the permeability of the caldera margin, and hence she will also test some of the granite fault rock facies described in Chapter 2. I have already met and worked with Rachel in selecting samples that represent the diversity of rock types and alteration associations at Lake City, and it is hoped that her work will lead to interesting future collaborations and publications.

Recently it is becoming accepted that the North Island volcanic arc in New Zealand has had a NE-SW orientation for at least the last ~20 Ma, and the apparent NNW trend of the Coromandel Volcanic Zone is due to faulting associated with development of the Hauraki Rift (Fig. 1a) (Seebeck et al., 2014; Wilson and Rowland, 2016). The Coromandel Volcanic Zone (CVZ) is richly mineralised, and home to the Hauraki Goldfield (Mauk et al., 2011), however similar deposits are apparently absent in much of the rest of the proposed former arc. If this hypothesis is accepted, then an important question is why the part of the arc represented by the Hauraki Goldfield was host to considerably more mineralisation than the adjacent parts of the arc, over a period of more than ten million years. This situation has some similarities to the Colorado Mineral Belt, which is discordant to the orientation of the general Southern Rocky Mountains Volcanic Field arc and hosted mineralisation over a period of tens of millions of years (Chapin, 2012). Similar explanations that have been proposed for the Colorado Mineral Belt, such as inherited basement structures, and structures in the subducting slab (Chapin, 2012), could be investigated for the Hauraki Goldfield. The CVZ is

the only part of the former arc where products of major silicic volcanism have been identified (Fig. 1a). It is possible that the anomalously high mantle flux conditions that may have accompanied the onset of silicic volcanism in the part of the arc represented by the CVZ (Gravley et al., 2016) were also an important factor. However, in the Hauraki Goldfield, mineralisation is much less widespread in and near silicic calderas than in the more voluminous andesite and dacite (Christie et al., 2007). If the NNW trend of the Hauraki Goldfield is extrapolated southwards into the modern TVZ, it would encompass the area approximately between the eastern margins of Okataina and Whakamaru calderas. Some of the geothermal systems in this area (e.g. Rotokawa) have significant hydrothermal fluxes of gold and silver, however no major ore mineralisation has been found at depth (Simmons and Brown, 2007; Simmons et al., 2016). An interesting area of future research would be to determine if geothermal systems in this area have any distinguishing features compared to systems outside of it, that may represent a possible modern continuation of the Hauraki Goldfield, or if the whole central TVZ represents a modern continuation of the anomalous CVZ and Hauraki Goldfield.

5.6. REFERENCES CITED

Ashwell, P.A., Kennedy, B.M., Gravley, D.M., von Aulock, F.W., and Cole, J.W., 2013, Insights into caldera and regional structures and magma body distribution from lava domes at Rotorua Caldera, New Zealand: Journal of Volcanology and Geothermal Research, v. 258, p. 187–202, doi: 10.1016/j.jvolgeores.2013.04.014.

Barker, S.J., Wilson, C.J.N., Smith, E.G.C., Charlier, B.L.A., Wooden, J.L., Hiess, J., and Ireland, T.R., 2014, Post-supereruption magmatic reconstruction of Taupo volcano (New Zealand), as reflected in zircon ages and trace elements: Journal of Petrology, v. 55, p. 1511–1533, doi: 10.1093/petrology/egu032.

Bertrand, E.A., Caldwell, T.G., Bannister, S., Soengkono, S., Bennie, S.L., Hill, G.J., and Heise, W., 2015, Using array MT data to image the crustal resistivity structure of the southeastern Taupo Volcanic Zone, New Zealand: Journal of Volcanology and Geothermal Research, v. 305, p. 63–75, doi: 10.1016/j.jvolgeores.2015.09.020.

Bibby, H.M., Caldwell, T.G., Davey, F.J., and Webb, T.H., 1995, Geophysical evidence on the structure of the Taupo Volcanic Zone and its hydrothermal circulation: Journal of Volcanology and Geothermal Research, v. 68, p. 29–58, doi: 10.1016/0377-0273(95)00007-H.

Bove, D.J., Hon, K., Budding, K.E., Slack, J.F., Snee, L.W., and Yeoman, R.A., 2001, Geochronology and geology of late Oligocene through Miocene volcanism and mineralization in the western San Juan Mountains, Colorado: U.S. Geological Survey Professional Paper 1642, 30 p.

Branney, M.J., and Kokelaar, P., 1994, Volcanotectonic faulting, soft-state deformation, and rheomorphism of tuffs during development of a piecemeal caldera, English Lake District: Geological Society of America Bulletin, v. 106, p. 507–530, doi: 10.1130/0016-7606(1994)106<0507:VFSSDA>2.3.CO;2.

Browne, P.R.L., 1970, Hydrothermal alteration as an aid in investigating geothermal fields: Geothermics, v. 2, p. 564–570, doi: 10.1016/0375-6505(70)90057-X.

Caldwell, T.G., and Bibby, H.M., 1992, Geothermal implications of resistivity mapping in Lake Taupo: Proceedings 14th New Zealand Geothermal Workshop, Auckland, New Zealand, 4-6 November 1992, p. 207–212.

Caratori Tontini, F., de Ronde, C.E.J., Scott, B.J., Soengkono, S., Stagpoole, V., Timm, C., and Tivey, M., 2016, Interpretation of gravity and magnetic anomalies at Lake Rotomahana: Geological and hydrothermal implications: Journal of Volcanology and Geothermal Research, v. 314, p. 84–94, doi: 10.1016/j.jvolgeores.2015.07.002.

Chambefort, I., Lewis, B., Simpson, M.P., Bignall, G., Rae, A.J., and Ganefianto, N., 2017a, Ngatamariki geothermal system: Magmatic to epithermal transition in the Taupo Volcanic Zone, New Zealand: Economic Geology, v. 112, p. 319–346, doi: 10.2113/econgeo.112.2.319.

Chambefort, I., Lewis, B., Wilson, C.J.N., Rae, A.J., Coutts, C., Bignall, G., and Ireland, T.R., 2014, Stratigraphy and structure of the Ngatamariki geothermal system from new zircon U-Pb geochronology: Implications for Taupo Volcanic Zone evolution: Journal of Volcanology and Geothermal Research, v. 274, p. 51–70, doi: 10.1016/j.jvolgeores.2014.01.015.

Chambefort, I., Wilson, C.J.N., Rowland, J. V, Gravley, D.M., Bignall, G., Alcaraz, S.A., Milicich, S.D., Villamor, P., and Rosenberg, M.D., 2017b, The deep controls on high enthalpy geothermal systems: A multi-disciplinary overview from New Zealand: Proceedings 39th New Zealand Geothermal Workshop, Rotorua, New Zealand, 22-24 November 2017.

Chapin, C.E., 2012, Origin of the Colorado Mineral Belt: Geosphere, v. 8, p. 28–43, doi: 10.1130/GES00694.1.

Christie, A.B., Simpson, M.P., Brathwaite, R.L., Mauk, J.L., and Simmons, S.F., 2007,

Epithermal Au-Ag and related deposits of the Hauraki Goldfield, Coromandel Volcanic Zone, New Zealand: Economic Geology, v. 102, p. 785–816, doi: 10.2113/gsecongeo.102.5.785.

Cole, J.W., and Spinks, K.D., 2009, Caldera volcanism and rift structure in the Taupo Volcanic Zone, New Zealand: Geological Society, London, Special Publications, v. 327, p. 9–29, doi: 10.1144/SP327.2.

Cornejo, P., Tosdal, R.M., Mpodozis, C., Tomlinson, A.J., Rivera, O., and Fanning, C.M., 1997, El Salvador, Chile Porphyry Copper Deposit Revisited: Geologic and Geochronologic Framework: International Geology Review, v. 39, p. 22–54, doi: 10.1080/00206819709465258.

Davey, F.J., Henrys, S. a., and Lodolo, E., 1995, Asymmetric rifting in a continental back-arc environment, North Island, New Zealand: Journal of Volcanology and Geothermal Research, v. 68, p. 209–238, doi: 10.1016/0377-0273(95)00014-L.

Downs, D.T., Rowland, J. V., Wilson, C.J.N., Rosenberg, M.D., Leonard, G.S., and Calvert, a. T., 2014a, Evolution of the intra-arc Taupo-Reporoa Basin within the Taupo Volcanic Zone of New Zealand: Geosphere, v. 10, p. 185–206, doi: 10.1130/GES00965.1.

Downs, D.T., Wilson, C.J.N., Cole, J.W., Rowland, J. V., Calvert, A.T., Leonard, G.S., and Keall, J.M., 2014b, Age and eruptive center of the Paeroa Subgroup ignimbrites (Whakamaru Group) within the Taupo Volcanic Zone of New Zealand: Bulletin of the Geological Society of America, v. 126, p. 1131–1144, doi: 10.1130/B30891.1.

Ellis, A.J., 1970, Quantitative interpretation of chemical characteristics of hydrothermal systems: Geothermics, v. 2, p. 516–528.

Fischer, M., Röller, K., Küster, M., Stöckhert, B., and McConnell, V.S., 2003, Open fissure mineralization at 2600 m depth in Long Valley Exploratory Well (California) - Insight into the history of the hydrothermal system: Journal of Volcanology and Geothermal Research, v. 127, p. 347–363, doi: 10.1016/S0377-0273(03)00176-8.

Goff, F., and Gardener, J.N., 1994, Evolution of a mineralized geothermal system, Valles Caldera, New Mexico: Economic Geology, v. 89, p. 1803–1832.

Goff, F., and Janik, C.J., 2002, Gas geochemistry of the Valles caldera region, New Mexico and comparisons with gases at Yellowstone, Long Valley and other geothermal systems: Journal of Volcanology and Geothermal Research, v. 116, p. 299–323, doi: 10.1016/S0377-0273(02)00222-6.

Gravley, D.M., Deering, C.D., Leonard, G.S., and Rowland, J. V., 2016, Ignimbrite flare-ups and their drivers: A New Zealand perspective: Earth-Science Reviews, v. 162, p. 65–82,

doi: 10.1016/j.earscirev.2016.09.007.

Gravley, D.M., Wilson, C.J.N., Leonard, G.S., and Cole, J.W., 2007, Double trouble: Paired ignimbrite eruptions and collateral subsidence in the Taupo Volcanic Zone, New Zealand: Geological Society of America Bulletin, v. 119, p. 18–30, doi: 10.1130/B25924.1.

Heise, W., Caldwell, T.G., Bertrand, E.A., Hill, G.J., Bennie, S.L., and Palmer, N.G., 2016, Imaging the deep source of the Rotorua and Waimangu geothermal fields, Taupo Volcanic Zone, New Zealand: Journal of Volcanology and Geothermal Research, v. 314, p. 39-48, doi: 10.1016/j.jvolgeores.2015.10.017.

Heise, W., Caldwell, T.G., Bibby, H.M., and Bennie, S.L., 2010, Three-dimensional electrical resistivity image of magma beneath an active continental rift, Taupo Volcanic Zone, New Zealand: Geophysical Research Letters, v. 37, p. 2–6, doi: 10.1029/2010GL043110.

Hildreth, W., 2017, Fluid-driven uplift at Long Valley Caldera, California: Geologic perspectives: Journal of Volcanology and Geothermal Research, v. 341, p. 269–286, doi: 10.1016/j.jvolgeores.2017.06.010.

Hildreth, W., 2004, Volcanological perspectives on Long Valley, Mammoth Mountain, and Mono Craters: Several contiguous but discrete systems: Journal of Volcanology and Geothermal Research, v. 136, p. 169–198, doi: 10.1016/j.jvolgeores.2004.05.019.

Hildreth, W., Fierstein, J., and Calvert, A., 2017, Early postcaldera rhyolite and structural resurgence at Long Valley Caldera, California: Journal of Volcanology and Geothermal Research, v. 335, p. 1–34, doi: 10.1016/j.jvolgeores.2017.01.005.

Hon, K.A., 1987, Geologic and petrologic evolution of the Lake City caldera, San Juan Mountains, Colorado [Ph.D. thesis]: University of Colorado at Boulder, 244 p.

Houghton, B.F., Wilson, C.J.N., McWilliams, M.O., Lariphere, M.A., Weaver, S.D., Briggs, R.M., and Pringle, M.S., 1995, Chronology and dynamics of a large silicic magmatic system. Central Taupo volcanic zone, New Zealand: Geology, v. 23, p. 13–16, doi: 10.1130/0091-7613(1995)023<0013:CADOAL>2.3.CO;2.

Hulen, J.B., and Nielson, D.L., 1990, Possible volcanotectonic controls on high-temperature thermal fluid upflow in the Valles caldera, New Mexico: Geothermal Resources Council Transactions, v. 14, p. 1457–1464, doi: 10.18553/jmcp.2008.14.S6-B.21.

Hulen, J.B., Nielson, D.L., Goff, F., Gardner, J.N., and Charles, R.W., 1987, Molybdenum mineralization in an active geothermal system, Valles caldera, New Mexico (USA).: Geology, v. 15, p. 748–752, doi: 10.1130/0091-

7613(1987)15<748:MMIAAG>2.0.CO;2.

Hurwitz, S., Farrar, C.D., and Williams, C.F., 2010, The thermal regime in the resurgent dome of Long Valley Caldera, California: Inferences from precision temperature logs in deep wells: Journal of Volcanology and Geothermal Research, v. 198, p. 233–240, doi: 10.1016/j.jvolgeores.2010.08.023.

Kennedy, B., Wilcock, J., and Stix, J., 2012, Caldera resurgence during magma replenishment and rejuvenation at Valles and Lake City calderas: Bulletin of Volcanology, v. 74, p. 1833–1847, doi: 10.1007/s00445-012-0641-x.

Larson, P.B., and Taylor, H.P., 1986, An oxygen isotope study of hydrothermal alteration in the Lake City caldera, San Juan Mountains, Colorado: Journal of Volcanology and Geothermal Research, v. 30, p. 47–82.

Lipman, P.W., 1976, Caldera-collapse breccias in the western San Juan Mountains, Colorado: Geological Society of America Bulletin, v. 87, p. 1397–1410.

Lipman, P.W., Fisher, F.S., Mehnert, H.H., Naeser, C.W., Luedke, R.G., and Steven, T.A., 1976, Multiple ages of mid-Tertiary mineralization and alteration in the Western San Juan Mountains, Colorado: Economic Geology, v. 71, p. 571–588.

Lucic, G., Stix, J., and Wing, B., 2015, Structural controls on the emission of magmatic carbon dioxide gas, Long Valley Caldera, USA: Journal of Geophysical Research: Solid Earth, v. 120, p. 2262–2278, doi: 10.1002/2014JB011760.

Mauk, J.L., Hall, C.M., Chesley, J.T., and Barra, F., 2011, Punctuated evolution of a large epithermal province: The Hauraki goldfield, New Zealand: Economic Geology, v. 106, p. 921–943, doi: 10.2113/econgeo.106.6.921.

McConnell, V.S., Shearer, C.K., Eichelberger, J.C., Keskinen, M.J., Layer, P.W., and Papike, J.J., 1995, Rhyolite intrusions in the intracaldera Bishop Tuff, Long Valley Caldera, California: Journal of Volcanology and Geothermal Research, v. 67, p. 41–60, doi: 10.1016/0377-0273(94)00099-3.

Milicich, S.D., Wilson, C.J.N., Bignall, G., Pezaro, B., Charlier, B.L.A., Wooden, J.L., and Ireland, T.R., 2013, U–Pb dating of zircon in hydrothermally altered rocks of the Kawerau Geothermal Field, Taupo Volcanic Zone, New Zealand: Journal of Volcanology and Geothermal Research, v. 253, p. 97–113, doi: 10.1016/j.jvolgeores.2012.12.016.

Milner, D.M., Cole, J.W., and Wood, C.P., 2002, Asymmetric, multiple-block collapse at Rotorua Caldera, Taupo Volcanic Zone, New Zealand: Bulletin of Volcanology, v. 64, p. 134–149, doi: 10.1007/s00445-001-0191-0.

Moore, J.N., Powell, T.S., Norman, D.I., and Johnson, G.W., 1997, Hydrothermal alteration and fluid-inclusion systematics of the reservoir rocks in Matalibong-25, Tiwi, Philippines, *in* Proceedings, Thirty-Second Workshop on Geothermal Reservoir Engineering, Stanford, California, 22-24 January 2007, p. 447–456.

Phillips, E.H., Goff, F., Kyle, P.R., McIntosh, W.C., Dunbar, N.W., and Gardner, J.N., 2007, The 40Ar/39Ar age constraints on the duration of resurgence at the Valles caldera, New Mexico: Journal of Geophysical Research: Solid Earth, v. 112, p. 1–15, doi: 10.1029/2006JB004511.

Reyes, A., 1990, Petrology of Philippine geothermal systems and the application of alteration mineralogy to their assessment: Journal of Volcanology and Geothermal Research, v. 43, p. 279–309.

Rosenberg, M., 2017, Volcanic and tectonic perspectives on the age and evolution of the Wairakei-Tauhara geothermal system [Ph.D. thesis]: Wellington, New Zealand, Victoria University of Wellington, 330 p.

Rosenberg, M.D., Bignall, G., and Rae, A.J., 2009, The geological framework of the Wairakei–Tauhara Geothermal System, New Zealand: Geothermics, v. 38, p. 72–84, doi: 10.1016/j.geothermics.2009.01.001.

Rowland, J.V., and Sibson, R.H., 2004, Structural controls on hydrothermal flow in a segmented rift system, Taupo Volcanic Zone, New Zealand: Geofluids, v. 4, p. 259–283, doi: 10.1111/j.1468-8123.2004.00091.x.

Rowland, J.V., and Simmons, S.F., 2012, Hydrologic, magmatic, and tectonic controls on hydrothermal flow, Taupo Volcanic Zone, New Zealand: Implications for the formation of epithermal vein deposits: Economic Geology, v. 107, p. 427–457, doi: 10.2113/econgeo.107.3.427.

Rowland, J. V., Wilson, C.J.N., and Gravley, D.M., 2010, Spatial and temporal variations in magma-assisted rifting, Taupo Volcanic Zone, New Zealand: Journal of Volcanology and Geothermal Research, v. 190, p. 89–108, doi: 10.1016/j.jvolgeores.2009.05.004.

Rymer, H., and Brown, G.C., 1986, Gravity fields and the interpretation of volcanic structures: Geological discrimination and temporal evolution: Journal of Volcanology and Geothermal Research, v. 27, p. 229–254, doi: 10.1016/0377-0273(86)90015-6.

Sanford, R.F., 1992, Lead isotopic compositions and paleohydrology of caldera-related epithermal veins, Lake City, Colorado: Geological Society of America Bulletin, v. 104, p. 1236–1245.

Seebeck, H., and Nicol, A., 2009, Dike intrusion and displacement accumulation at the

intersection of the Okataina Volcanic Centre and Paeroa Fault zone, Taupo Rift, New Zealand: Tectonophysics, v. 475, p. 575–585, doi: 10.1016/j.tecto.2009.07.009.

Seebeck, H., Nicol, A., Giba, M., Pettinga, J., and Walsh, J., 2014, Geometry of the subducting Pacific plate since 20 Ma, Hikurangi margin, New Zealand: Journal of the Geological Society, v. 171, p. 131–143, doi: 10.1144/jgs2012-145.

Seebeck, H., Nicol, A., Stern, T.A., Bibby, H.M., and Stagpoole, V., 2010, Fault controls on the geometry and location of the Okataina Caldera, Taupo Volcanic Zone, New Zealand: Journal of Volcanology and Geothermal Research, v. 190, p. 136–151, doi: 10.1016/j.jvolgeores.2009.04.011.

Self, S., 1983, Large-scale phreatomagmatic silicic volcanism: A case study from New Zealand: Journal of Volcanology and Geothermal Research, v. 17, p. 433–469.

Self, S., Goff, F., Gardner, J.N., Wright, J. V., and Kite, W.M., 1986, Explosive rhyolitic volcanism in the Jemez Mountains: Vent locations, caldera development and relation to regional structure: Journal of Geophysical Research, v. 91, p. 1779–1798.

Simmons, S.F., and Brown, K.L., 2007, The flux of gold and related metals through a volcanic arc, Taupo Volcanic Zone, New Zealand: Geology, v. 35, p. 1099, doi: 10.1130/G24022A.1.

Simmons, S.F., Brown, K.L., Browne, P.R.L., and Rowland, J.V., 2016, Gold and silver resources in Taupo Volcanic Zone geothermal systems: Geothermics, v. 59, p. 205–214, doi: 10.1016/j.geothermics.2015.07.009.

Simmons, S.F., Keywood, M., Scott, B.J., and Keam, R.F., 1993, Irreversible change of the Rotomahana-Waimangu hydrothermal system (New Zealand) as a consequence of a volcanic eruption: Geology, v. 21, p. 643–646, doi: 10.1130/0091-7613(1993)021<0643:ICOTRW>2.3.CO;2.

Simpson, M.P., and Bignall, G., 2016, Undeveloped high-enthalpy geothermal fields of the Taupo Volcanic Zone, New Zealand: Geothermics, v. 59, p. 325–346, doi: 10.1016/j.geothermics.2015.08.006.

Smith, B.M., and Suemnicht, G.A., 1991, Oxygen isotope evidence for past and present hydrothermal regimes of Long Valley caldera, California: Journal of Volcanology and Geothermal Research, v. 48, p. 319–339.

Sorey, M.L., Suemnicht, G.A., Sturchio, N.C., and Nordquist, G.A., 1991, New evidence on the hydrothermal system in Long Valley caldera, California, from wells, fluid sampling, electrical geophysics, and age determinations of hot-spring deposits: Journal of Volcanology and Geothermal Research, v. 48, p. 229–263, doi: 10.1016/0377-

0273(91)90045-2.

Spinks, K.D., Acocella, V., Cole, J.W., and Bassett, K.N., 2005, Structural control of volcanism and caldera development in the transtensional Taupo Volcanic Zone, New Zealand: Journal of Volcanology and Geothermal Research, v. 144, p. 7–22, doi: 10.1016/j.jvolgeores.2004.11.014.

Stagpoole, V.M., 1994, Interpretation of refraction seismic and gravity data across the eastern margin of the Taupo volcanic zone, New Zealand: Geothermics, v. 23, p. 501–510.

Suemnicht, G.A., and Varga, R.J., 1988, Basement structure and implications for hydrothermal circulation patterns in the western moat of Long Valley caldera, California: Journal of Geophysical Research, v. 93, p. 13191–13207, doi: 10.1029/JB093iB11p13191.

Villamor, P., and Berryman, K., 2001, A late quaternary extension rate in the Taupo Volcanic Zone, New Zealand, derived from fault slip data: New Zealand Journal of Geology and Geophysics, v. 44, p. 243–269, doi: 10.1080/00288306.2001.9514937.

Villamor, P., Berryman, K.R., Nairn, I.A., Wilson, K., Litchfield, N., and Ries, W., 2011, Associations between volcanic eruptions from Okataina volcanic center and surface rupture of nearby active faults, Taupo rift, New Zealand: Insights into the nature of volcano-tectonic interactions: Bulletin of the Geological Society of America, v. 123, p. 1383–1405.

Villamor, P., Clark, K., Watson, M., Rosenberg, M., Lukovic, B., Ries, W., and González, Á., 2015, New Zealand geothermal power plants as critical facilities: An active fault avoidance study in the Wairakei Geothermal Field, New Zealand: Proceedings of the World Geothermal Congress, Melbourne, Australia, 19-25 April 2015.

Villamor, P., Nicol, A., Seebeck, H., Rowland, J., Townsend, D., Massiot, C., Mcnamara, D.D., Milicich, S., Ries, W., and Alcaraz, S., 2017, Tectonic structure and permeability in the Taupō Rift: New insights from analysis of LiDAR derived DEMs: Proceedings 39th New Zealand Geothermal Workshop, Rotorua, New Zealand, 22-24 Novemeber 2017.

Villaseñor, L.B., and Vicedo, R.O., 2010, Exclusion of acid sulfate fluid in wells at Tiwi Geothermal Field, Albay Province, Philippines: Proceedings of the World Geothermal Congress 2010, Bali, Indonesia, 25-30 April 2010.

Walker, G.P.L., 1984, Downsag calderas, ring faults, caldera sizes, and incremental caldera growth: Journal of Geophysical Research, v. 89, p. 8407–8416.

Walker, G.P.L., 1985, Origin of coarse lithic breccias near ignimbrite source vents: Journal of

Volcanology and Geothermal Research, v. 25, p. 157–171, doi: 10.1016/0377-0273(85)90010-1.

Wilson, C.J.N., 1993, Stratigraphy, Chronology, Styles and Dynamics of Late Quaternary Eruptions from Taupo Volcano, New Zealand: Philosophical Transactions of the Royal Society A: Mathematical, Physical and Engineering Sciences, v. 343, p. 205–306, doi: 10.1098/rsta.1993.0050.

Wilson, C., 2001, The 26.5ka Oruanui eruption, New Zealand: An introduction and overview: Journal of Volcanology and Geothermal Research, v. 112, p. 133–174, doi: 10.1016/S0377-0273(01)00239-6.

Wilson, C.J.N., Houghton, B.F., Mcwilliams, M.O., Lanphere, M.A., Weaver, S.D., and Briggs, R.M., 1995, Volcanic and structural evolution of Taupo Volcanic Zone, New Zealand : A review: Journal of Volcanology and Geothermal Research, v. 68, p. 1–28.

Wilson, C.J.N., and Rowland, J. V., 2016, The volcanic, magmatic and tectonic setting of the Taupo Volcanic Zone, New Zealand, reviewed from a geothermal perspective: Geothermics, v. 59, p. 168–187, doi: 10.1016/j.geothermics.2015.06.013.

Wilson, C.J.N., and Walker, G.P.L., 1985, The Taupo Eruption, New Zealand I. General Aspects: Philosophical Transactions of the Royal Society A: Mathematical, Physical and Engineering Sciences, v. 314, p. 199–228, doi: 10.1098/rsta.1985.0019.

Wood, C.P., 1994, Aspects of the geology of Waimangu, Waiotapu, Waikite and Reporoa geothermal systems, Taupo Volcanic Zone, New Zealand: Geothermics, v. 23, p. 401–421.

Wood, C.P., 1992, Geology of the Rotorua geothermal system: Geothermics, v. 21, p. 25–41, doi: 10.1016/0375-6505(92)90066-I.

Wyering, L.D., Villeneuve, M.C., Wallis, I.C., Siratovich, P.A., Kennedy, B.M., and Gravley, D.M., 2015, The development and application of the alteration strength index equation: Engineering Geology, v. 199, p. 48–61, doi: 10.1016/j.enggeo.2015.10.003.

Wyering, L.D., Villeneuve, M.C., Wallis, I.C., Siratovich, P.A., Kennedy, B.M., Gravley, D.M., and Cant, J.L., 2014, Mechanical and physical properties of hydrothermally altered rocks, Taupo Volcanic Zone, New Zealand: Journal of Volcanology and Geothermal Research, v. 288, p. 76–93, doi: 10.1016/j.jvolgeores.2014.10.008.

APPENDICES

All appendices are submitted in electronic form, and can be found on a compact disc accompanying the printed version of this thesis, or in a folder entitled "Electronic Appendices" accompanying the electronic version of the thesis. The appendices consist of the following supplementary information:

Chapter 2 Appendices

Appendix A – Scanline logs

The raw data collected along scanlines, which is presented in Chapter 2. A guide to the notation used in the scanline logs is also included.

Appendix B – Published paper

A copy of the version of this chapter that has been published in the journal Geosphere.

Chapter 3 Appendices

Appendix C – Sample locations and analyses

A tabulated summary of all the samples that were collected for this thesis, their locations, and a list of the analyses that were conducted on each sample.

Appendix D – Raw TerraSpec data

A spreadsheet of the raw data from all of the TerraSpec analyses that were conducted.

Appendix E – Corescan and TerraSpec summary data

The averaged Corescan and TerraSpec white mica AlOH wavelength data for each sample for which both techniques were used. The raw Corescan data are not included due to the large size of the files, but are available on request.

Appendix F – SEM EDS data

The SEM EDS data used to determine white mica composition. The data have been already cleaned to remove analyses that were not of white mica.

Appendix G – Corescan white mica composition data

The averaged Corescan white mica AlOH wavelength data for each sample and averaged for each location. The raw Corescan data are not included due to the large size of the files, but are available on request.

Chapter 4 Appendices

Appendix H - Sample locations and analyses

A tabulated summary of all the samples that were collected for this thesis, their locations, and a list of the analyses that were conducted on each sample.

Appendix I – Corescan mineralogy data

The maximum mineral abundance for each sample and each location as determined using Corescan, used to determine the mineralogy of each sample. See section 4.4.4 for the explanation of how these were computed. The raw Corescan data are not included due to the large size of the files, but are available on request.

Appendix J – Corescan white mica composition data

The averaged Corescan white mica AlOH wavelength data for each sample and averaged for each location. The raw Corescan data are not included due to the large size of the files, but are available on request.

Appendix K – Vein texture data

A tabulated summary of the locations where vein boiling textures were identified versus where they were absent. See section 4.4.2 for the explanation of what textures are considered boiling textures.

Appendix L – Fluid inclusion data

Spreadsheet of all raw fluid inclusion microthermometry data collected during this thesis.